THE ROLE OF NEUTROPHIL MICROPARTICLES IN RHEUMATOID ARTHRITIS

Miss Sarah Emily Headland

A thesis submitted in partial fulfilment of the requirements of the University of London for the Degree of Doctor of Philosophy

Centre for Biochemical Pharmacology,
William Harvey Research Institute,
Barts and the London School of Medicine and Dentistry,
Charterhouse Square, London, EC1M 6BQ.

I, Sarah Emily Headland, confirm that the research included within this thesis is my own work or that where it has been carried out in collaboration with, or supported by others, that this is duly acknowledged below and my contribution indicated. Previously published material is also acknowledged below.

I attest that I have exercised reasonable care to ensure that the work is original, and does not to the best of my knowledge break any UK law, infringe any third party's copyright or other Intellectual Property Right, or contain any confidential material.

I accept that the College has the right to use plagiarism detection software to check the electronic version of the thesis.

I confirm that this thesis has not been previously submitted for the award of a degree by this or any other university.

Details of collaboration and publications:

This work was supported by the Oliver Bird Rheumatism Programme, The Nuffield Foundation.

All samples were generated by myself, I collected and analysed the data presented herein, with the following exceptions. Immunogold staining and transmission electron microscopy was kindly performed by Dr Cristiane Damas Gil with Professor Sonia Oliani. Western blotting analysis for phosphorylated Akt and ERK1/2 was kindly performed by Dr Sadani Cooray, Real-Time PCR data presented in Section 4.4.2 was kindly performed by Dr Trinidad Montero-Melendez. TGF-β1 cytokine bead array was kindly performed by Mr Hefin Rhys Jones. Microcapsules were a kind gift from Prof Gleb Sukhorukov.

Signed: 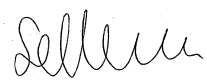

Date: 2nd April 2014

ABSTRACT

Microparticles are small subcellular vesicles, which function in inter-cellular communication by transferring RNA, bioactive lipids, proteins and receptors to target cells. Neutrophil microparticles are abundant in rheumatoid arthritis synovial fluids. Current dogma dictates that cartilage is an impenetrable avascular matrix through which metabolites from the synovial fluid must diffuse; we present the first evidence that microparticles can access chondrocytes through the cartilage. Addition of neutrophil microparticles to chondrocytes *in vitro* and *in vivo* afforded protection from arthritogenesis, evidenced by reduced extracellular matrix degradation, increased expression of genes involved in cartilage matrix synthesis and reduced inflammatory mediator production. Adoptive transfer of fluorescently labelled neutrophils into mice with inflammatory arthritis migrated to the inflamed joints and released microparticles, which could be found abundantly within the cartilage. We propose a mechanism whereby microparticles deliver the pro-resolving protein Annexin A1, which engages the receptor FPR2/ALX on the chondrocyte, eliciting tissue protection. This protection could be blocked in part by TGF-β neutralising antibodies and by preventing microparticle phosphatidylserine interaction with chondrocytes by coating with Annexin V. Intriguingly, microparticle treatment directly inhibited the phosphorylation of Hsp27. Hsp27 exists as large oligomers within the resting cell, and upon phosphorylation are released as monomers which function to stabilise the mRNA of certain pro-inflammatory genes such as IL-8, IL-6 and COX-2; which were effects seen during microparticle/chondrocyte coculture. Thus, microparticles may directly reprogram chondrocytes to prevent the expression of pro-inflammatory cytokines and mediators, but also they exert anti-inflammatory effects via the exposure of phosphatidylserine and induce the production of protective TGF-β by chondrocytes. As cartilage has limited capacity for self-repair, there is an unmet need for therapies that actively repair or protect cartilage, especially in Rheumatoid Arthritis. We envisage these microparticles could offer therapeutic possibilities in the protection of cartilage in situ in these difficult-to-treat patients.

“Nature makes nothing incomplete, and nothing in vain.”

Aristotle

ACKNOWLEDGEMENTS

Firstly, I would like to thank Professor Mauro Perretti, for your energy, enthusiasm and support. Thank you for the freedom you gave me to undertake and shape my project in a manner that made me feel as if it were the fruit of my own ideas, even though your wisdom and vision led my work every step of the way. Thank you for this challenging and rewarding project, for the unlimited time you always gave me, and for the opportunity to develop as a person.

I could not have completed this work without building on what was discovered before, and I would like to thank Lucy Norling, Jesmond Dalli and Karin Greco for providing the foundation, and then helping me build, my research. Lucy, you obviously deserve a special mention, as you have been an inspiration over the past four years. Your unceasing patience, effort and attention to detail are qualities that I can only try to emulate during the rest of my career. I hope we can continue to work together in the future, but moreover, I hope we remain firm friends.

I would like to thank my colleagues past and present in Biochemical Pharmacology, especially Beatrice Gittens, Rachael Wright, Patricia Soares de Souza, Hetal Patel and Hefin Jones; without the constant support from you all, I would have been lost, or been driven mad.

I would also like to thank my second supervisor, Professor Francesco Dell'Accio for all the advice you've given me, both about my project, and strategic input in how to progress during my career. I need to thank my friends in other departments, those who have provided technical guidance, such as Mrs Rita Jones, Dr Rebecca Hands, Arif Mustafa and Dr Mike Seed, and those who have provided academic, but also social, support. Andrew Moore, Fu Liang Ng, Suzanne Eldridge, Bethan Thomas, Christopher Schultz, William Day, Paul Armstrong, Ahuva Nissim, Janice Haycocks and many more.

I would like to thank my funding body, The Oliver Bird Programme, for providing world-class opportunities for people like myself to take part in such a fulfilling four-year PhD programme.

On a personal note, I would like to thank my partner Dennis who has provided me with the strength I've needed over the past four years. It's the small kindnesses you show me every day that make taking on huge challenges possible, I couldn't have done it without you. To my Mum and Dad, thank you a million times over. And thank you to the rest of my family for being so supportive. And to Natalie Ainscough, whenever I feel overwhelmed, I think about you, moving to Australia, on your own, whilst working 70 hours a week and doing the hardest distance Masters Degree I've ever come across. On top of that, you have always made time for me, thank you.

Finally, I would like to mention some of the people who have helped me join the dots from school education to PhD, from Mrs Julia Chant, to Kim Lewry and Niall McMullan, without your encouragement, I would never have dreamed of doing a PhD.

TABLE OF CONTENTS

LIST OF FIGURES

LIST OF TABLES

LIST OF ABBREVIATIONS

3D	Three-dimensional
ABCA1	ATP-Binding Cassette A1
Ac2-26	N-terminal Annexin A1 derived peptide amino acids 2-26
ACAN	Aggrecan
ADAMTS	A disintegrin and metalloproteinase with thrombospondin motifs
AHAC	Adult human articular chondrocytes
ANOVA	Analysis of Variance
Anx V	Annexin V
AnxA1	Annexin A1
AP-1	Activator protein-1
APC	Antigen presenting cell
APS	Ammonium persulfate
AREs	AU-rich Element
ATP	Adenosine triphosphate
AU	Adenylate Uridylate
AU	Arbitrary units
AUUUA	Adenine-uridine-uridine-uridine-adenine
BACE1	Beta-secretase 1
BAPTA-AM	1,2-*Bis*(2-aminophenoxy)ethane-*N,N,N′,N′*-tetraacetic acid tetrakis(acetoxymethylester)
BCA	Bicinchoninic acid
bFGF	Basic fibroblast growth factor
BLyS	B-lymphocyte stimulator
BP	Band pass
BSA	Bovine serum albumin
C/EBPα	CCAAT enhancer-binding protein alpha
C3	Complement component 3
C3a	Complement component 3a
C5a	Complement component 5a
C5b-9	Complement components 5b-9
Ca^{2+}	Calcium
CCL2	CC-type chemokine 2
CCL4	CC-type chemokine 4
CCL5	CC-type chemokine 5
CCL8	CC-type chemokine 8
CCR5	C-C chemokine receptor type 5
CCR7	C-C chemokine receptor type 7
CD	Cluster of differentiation
cDNA	Coding DNA
CIA	Collagen-induced arthritis
CMP	Control neutrophil microparticle
CO_2	Carbon dioxide
COL2A1	Type II collagen
COX-2	Cyclooxygenase 2
COX2	Cyclooxygenase 2
CP	Ceruloplasmin
CRISPRs	Clustered, regularly interspaced short palindromic repeats
CRP	C-reactive protein

Ct	Cycle threshold
CXCL1	C-X-C motif ligand 1 chemokine
CXCL5	C-X-C motif ligand 5 chemokine
CXCL8	C-X-C motif ligand 8 chemokine
CXCR2	C-X-C chemokine receptor type 2
CXCR4	C-X-C chemokine receptor type 4
CycH	Cyclosporin H
DAPI	4',6-diamidino-2-phenylindole
DCs	Dendritic cells
DHA	Docosahexaenoic acid
$DiOC_6$	3,3'-dihexyloxacarbocyanine iodide
DMARDs	Disease modifying anti-rheumatic drugs
DMEM	Dulbecco's Modified Eagle Medium
DMM	Destabilisation of the Medial Meniscus
DMMB	1,9-dimethylmethylene blue
DMSO	Dimethylsulfoxide
DNA	Deoxyribonucleic acid
DPX	Distrene, plasticiser, xylene
dsDNA	Double-stranded DNA
DTT	Dithiothreitol
dUTPs	Deoxyuridine triphosphate
EAE	Experimental autoimmune encephalomyelitis
ECM	Extracellular Matrix
EDTA	Ethylene-(2,2)-diamine-tetracetic acid
EIA	Enzyme immunoassay
ELISA	Enzyme-linked immunosorbent assay
ELR	Enzyme-linked receptor
eNOS	Endothelial nitric oxide synthase
ERK1/2	Extracellular signal-regulated kinase ½
ESAM-1	Endothelial cell selective adhesion molecule-1
ESL-1	E-selectin ligand-1
FasL	Fas ligand
FBS	Foetal bovine serum
Fc	Fragment crystallisable
FCS	Foetal calf serum
FFPE	Formalin-fixed paraffin embedded
FGF	Fibroblast growth factor
FITC	Fluorescein isothiocyanate
FL1	Fluorescence channel 1
fMLP	Formyl-methionine-leucine-phenylalanine
FPR1	Formyl Peptide Receptor 1
Fpr2/3	Formyl Peptide Receptor 2/3 (murine)
FPR2/ALX	Formyl Peptide Receptor 2/Lipoxin A4 receptor
FSC	Forward scatter
G-CSF	Granulocyte colony stimulating factor
GAPDH	Glyceraldehyde phosphate dehydrogenase
GFP	Green fluorescent protein
GM-CSF	Granulocyte-macrophage colony stimulating factor
GP	Glycoprotein
GPCR	G-protein coupled receptor
GROα	Growth regulated oncogene-alpha; CXCL1
GTP	Guanosine triphosphate
H&E	Haematoxylin and eosin
H_2O	Water

H_2SO_4	Sulphuric acid
HCl	Hydrochloric acid
HEK293	Human embryonic kidney 293 cells
HEPES	2-[4-(2-hydroxyethyl)piperazin-1-yl]ethanesulfonic acid
HIV	Human immunodeficiency virus
HLA	Human leukocyte antigen
HMDMs	Human monocyte derived macrophages
HMGB1	High-mobility group protein B1
HRP	Horse radish peroxidase
Hsp27	Heat shock protein 27
Hsp72	Heat shock protein 72
i.a.	Intra-articular
i.p.	Intraperitoneal
ICAM	Intercellular cell adhesion molecule
Ig	Immunoglobulin
IGF-1	Insulin growth factor
IKBK	Nuclear factor kappa-B inhibitor kinase beta
IL-10	Interleukin-10
IL-12	Interleukin-12
IL-1β	Interleukin 1β
IL-6	Interleukin-6
IL-8	Interleukin-8
il1b	IL-1β gene
IMP	IL-8 stimulated neutrophil microparticle
IQR	Interquartile range
Iso	Isotype
IS^X	ImageStream^X
ITS	Insulin transferrin selenium supplement
JAG1	Jagged 1
JAM	Junctional adhesion molecule
JAM3	Junctional adhesion molecule 3
JNK	c-Jun N-terminal kinase
KO	Knockout
LAMP2	Lysosomal associated membrane protein-2
LAP	Latency Associated Protein
LED	Light-emitting diode
LFA-1	Lymphocyte function-associated antigen-1
LP	Long pass
LPS	Lipopolysaccharide
LRP-1	Low-density lipoprotein receptor protein-1
mA	Milliamps
MAC	Membrane attack complex
MAC-1	Macrophage antigen-1
MAPK	Mitogen activated protein kinase
MAPKAPK2	Mitogen activated protein kinase-activated protein kinase 2
MCP-1	Monocyte chemotactic protein-1
MerTK	Mer receptor tyrosine kinase
MFI	Mean fluorescence intensity
MHC	Major histocompatibility complex
MIP	Macrophage inflammatory protein
MK2	MAPKAPK2
MLCK	Myosin light chain kinase
mm	Millimetre
MMP	Matrix Metalloproteinase

MMP1	Matrix metalloproteinase 1; collagenase
MMP13	Matrix metalloproteinase 13
MMP14	Membrane type I matrix metalloproteinase 14
MMP3	Matrix metalloproteinase 3
MMP9	Matrix metalloproteinase-9; neutrophil gelatinase
mPGES-1	Microsomal prostaglandin E_2 synthase-1
mRNA	Messaging Ribonucleic acid
MRP14	Myeloid-Related Protein 14
MRP8	Myeloid-Related Protein 8
MVB	Multivesicular body
NACHT	NAIP (NLR family, apoptosis inhibitory protein/baculoviral IAP repeat-containing protein 1), CIITA (class II major histocompatibility complex, transactivator), HET-E and TP1 domains
NaCl	Sodium chloride
NADPH	Nicotinamide adenine dinucleotide phosphate oxidase
NALP3	NACHT-leucine-rich repeat-and pyrin-domain-containing protein
NaOH	Sodium hydroxide
NED	*N*-1-napthylethylenediamine dihydrochloride
NETs	Neutrophil extracellular traps
NF-κB	Nuclear Factor kappa B
NK	Natural killer cell
nm	Nanometre
NO	Nitric oxide
NO_2-	Nitrite
NTA	Nanoparticle Tracking Analysis
OCT	Optimal cutting temperature compound
OD	Optical density
OH	Hydroxy
PAD4	Peptidyl arginine deiminase type 4
PAGE	Polyacrylamide gel electrophoresis
PBMC	Peripheral blood mononuclear cells
PBS	Phosphate buffered saline
PC	Phosphatidylcholine
PCD6IP	Programmed cell death 6 interacting protein
PCR	Polymerase chain reaction
PDGF	Platelet derived growth factor
PE	Phycoerythrin
PE	Phosphatidylethanolamine
PECAM-1	Platelet/endothelial cell adhesion molecule 1
PFA	Paraformaldehyde
PGE_2	Prostaglandin E_2
PI3K	Phoshoinositide-3 kinase
PLA_2	Phospholipase A_2
PMN	Polymorphonuclear cells
PMT	Photomultiplier tube
PRP	Platelet-rich plasma
PS	Phosphatidylserine
PSGL-1	P-selectin glycoprotein ligand-1
PTPN22	Protein tyrosine phosphatase, non-receptor type 22 (lymphoid)
RA	Rheumatoid Arthritis
RAGE	Receptor for Advanced Glycation End Products
RALS	Right-angled light-scatter
RANTES	Regulated on activation, normal T cell expressed and secreted

RBC	Red blood cell
RNA	Ribonucleic acid
ROCK	Rho-associated kinase-1
ROI	Region of interest
ROS	Reactive oxygen species
RPL32	Ribosomal protein L32
RPMI	Roswell Park Memorial Institute 1640 medium
RT-PCR	Real-time Polymerase chain reaction
RvD1	Resolvin D1
S100A8	s100 calcium binding protein A8
S100A9	s100 calcium binding protein A9
SAA	Serum Amyloid A
SDF-1	Stromal-derived factor-1
SDS	Sodium dodecylsulphate
SEM	Standard error of the mean
sGAG	Sulphated glycosaminoglycans
SGPP2	Sphingosine-1-phosphate phosphatase type 2
SLE	Systemic lupus erythematosus
SOCS3	Suppressor of cytokine secretion
SOX9	Sex determining region y-box 9
SP	Sphingomyelin
SP1	Specificity protein 1
$sPLA_2$	Secretory phospholipase A_2
spp.	Species
SPP2	Sphingosine-1-phosphate phosphatase type 2
SRY	Sex-determining region Y
SSC	Side scatter
STAT4	Signal transducer and activator of transcription 4
TBS	Tris-buffered saline
TBST	Tris-buffered saline containing 0.1% Tween 20
TdT	Deoxynucleotidyltransferase
TEMED	Tetramethylethlenediamine
TGF-β	Transforming Growth Factor β
TGF-β1	Transforming Growth Factor β isoform 1
TIM4	T-cell immunoglobulin mucin receptor 4
TLR4	Toll-like receptor 4
TMEM16F	Transmembrane protein 16F; Anoctamin 6
TMP	TNF-α stimulated neutrophil microparticle
TNF-α	Tumour Necrosis Factor α
TUNEL	Terminal deoxynucleotidyl transferase deoxyuridine triphosphate nick end labelling
UTR	Untranslated region
v/v	Volume to volume
VEGF	Vascular endothelial growth factor
w/v	Weight to volume
WGA	Wheat Germ Agglutinin
WRW_4	WRWWWW-NH2
WT	Wild-type
ZIA	Zymosan-induced arthritis

CHAPTER 1: INTRODUCTION

1.1 Inflammation

1.1.1 Overview

Inflammation is a dynamic tissue response mechanism, which has developed throughout evolution to defend the host against invasion by pathogens. All animals have innate mechanisms for dealing with pathogen invasion and injury, and even simple organisms such as protozoans are able to phagocytose infective agents (Withers, 1992). Interestingly, bacterial defence against bacteriophages and plasmids by clustered, regularly interspaced short palindromic repeats (CRISPRs) has recently been discovered. These sequences represent an adaptive, but also heritable record of past infections and encode small RNAs that target invasive nucleic acids, providing evidence that all kingdoms of life develop protection from other invading organisms (Mojica et al., 2000). Higher organisms, especially those with developed vasculature are not only able to sense and react to pathogen presence, but also to detect host tissue injury and initiate repair programmes.

Inflammation occurs primarily due to tissue infection or injury. Mammals and other vertebrates detect microbial presence directly by detecting conserved molecules produced by classes of microbes using receptors on innate immune cells: toll-like receptors and nucleotide-binding oligomerisation-domain protein-like receptors. The presence of microbes can also be detected indirectly. Pore forming toxins from gram-positive bacteria self-assemble in the plasma membrane of the host cells causing an influx of intracellular K^+ ions. This activates the NALP3 (NACHT-, leucine-rich repeat- and pyrin-domain-containing protein) inflammasome inducing the release of IL-1β, which elicits immune-cell recruiting responses. The host can also detect the non-specific and indirect presence of microbes or injury by sensing products of cellular death. The desequestration of cellular components that are normally restricted to intracellular compartments, such as adenosine triphosphate (ATP), high-mobility group protein B1 (HMGB1) and S100 proteins A8 and A9, acts as an early warning of infectious invasion. Initial sensing responses are usually mediated by tissue resident macrophages and mast cells. Once an insult is sensed, inflammatory mediators are released to amplify the immune response, such as cytokines, chemokines, leukotrienes and eicosanoids, vasoactive amines and products of the complement cascade. The net result of the release of these mediators is an increase in vascular permeability leading to the delivery of plasma products, and the selective extravasation of neutrophils to the site of injury (Medzhitov, 2008).

1.1.2 Neutrophil Recruitment

Neutrophils are the body's main line of defence against invading pathogens such as bacteria, and make up 40-60% of all white blood cells in humans (Wright et al., 2010, Majno, 1996). These cells are critical to the defence of the host, and as such, two-thirds of the activity of the bone marrow is dedicated to granulopoiesis (Borregaard, 2010). Neutropenia can be catastrophic for the host, often leading to death from infections normally dealt with asymptomatically. Granulocytes are endowed with a non-redundant anti-microbial armoury: they release reactive oxygen species, proteolytic enzymes and an array of bactericidal proteins (Witko-Sarsat et al., 2000) in a time and space-dependent manner.

1.1.2.1 Neutrophil Capture

The recruitment of leukocytes is a multistep process governed by chemokines, selectins and integrins on both the leukocyte and endothelial cells. These elements engage in a sequential, step-wise manner to activate intracellular signals and initiate adhesive bond formation to capture cells from the circulation to the site of injury (Dixit and Simon, 2012). Firstly, capture of the neutrophils from the circulation by the endothelium takes place by the exposure of E- and P-selectin on the apical surface of the endothelial membrane. Under resting conditions, P-selectin is stored in Weibl-Palade bodies within the endothelium, but upon stimulation with histamine, cysteinyl-leukotrienes and cytokines, these bodies fuse with the plasma membrane and P-selectin, along with von Willebrand factor, is exposed. E selectin is synthesised *de novo* by the endothelium when stimulated. These selectins capture ligands on the neutrophil surface such as P-selectin glycoprotein ligand-1 (PSGL-1) or E-selectin ligand-1 (ESL-1) and CD44 (Phillipson and Kubes, 2011) via sialyl Lewis x motifs. These selectins have overlapping functions and ensure the maximal recruitment of neutrophils (Kolaczkowska and Kubes, 2013).

1.1.2.2 Neutrophil Rolling

Neutrophil rolling is achieved by catch-bond formation of these selectins and their ligands, and is crucial for slowing the leukocytes in order for their arrest. Rolling on selectins allows neutrophils to encounter immobilised intravascular chemokine gradients. Chemokines are small positively charged molecules which bind heparan sulphate on the apical side of the endothelium (Phillipson and Kubes, 2011), thus allowing the generation of a stable gradient unaffected by the flow of blood (Kolaczkowska and Kubes, 2013). Chemokines are sensed by G-protein coupled receptors (GPCRs) on the neutrophil surface and along with E selectin, induce integrin-dependent arrest (Dixit and Simon, 2012) by inside-out signalling.

1.1.2.3 Neutrophil Arrest and Crawling

Inside-out signalling is the conformational changes of integrins (that arises after GPCR ligation) from low-affinity and bent as on circulating neutrophils, to intermediate affinity and extended and finally to high-affinity extended and open. β_2 integrins are responsible for discrete end-points within the recruitment cascade. For example, lymphocyte function-associated antigen-1 (LFA-1; $\alpha_L\beta_2$-integrin or CD11a/CD18) allows firm adhesion of the neutrophil to the endothelium whereas macrophage antigen-1 (MAC-1; $\alpha_M\beta_2$-integrin, CD11b/CD18) is required for intravascular crawling once arrested (Phillipson and Kubes, 2011).

In order to achieve arrest, chemokine receptors, such as CXCR2 on neutrophils interact with endothelial ligand CXCL1 causing further activation of inside-out signalling to induce the extension and opening to the high affinity conformation (Pick et al., 2013). Once extended and open, integrins bind ICAM-1 and -2 on the endothelium (Wright et al., 2010), after which the lamellipodium forms at the leading neutrophil edge to allow the cell to crawl to an optimal location to transmigrate. Crawling is achieved by the rapid polymerisation and depolymerisation of the actin cytoskeleton allowing the cell to move in a directed manner (Wang et al., 2006).

1.1.2.4 Neutrophil Transmigration

For neutrophils to reach sites of inflammation, they must first cross the endothelium in a process termed transendothelial migration or diapedesis. Neutrophils transmigrate preferentially between endothelial cells (known as paracellular transmigration), which is a dynamic process in which the endothelial cells play an active role by forming docking structures to allow the neutrophils to pass through (Voisin and Nourshargh, 2013). The best-characterised molecule involved in the transmigration process is PECAM-1, which can bind integrin $\alpha v\beta_3$, but other molecules are highly involved, e.g. ESAM-1, ICAM-2 and junctional adhesion molecules (JAMs) (Wang et al., 2006). Endothelial JAMs, which bind homotypically to molecules on the opposing endothelial cell surface under resting conditions, are able to bind neutrophil-expressed adhesion molecules to allow the cell to pass through (Muller, 2003). Occasionally, and under conditions of high ICAM-1, neutrophils may transmigrate through an endothelial cell, known as transcellular transmigration. Here, the endothelial cell extends its membrane up and around the neutrophil to allow the cell to pass through in a directed manner (Kolaczkowska and Kubes, 2013).

1.1.2.5 Neutrophil Migration Across the Basement Membrane

The basement membrane is a dense network of extracellular matrix proteins, generated by both the endothelial cells, pericytes and smooth muscle cells, which must be crossed by neutrophils to reach the inflammatory site. It has become clear that neutrophils pass through the sub-endothelial basement membranes by seeking out areas of low collagen IV and laminin extracellular matrix protein by crawling in an amoeboid manner, which is followed by migration through the interstitial tissue to the site of inflammation (Wang et al., 2006, Pick et al., 2013).

1.1.2.6 Neutrophil Antibacterial Activity

At the site of insult or injury, the neutrophils release CXCL8 (IL-8), CXCL1 and leukotriene B_4 to recruit further neutrophils, and the cells degranulate, releasing their proteolytic cargo from pre-formed intracellular stores. The contents of the granules include antimicrobial proteins such as lactoferrin, cathepsins and defensins, and degradative enzymes such as elastase and matrix metalloproteinase (MMP)-9. Neutrophils generate reactive oxygen species to damage invading bacteria. For hydrogen peroxide generation, nicotinamide adenine dinucleotide phosphate oxidase (NADPH) is required, a complex multicomponent enzyme, which assembles at the cell membrane during priming. Hypochlorous acid can also be generated by neutrophils by the action of myeloperoxidase. Neutrophils phagocytose bacterial pathogens and kill them via the fusion of the endosome with lysosomes, which exposes them to lysozyme (Kolaczkowska and Kubes, 2013). It has been shown that activated tissue neutrophils have more phagocytic capacity than circulating neutrophils (Borregaard, 2010). Under extreme circumstances, it has been found that neutrophils extrude their DNA forming NETs (neutrophil extracellular traps), in which bacteria become trapped, allowing for easier phagocytosis. Bacteria also become exposed to anti-microbial histones within the NETs, as well as other small antimicrobial proteins, further facilitating bacterial killing and clearance (Kolaczkowska and Kubes, 2013). Recently, a new mode of antibacterial activity has been shown for neutrophils. Neutrophils release microparticles from their plasma membrane that have been shown to have antibacterial functions. These microparticles exhibit bacteriostatic activity by aggregating bacteria, and are as potent as their parent cells at inhibiting microbial infection (Timar et al., 2013).

1.1.2.7 Inflammation Outcomes

The outcome of the inflammatory reaction is dictated by the way in which the process starts. For example, the activation of neutrophils by prostaglandins during the normal pro-inflammatory stage is known to “reprogram” the cells to produce anti-inflammatory

lipoxins upon further stimulation, initiating the end phase of inflammation (Levy et al., 2001). The successful elimination of bacteria or cause of injury results in the initiation of resolution and tissue repair programmes, but when the acute inflammatory response fails, inflammation persists and acquires new characteristics. Neutrophils that have migrated into the tissue are replaced by inflammatory macrophages and in the case of infection, with T cells. If this further response is insufficient, chronic inflammation ensues, characterised by the formation of granulomas and tertiary lymphoid organs. Chronic inflammation can also arise due to the generation of autoantibodies, which propagate inflammation by binding self-antigens in perpetuity.

1.1.3 The Resolution of Inflammation

In order to prevent the progression from acute to persistent inflammation, the inflammatory reaction must be actively resolved, inhibiting further tissue damage. Historically, it was believed that the resolution of inflammation was a passive process involving the dilution of chemokine gradients over time, thus circulating leukocytes would no longer sense gradients and be recruited to the site of injury. However, extensive work over the past few decades have revealed that the resolution of inflammation is a carefully managed active process, and deficiencies in any of its components leads to over-active, uncontrolled chronic inflammation. One example of this is chronic airway inflammation seen in patients with cystic fibrosis, allergic airway disease and asthma, who have been shown to produce reduced levels of anti-inflammatory lipoxin A_4 (Levy, 2005).

The resolution of inflammation represents a return to tissue homeostasis, defined as the clearance of tissue migrated neutrophils, and a reduction in the number of monocytes and macrophages accompanied by a return of these cells to the pre-inflamed phenotype. The resolution process occurs in four stages: firstly, leukocytes that have fulfilled their pro-inflammatory function undergo apoptosis, which is followed by the clearance of these cells by macrophages (Reville et al., 2006), which then reprogram to switch their mediator production from pro- to anti-inflammatory, and finally, these phagocytes leave the tissue via the lymphatics to fulfil the requirements of a return to homeostasis (Serhan and Savill, 2005).

The resolution of inflammation is governed in part by tissue macrophages. These cells perform a variety of functions that down-regulate inflammatory signals and clear cytokines. Macrophages release proteases at the site of inflammation to cleave chemokines at their ELR motifs, which are required for chemokine-receptor binding.

This renders the chemokines inactive, and clears chemokine gradients preventing neutrophil recruitment. Macrophages also control the lifespan of neutrophils by releasing death receptor ligands such as Fas ligand and tumour necrosis factor (TNF) - α. When released in low concentrations, FasL prolongs the lifespan of neutrophils, but at higher concentrations, it induces their apoptosis. Apoptotic neutrophils release bioactive resolving proteins, such as Annexin A1, which translocates to the plasma membrane, binds the formyl-peptide receptor 2/ALX (FPR2/ALX) and suppresses further neutrophil recruitment whilst inducing apoptosis in neighbouring cells (Ortega-Gomez et al., 2013).

Apoptotic neutrophils release “find me” signals, such as lysophosphatidylserine, which promotes the migration of macrophages towards them. The membrane of apoptotic neutrophils undergoes rearrangement so that phosphatidylserine is expressed on the outer envelope. Phosphatidylserine acts as an “eat me” signal and induces clearance of apoptotic neutrophils by macrophages by engaging the TIM4 receptor (Ortega-Gomez et al., 2013). Annexin A1 can also act as a bridging molecule to enhance the binding of apoptotic cells to phagocytes (Serhan and Savill, 2005), and N-terminal derived peptides of Annexin A1 can also act as “eat me” signals (Ortega-Gomez et al., 2013).

Engulfment of apoptotic neutrophils induces a phenotypic switch in macrophages from a pro-inflammatory M1 to an anti-inflammatory M2 phenotype. Anti-inflammatory macrophages alter their metabolism of lipids from proinflammatory prostaglandins and leukotrienes to pro-resolving bioactive lipids such as lipoxins and resolvins, protectins and maresins (Ortega-Gomez et al., 2013). Lipoxins are able to suppress neutrophil chemotaxis, reduce vascular dilatation and permeability and promote the efferocytosis of apoptotic neutrophils by macrophages and promote their egress from the tissue via the lymphatics (Nathan and Ding, 2010). These anti-inflammatory lipid mediators suppress neutrophil and enhance monocyte recruitment, which aids in the further clearance of apoptotic cells (Ortega-Gomez et al., 2013). M2 macrophages also secrete anti-inflammatory cytokines such as IL-10, which inhibits proinflammatory cytokine production (such as TNF-α and IL-1β) by recruiting suppressor of cytokine secretion 3 (SOCS3); and transforming growth factor β (TGF-β), which has a broad range of anti-inflammatory functions. TGF-β can induce neutrophil apoptosis, inhibit T cell proliferation and induce monocyte differentiation to macrophages (Rossol et al., 2011) and is a potent suppressor of proinflammatory (classical) monocyte activation (Nathan and Ding, 2010).

After phagocytosing apoptotic neutrophils, macrophages down-regulate their CD11b and become unresponsive to TLR4 signals, which hints at a “satiated” phenotype. These cells egress via the lymphatics (Schif-Zuck et al., 2011), returning the tissue to the pre-inflammatory state.

1.2 Rheumatoid Arthritis

1.2.1 Introduction

Rheumatoid arthritis is a chronic systemic inflammatory disease of unknown aetiology that affects approximately one per cent of the population, causing symmetrical irreversible damage of the diarthrodial joints. Disease onset typically occurs between forty and fifty years of age and patients present with stiffness, swelling and joint pain often accompanied by weight loss, fever and fatigue. The disease is associated with a reduction in life expectancy by around 10 years.

1.2.2 Rheumatoid Arthritis Aetiology

Rheumatoid arthritis is unique among inflammatory diseases in that no aetiological agent has been identified, despite extensive efforts to determine joint-specific self-antigens. However, rheumatoid arthritis is a systemic disease that manifests most visibly in joint destruction, implying that there may be systemic defects in the immune system, in combination with a pathological process occurring in the synovial joint, which results in persistent chronic inflammation. In terms of susceptibility, the majority of patients are female, and outnumber male patients 3:1 (Patel, 2010). Rheumatoid arthritis is a complex and multifactorial disease with a mild to moderate genetic association. Genetic and environmental factors, including lifestyle choices such as smoking, may have an impact on individual susceptibility. Genetic linkage studies have shown a strong association between destructive forms of rheumatoid arthritis and certain major histocompatibility complex (MHC) class II alleles (human leukocyte antigen (HLA) DR4). The association is with a sequence motif of amino acids 70-74 in the 3rd hyper variable region of the β1 domain of the HLA-DR4 molecule (Mallone and Nepom, 2004) and is mainly associated with the expression of the “shared epitope”. This region encodes genes for MHC class II molecules, which bind and present antigen to the T cell receptors of CD4^{+} T cell (Trouw et al., 2013). Other susceptibility genes include PTPN22 and STAT4 (Imboden, 2009), genes that are highly involved in T cell survival, T cell effector responses (Rieck et al., 2007) and immune regulation (Remmers et al., 2007).

1.2.3 Rheumatoid Arthritis Pathogenesis

The disease process is characterized by an adaptive immune response mediated by B cells and T cells, which results in a cascade of inflammatory events leading to the recruitment of neutrophils, macrophages and further lymphocytes (Distler et al., 2005b). The progressing disease culminates in tissue and joint damage as the leukocytes and reactive synovium invade the cartilage and bone and produce cytokines and degradative enzymes. The synovial tissue transforms into an aggressive hyperplastic tumour-like organ which projects into the joint space, coming into direct contact with the cartilage to degrade matrix components and bone, causing extensive disability (D'Aura Swanson et al., 2009).

1.2.3.1 Autoantibodies

The formation of autoantibodies characterises autoimmune diseases such as rheumatoid arthritis. Physiological mechanisms exist (such as deletion, receptor editing and induction of anergy of potentially autoreactive lymphocytes) to prevent the adaptive immune system from reacting to autoantigens whilst still allowing a response to foreign antigens. Autoreactive cells sometimes survive, which are required to be supressed by regulatory cells, but if these processes fail, self-tolerance can be broken, allowing self-reactive lymphocytes to mature. The autoantigen becomes the target of the immune response, leading to chronic autoimmune disease, as the autoantigen can never be successfully cleared from the body.

1.2.3.2 Complement Cascade

The complement cascade is an enzymatic network critical for the innate immune system to dispatch invading pathogens by the production of self-assembling lytic factors, which form pores in the membrane of bacteria. The cascade can be activated in three ways: via the classical, lectin or alternative pathways, of which the classical pathway is the most relevant to rheumatoid arthritis. Here, complement is activated by the presence of the IgM and IgG immune complexes, and transactivates downstream proteins to convertases, ultimately culminating in the generation of membrane attack complex (MAC) and the lysis of cells. Prior to the generation of MAC, several of the convertases have immune-cell stimulating capabilities. For example, C3 is the most highly abundant complement protein and is activated to C3a, which can directly stimulate mast cell degranulation. A second complement product, C5a, has important implications for rheumatoid arthritis as it is able to interact with neutrophil receptors and prime or directly activate these cells to induce intracellular calcium flux, chemotaxis and the generation of oxygen radicals (Ward, 2010). C5a is locally increased in the synovial fluid of rheumatoid arthritis patients, but not in their plasma (Jose et al., 1990).

1.2.3.3 Synovial Fibroblasts in Rheumatoid Arthritis

The normal physiology of the joint includes a single-cell layer of synovium surrounding the joint capsule, and consists of macrophage-like synoviocytes and synovial fibroblasts (Filer et al., 2008). Its function is to produce the synovial fluid that lubricates and nourishes the joint tissues, including the cartilage. In the early phases of inflammatory arthritis, tissue oedema becomes prominent, angiogenesis occurs, and the synovial lining becomes hyperplastic. As the disease progresses, the synovium forms multiple folds and villi, and the subintima becomes chronically infiltrated by T cells, B cells, macrophages and dendritic cells. The synovial fibroblasts act as immune sentinel cells that bridge the innate and adaptive immune systems and the stromal compartment to orchestrate the complex immune response by releasing a broad array of inflammatory mediators.

Subsets of synovial fibroblasts express CD40, which, upon engagement of the CD40 ligand (CD40L) expressed on activated T cells, leads to the production of cytokines and the production of antibodies by CD40-expressing plasma cells. Adaptive immune cells migrate to the joint in response to fibroblast-secreted CXC- and CC-type chemokines, and neutrophils are recruited by interleukin IL-8, CXCL5 and CXCL1 (GROα). Monocytes are also recruited via CCL2 (also known as MCP-1), CCL4 and CCL5. Synovial fibroblasts become invasive and directly damage tissue via the secretion of matrix-metalloproteinases (MMPs) and cathepsins that degrade cartilage matrix and bone (Neumann et al., 2010). This aggressive phenotype, characteristic of the persistently activated rheumatoid synovial fibroblast, is stable and can persist through passaging *in vitro* for several months (Filer, 2010).

Multiple factors contribute to the phenotypic acquisition of fibroblasts, including exposure to growth factors such as fibroblast growth factor (FGF), transforming-growth factor β (TGF-β) and platelet-derived growth factor (PDGF). Direct contact with cartilage matrix via adhesion molecules such as cadherin-11 and integrins and exposure to fragments of degraded matrix such as vitronectin and fibronectin induce MMP synthesis. Contact with matrix which has been denuded by these enzymes further influences invasive behaviour and migration (Neumann et al., 2010).

1.2.3.4 Lymphocytes in Rheumatoid Arthritis

T cells are present in the synovial fluid of rheumatoid arthritis patients, and early arthritis (less than 3 months' duration) is characterised by a transient increase of T-cell modulating cytokines indicating T cell (and stromal cell) activity (Raza et al., 2005).

Dendritic cells and macrophage-derived cytokines activate auto-reactive $CD4^+$ T cells to provide help to B cells to differentiate into arthritogenic autoantibody-producing plasma cells. Activated T cells produce their own cytokines which act upon the cells present in the joint to increase inflammation (Murphy, 2008). In around 10% of cases T cells along with B cells develop into highly organised secondary and tertiary lymphoid structures, often with germinal centres (Weyand and Goronzy, 2003) further highlighting the chronicity of the inflammation in this disorder.

1.2.3.5 Neutrophils in Rheumatoid Arthritis

Although rheumatoid arthritis disease progression resembles non-resolving chronic inflammation, the role of the neutrophils in this disease suggests reinitiation of an acute inflammatory process. Neutrophils are the most numerous cells within the synovial fluid during flares, and the influx of neutrophils into the joint space can exceed 1 billion neutrophils per day, and a half-life estimated at approximately four hours (Nathan and Ding, 2010). These cells have been shown to have a pre-activated or "primed" phenotype suggesting that they have previously been exposed to activating stimuli (Nemeth and Mocsai, 2012) and produce a large variety of cytokines and proteinases which contribute to joint destruction (Cassatella, 1995, Cassatella et al., 1997, Quayle et al., 1994, Quayle et al., 1995, Quayle et al., 1997, Tecchio and Cassatella, 2014, White et al., 1996). In normal physiology, neutrophils undergo apoptosis when redundant and are cleared by macrophage engulfment, preventing inflammation. In rheumatoid arthritis, the synovial fluid contains a both pro- and anti-apoptotic factors, dysregulating the usually constitutive and controlled apoptosis of neutrophils (Cross et al., 2006). Neutrophils contain a variety of degradative enzymes in their armamentarium meant for combatting invading pathogens and these enzymes become aberrantly released during necrosis. One of these enzymes, peptidyl arginine deiminase type 4 (PAD4) converts side chains of L-arginine residues generating citrulline, and citrullinated proteins (Nathan and Ding, 2010). Autoantibodies in rheumatoid arthritis have been shown to react with citrullinated peptides, and further, type II collagen, the major collagenous constituent of cartilage, has been shown to be citrullinated in rheumatoid arthritis patients (Uysal et al., 2009). Thus, dying neutrophils are thought to sustain self-antigen production by releasing PAD4 to citrullinate proteins, which once bound by autoantibodies, recruit neutrophils further to release destructive reactive oxygen species and proteases (Nathan and Ding, 2010).

1.2.3.6 Chondrocytes in Rheumatoid Arthritis

The ultimate end-point of joint erosion is the destruction of the bone and cartilage. Cartilage is composed solely of chondrocytes, which in a resting state turn over the

cartilage matrix very slowly. They do this by producing cartilage extracellular matrix proteins such as type II collagen (with a half-life of 120 years) and aggrecan (with a half-life of 120 days) and the enzymes required for their degradation (including MMPs and a disintegrin and metalloproteinase with thrombospondin motifs (ADAMTSs)).

During the development of the skeleton, chondrogenesis occurs: chondrocytes arise from mesenchymal progenitor cells to synthesize the cartilage anlagen (template) for the developing limbs. Following chondroprogenitor cell differentiation, the chondrocytes undergo proliferation, followed by terminal differentiation, hypertrophy and then apoptosis, where the hypertrophic cartilage is replaced by calcified bone in a process termed endochondral ossification (Goldring, 2012). Transcription factors such as Sox9 (Bi et al., 1999) and Runx2, and various signalling pathways, play stage-specific roles in chondrogenesis. The resulting articular cartilage in adults is composed of four regions from the superficial tangential zone, nearest the synovial space, through to the middle zone, deep zone and finally the calcified zone nearest the subchondral bone. The territorial (or pericellular) matrix adjacent to the cells contains little or no fibrillar collagen but does contain type VI collagen microfibrils. The interterritorial matrix is composed of a fibrillar collagen network, with type II collagen fibrils interwoven with type XI collagen, and type IX collagen integrated into the fibril surface allowing retention of proteoglycans and permitting association with other matrix components (van den Berg, 2008). Compressive resistance is maintained by the retention of water molecules by the expression of aggrecan, a large aggregating proteoglycan. The expression of cartilage specific proteins, and the alignment of the collagen fibrils differs between each of the zones, and allows mechanical pressure to be distributed correctly (Goldring and Marcu, 2009).

Aberrant production of cartilage degrading enzymes occurs in rheumatoid arthritis, due to the influx and stimulation of immune cells, and the activation of synovial fibroblasts; these enzymes tip the equilibrium of cartilage production and remodelling to outright degradation. The principal MMPs responsible for cartilage degradation are the collagenases (MMP-1, MMP-8 and MMP-13), the gelatinases (MMP-2 and MMP-9), stromelysin (MMP-3) and membrane type I MMP (MMP-14). ADAMTS-4 and -5 are regarded as the principle aggrecan-degrading enzymes (Stanton et al., 2011).

Rheumatoid arthritis differs from osteoarthritis in terms of cartilage degradation in that in rheumatoid arthritis chondrocytes display intrinsic chondrolytic activity and contribute to their own cartilage degradation, not only at the cartilage-pannus junction but also

within deeper zones of the cartilage. In osteoarthritis, cartilage degradation usually manifests as a surface lesion with evidence of pericellular cartilage degradation only in late disease progression. Chondrocytes produce, and react to, inflammatory cytokines such as TNF-α (Saklatvala, 1986) and IL-1β, and respond by producing prostaglandins, nitric oxide and proteases. In addition, chondrocytes produce, and express the receptors for chemokines such as CXCL8, which may play a role in cartilage catabolism (Fernandes et al., 2002). IL-1β is known to suppress the expression of a number of genes associated with the differentiated chondrocyte phenotype, such as the type II collagen gene *COL2A1*, by activating transcription factors including nuclear factor-kappa-B (NF-κB), CCAAT enhancer-binding protein (C/EBP), activator protein (AP-1) and E26 transformation specific family members, which regulate inflammation and stress-induced signalling (Fan et al., 2007).

Degraded articular cartilage has limited capacity for repair, and a multitude of techniques are currently being investigated to try to enhance chondrogenesis in patients suffering cartilage trauma or loss due to diseases such as osteo- or rheumatoid arthritis. So far, treatment of large cartilage lesions has involved tissue-engineering strategies to try to enhance chondrogenesis using synthesised cartilage scaffolds, stem cells and autologous chondrocyte reimplantation, but their routine clinical efficacy is lacking. Ultimately, severe cartilage injury or degradation is overcome by total joint replacement, but the development of multidisciplinary approaches to achieve cartilage regeneration would improve quality of life for arthritis patients (Tuan et al., 2013).

1.2.4 Rheumatoid Arthritis Therapy

Although some of the molecular mechanisms behind the disease have been elucidated, especially by the use of mouse models, the underlying cause of the disease remains a mystery (Patel, 2010). Further, the presence of Rheumatoid Factor in some normal individuals, and in other diseases, and the absence of such antibody in some rheumatoid arthritis patients highlights a lack of basic understanding of the processes which lead to clinical disease (Majno, 1996). Further, citrullinated proteins that are putative auto-antigens are not synovium-specific (Vossenaar and van Venrooij, 2004). Nonetheless, new treatments for rheumatoid arthritis have recently represented a revolution in disease management. Modern rheumatoid arthritis therapy centres on the use of non-steroidal anti-inflammatory drugs, glucocorticoids and disease modifying anti rheumatic drugs (DMARDs). Glucocorticoids are effective at reducing joint swelling and stiffness as well as pain, but the risk of considerable side effects such as

osteoporosis is high. The bulk of treatment relies on the use of DMARDs, which slow the progression of joint destruction, reduce swelling associated with synovitis and preserve joint function. Methotrexate, leflunomide and sulfasalazine represent the mainstay of synthetic DMARD options, but with progressing disease, biological drugs are required. Biological treatments are usually humanized antibodies or recombinant human proteins that target the cytokine network present within the rheumatoid joint. The most widely used are the TNF inhibitors, such as etanercept, infliximab, adalimumab, or the IL-1 receptor antagonist anakinra, but other biologicals exist and target the IL-6 receptor (tocilizumab), deplete B-cells by targeting CD20 (rituximab) or inhibit T cell co-stimulation by binding CD80 (abatacept) (Herold, 2012). Despite this revolution in therapy for rheumatoid arthritis, a large proportion of patients (30-40% in terms of anti-TNF therapy) remain refractory to treatment (Hyrich et al., 2006, Patel, 2010), and few markers are available to predict which patients will respond to treatment. An intriguing study by Wright et al. (2012) found that patients that went on to be responders to anti-TNF therapy had elevated synovial fluid levels of T-cell-derived cytokines, such as IL-2, and that Treg function, suppressed by high levels of TNF-α could be restored by TNF blockade. Patients without a T-cell driven inflammatory phenotype did not respond to anti-TNF therapy, as their persistent inflammation is likely dominated by different cellular microenvironments within their synovial joints that could instead make them candidates for anti-IL-6 therapy. Furthermore, this study highlighted the fact that circulating cytokines in RA patients did not necessarily correspond to the levels of cytokines present in the synovial fluid, and that the levels of local cytokine production provided a clearer indication of patient therapy stratification. Still, few rheumatoid arthritis patients achieve lasting remission after cessation of DMARD or biological treatments (Nathan and Ding, 2010). Thus, there is an unmet need of both understanding the fine detail of how the disease develops and progresses, as well as new treatments which can halt the over-active chronic inflammation, and push the disease to fully resolve.

1.3 Microparticles

1.3.1 Introduction

Microvesicles are small plasma membrane coated bodies released from cells in a variety of circumstances. The umbrella term “microvesicle” refers to exosomes, microparticles, and small apoptotic bodies, and distinct rules for their classification have not been devised. Their size and functions often overlap, but there exist certain

markers that may be used to help in determining the population in question. For example, exosomes are thought to be formed right side out, from multivesicular bodies (MVB) within the cell. Exosomes are therefore usually preformed; they bud from the internal MVB membrane within the cell (Figure 1.3.1), and carry tetraspannins, which can be used to identify them. Their protein repertoire is also more restricted (Roos et al., 2010) and their size smaller (between 30-100nm). Microparticles are small, membrane-coated, microstructures between 100nm and 1μm in size and bud from the plasma membrane of the parent cell (Deregibus et al., 2007). They are released from many, if not all, eukaryotic cell types and have a diverse range of functions. Their increased levels have been associated with many disease states (Distler et al., 2005b, Distler et al., 2005a) including atherosclerosis and coronary disorders (Inal et al., 2012, New et al., 2013, Kapustin et al., 2011), type II diabetes mellitus (Omoto et al., 2002), inflammation and rheumatoid disease (Distler et al., 2005b) as well as cancer (Lima et al., 2009) when released from platelets, endothelial cells, lymphocytes, monocytes and other cell types.

Microparticles were first discovered indirectly, by Chargaff and West (1946), who noted that ultracentrifuged plasma displayed delayed clotting times, and that re-adding the isolated pellet to plasma rescued coagulation. But it was not until 20 years later that it was found that the ultracentrifuged pellet contained spherical vesicle-like structures with a plasma membrane coating (Wolf, 1967), but these were regarded incorrectly as inert cellular debris. Preliminary studies in thrombosis provided strong evidence of the potency of microparticles to promote coagulation due to the phosphatidylserine expression on the outer microparticle membrane, which provides a negatively charged surface for coagulation factor binding. Microparticles have also been shown to display tissue factor under certain circumstances (Boilard et al., 2010, Beyer, 2010). The exposure of phosphatidylserine on the microparticles is one of the features that can be used to discriminate them from other membrane vesicles, such as exosomes (Ratajczak et al., 2006). Microparticles, although released during early apoptosis, differ from apoptotic bodies that occur during the final stages of cell death. Apoptotic bodies are usually much larger than microparticles (around 4μm) and contain histones and nuclear material.

1.3.2 Microparticle Formation

Microparticles are formed by vesiculation (Figure 1.3.2). Firstly, cytoskeletal rearrangement occurs consequent to a sustained influx of calcium (Hugel et al., 2005). The activation of calcium-dependent proteases calpain and gelsolin (Inal et al., 2012) cleave talin and α-actinin, freeing the plasma membrane from the cytoskeleton

(Miyoshi et al., 1996). The cytoskeleton itself is also transformed by these enzymes as they cleave the actin filaments facilitating microparticle shedding (Inal et al., 2012). The cytoskeleton is further modified by the phosphorylation of myosin light-chain kinase which enhances the contractility of myosin "resulting in the production of sliding forces" and the activation of Rho-associated kinase-1, which decouples actin-myosin filaments from the plasma membrane (Distler et al., 2006).

Second, the directional segregation of the phospholipid bilayer is disrupted due to the activation of membrane-direction governing proteins (Morel et al., 2011), such as floppase and scramblase by calcium, and the inactivation of flippase (Hugel et al., 2005). This causes the normal physiological state of the plasma membrane to be unsegregated: phosphatidylserine and phosphatidylethanolamine, anionic aminophospholipids (Inal et al., 2012), normally reside on the inner membrane leaflet, whereas phosphatidylcholine and sphingomyelin (the choline-phospholipids) reside on the external membrane leaflet (Morel et al., 2011). Transposing of the membrane to expose phosphatidylserine precedes the formation of microparticles and in THP-1 monocytes this event occurs 2-10 seconds after stimulation of the $P2X_7$ receptor with an ATP mimetic. Vesicle blebbing occurred 40-150 seconds after stimulation (MacKenzie et al., 2001).

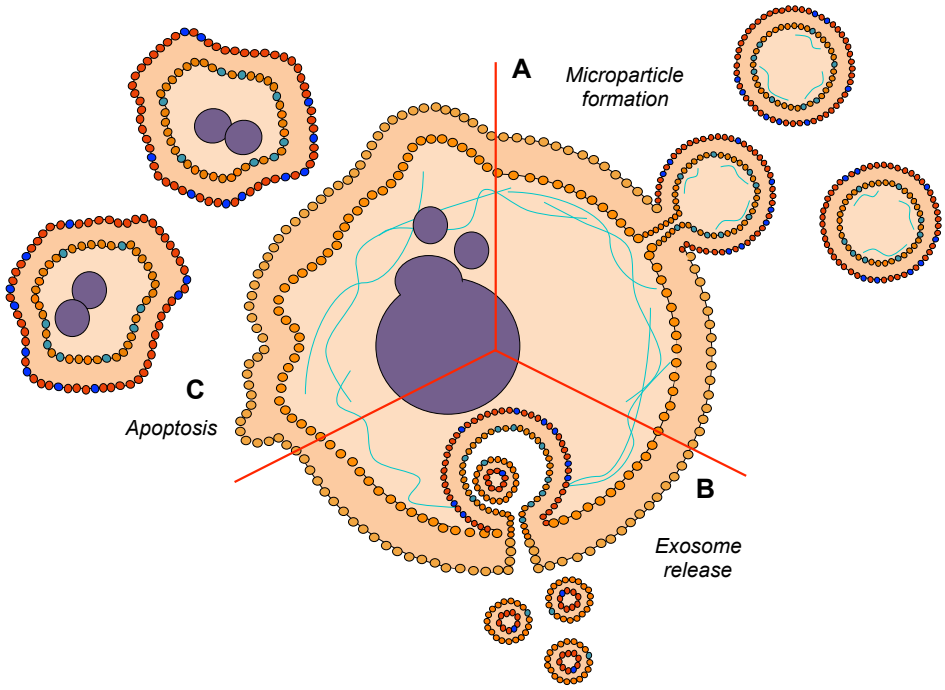

Figure 1.3.1 Types of extracellular vesicles and their formation. Several types of extracellular vesicles exist, and are formed by different mechanisms. (A) Microparticles are formed *de novo* via budding from the surface of activated cells, and express phosphatidylserine on their outer surface. (B) Exosomes are formed within multivesicular bodies and are released from the cell when this structure fuses with the plasma membrane, expelling the exosomes. (C) Apoptotic bodies are released from cells undergoing programmed cell death and contain nuclear material such as histones.

Finally, the plasma membrane of the cell and microparticle must undergo resealing prior to microparticle shedding to ensure retention of membrane integrity (MacKenzie et al., 2001). Investigations into how nucleated cells protect themselves from attack by pore-forming toxins have led to an increased understanding of the events surrounding this process. Injury of the plasma membrane by pore-forming toxin streptolysin O leads to an influx of extracellular calcium. This rise in calcium ions is sensed by intracellular Annexin A6, which induces recruitment of this protein to the damaged plasma membrane. Annexin A6 facilitates the formation of lesion-containing microparticles by binding the membrane and resealing the lesion outside of the cell, which is then shed. If the cell has to deal with larger, or multiple, injuries, a global rise in calcium induces homogeneous binding of Annexin A6 to the entire plasma membrane, regardless of proximity to injury. In this case, Annexin A6 can no longer repair the lesion, and Annexin A1, a less sensitive calcium-binding annexin, translocates to the injured area of the plasma membrane, which retains a higher calcium concentration, especially in an area of cellular protrusion. Here, Annexin A1 can efficiently seal off the lesion resulting in the release of microparticles containing both Annexin A1 and A6 as well as the lesion (Potez et al., 2011). Although these studies were carried out in transfected HEK293 cells injured with streptolysin O, the findings could be extrapolated to the release of microparticles due to stimulation of cells.

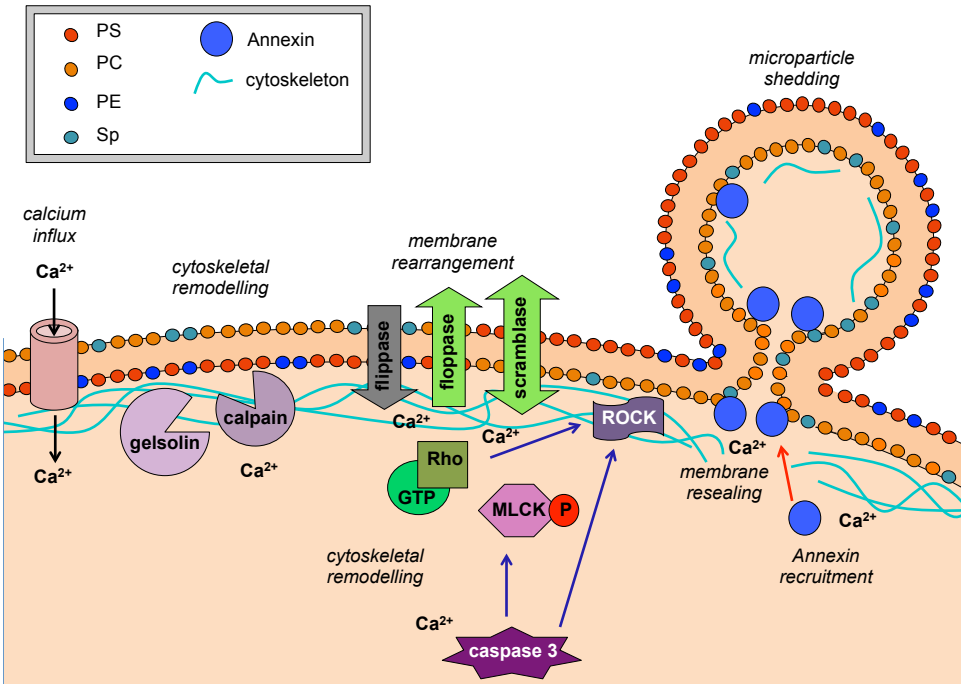

Figure 1.3.2 Microparticles are shed through an orchestrated process of cytoskeletal remodelling, membrane rearrangement and resealing. PS, phosphatidylserine; PE, phosphatidylethanolamine; PC, phosphotidylchloline; Sp, sphingomyelin; ROCK, Rho-associated kinase-1; MLCK, myosin light-chain kinase; GTP, guanosine triphosphate; P, phosphorylation.

The binding of ligand to GPCRs induces receptor-operated calcium entry, a moderate influx of calcium from stores in the endoplasmic reticulum. This process is followed by a global rise in calcium by store operated calcium entry, where calcium-sensing molecules translocate to membrane-associated calcium ion channels to induce an influx of calcium from the extracellular milieu (Hillson and Hallett, 2007). These rises in calcium are sufficient to achieve the activation of calcium-dependent enzymes that cleave cytoskeletal-anchoring proteins (Dixit and Simon, 2012) and could conceivably induce translocation of annexins to the plasma membrane to operate in microparticle-associated membrane sealing. The transverse migration of phosphatidylserine to the outer membrane leaflet, coupled with the disassociation of the plasma membrane from the cytoskeleton, and sealing of the membranes equal the shedding of microparticles (Inal et al., 2012).

1.3.3 Microparticle Function

The ubiquity of microparticles suggests a role in cell regulation, in addition to providing a surface upon which the coagulation cascade takes place (Inal et al., 2012). Microparticles possess characteristic signatures of the cells from which they originate (Beyer, 2010); in addition, the activation status of the parent cells influences the composition and function of the offspring microparticles (Mause, 2010, Timar et al., 2013). For example, although both cell activation and early apoptosis give rise to microparticle production, their resultant microparticles differ both phenotypically and quantitatively: microvascular endothelial cell-derived microparticles preferentially express CD51 and ICAM-1 (CD54) when produced by activation, whereas PECAM-1 and E-selectin were more highly expressed when produced via apoptosis (Jimenez et al., 2003). This is also true in terms of their differential functions. Timar et al. (2013) have shown that microparticles generated by neutrophils stimulated with opsonised *Staphylococcus aureus* particles inhibited the growth of *S. aureus* bacteria by forming microparticle-bacterial aggregates, but microparticles generated by stimulating neutrophils with other pro-inflammatory agents (e.g. fMLP) did not display antibacterial activity. Microparticles are enriched in certain phospholipids and bioactive lipids depending on stimulus applied to the parent cell (Distler et al., 2005a). The cytoplasmic component contained by the microparticle may also have pre-selected contents. MacKenzie et al. (2001) found that THP-1 monocytes formed microparticles when stimulated with various agents, but that the resulting microparticles contained IL-1β only when stimulated with a $P2X_7$ receptor antagonist. Shedden et al. (2003) found that solid tumour cells that were chemotherapy-resistant expressed more genes associated

with vesicle shedding and the vesicles shed from these cells contained higher concentrations of doxorubicin compared to the cells from which they were generated. Similar results have been found in cisplatin resistant cells, where microparticles from resistant cells contained 2.6-fold more than those released from sensitive cells leading to increased expulsion (Safaei et al., 2005). These cells also expressed more genes associated with microvesicle shedding suggesting that preferential loading of microparticles, as expropriated here by chemotherapy-resistant cancer cells, has specific genetic machinery.

Microparticles contain a wide variety of intracellular proteins, RNA and lipids and these components may undergo extensive remodelling to enable adaptive or specialised functions (Muralidharan-Chari et al., 2010). Electron and confocal microscopic analysis of microparticle formation has shown selective arrangement processes occurring in cells stimulated with C5b-9 complexes (Moskovich and Fishelson, 2007) so that the subsequent phenotype of the shed vesicles is not random. Raft domains and the lateral organisation of the plasma membrane segregate particular proteins and lipid species and confer this inclusive or exclusive sorting (Hugel et al., 2005). Lipid rafts are membrane micro domains enriched in certain proteins and cholesterols. It has been shown that microparticles may be shed from lipid raft regions: Jy et al. (2002) showed that prior to microparticle release, PECAM-1 clustered on the cell surface in lipid rafts and the subsequent microparticles generated by these cells were enriched in PECAM-1. Further, disruption of lipid-rich domains using either nystatin or methyl-β-cyclodextrin impairs the ability of endothelial cells to produce microparticles (Burger et al., 2011). Proteins known to co-localise with lipid rafts have also been found in microparticles, in particular CD39, flotillin-2, eNOS and caveolin-1 (Banz et al., 2008, Burger et al., 2011).

Microparticles are able to signal as discrete elements by possessing a large array of bioactive substances, adhesion molecules and membrane-anchored receptors on their surface. They contain cytokines, enzymes, signalling proteins and functioning mRNA and miRNA (Andaloussi et al., 2013), where the incorporation of the microparticle into the target cell is required before the content of the microparticle may exert its effects (Mause, 2010). The transfer of RNA by exosomes or extracellular vesicles has been characterised more extensively. Extracellular vesicles have been shown to deliver mRNA that can be translated into protein by the recipient cell – human mast cell-derived exosomes delivered mRNA to mouse mast cells, which translated the human protein (Valadi et al., 2007). Artificially, reporter mRNA carried by extracellular vesicles

derived from glioma cells could be transferred and expressed in recipient cells (Skog et al., 2008). Further, extracellular vesicles from a variety of cell types have been shown to contain machinery associated with RNA processing and transport (Andaloussi et al., 2013). Interestingly, Bolukbasi et al. (2012) may have identified a potential "post-code" located in the 3' untranslated region of mRNAs that lead to their incorporation into extracellular vesicles, showing that even the enrichment of mRNA into microvesicles is pre-selected by the cell. Although these are examples of exosomal RNA transportation, given the lack of consensus on definitions and with a lack of a gold standard in isolation techniques, these mechanisms could conceivably be part of the microparticle functional repertoire.

Microparticles not only act in the neighbourhood of their parent cells, but also at target sites much further away. For example, cancers release microparticles rich in MMP-2 and MMP-9, which when disseminated via the vasculature, are capable of degrading the basement membrane collagen and other ECM components allowing the tumour to metastasise (Graves et al., 2004). It is also likely that microparticles contribute to tumour metastasis by the induction and support of angiogenesis; in fact Baj-Krzyworzeka et al. (2006), Baj-Krzyworzeka et al. (2007) demonstrated that upon fusion of tumour-derived microparticles with monocytes, the transfer of nucleic acid material occurs resulting in the induction of VEGF and hepatocyte growth factor, demonstrating transfer of functional transcribed messages.

Microparticles do not only convey chemical signals to target cells, but can also endow them with new functions. Rozmyslowicz et al. (2003) and Majka et al. (2000) showed that CD4+/CXCR4-null cells were able to acquire CXCR4, the principle co-receptor for lymphotrophic HIV-1 strain infection, from platelet and megakaryocyte microparticles rich in the receptor; in this manner they became vulnerable to HIV-1 infection, demonstrating transfer *and* retention of functional receptors. Comparable results have been shown with another chemokine receptor, CCR5, which was transferred to null macrophages via peripheral blood monocyte-derived microparticles, rendering them susceptible to a macrophage-tropic strain of HIV (Mack et al., 2000). Similarly, platelet-derived microparticles have been shown to transfer the CD41 antigen ($\alpha_{IIb}\beta_3$ integrin) to lung cancer cells, increasing their adhesiveness to the endothelium and the rate of metastasis (Janowska-Wieczorek et al., 2005). Further, endothelial progenitor cell-derived microparticles function by reprogramming quiescent endothelial cells to endow them with angiogenic properties, a process reliant on α_4 and β_1 integrins and the transfer of RNA (Deregibus et al., 2007). Combes et al. (2005) demonstrated that the

ATP-binding cassette transporter A1 (ABCA-1), a receptor which regulates the distribution of phosphatidylserine to the outer membrane leaflet during microparticle shedding, played a key role in the development of cerebral malaria. They showed that ABCA-$1^{-/-}$ mice were resistant to cerebral malaria infection and produced a diminished level of plasma microparticles. Administration of microparticles isolated from ABCA-$1^{+/+}$ mice however, transferred the receptor and rendered the animals susceptible to cerebral malaria.

1.3.4 Microparticles as Biomarkers of Disease

Circulating microparticles and the proteins they express have become an attractive putative biomarker for several diseases, and their increased levels noted in atherosclerotic lesions (Baron et al., 2011), heatstroke, cancer and immunological diseases such as lupus and rheumatoid arthritis (Nielsen et al., 2012). Low levels of circulating MPs in patients with septic shock were correlated with organ dysfunction and higher mortality rates. Furthermore, data from this laboratory show that the phenotype of surface molecules on circulating microparticles in sepsis patients is an indicator of survival (Dalli et al., 2014).

Urinary microparticles, attractive as potential biomarkers of disease due to ease of sampling, have been used to identify diagnostic markers for both nephrotic syndrome (Rood et al., 2010) and prostate cancer (Rood et al., 2010, Nilsson et al., 2009). Microparticles as biomarkers of rheumatic diseases have become relatively well characterised in recent years. The levels of platelet microparticles, as identified by the expression of either CD41 or CD61 are increased in the plasma of patients with systemic lupus erythematosus (Lazarus et al., 2000, Joseph et al., 2001, Nagahama et al., 2001, Pereira et al., 2006), systemic sclerosis (Guiducci et al., 2008, Nomura et al., 2008) and rheumatoid arthritis (Knijff-Dutmer et al., 2002). Leukocyte microparticles, derived from a broad spectrum of immune cells, have also been identified in these diseases, especially in diseases with more vascular manifestations. For instance Nagahama et al. (2003) reported higher macrophage-derived microparticles (CD14 positive) in the plasma of anti-phospholipid syndrome patients; Guiducci et al. (2008) reported increased numbers of CD45-positive leukocyte-derived microparticles in systemic sclerosis; Daniel et al. (2006) showed higher levels of neutrophil-derived (CD66b positive) microparticles in systemic vasculitis patients. In agreement with this, Erdbruegger et al. (2008) found increased levels of CD45 and CD11b positive microparticles in acute vasculitis. Berckmans et al. (2005) characterised microparticles present within rheumatoid arthritis synovial fluid and found various leukocyte-derived

microparticles positive for CD4, CD8, CD14, CD20, CD66b and CD66e suggesting a complex contribution of not only these cells but also their resultant offspring microparticles to the disease pathogenesis.

1.3.5 Scott Syndrome

Although most reports centre on the inflammatory nature of microparticles, complete absence of these structures results in pathology. Platelets possess the highest flippase and scramblase rate of all cells and the microparticles derived from platelets provide a substrate surface that is 50-100 fold more pro-coagulant than platelets themselves. The importance of microparticles in haemostasis is demonstrated most clearly by the phenotype of patients with a rare bleeding disorder caused by a deficiency in microparticle shedding, known as Scott syndrome. These patients suffer episodes of moderate bleeding due to the inability to expose phosphatidylserine via microparticles, and the exact genetic identification of the trait has only recently been elucidated due to the rarity of human cases (Yang et al., 2012, Castoldi et al., 2011, Suzuki et al., 2010). Mutations in phospholipid scramblase TMEM16F (Anoctamin 6) are responsible for this phenotype. A similar disorder has been noted in German Shepherd dogs, where platelets display a similar lack of pro-coagulant activity (Morel et al., 2011), and could provide a good experimental model for investigations into microparticle shedding.

Inhibiting extracellular vesicle production or release and inhibition of the uptake of extracellular vesicles by recipient cells has been suggested to model their functions *in vivo*. This approach, required to determine the true physiological role of microparticles, is technically challenging and may not be possible experimentally. For example, inhibiting ceramide formation (important in protein sorting and exosome biogenesis) or PCD6IP (required for exosome formation) to limit exosome generation; or the interference of RAB27a to inhibit exosome release have been shown to limit the effects of exosomes, but also inhibit other non-specific cellular processes (Andaloussi et al., 2013). Treatment with the blood-pressure lowering drug dimethyl amiloride has been shown to attenuate endocytic vesicle recycling and inhibit exosome release, and *in vivo* has been shown to reduce mouse and human tumour cell growth by blocking the release of exosomes bearing Hsp72 which would otherwise exhibit immunosuppressive effects (Chalmin et al., 2010). Although off-target effects may have occurred during this study, it is interesting to note that therapeutic inhibition of microvesicle release is efficacious in certain circumstances. Prevention of microvesicle uptake by recipient cells would require blocking of phosphatidylserine receptor which is known to have far-reaching and catastrophic consequences (Andaloussi et al., 2013).

Phosphatidylserine receptor knockout mice are known to die at birth and histological analysis of the internal organs revealed profound inflammation and the presence of a large number of apoptotic bodies (Li et al., 2003). Thus, blocking of this receptor is likely to have severe consequences aside from blocking the uptake of microparticles. TMEM16F null mice also suffer a high rate of perinatal mortality, and thus, conditional knockouts must first be generated in order to elucidate their full role in physiology.

1.3.6 Microparticles as Potential Therapeutic Vectors

Encompassing all types of extracellular vesicles, reports exist of the therapeutic capabilities of certain vesicles when administered exogenously. For example, extracellular vesicles derived from mesenchymal stem cells have been used to stimulate cardiac tissue repair following myocardial infarction in mice (Andaloussi et al., 2013) and extracellular vesicles derived from tumour antigen-pulsed dendritic cells have been exploited in cancer immunotherapy (Zitvogel et al., 1998). Extracellular vesicles have been shown to induce pro-angiogenic programs in endothelial cells and to stimulate proliferation by delivering mRNA associated with the PI3K and Akt pathway (Deregibus et al., 2007).

Although the functions of microparticles may be exploited for therapy, these structures are also amenable to molecular manipulation and can even be used as non-viral vectors of nucleic acids. For example, it has been shown that extracellular vesicles derived from pre-transfected parent cells so that they carry suicide gene mRNA reduced schwannoma tumour burden in mice (Mizrak et al., 2013). Extracellular vesicles, when generated from autologous patient-derived cells as immunologically inert and biocompatible (Andaloussi et al., 2013). Furthermore, extracellular vesicles have access to physiological sites that remain privileged to the parent cells: for example, platelet microparticles can enter rheumatoid synovial fluid where intact platelets cannot (Boilard et al., 2010). Alvarez-Erviti et al. (2011) have demonstrated that extracellular vesicles are capable of crossing the blood-brain barrier: immature dendritic cells transfected with a plasmid encoding LAMP2 (an exosomal membrane protein) fused with a brain-specific peptide (rabies virus glycoprotein-derived peptide) which allowed brain-specific targeting of offspring exosomes. These targeted exosomes were then loaded via electroporation with siRNA that silenced *GAPDH*, a ubiquitous and highly expressed housekeeping gene, or *BACE1*, a strong candidate for anti-Alzheimer's disease therapeutics. Strong inhibition of *GAPDH* was noted in the brains of mice receiving *GAPDH* modified exosomes by tail-vein injection, with only minimal silencing effects seen in the liver and spleen. However, in mice receiving

exosomes containing *BACE1* silencing RNA, a brain specific knockdown of *BACE1* mRNA (60%) and BACE1 protein (62%) could be seen. This study demonstrates not only that exosomes are capable of crossing the blood-brain barrier, but also that these exosomes can easily be manipulated for targeting to specific organs.

Norling et al. (2011) harnessed neutrophil microparticles and enriched them with bioactive lipid mediators to enhance their efficacy, creating “nanomedicines”. These structures were inherently anti-inflammatory, and increased the potency of aspirin-triggered Resolvin D1 and a stable analogue of lipoxin A_4 so that much lower concentrations were effective at reducing neutrophil recruitment in models of acute inflammation (the zymosan peritonitis model) and temporomandibular joint inflammation.

1.3.7 Microparticles in Inflammation and Rheumatoid Arthritis

Microparticles have been found to play pathogenic roles in rheumatoid arthritis. It has been shown that microparticles produced by platelets are increased in the plasma of rheumatoid arthritis patients, and levels correlate with disease scores and activity (Knijff-Dutmer et al., 2002). It has been demonstrated that these microparticles are formed during stimulation of the platelet glycoprotein receptor VI by collagen, and are present in the synovial fluid of rheumatoid arthritis patients where intact platelets are absent. These platelet microparticles were rich in IL-1 and elicited pro-inflammatory responses when interacting with synovial fibroblasts (Boilard et al., 2010). Additionally, patients with rheumatoid arthritis have a disproportionately high cardiovascular mortality risk compared to the normal population. A causal relationship between the increased levels of highly pro-coagulant platelet-derived microparticles and the risk of thrombosis has been suggested by experiments *in vitro,* and high levels of microparticles were found in atherosclerotic plaques (Knijff-Dutmer et al., 2002). Microparticles isolated from rheumatoid joints patients are capable of also coagulating the synovial fluid, and induces the formation of fibrin macro-aggregates, known as rice bodies (Berckmans et al., 2002).

Microparticles from various cellular origins have been shown to be present in rheumatoid synovial fluid, with high levels of granulocyte-derived (CD66b positive) and monocyte-derived (CD14 positive) microparticles. $CD4^+$ and $CD8^+$ T cell, platelet and erythrocyte microparticles are also present, but in much lower numbers (Berckmans et al., 2002). As synovial fibroblasts are localised in the intimal lining layer, in direct

contact with the synovial fluid, it is possible for microparticles to interact with synovial fibroblasts directly, influencing the release of an array of pro-inflammatory mediators (Berckmans et al., 2005). Microparticles produced by primary T cells and monocytes strongly induce MMPs -1, -3, -9 and -13 when co-cultured with rheumatoid synovial fibroblasts. Importantly, the induction of these enzymes in response to monocyte and T-cell microparticles seems to be specific for fibroblasts as no significant effects were noted when MCF-7 and BT549 breast cancer cells were exposed to microparticles. Further, co-incubation of microparticles with rheumatoid synovial fibroblasts induced the production of IL-6, IL-8 and CCL2 and CCL8 (Distler et al., 2005a, Morel et al., 2011) plus soluble ICAM-1 and RANTES (Berckmans et al., 2005). Immune cells occur abundantly in the rheumatoid synovium and the microparticles produced by these cells may induce and amplify pathways of activation and destruction without the need for direct cell-to-cell interaction.

Microparticles may play an important role in the development of autoantibodies by displaying intracellular self-antigens on their surface that, if recognised by antigen presenting cells, could elicit a T-cell response that through interactions with B cells could trigger the production of autoantibodies. Further display of the same autoantigens for recognition by autoantibodies has been shown to induce immune-complex formation on microparticles in patients with Systemic Lupus Erythematosus (SLE) (Nielsen et al., 2012). This correlates with a report by Ullal et al. (2011) who found that anti-double stranded (ds) DNA antibodies bound plasma microparticles in SLE patients, and that increased microparticle-immune complex aggregates correlated with high anti-dsDNA titres. The report by Nielsen et al. (2012) went further in identifying double-labelled microparticles (Annexin V positive) in the circulation, positive for IgG which then correlated to anti-histone and anti-Sm/RNP levels in SLE patient serum. These microparticles may activate complement resulting in further damage. Reduced clearance of these microparticles may be the key to autoantibody formation increasing the likelihood of recognition by antigen presenting cells.

Microparticles have been shown to promote adhesion and rolling of leukocytes *in vitro* and to activate complement, suggesting a contributing role in inflammation (Distler et al., 2005b). Microparticles can contain cytokines and are able to disseminate into regions that are inaccessible to the parent cells. As mentioned previously, platelets activated through the GP VI by collagen release IL-1β-enriched microparticles, which were shown to be present within synovial joint fluid of rheumatoid arthritis patients, where intact platelets are rarely present (Boilard et al., 2010). Additionally, IL-1β

secretion occurs preferentially *via* microparticles. The synthesis of IL-1β by cells is unconventional in terms of protein export, in that it does not follow the classical endoplasmic-reticulum-to-Golgi pathway and does not have a secretory signal sequence and there is no evidence that is stored preformed intracellularly (MacKenzie et al., 2001). It has been shown that mature IL-1β secretion from macrophages relies on ABCA1, a pivotal gene in the regulation of cellular cholesterol homeostasis (Zhou et al., 2002) and key for microparticle release.

Microparticles may directly release lipid mediators such as oxidised phospholipids, lysophosphatidic acid and arachidonic acid, especially where microparticles are exposed to high levels of secretory phospholipase A_2 ($sPLA_2$) as it does occur in the rheumatoid joint (Berckmans et al., 2005, Pruzanski et al., 1988). Secretory PLA_2, derived mainly from activated platelets and neutrophils, catalyses the release of arachidonic acid from phospholipids, which is in turn enzymatically converted into prostaglandins by cyclooxygenase-2 (COX-2) (Knijff-Dutmer et al., 2002). High levels of prostaglandin E_2 play key roles in the pathogenesis of rheumatoid arthritis and mediate not only pain sensitivity and inflammation but also stimulate angiogenesis. Its biosynthesis is strictly controlled by PLA_2, cyclooxygenases and prostaglandin E synthases (Jungel et al., 2007). COX-2 in particular is unregulated in the rheumatoid synovium and correlates with the level of inflammation present. Platelet microparticles can carry arachidonic acid, stimulating the expression of COX-2 in endothelial cells, increasing the production of prostaglandins (Barry et al., 1998, Barry et al., 1997). T cell- and monocyte-derived microparticles are also capable of inducing Prostaglandin E_2 synthesis when co-incubated with rheumatoid arthritis synovial fibroblasts, by up-regulating the enzymes involved in the conversion of arachidonic acid to Prostaglandin E_2, namely COX-2 and mPGES-1.

Microparticles express phosphatidylserine, which is sensed as an “eat me” signal by phosphatidylserine receptors on macrophages, which are responsible for the clearance of apoptotic cells and cellular debris. As microparticles in the synovial fluid bind less annexin V than the microparticles found in plasma, the phagocytic removal of these particles may be impaired. The reduced binding may be due to the exposure of microparticles to $sPLA_2$ which catalyses the phosphatidylserine into other compounds thus reducing annexin V binding (Knijff-Dutmer et al., 2002).

1.3.8 Neutrophil Microparticles

Gasser and Schifferli (2004) proposed that neutrophil microparticles feature immunosuppressive and anti-inflammatory qualities, which further challenges the linear model of inflammation, suggesting pro-inflammatory and anti-inflammatory events are initiated and coincide in a parallel manner. Neutrophil microparticles were shown not to induce IL-8, TNF-α and IL-10 secretion when co-incubated with human monocyte derived macrophages (HMDMs) as predicted. Instead, an increase in the anti-inflammatory cytokine TGF-β was observed. Furthermore, when co-incubated with HMDMs, neutrophil microparticles dose-dependently blocked the LPS-dependent production of TNF-α and reduced the release of IL-8 and IL-10 compared to HMDMs stimulated LPS alone. This effect was not dependent on the phagocytosis of the microparticles by the HMDMs, as demonstrated by inhibiting phagocytosis with the addition of cytochalasin D, rather binding of the microparticles to the cells or the microparticle membranes alone, was sufficient for the anti-inflammatory effects to be exerted. Neutralizing antibodies to TGF-β partially inhibited the anti-inflammatory effects of the microparticles by blockade of IL-8 production and reduction of IL-10 and TNF-α suggesting only a partial contribution of TGF-β in the anti-inflammatory activity of these microparticles. Potentially, the anti-inflammatory effects of microparticles observed here could be due to the engagement of the phosphatidylserine receptor on the HMDMs by phosphatidylserine-exposing microparticles, as this process, as mentioned earlier, is crucial for the production of TGF-β.

Neutrophil microparticles have been shown to inhibit dendrite formation in dendritic cells (DCs) matured with LPS, with cellular morphology directly altered by exposure to these microparticles with or without LPS stimulation. Furthermore, microparticle treatment reduced the phagocytic capabilities of both immature and mature DCs, inhibited the up-regulation of key surface markers (CD40, CD80, CD83, CD86 and HLA-DP DQ DR) and the release of inflammatory cytokines (IL-8, IL-12, IL-10, TNF-α) by LPS-matured monocyte-derived DCs. Dendritic cells treated with neutrophil microparticles at the time of LPS stimulation induced significantly less T cell proliferation compared to LPS-stimulation alone. Co-incubation of the cells with neutrophil microparticles also elicited a pro-resolving response, similar to that described by Gasser and Schifferli (2004), where the release of TGF-β1 was consistently induced, regardless of whether the cells were immature, LPS-matured, or even from non-autologous donors. The chemokine receptor CCR7 is inhibited by TGF-β1, in agreement, down-regulation of this receptor was observed in these experiments. Both the anti-inflammatory and pro-resolving effects of these microparticles were

partially inhibited by annexin V binding showing that these effects were mediated at least partly by phosphatidylserine recognition (Eken et al., 2008). The content of the microparticles may be contributing more to this anti-inflammatory process however, as Hoffmann et al. (2005) were able to demonstrate that phosphatidylserine and binding of its receptor was sufficient to generate anti-inflammatory effects in the majority of adaptive immune cells, except dendritic cells. The phosphatidylserine receptor cloned by this group was also not expressed on dendritic cells and thus phosphatidylserine liposomes could not induce TGF-β production in these cells. The anti-inflammatory effects reported by Eken et al. (2008) and the subsequent partial blocking of these effects by annexin V binding to phosphatidylserine in dendritic cells should be interpreted with caution. The authors state that annexin V coated neutrophil microparticles alone induced TNF-α release when incubated with immature dendritic cells, indicating that annexin V may have induced or blocked other interactions not directly related to phosphatidylserine binding.

Some of these effects may be explained by analysing the signalling cascades modulated by the microparticles. Eken et al. (2010) demonstrated that neutrophil microparticles significantly supressed the phosphorylation of NFκB p65 at Ser^{536}, a position which is reported to enhance transcriptional activation of NFκB. NFκB is a key transcription factor involved in the control of major pro-inflammatory genes as well as proliferation, differentiation and cell survival. The neutrophil microparticles also prevented the translocation of NFκB to the nucleus and its subsequent transactivation. The inhibition of NFκB p65 phosphorylation was lost when blocking antibodies to MerTK were added demonstrating that MerTK is required for the biological activity of neutrophil microparticles in this setting. Upstream, it was shown that PI3K and Akt were involved in the inhibition afforded by neutrophil microparticles. Downstream, the mRNA of six genes associated with NFκB signalling were measured: TNF-α, IL-1β, IL-6, IL-8, IL-10 and IL-12, all of which were significantly down regulated in HMDMs treated with neutrophil microparticles and zymosan compared to zymosan treatment alone, as were the supernatant levels of these cytokines.

Microparticles are intercellular communicators able to deliver lipid-mediators to aid in the resolution of inflammation (Norling et al., 2011). Deuterium-labelled d_5DHA was incorporated into neutrophil microparticles when administered during the onset of inflammation in a mouse model of zymosan peritonitis. These microparticles contained enzymatic metabolites of d_5DHA: d_5-17-HDHA and d_5-14-HDHA, which are biosynthetic pathway markers of D-series resolvins and maresin. This implicates microparticles as

intercellular communicators that act by delivering pro-resolving lipid mediator precursors to inflammatory sites to be metabolised into resolvins and maresins. Resolvins and maresins are extremely potent anti-inflammatory poly-unsaturated fatty acids, generated during the resolution phase of inflammation (Serhan and Petasis, 2011). Therefore, neutrophil microparticles may contribute to the balance of pro-resolution versus pro-inflammation in rheumatoid arthritis by carrying bioactive lipid precursors.

Secretory PLA_2 is secreted constitutively by neutrophils, and by chondrocytes, the cells which produce cartilage, when stimulated with cytokines (Fourcade et al., 1995) and $sPLA_2$ levels are elevated within synovial fluid (Berckmans et al., 2002) and during the resolution phase of inflammation (Norling et al., 2011). Secretory PLA_2 readily hydrolyses phosphatidylserine and phosphatidylethanolamine into lysophosphatidylserine and lysophosphatidylethanolamine, but cannot penetrate inside cellular membranes and therefore has limited action on intact cells. As microparticles express both of these anionic lipids on their outer leaflet, it has been suggested that microparticles are the biological substrate for $sPLA_2$ action. Further, when neutrophils were incubated with deuterium-labelled DHA, microparticles were generated containing both d_5-DHA and d_5-HDHA esterified into phosphatidylcholine which when co-incubated with $sPLA_2$ liberated esterified pro-resolving mediator precursors from the microparticle surface (Norling et al., 2011). It has been shown that another lipid present in the microparticle membrane, phosphatidic acid, has anti-inflammatory properties when hydrolysed by $sPLA_2$ into lysophosphatidic acid (Fourcade et al., 1995). Similarly, orally administered 2-polyunsaturated lysophosphatidylethanolamine significantly inhibited leukocyte migration into the peritoneal cavity in a model of zymosan-induced peritonitis, reduced the production of the inflammatory cytokines TNF-α, IL-1β and IL-6, and of the chemokines MIP-1α, MCP-1 and MIP-2; and significantly up-regulated IL-10, a potent anti-inflammatory cytokine (Hung et al., 2011). Microparticles characterised in patients with arthritis did express high levels of lysophosphatidylethanolamine and lysophosphatidylserine (Fourcade et al., 1995) but subsequent investigation of the role of these microparticles has not been carried out.

The anti-inflammatory effects of neutrophil microparticles are not broadly immunosuppressive, like simple anti-inflammatory cytokines such as IL-10, but instead play tightly restricted roles that depend on the inflammatory circumstances. Timar et al. (2013) have shown that in a context-dependent setting, neutrophils stimulated with opsonised *Staphylococcus aureus* bacteria produce microparticles with antibacterial

properties that were capable of aggregating bacteria to prevent their growth. Furthermore, opsonised *S. aureus* generated microparticles that were as effective as their parent neutrophils at inhibiting bacterial activity. In this way, the antibacterial activity of neutrophils is enhanced, without the broad suppression of the immune system.

Our laboratory has extended the study of neutrophil microparticles. Dalli et al. (2013) have shown that neutrophils stimulated in suspension produce microparticles with a proteome distinct from those produced by neutrophils in contact with the endothelium. In both neutrophil microparticle subsets, myeloperoxidase, Annexin A1, cathepsins G and S100A8 (also known as myeloid-related protein 8; MRP8) are highly abundant. Suspension neutrophil microparticles generated *in vitro* express higher amounts of heat shock protein 71 compared to adherent neutrophil microparticles, which are enriched in α_2-macroglobulin and ceruloplasmin, and this protein profile reflects the function of the microparticles. When co-incubated with human umbilical vein endothelial cells, each microparticle subset modulated the transcriptional phenotype of the cells: suspension neutrophil microparticles altered the gene expression pattern of 1154 genes, most closely representing genes modulated during anti-inflammatory drug treatment; whereas adherent neutrophil microparticles influenced the transcription of 501 genes, which most closely resembled those modulated during antibacterial or antifungal drug treatments. These microparticles were also seen to have chemotactic properties capable of migrating towards a chemokine gradient, which has exciting implications for these structures, which were once considered inert, empty cellular debris.

So far, the functional effects of microparticles or the contribution of microparticles to the pathogenesis of rheumatoid arthritis has been studied only in relation to the pro-inflammatory effects of these structures, particularly to fibroblast-like synoviocytes. Microparticles from arthritic joints have been shown in vitro to stimulate synovial fibroblasts to release chemokines (CCL2, CCL8, CCL5), cytokines (IL-6, IL-8) and adhesion molecules (ICAM-1) (Distler et al., 2005b) and to induce the production of cartilage-matrix degrading enzymes such as MMP-3, -9 and -13. All of these effects contribute to the inflammation and degradation characterising this disease (Beyer, 2010). As of yet the role of neutrophil microparticles in rheumatoid arthritis remains unclear, and, overall, the effects of microparticles on the cartilage and the chondrocytes have not been explored.

Endogenously produced microvesicles of chondrocyte and osteocyte origin are involved in the calcification of bone in both development and adult bone remodelling (Balcerzak et al., 2003, Balcerzak et al., 2008), where the combination of phosphatidylserine exposure and Annexin A1 promote hydroxyapatite crystal formation by nucleation. Similar effects have been reported in extracellular vesicles associated with calcification during atherosclerosis, where vesicles were shown to associate with collagen fibrils (Kapustin et al., 2011, New et al., 2013). No reports exist of the functional relevance of microparticles in relation to mature, adult healthy or arthritic cartilage, but these extracellular matrix-associating properties indicates that microparticles may have a propensity for interaction. Neutrophil microparticles, due to their abundance in the inflamed joint make ideal candidates assessing any possible relationship. This project aims to investigate the role of neutrophil microparticles in the rheumatoid joint, and if any, the contribution of the proteins expressed within the microparticles as determined by previous proteomic analysis. Particular attention will be paid to their effects on the chondrocytes within both healthy and rheumatoid joints.

1.4 Hypothesis and Aims

Previous reports have demonstrated that neutrophil microparticles have potent anti-inflammatory effects *in vitro* when co-cultured with innate immune cells and stromal cells, and that Annexin A1 may be a contributing player in these settings.

This thesis challenges the hypothesis that neutrophil microparticles could have protective actions on non-immune cell types, such as the chondrocytes and the extracellular matrix, as microparticles have previously been shown to associate with collagen fibrils, and are abundantly present within the joint.

Thus, the overall aim of the thesis is to dissect the role of neutrophil microparticles using experiments that represent the physiology of the human joint, in the setting of rheumatoid arthritis pathology.

Objectives:

***In Vitro* Assays**

- Generate neutrophil-derived microparticles *in vitro* and assess their characteristics, number and mode of formation with different stimuli
- Elucidate the roles of the extracellular matrix in microparticle production
- Determine the effects of neutrophil microparticles in co-culture with chondrocyte cell lines cultured in high-density micromasses
- Explore the involvement in Annexin A1 in the chondroprotection seen, including the roles of the Annexin A1 receptor
- Assess the contribution of other microparticle components on chondroprotection

***Ex Vivo* Assays**

- Generate an *ex vivo* culture system for the study of cartilage-native chondrocytes
- Investigate the relationship between microparticles and cartilage native chondrocytes using imaging techniques

***In Vivo* Assays**

- Assess the effect of systemic neutrophil microparticle administration during on-going inflammatory arthritis
- Assess the effect of local neutrophil microparticle administration during on-going arthritis with both histological and live-imaging tools
- Determine the requirement for the Annexin A1 receptor during microparticle-induced chondroprotection
- Generate an *in vivo* protocol to elucidate the physiological process of neutrophil trafficking and microparticle generation in inflamed joints

CHAPTER 2: MATERIALS AND METHODS

2.1 Materials

All antibody suppliers, clones and concentrations are listed in Table 2.1.1. All chemicals and reagents were purchased from Sigma-Aldrich, Poole, UK, unless otherwise stated, including 0.1μm, 0.5μm and 1μm latex calibration beads, cytoskeletal inhibitors, recombinant human lactoferrin, histology reagents, dyes and tissue cassettes. Power SYBRgreen mastermix was purchased from Applied Biosystems Inc., CA, USA. Isoflurane inhalable gas anaesthetic was purchased from Baxter, Norfolk, UK. Human Fc block, TGFβ1 cytokine bead array, transwell inserts and FITC-Annexin V apoptosis detection kit I were purchased from BD Bioscience, Abingdon, UK. Polystyrene ultracentrifuge tubes were purchased from Beckman Coulter, High Wycombe, UK. Laemmli buffer was purchased from Bio-Rad, Hemel Hempstead, UK, Genomic DNA from Bioline, London, UK and Alcian Blue 8GS dye from Carl Roth, Karlsruhe, Germany. Prostaglandin E_2 EIA and resolvin D1 was purchased from Cayman, Ann Arbor, MI, USA; Neubauer Chamber from Celeromics, Valencia, Spain and Wax Pens from Dako, Glostrup, Denmark. Mouse Fc block, Cell Fix/Permeabilisation kit and IL-8 Ready-Set-Go! ELISA kit were purchased from eBioscience, Hatfield, UK. Histoclear and Hoefer Western Blotting equipment were purchased from Fisher Scientific, Loughborough, Leicestershire, UK. Hyperfilm and High-range rainbow molecular weight markers were from GE Healthcare, Little Chalfont, UK and ITS supplement, Foetal bovine serum (both heat inactivated and non-heat inactivated) and trypsin/EDTA were purchased from Gibco, Invitrogen, Paisley, UK. Hamilton syringes were from Hamilton, Bonaduz, Switzerland. Bodipy FL N-(2-aminoethyl)maleimide), DAPI, Dithiothreitol, First Strand Buffer, AlexaFluor 546-conjugated Phalloidin, ProLong immunogold antifade reagent, PureLink FFPE Total RNA Isolation kit, RNAse OUT, Superscript III, SYBRgreen I dye and AlexaFluor 633-conjugated Wheat Germ Agglutinin were all purchased from Invitrogen, Paisley, UK. Dextran (MW 450,000-650,000), $DiOC_6$ dye, GelRed, HEPES, $Oligo_{(dT)}$, 1μm fluorescent beads, 500nm fluorescent beads, collagenase type II and cytochalasin D were all purchased from Life Technologies, Invitrogen, Paisley, UK. Primary adult human articular chondrocytes (AHAC), AHAC growth medium, AHAC differentiation medium and trypsin deactivation solution were purchased from Lonza. Mowiol and human recombinant ceruloplasmin were purchased from Merck Millipore, Darmstadt, Germany. 0.22μm and 0.70μm filters, Accutase, Luminata forte, Polyvinylidene difluoride membranes and ApopTag fluorescein in situ apoptosis detection kit were purchased from Millipore, Watford, UK. Polyacrylamide Protogel, Resolving Buffer and

Stacking Gel Buffer were from National Diagnostics, Charlotte, NC, USA. Bovine serum albumin, DMEM high glucose, penstrep and phenol red-free RPMI were purchased from PAA, Somerset, UK. IL-8 was purchased from Peprotech, EC, London, UK, BCA Assay from Pierce, Rockford, IL, USA and dNTP mix and Griess Reagent System were from Promega, Madison, WI, USA. RNeasy minikit and Gene primers (see Table 2.1.2) were purchased from Qiagen, Hilden, Germany. IL-1β was from R&D Systems, Abingdon, UK and OCT Tissue-Tek compound from Sakura Finetek, Europe. Diamond microtome blades were from C.L. Sturkey, Lebanon, PA, USA and all needles including 21 Gauge Butterfly needles were purchased from Terumo, Heverlee, Belgium. Glass microscope slides and ThermoPrime ReddyMix PCR Mastermix were from ThermoScientific, Leicestershire, UK. All cell culture flasks, plates and plastics were from Corning Amsterdam, NL.

Software packages utilised during this project were IDEAS and INSPIRE software, Amnis Corporation, Seattle, WA, USA; FCAP Assay Software, BD Bioscience, Abingdon, UK; Zeiss Imaging Software, Carl Zeiss, Cambridge, UK; Living Imaging 3.0, Caliper, Hopkinton, MA; FlowJo Software, FlowJo, Stanford, CA, USA; Lucia Imaging Software, Lucia Laboratory Imaging, Prague, CZ; ND 1000 software, NanoDrop Technologies, Wilmington, DE; NTA software version 2.3, NanoSight Ltd., Amesbury, UK and ImageJ software, NIH, Bethesda, MD, USA.

Analytical hardware included Imagestream^X mk. II, Amnis corporation, Seattle, WA, USA; ABI Prism 7900 real-time PCR system, Applied Biosystems Inc., CA, USA; BD LSRFortessa and BD FACSCalibur, BD Bioscience, Abingdon, UK; IVIS 200 bioluminescence imaging system, Caliper, Hopkinton, MA, USA; Zeiss LSM 510 laser scanning confocal microscope, Carl Zeiss, Cambridge, UK; EVOS LED Fluorescence microscope, Invitrogen, Paisley, UK; Multiskan Bichromatic 348 Spectrophotometer, Labsystems, Finland; Leica tissue processor and Leica microtome, Leica Microsystems, Milton Keynes, UK; NanoDrop Spectrophotometer, NanoDrop Technologies, Wilmington, DE; NanoSight LM10 system, NanoSight Ltd, Amesbury, UK; Nikon DXM1200 digital camera, Nikon, Melville, NY, USA; Olympus BH-2 light microscope, Olympus, Tokyo, Japan; FluorChem E digital darkroom, Protein Simple, Santa Clara, CA, USA; TECAN M200 Spectrophotometer, Tecan, Mannedorf, Switzerland and Abgene Thermal Cycler, ThermoScientific, Leicestershire, UK.

Table 2.1.1 Antibody concentrations, suppliers and clones.

Antigen	Clone, host	Company	Fluorochrome	Ig type	Final Concentration
CD11b (human)	ICRF44, mouse	eBioscience	APC	IgG1κ	0.1μg/ml
CD62L (human)	DREG56, mouse	eBioscience	PECy5	IgG1κ	0.1μg/ml
CD66b (human)	G10F5, mouse	Biolegend	PE	IgM	10μg/ml
MRP8/S100A8 (Human)	CF-145, mouse	Lifespan Biosciences	FITC	IgG2b	20μg/ml for flow cytometry, 50μg/ml Immunofluorescence
MRP14/S100A9 (human)	MRP 1H9, mouse	Pierce	FITC	IgG1κ	10μg/ml
MRP14 (mouse)	Goat polyclonal	LSbio	Purified	IgG	15μg/ml
α2-Macroglobulin (human)	257316, mouse	R&D Systems	Purified	IgG1	5μg/ml
Ceruloplasmin (human)	8, mouse	BD Transduction labs	Purified	IgG1	20μg/ml
Heat-shock Protein 70 (human)	4E7, mouse	AbD Serotec	Purified	IgG1	40μg/ml
Annexin A1 (Human)	1b, mouse	In house generated	Purified	IgG1	50μg/ml for flow cytometry and immunofluorescence, 2μg/ml Westerns
Secondary Ab (mouse)	Goat	Invitrogen	Alexa 594	IgG1	20μg/ml
Secondary Ab (Rabbit)	Goat	Life Technologies	Alexa 594	IgG	20μg/ml
Ly6G (mouse)	1A8 (rat)	BD Biosciences	FITC	IgG2aκ	0.5μg/ml
Annexin A1 (human, cross reacts with mouse, rat)	Polyclonal, rabbit	Thermo Scientific	Purified	IgG	20μg/ml Immunofluorescence

FPR2 (human)	304405, mouse	R&D Systems	Purified	IgG2b	2.5μg/ml
FPR1 (human)	350418, mouse	R&D Systems	Purified	IgG2a	2.5μg/ml
TGF-β (human isoforms 1, 2 & 3)	Ab66043, Rabbit polyclonal	Abcam	Purified	IgG	20μg/ml for blocking experiments
Isotype 17-4714 (CD11b)	Mouse	eBioscience	APC	IgG1κ	0.1μg/ml
Isotype (CD62L)	Mouse	eBioscience	PECy5	IgG1κ	0.1μg/ml
Isotype (CD66b)	Mouse	Biolegend	PE	IgM	10μg/ml
Isotype (MRP8)	Mouse	Lifespan	FITC	IgG2b	20μg/ml
Isotype (MRP14)	Mouse	Pierce	FITC	IgG1κ	10μg/ml
Isotype (Ly6G)	R35-95 (Rat)	BD Biosciences	FITC	IgG2aκ	0.5μg/ml

Table 2.1.2 Primers used for mRNA expression analysis

Gene code	Catalogue Number	Gene code	Catalogue Number
Hs_COL2A1	QT00049518	Hs_SP1	QT01870449
Hs_ACAN	QT00001365	Hs_JAG1	QT00031948
Hs_GAPDH	QT01192646	Hs_JAM3	QT00024997
Hs_RPL32	QT01668198	Mm_Adamts5	QT00131376
Hs_Sox9	QT00001498	Mm_Il1b	QT01048355
Hs_Anxa1	QT00078197	Mm_Mmp13	QT00111104
Hs_FPR2	QT00204295	Mm_Acan	QT00175364
Hs_FPR1	QT00199745	Mm_Col2a1	QT01055523
Hs_SGPP2	QT00041832	Mm_Sox9	QT00163765

2.2 Development, Validation and Optimisation of Techniques

This PhD project presented several opportunities to develop and optimise various methods and techniques. Primarily, as the field of microparticle study is relatively new, the techniques used for microparticle detection and measurement are not standardised, and as yet no gold standard exists. With the tools available to me, I have endeavoured to ensure that the data collected, especially in terms of microparticle assays, were as robust as possible. Where limitations cannot be overcome, such as with the direct measurement of the size of the microparticles, I have tried to build up a portfolio of evidence using techniques including flow cytometry, Imagestream^X imaging cytometry, nanoparticle tracking analysis, confocal microscopy and live cell fluorescence microscopy to give confidence that the microparticles fall below the prescribed 1μm upper size limit. In the future it is likely that technologies will be combined so that the concentration, size and biochemical characteristics of microparticles can be measured simultaneously in high-throughput assays. Until then, the optimisations performed on these individual techniques are described herein.

2.2.1 Microparticle Generation

Microparticles were generated from human or mouse neutrophils. Human neutrophils, from healthy donors, were isolated from the peripheral blood using a Dextran/Histopaque density gradient (see section 2.3.1). Mouse neutrophils were recruited to the peritoneum using zymosan peritonitis before collection and stimulation. Cell populations were analysed by flow cytometry to determine purity and/or activation status (see section 2.3.2)

2.2.1.1 Microparticle Generation for Co-Culture and Flow Cytometry

Every effort was made to keep microparticle preparations sterile to ensure co-culture of cells with microparticles was free of contamination. Microparticles were generated from freshly isolated neutrophils. Cells (2 x 10^7/ml) were stimulated with TNF-α (50ng/ml, Sigma) or IL-8 (50ng/ml, Peprotech) or vehicle (PBS) for 20 minutes at 37°C. Cells were then pelleted by centrifugation at 4500 x g for 15 minutes at 4°C and collected for flow cytometric analysis (see section 2.3.2.1), and any residual platelets depleted by a second centrifugation at 10,000 x *g* at 4°C for 2 minutes. Microparticles were pelleted

from the supernatant by ultracentrifugation at 100 000 x *g* for 1 hour at 4°C. Microparticle pellets were resuspended in 200μl 0.22μm filtered sterile PBS and 10μl per sample was taken for flow cytometric analysis. The remaining microparticle suspension was kept at -80°C until further use.

2.2.1.2 Fluorescent Microparticle Generation for Visualisation in Confocal Microscopy and Fluorescent Microscopy

For generation of fluorescent microparticles (used in fluorescence and confocal microscopy) 2 x 10^7/ml neutrophils were stained with Bodipy-maleimide stain in DMSO (2.5μM) on ice for 10 min prior to stimulation. After staining, cells were washed with 40ml PBS and centrifuged at 300 x *g* for 10 minutes, resuspended to 2 x 10^7 per ml in phenol-red free RPMI. Cells were stimulated with TNF-α (50ng/ml) or vehicle (PBS) for 20 minutes in the dark at 37°C. Following incubation, samples were centrifuged at 4500 x *g* for 15 minutes at 4°C to pellet cells, then 10,000 x *g* for 2 minutes to pellet platelets, which were then discarded, and the microparticles pelleted from the supernatant by ultracentrifugation at 100 000 x *g* for 1 hour at 4°C ensuring that all sample handling occurred in the dark. Microparticle pellets were resuspended in 200μl 0.22μm filtered sterile PBS and stored at -80°C until use.

2.2.1.3 Generation of Microparticles from Neutrophils Treated with Cytoskeletal Function Modifying Drugs and Calcium Chelator

To investigate the requirements for microparticle generation, freshly isolated neutrophils (1x10^6 in 100μl) were treated for 10 minutes with Cytochalasin D (2μM), Jasplakinolide (1μM), Blebbistatin (10μM), ML-7 (20μM) or 1,2-*Bis*(2-aminophenoxy)ethane-*N,N,N',N'*-tetraacetic acid tetrakis(acetoxymethylester) (BAPTA-AM; 20μM) at 37°C. Neutrophils were then plated into 96-well plates and centrifuged briefly and gently at 200 x *g* for 30 seconds at room temperature, following by washing in PBS (supplemented with 1% bovine serum albumin). Cells were then stimulated with TNF-α (50ng/ml) or vehicle (PBS) for 20 minutes. Supernatants were collected, stained with Bodipy-maleimide (2.5μM) and immediately acquired with an ImageStream^X mk. II to quantify microparticle number and size.

To ensure that these drugs did not interfere with neutrophil viability, Trypan blue dye was added to the cell suspension (1:2 dilution), 10μl applied to a Neubauer counting chamber, and 200 cells were assessed for Trypan blue exclusion, an indicator of cell viability. These cells appeared bright, whereas the dead cells that could not exclude

this dye were a deep blue colour. The percentage of live to dead cells was then recorded.

2.2.1.4 Generation of Microparticles with Annexin V Coating

In order to inhibit microparticle interaction with chondrocytes, microparticles were coated with Annexin V in the presence of calcium ions. Microparticle aliquots were removed from -80°C and thawed quickly to 37°C. Calcium binding buffer (2X, diluted with microparticles 1:2 to generate a 1X solution) was added, then FITC-conjugated Annexin V in excess (25μg in 100μl) was added to coat the microparticles for 20 minutes at room temperature in the dark. An aliquot of coated microparticles was analysed by flow cytometry to determine their Annexin V expression (see section 2.2.2.3). Microparticles were immediately used for co-culture experiments.

2.2.1.5 Generation of Murine Neutrophil Microparticles

Neutrophils were obtained by zymosan peritonitis (Figure 2.2.1). Male 8-week old wild type or *Anxa1* -/- C57BL/6 mice were injected with 1mg Zymosan A diluted in PBS and sacrificed at 4 hours. Cells were collected in ice-cold PBS by peritoneal lavage: skin was resected and the peritoneum exposed. Using a 23-gauge needle, 4ml saline was injected into the peritoneum taking care not to touch any organs within the peritoneal cavity. The needle was removed and the hole pinched closed. Using gentle massage, the cells were loosened from within the peritoneum then collected using the same syringe. The cells were counted, then stained with Ly6G antibodies (a neutrophil marker) and analysed by flow cytometry (see section 2.3.2.1). Cells (2×10^7/ml) were stimulated with recombinant mouse TNF-α (50ng/ml) for 20 minutes at 37°C and isolated by centrifugation and ultracentrifugation in the same way as human microparticles. Microparticles were then pooled according to genotype and counted by flow cytometry (see section 2.2.2).

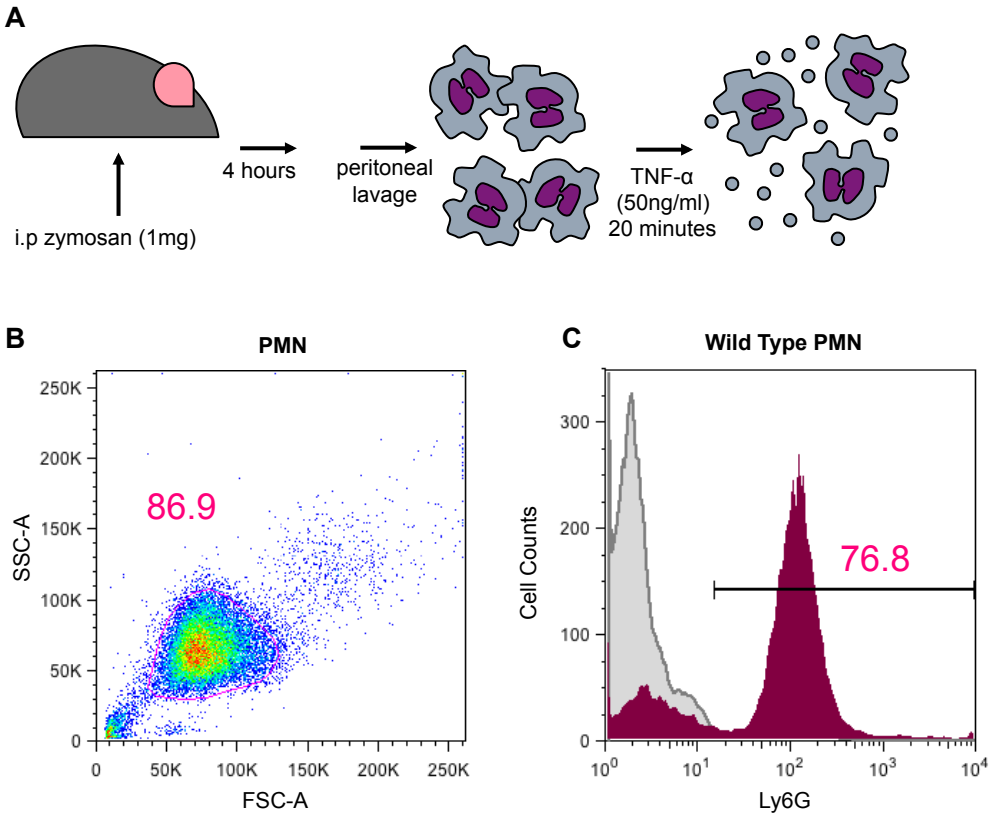

Figure 2.2.1 Schematic for mouse neutrophil microparticle generation. (A) Schematic of experimental procedure. (B) Neutrophils were analysed by flow cytometry and appeared as a homogenous population on the forward/side scatter. (C) Approximately 75% of the total events collected were Ly6G positive, indicating that they were of neutrophil origin.

2.2.2 Microparticle Detection and Measurement by Flow Cytometry

Flow cytometry is the simultaneous detection of multiple parameters, such as the size, granularity (internal complexity), surface topography and biochemical makeup, of a population of cells in suspension. Cells guided in a hydrodynamically focussed stream pass one-by-one through a flow cell. Fixed alignment lasers transmit light through the flow cell, and as the cell passes through the beam, an optical signal is generated. This optical signal reaches a detector, which translates the signal to an electronic one. Two types of detector are used in this system, photomultiplier tubes (PMT), used to detect weaker signals such as those generated by fluorescent labels and the side scatter (a measure of internal cellular complexity), and photodiodes, used to detect stronger forward scatter signals (a rough measure of cellular size).

To allow accurate detection of different fluorescent signals, the signals pass though filters and mirrors arrayed around the flow cell (Figure 2.2.2). Long pass dichroic filters, placed in front of the PMT detectors transmit wavelengths that are longer than a specified value, steering shorter wavelengths of light to the next PMT so that progressively shorter wavelengths are detected by the last PMT. Band-pass filters are used to only transmit a narrow bandwidth of light to the detector.

The digital signals generated using this system can be used to probe multiple parameters of cellular phenotype, and data generated are usually displayed in histograms of one parameter, such as fluorescence intensity, or in 2-parameter scatter plots, such as forward/side scatter (showing size and complexity).

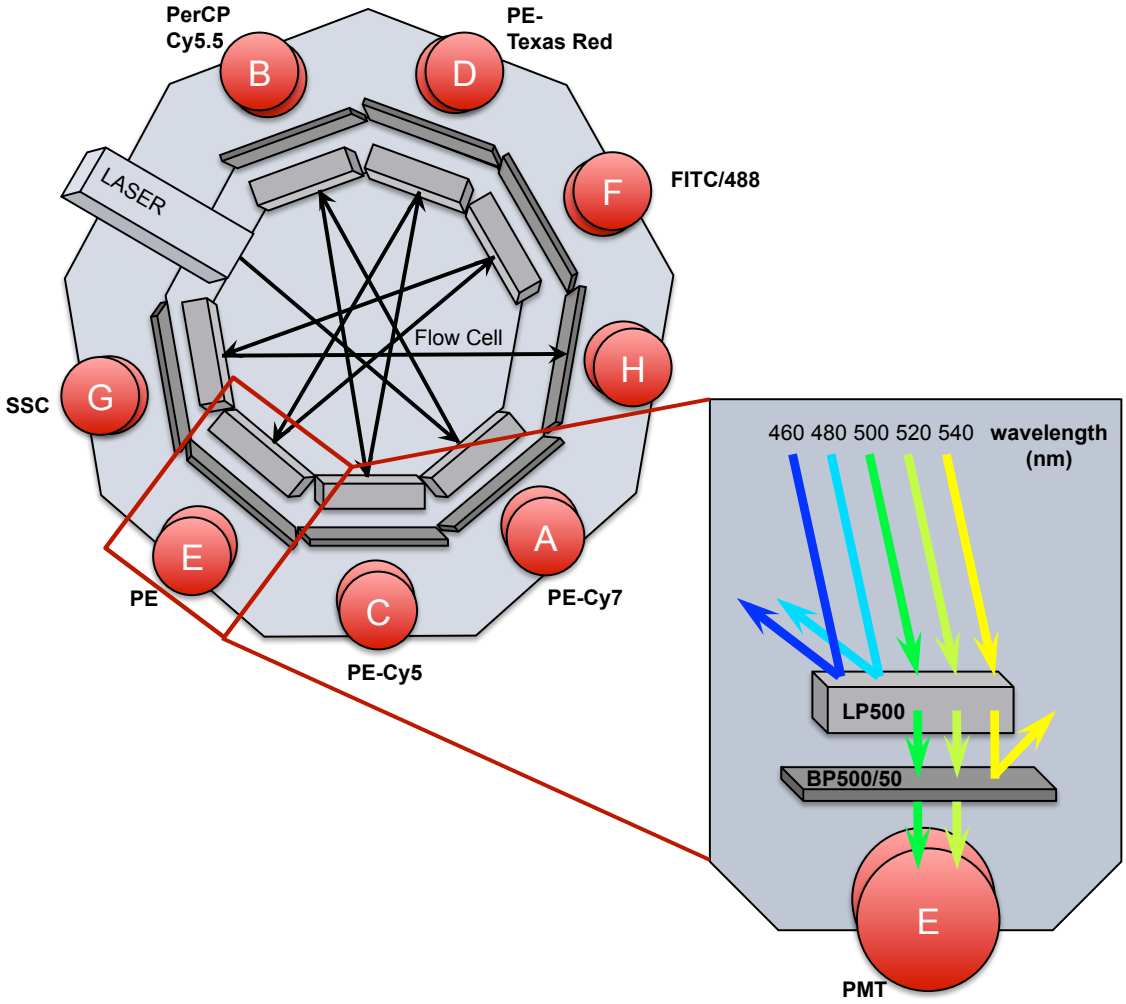

Figure 2.2.2 The laser and detector configuration of a BD LSR Fortessa flow cell. As a single cell passes into the flow cell it is interrogated via laser. The resulting optical signal generated by fluorescently-labelled cells is then detected by photomultiplier tubes (PMT) placed behind long-pass (LP) dichroic filters (inner rings) which redirect progressively shorter wavelengths to the next PMT, starting from PMT A. Band-pass (BP) filters (outer ring) transmit only a narrow spectrum of light allowing for a defined signal. The bandwidth of transmitted light is defined by specified numbers: Long-pass 500 filters only transmit wavelengths longer than 500nm and Band-pass filter 500/50 has a bandwidth of 50nm centred at 500nm wavelength. Finally, the narrowed optical signal is collected by the PMT and converted into an electronic signal. Figure adapted from BDLSR Fortessa product brochure accessed from the Biosciences website (2010).

2.2.2.1 Principles and Limitations of Flow Cytometric Analysis of Microparticles

The primary method used to detect and characterize microparticles in the published literature is flow cytometry. Microparticles in suspension are stained using antibodies raised against a specific antigen of interest and conjugated to a fluorochrome. The fluorescence intensity and the size of the particle are then measured using a flow cytometer.

During classical flow cytometric analysis, the suspension of cells is hydro-dynamically focused, which ensures single cells are measured individually. The size of cells is measured using a detector placed in line with the laser beam – the "forward scatter" – as particles larger than the wavelength of light produce a scatter predominantly in a forward direction (Figure 2.2.3). The granularity is a measure of the anatomy within the cell, as organelles are usually similar in size to the wavelength of light (>500nm), so they scatter light predominantly in a perpendicular direction. Thus, the size of the cell and its contents can be measured by analysis of both the forward- and side-scatter signals (Van der Pol, 2010, Nebe-von-Caron, 2009).

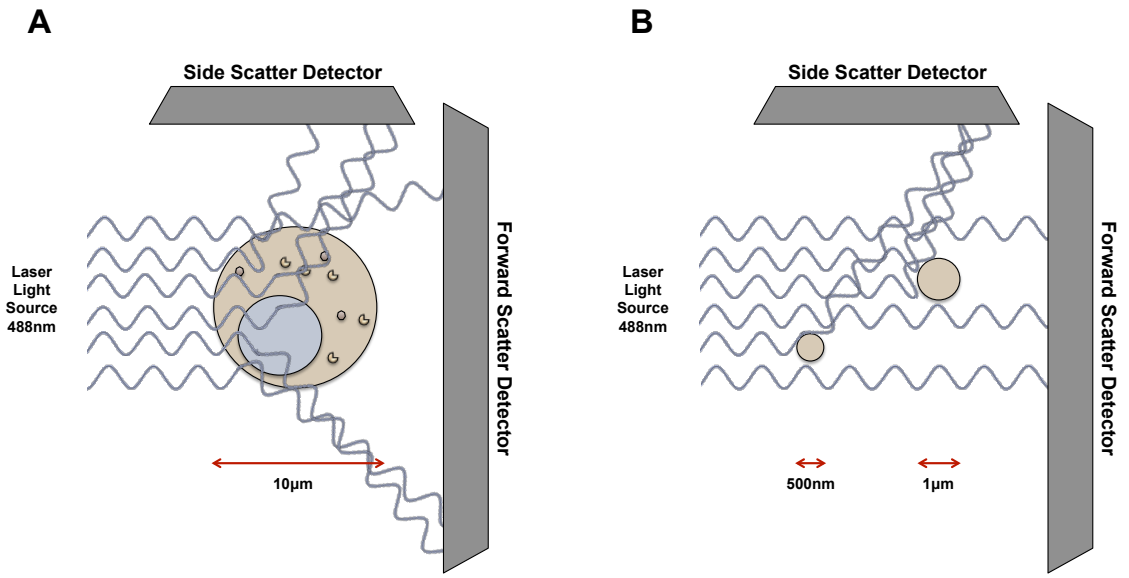

Figure 2.2.3 Light scattering of cells versus microparticles. (A) Cells passing through the laser beam scatter light in a forward direction, which can be used to approximate its size, and perpendicularly, which is collected by the sensitive side-scatter detector to produce a measure of granularity. This gives an indicator of the complexity of the cell's interior. (B) Microparticles are often smaller than the wavelength of light used to illuminate the sample and do not scatter light significantly in a forward direction. Forward scatter detection can therefore not be used to size microparticles. However, microparticles do scatter light in a perpendicular direction, and teamed with fluorescent labelling, can aid in microparticle detection and phenotyping.

Using flow cytometric analysis to obtain size information about microparticles, however, is difficult. The lower detection limit of the BD LSRFortessa is 500nm and for the BD FACScalibur around 400nm (BDLSR Fortessa brochure (2010)). The smallest polystyrene beads that can be detected by commercial flow cytometers are between 200nm and 300nm. However, as microparticles have a refractive index and scatter light approximately 10-fold less efficiently than polystyrene beads, the smallest single vesicles that can be detected using the forward scatter detector must be larger than 500nm (van der Pol et al., 2012). As microparticles range in size from approximately 100nm to 1μm, a significant proportion of the population is smaller than the lower detection limit of most cytometers (Van der Pol, 2010). The microparticles that fall below the detection limit of the forward scatter are then placed erroneously along the forward-scatter axis, thus discriminating between microparticles and noise using the forward scatter (as in most published literature) is not possible. Whilst fairly robust for the measurement of cells, the forward scatter detector also gives a variable signal between instruments, affecting reproducibility between institutes. It is the most alignment critical detector within the cytometer and can be affected by multiple variables, including mismatches in the refractive index between the sheath fluid and sample, beam geometry, polarisation, stop position and collection angle. The forward scatter position of microparticles of different sizes does not therefore follow their relative order in physical size. Furthermore, resolving two microparticles requires a difference in size between them of at least 280nm (Nebe-von-Caron, 2009). The paucity in accurate forward-scatter data collection can be demonstrated with the use of calibration beads (Figure 2.2.4). Although 1μm beads are placed with confidence in small discrete populations (Figure 2.2.4A), from forward/side-scatter plots of 500nm beads, “comet-tails” appear where the forward scatter is unable to size these beads accurately (Figure 2.2.4B).

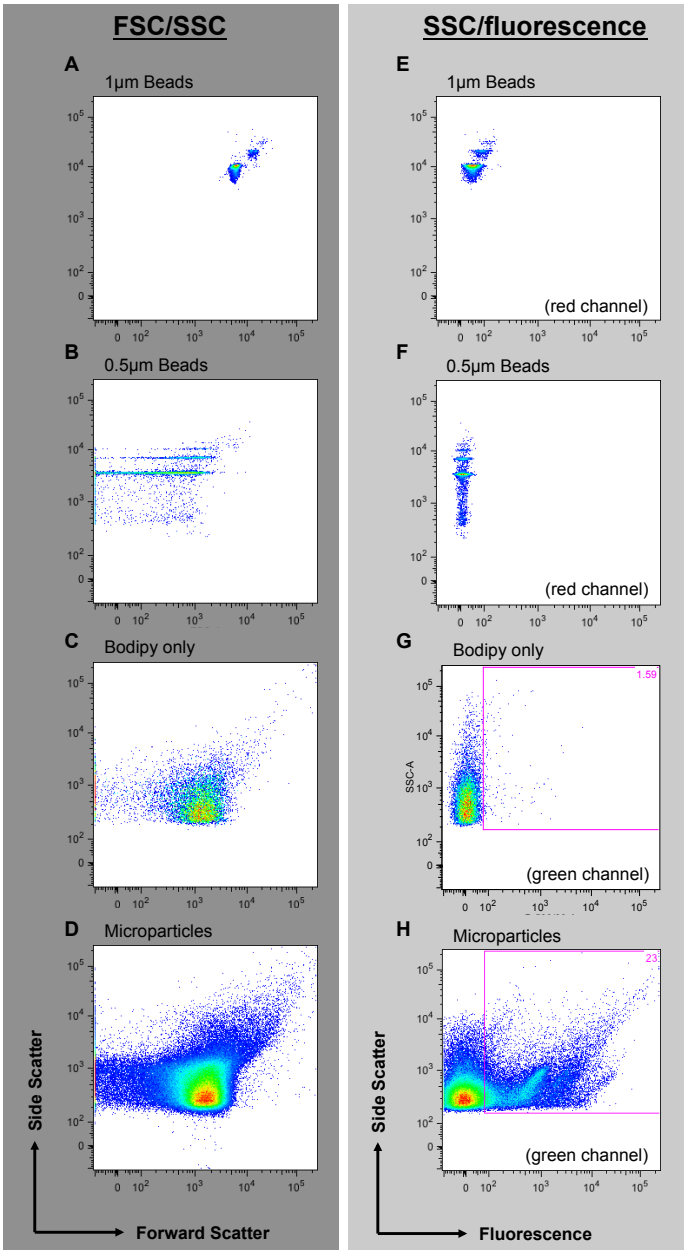

Figure 2.2.4 Comparison of the sensitivity of the Forward/Side scatter classical cytometry plots with the improved sensitivity Side scatter/fluorescence analysis. (A) The forward scatter of the BD LSR Fortessa is sensitive enough to resolve 1µm beads accurately, but not (B) 0.5µm beads. Thus, the presence of machine noise (C) overlaps with the (D) microparticle population using these plots. A more sensitive method is to use the fluorescence versus side-scatter, where (E) 1µm and (F) 0.5µm beads can both be resolved accurately, but due to brightness are viewed with the red laser. This removes (G) electronic instrument noise from the (H) positively stained microparticle population.

In contrast, side-scatter or "right-angled light scatter" (RALS, Figure 2.2.3) shows good correlation to size. This is because all instruments aim for maximal light collection and are therefore designed to achieve similar numerical apertures. This makes the side-scatter a more robust discriminator, especially between instruments (Nebe-von-Caron, 2009). Side-scatter information teamed with fluorescence labelling allows further discrimination between cell fragments, noise and true microparticles (Figure 2.2.4). Setting the axis parameters to side-scatter versus fluorescence allows the more accurate placement of 0.5µm beads (Figure 2.2.4F compared to B) and eliminates background noise from overlapping with the microparticle populations.

As microparticles expose antigens from their parent cell, fluorescence versus side-scatter analysis provides information on the biochemical composition of microparticles (Van der Pol, 2010). To achieve side scatter versus fluorescence plots, Bodipy-maleimide dye is employed to label the entire microparticle population. Bodipy-maleimide attaches to biological membranes via cysteine residues and thiol groups in proteins and its fluorescent nature enables its use in flow cytometry (Enjeti et al., 2008). The entire cytosolic compartment of cells and microparticles, and the membrane therefore become positively labelled. This dye does not allow exclusion of contaminating platelets, or cellular debris, apoptotic bodies or exosomes however, but allows the detection of biological particles from machine noise. Furthermore, membrane-labelling dyes such as PKH-26 are less suitable for microparticle analysis as the labelling reaction must be stopped by the addition of protein to the samples, usually serum or bovine serum albumin. This interferes with flow cytometric analysis of microparticle suspensions and generates high noise levels. These dyes are also incompatible with the polystyrene tubes used for ultracentrifugation, as these plastics irreversibly sequester the dye from the samples.

Fluorescence-associated cytometry does have its limitations as a method for detecting microparticles, even when using the side-scatter method for analysis. Firstly, accurate staining relies heavily on the properties and quality of the antibodies being used. Antibodies bind not only to their specific epitope, but also bind FC receptors on the surface of cells and microparticles and adhere to sticky proteins such as albumin and fibrinogen, or bind non-specifically. To control for this background fluorescence isotype antibodies are used. The isotype antibody is an irrelevant antibody of the same Ig type, bound to the same fluorochrome and added at the same concentration as the test antibody. By analysing the background fluorescence of the isotype antibody, any fluorescence above this background is considered antibody-epitope binding. Positive and negative samples are compared to the isotype control. However, the addition of antibodies in excess to microparticle samples can cause immunoglobulin aggregation, which appear as positively fluorescent signals within the cytometer. These immunoglobulin complexes are insensitive to detergent treatment, whereas microparticle-antibody labelling is sensitive. Therefore it is possible to subtract the fluorescence remaining after microparticle lysis to generate a true microparticle-epitope-bound fluorescence measurement. This issue is compounded by multi-labelling microparticles with multiple markers as these samples are not washed between staining incubations, and instead it is relied upon that positive-microparticles will appear above background fluorescence.

A second practical obstacle in the multi-labelling of microparticle samples is coincidence (Figure 2.2.5). The fluidics of flow cytometers is designed for passing single cells in a hydro-dynamically guided stream through the cuvette (Figure 2.2.5A). Isolated polymorphonuclear cells, as one example, occupy 630μm^3 (Ladinsky and Westring, 1967), whereas microparticles are much smaller, and occupy around 2-3μm^3 (see Figure 3.1.3 in Results). This results in non-optimal fluidics flow allowing multiple microparticles to be interrogated at one time, especially in concentrated samples, where false double or triple, or more, false-positive single events may be recorded (Figure 2.2.5B). Performing dilutions of the sample so that microparticles travel more rarely through the cuvette may aid in the reduction in coincidence (Figure 2.2.5C), but this significantly lengthens sample collection time, from experience, from around 5 minutes per sample, to over 20 minutes or more per sample.

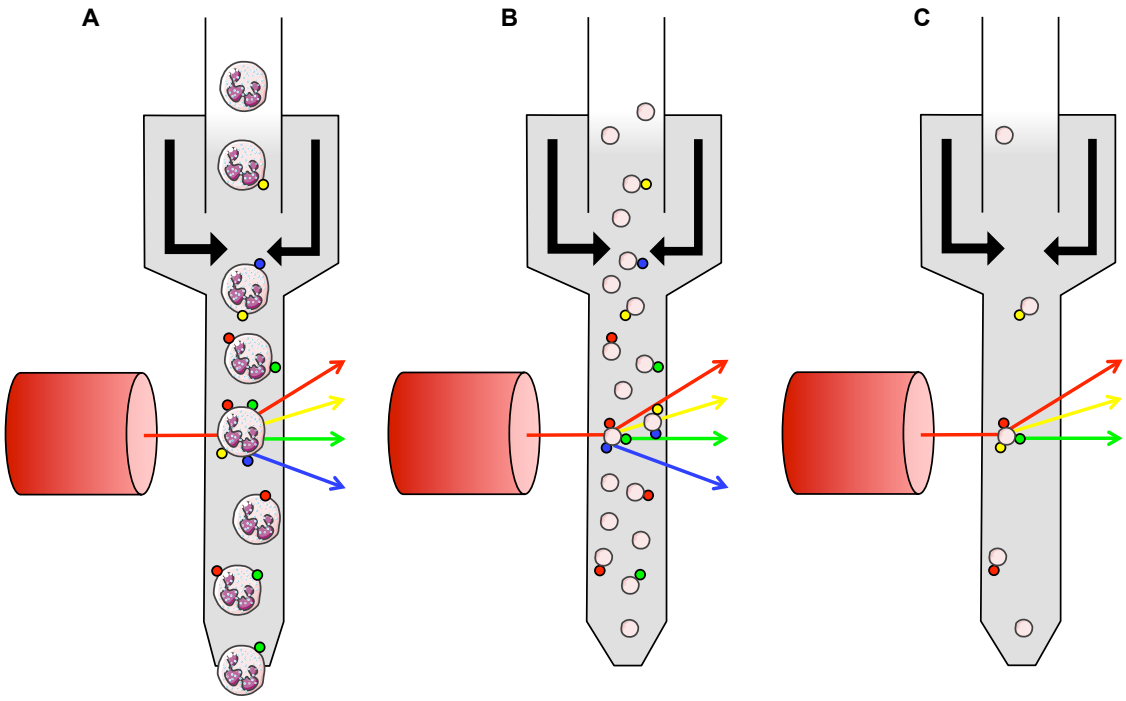

Figure 2.2.5 Coincidence within flow cytometry. (A) The fluidics of flow cytometers are designed to pass single cells through the flow cuvette for laser interrogation. (B) Microparticles are several orders of magnitude smaller than cells, and in concentrated samples, several microparticles may pass through the cuvette at once, generating false-positive signals. (C) Diluting the microparticle sample to ensure events are more rare may reduce coincidence.

Flow cytometers themselves require regular maintenance. Contamination from non-sterile sheath fluid or any microorganisms proliferating anywhere in the peripheral fluidics compartments of the flow cytometer (for example in tubing or tank-caps) significantly affects sample collection and analysis if they enter the sample line. A significant, sudden increase in machine noise can be indicative of this. By sterile-filtering and de-gassing the sheath fluid to remove small bubbles and impurities, and by deep-cleaning the cytometer before each use, noise can be minimised.

Although there may be limitations associated with the detection and characterization of microparticles using flow cytometry, there are many advantages to using this method. Not least is the availability, ease of use and relative low cost. By combining light-scatter measurements with that of fluorescence-labelling, accurate information about the biochemical composition, and cell of origin may be obtained, even if more sensitive equipment is required to elucidate detailed size measurements of microparticles. At present, analyses of microparticles have not been standardized. However, as this field of research progresses, it is hoped that the proposed side-scatter analysis method for microparticles will be more widely adopted.

2.2.2.2 Staining Microparticles for Characterisation by Flow Cytometry

All microparticle staining was carried out with double-filtered (0.22μm) sterile PBS. An aliquot (10 μl) of the microparticle suspension was stained using purified antibodies against α_2-macroglobulin, ceruloplasmin, Annexin A1 or heat shock protein 70 (see Table 2.1.1) for 30 minutes in the dark on ice before the addition of AlexaFluor 594-conjugated secondary antibody. The secondary antibody was incubated for 30 minutes in the dark on ice, followed by the addition of CD66b PE-conjugated antibodies for 20 minutes in the dark on ice. Immediately prior to running, Bio-maleimide dye (2.5μM) was added to label the entire microparticle population.

The structure and components of the microparticles were also investigated using specific labelling: Annexin V binding was used to assess phosphatidylserine expression and phalloidin was used to investigate the presence of cytoskeletal remnants. For Annexin V binding, microparticle aliquots (10μl) were diluted in 10μl 2x calcium binding buffer. This allows the calcium-dependent binding of the Annexin V to any exposed phosphatidylserine on the microparticle. Fluorescently conjugated Annexin V (5μl) alongside CD66b was then added to the microparticles for 20 minutes in the dark at room temperature to allow Annexin V binding to occur. For phalloidin staining, the addition of CD66b for 20 minutes in the dark on ice was followed by the

addition of Alexa546-conjugated phalloidin (final 0.01U/ml) for 10 minutes in the dark at room temperature. Immediately prior to running, Bio-maleimide dye (2.5μM) was added to label the entire microparticle population. Microparticle suspensions were not washed during preparation for flow cytometry to prevent loss of microparticles during this process.

As MRP8 and MRP14 antibodies had not been used previously, titration of the antibodies was performed on human neutrophils to determine the optimum concentration (Figure 2.2.6). Antibodies were tested at various dilutions with permeabilised neutrophils (see section 2.3.2.2 for permeabilisation protocol) for 30 minutes at room temperature before acquisition using a BD LSRFortessa. Final concentrations of 20μg/ml for MRP8 and 10μg/ml for MRP14 were selected as they had the highest signal-to-noise ratio. These concentrations were then used to stain microparticles, for 30 minutes at room temperature before the total population of microparticles was labelled with Bodipy-maleimide and CD66b.

Triple staining was carried out on each set of microparticles (i.e. antigen of interest plus CD66b and Bodipy-maleimide). Enumeration of microparticles is possible if the fluorescent staining appears above background and if the flow rate is known. The number of microparticles appearing Bodipy-maleimide medium to high and side-scatter positive was multiplied by the volume of sample measured, calculated from the flow rate, which if run on low equates to 12μl per minute.

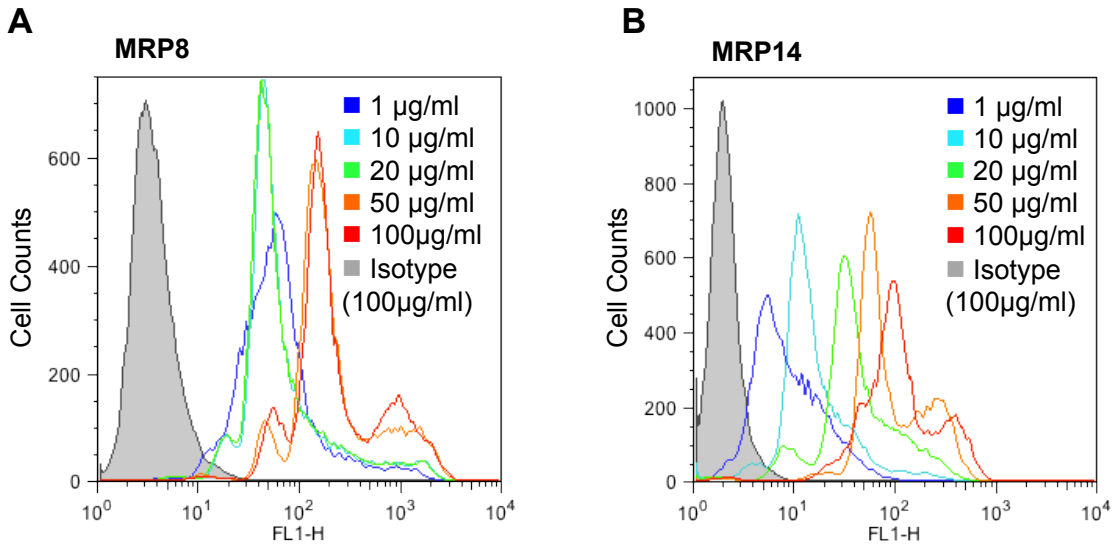

Figure 2.2.6 Antibody titration of MRP8 and MRP14. Increasing concentrations of antibody were tested to find optimum binding of (A) MRP8 and (B) MRP14 in permeabilised neutrophils. 10μg/ml was selected for MRP8 and 20μg/ml for MRP14.

2.2.2.3 Acquisition of Microparticles by Flow Cytometry

All microparticle sample acquisition was performed using a BD LSRFortessa with trigger set on side-scatter, with a voltage of 400V, gain of 1 and a threshold of 200 (as low as possible). 10,000 events that were double positive for both CD66b and Bodipy-maleimide were collected in order to calculate percentage positive microparticles and their mean fluorescence intensity. As a low threshold was applied to forward or side-scatter detectors, electronic, fluidic and optical noise contributed significantly to the events seen.

Events were analysed using FlowJo software, reapplying gates where necessary. Scatter plots of microparticle fluorescence signals in one channel plotted against fluorescence signals of another (for example, CD66b versus Bodipy-maleimide) do not form characteristic populations as seen in flow cytometric analysis of cells, as the fluorescence of a microparticle is a function of its size. Therefore, a highly positive microparticle with a small size will still only fall in the low-end of the Bodipy-maleimide fluorescence. Careful positive and negative gating was applied so that false-positive and false-negative results were not generated (Figure 2.2.7).

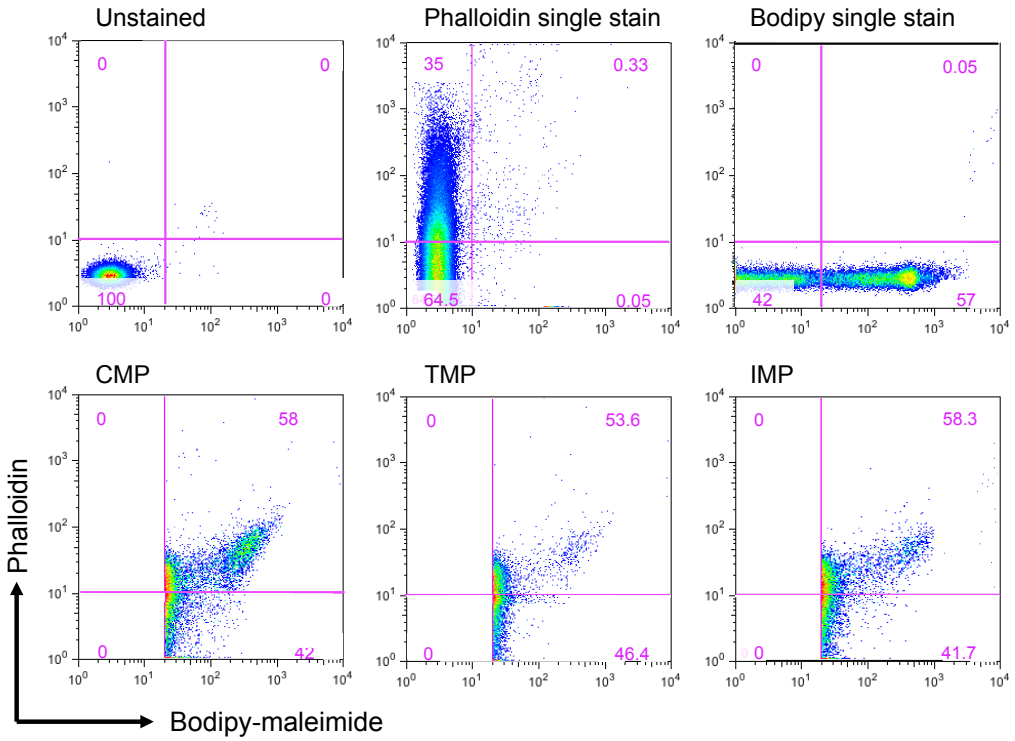

Figure 2.2.7 Determination of double-positive gates requires careful consideration. Unstained, phalloidin single-stained and Bodipy-maleimide single stains are used to set correct gates for double-stained microparticle samples. CMP, control microparticles, TMP, TNF-α microparticles and IMP, IL-8 microparticles.

2.2.3 ImageStream^{x} mk. II Analysis of Microparticles

We have recently gained access to a high sensitivity imaging cytometer, the Amnis Imagestream^{X} mk. II (ISX). This cutting edge instrument uses charge-coupled devices instead of PMTs and captures up to 12 images of each event as it passes through the flow cell. The machine was designed to allow the co-localisation of subcellular particles within cells and is equipped with a X60 objective in order to do this, and is subsequently amenable to microparticle detection and analysis. Acquisition parameters can be determined by a huge variety of physical parameters rather than just size, complexity and fluorescence intensity. In terms of microparticle research, this analyser represents important advancements in sample detection and measurement. Firstly, each event recorded is paired with a bank of images generated for each single event. Dot plots and image galleries are therefore searchable and can be used to corroborate event identity by eye. Furthermore, multicolour staining can be used for accurate identification of various subpopulations.

We have tried to define the lower limits of measurement parameters using commercially available sizing beads, 1μm, 0.5μm and 0.1μm in size (Figure 2.2.8). These could be placed confidently using their fluorescence intensity, but sizing according to area or diameter measurements were somewhat less useful, even when measured using the fluorescence channel. This is because, at such high magnification, a pixel still represents an area of 0.3μm^2, which is a large proportion of a 0.5μm diameter bead or microparticle. The masking applied to the fluorescence channel also requires alteration from the default setting to ensure stringent measurements can be made.

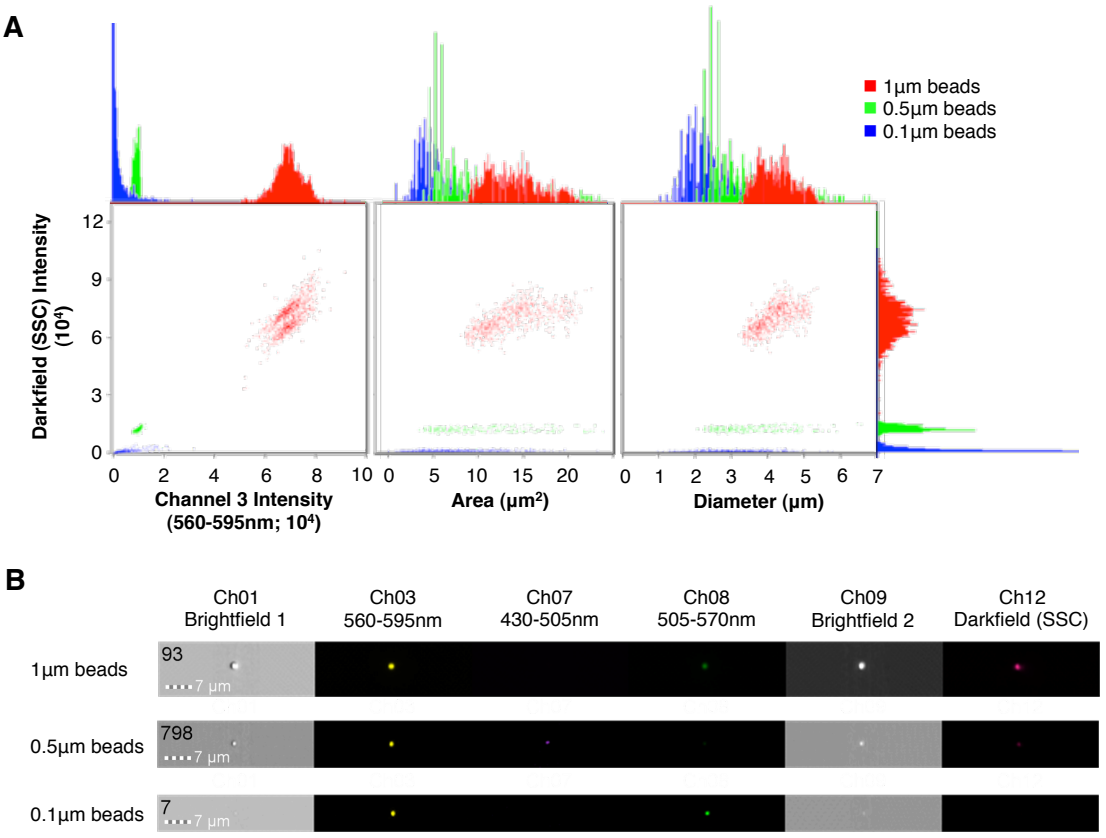

Figure 2.2.8 Detection of various sized calibration beads using the ImageStream^X mk. II imaging cytometer. Latex fluorescent calibration beads, 1µm, 0.5µm and 0.1µm in size were analysed using an ImageStream^X imaging cytometer. (A) Beads could be detected and separated according to size using fluorescence intensity and area and diameter measurements plotted against side-scatter. (B) Beads were visible in the fluorescence channels, but not always on the brightfield channel. Ch, Channel.

2.2.3.1 Generation of Microparticles for Analysis with ImageStream^X

For ImageStream^X analysis, it was not necessary to remove neutrophils from the supernatant to analyse the microparticle population. In this way it was possible to prepare isolated neutrophils and stimulate them immediately prior to microparticle acquisition to determine the rate at which microparticles are generated. To do this, freshly isolated neutrophils were resuspended at 1 x 10^6 cells per millilitre in phenol red-free RPMI and labelled with Bodipy-maleimide dye (2.5μM) 2 minutes prior to sample acquisition, then the sample loader lowered. TNF-α (50ng/ml) was added immediately prior to placing the eppendorf into the sample loader and loading. Acquisition of events was started immediately, and the events appearing in the microparticle population gate collected on low for 45 minutes (see section 2.2.3).

To assess microparticle number using IS^X analysis, pre-prepared microparticles were placed in a 1.5ml eppendorf after removal from -80°C and quick thawing to 37°C. Bodipy-maleimide (2.5μM) was added immediately prior to acquisition. Alternatively, freshly isolated, live neutrophils were stained with Bodipy-maleimide (2.5μM) then stimulated immediately prior to acquisition.

The instrument and INSPIRE software were set up as follows: Channels 01 (bright field), 02 (green fluorescence), 03 (spill-over from green fluorescent channel allowing visualisation of over-saturated Bodipy-maleimide loaded cells), 06 (bright field 2) and channel 12 (scattering channel) were made active, plus any other fluorescence channels required. Magnification was 60X, providing a pixel size of 0.3μm^2 and the lasers 488 and 745 activated for fluorescence and side-scatter, respectively; with or without 405 and 642 laser activation. The flow rate was set to low speed/high sensitivity and stream alignment was adjusted where necessary. To obtain a collection gate, a scatter plot of channel 02 fluorescence intensity was plotted against channel 12 (side scatter) signal intensity. This allows discrimination of speed beads, which are used as an internal calibrator for the machine's image capture system to determine the flow rate. These speed beads run continuously throughout both sample collection and while the machine is idle, but can be completely excluded from microparticle analysis as they form a discrete high-scatter intensity, low channel 02 fluorescence intensity population (Figure 2.2.9). Bodipy-maleimide labelled microparticles appear as a low-scatter, low to mid fluorescence intensity, and any contaminating cells appear as high fluorescence intensity (Figure 2.2.9 right hand panels). Each gated population was interrogated via the image gallery to determine the upper and lower limits of microparticle size and shape. Microparticles characteristically appear as small,

spherical green-fluorescent points, and can be discriminated from cells, which are much larger, or cellular debris, which is not uniformly spherical. Furthermore, coincidence, or the appearance of more than one microparticle in an image, does not skew analysis as it does with flow cytometry and the gates containing coincident microparticles may be included or excluded in the analysis.

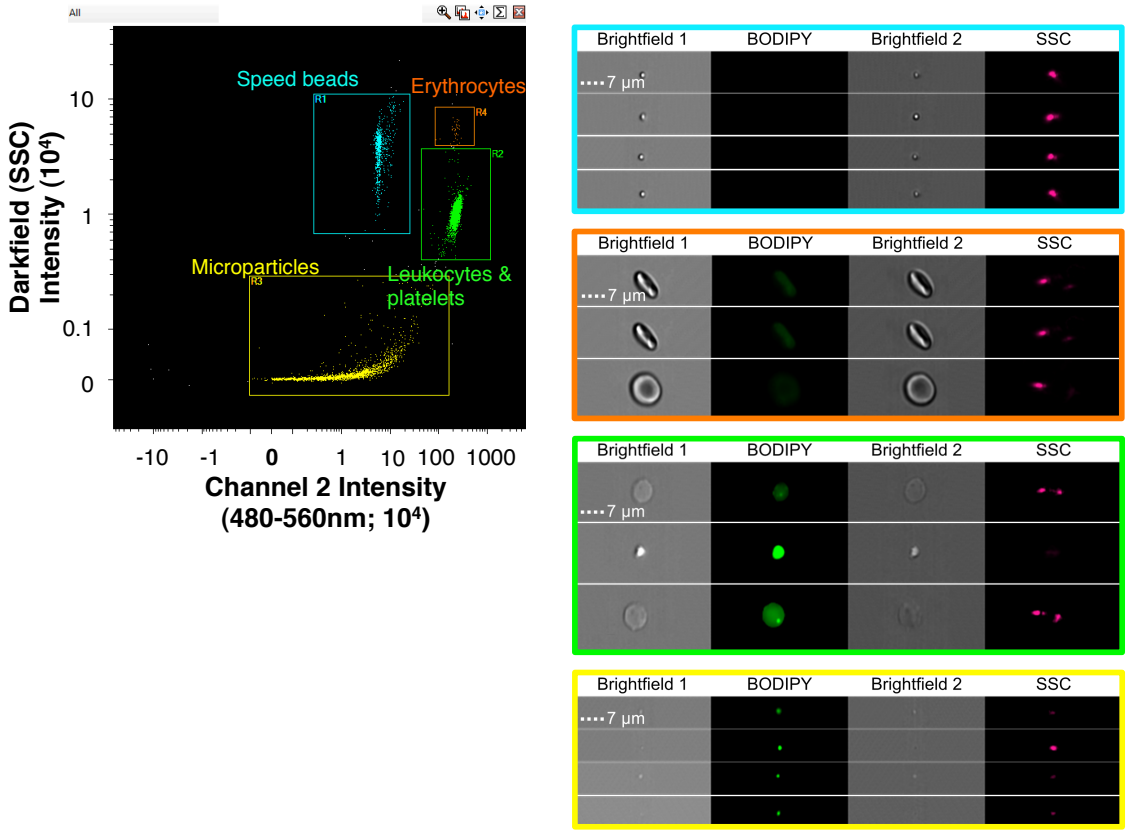

Figure 2.2.9 Acquisition of TNF-α-stimulated neutrophil samples allows differentiation between contaminating cells and microparticles. Acquisition of samples using a scatter plot of side-scatter (SSC; dark field) versus Channel 02 intensity allows for the accurate discrimination of microparticles from contaminating neutrophils, platelets, erythrocytes and speed beads when Bodipy-maleimide stain is used. Right hand panels show representative gallery images of events residing in each of the different colour-coded gates.

For real-time neutrophil microparticle generation experiments (see 2.2.3.1), the upper collection event gate was set to $1x10^6$ to prevent premature termination of sample acquisition. For simple enumeration of pre-prepared microparticle samples, the acquisition cut-off was set to 10,000 to prevent sample wastage. To determine the concentration of the sample, IDEAS software was used. Raw image files with the entire number of events were opened. A scatter plot showing channel 02 fluorescence intensity plotted against scattering intensity of channel 12 was generated and a microparticle gate re-applied and inspected visually to exclude inappropriate events. The gate was adjusted where necessary. The objects/mL feature was added to the analysis area, and applied to the microparticle gate under the channel 02 fluorescence trigger, after the default area mask had been adjusted to around 75%. This was more sensitive at capturing microparticles than the bright field as significant haloing contributes to the sample fluorescence, augmenting the signal. Other parameters, such as diameter and perimeter were determined by addition to the features list, after adjusting the mask in channel 02 to fit tightly around the event. To analyse the number of microparticles generated over the 45-minute sample acquisition, all events falling in the microparticle gate were plotted on a scatter graph showing time versus objects/sec or time versus objects/ml. Each plot was manually adjusted so that the machine noise generated at the beginning of acquisition was set to zero, allowing determination of the rate of microparticle production over time, regardless of the number of microparticles that were already present within the sample.

2.2.4 *In Vitro* Cartilage Models

2.2.4.1 Culture of C28/I2 Chondrocyte Cell Line.

The C28/I2 cell line was originally generated by immortalisation of primary human juvenile rib cartilage chondrocytes with simian virus-40 transfection, selection on agarose and expansion in serum-containing medium. These cells express type II collagen, one of the most labile features of cultured (primary and immortalised) chondrocytes, and produce matrix that reacts with antibodies to type II collagen, large proteoglycan and sulphated glycosaminoglycans. They also exhibit decreased expression of type II collagen and increased expression of matrix metalloproteinases (MMPs) in response to IL-1β stimulation (Goldring et al., 1994), reminiscent of the true chondrocytic phenotype.

Cells were cultured in Dulbecco's modified Eagle medium (DMEM) containing high glucose (4.5g/litre; PAA) supplemented with 10% non heat-inactivated foetal calf serum and 1% penstrep (complete medium) during monolayer culture. C28/I2 cells were cultured to confluence before subculture. Flasks were rinsed with PBS to remove any serum, and cells were detached with 0.25% warm trypsin/EDTA (Gibco, Invitrogen). Once cells had rounded and detached, the trypsin was deactivated by the addition of an equal volume of complete medium. Cells were resuspended in 30ml complete medium and transferred to new flasks (10ml per T75 flask) to achieve a 1:3 subculture. Cells were used between passage 3 and 20 for micromass culture.

2.2.4.2 Generation of C28/I2 Chondrocyte Micromass Cultures

C28/I2 can be differentiated into matrix-producing chondrocytes when cultured in high density and serum free conditions (Figure 2.2.10) (Greco et al., 2011). Confluent C28/I2 in monolayer (Figure 2.2.10A) were trypsinised with 0.25% trypsin-EDTA for 3 minutes at 37°C, collected in 10ml complete medium then centrifuged for 10 minutes at 400 x *g* before being resuspended in 5ml complete medium for counting. If required, cells were centrifuged a second time (400 x *g*, 10 minutes at room temperature) and resuspended to a volume of 2.5 x 10^7 cells/ml in complete medium. Using a reverse displacement Gilson pipette, 20μl of the thoroughly mixed cell suspension was placed into individual wells of a 48-well plate, so that the surface tension allowed a rounded drop to be formed on the floor of the well (Figure 2.2.10B). The 48-well plates were pre-filled with sterile PBS around the periphery to prevent evaporation of the medium containing the cells (Figure 2.2.11). Plates were carefully transferred to an incubator

without disrupting the pellets and cells were left to adhere for 3 hours at 37°C in 5% CO_2. After the 3-hour period, 2ml complete medium was added very slowly to each well, taking care not to dislodge the delicate cell pellet (Figure 2.2.10D). After 24 hours the medium was replaced with 1ml chondrocyte differentiation medium (serum free, phenol-red free RPMI containing 1% insulin/transferrin/selenium (ITS) supplement) and cells were treated 24 hours later.

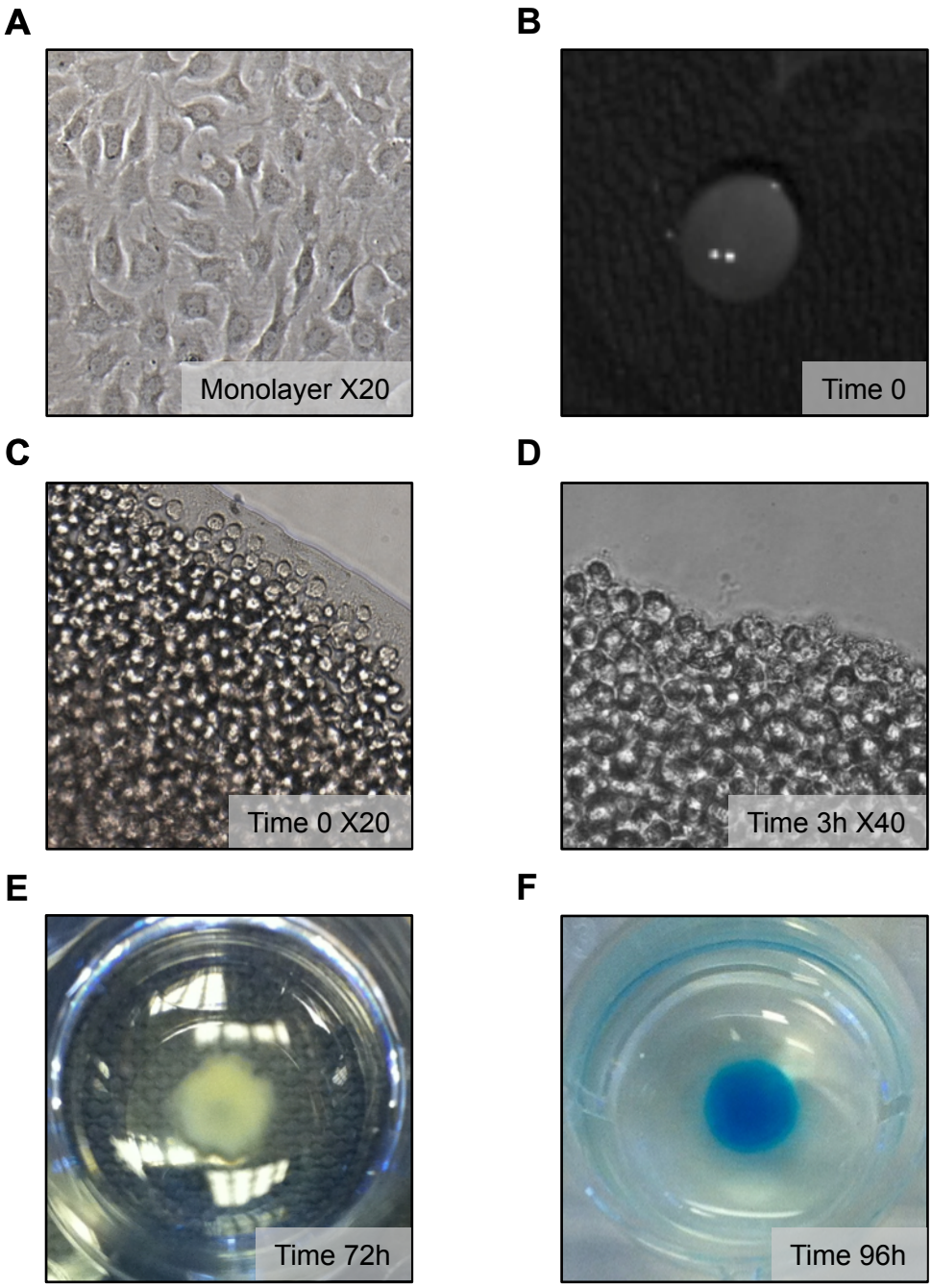

Figure 2.2.10 C28/I2 Micromass generation. (A) Confluent cells in monolayer were harvested and (B, C) reseeded at high density (5 x 10^5 cells in 20μl). (D) At 3 hours cells retained their spherical morphology and medium was added. Following 24-hour serum starvation and ITS supplementation, micromasses were stimulated for 24 hours. (E) micromasses were fixed then (E) proteoglycan content was quantified by Alcian blue staining.

Micromasses were treated with recombinant human IL-1β or TNF-α with or without CMP, TMP or IMP or Annexin A1-null TMP or wild type mouse TMP at the concentrations indicated. For FPR antagonist experiments, WRW_4 or CycH (10μM each) were added 10 minutes before stimulation. Recombinant ceruloplasmin and lactoferrin were added for 24 hours at various concentrations, diluted in PBS. Resolvin D1, stored in ethanol, then diluted in PBS was added for 24 hours at various concentrations. For TGFβ blocking experiments, TGFβ neutralising antibodies (see Table 2.1.1) were added (20μg/ml) at the same time as stimulation for 24 hours. Apoptosis experiments were performed as described in section 2.3.4. During neutrophil-transwell separation experiments, neutrophils were treated with or without cytoskeletal-altering drugs as described (see section 2.2.1.3) and treated with TNF-α for 10 minutes prior to addition to transwells with various pore-sizes placed above micromasses that had been stimulated with IL-1β (30ng/ml) for 1 hour. Transwells were removed 4 hours later, and micromasses fixed for Alcian blue staining at 24 hours. For RNA analyses, micromasses were stimulated for 6 hours, for westerns of unphosphorylated proteins, 24 hours, and for signalling westerns, for the times indicated. For Annexin V coated microparticles, see section 2.2.1.4.

Cells formed a visible gel-like matrix under serum-free conditions by 72 hours (Figure 2.2.10E), which could be stained with Alcian blue dye (Figure 2.2.10F). Micromasses were stimulated for a total of 24 hours for Alcian Blue dye measurement, or for 6 hours for PCR. All supernatants were collected and stored at -80°C for Prostaglandin E_2, cytokine or proteoglycan analysis.

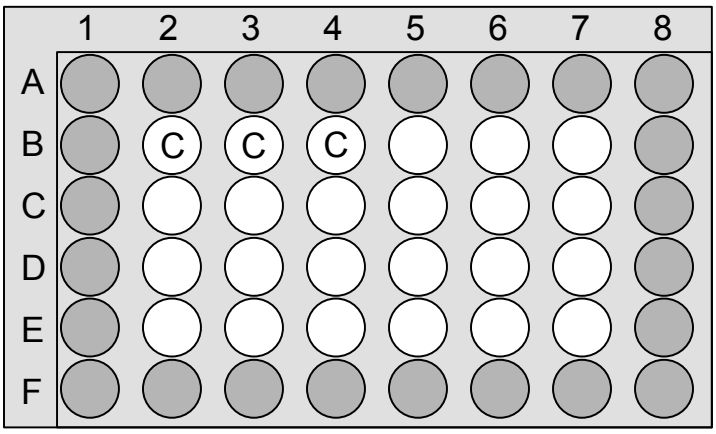

Figure 2.2.11 48-well plate plan for micromass culture. Grey outer circles represent wells filled with PBS prior to micromass seeding to prevent evaporation of the low volume of culture medium (20μl) during the 3-hour adhesion stage. C represents wells that act as control for every plate of micromasses seeded to prevent inter-plate variation.

2.2.4.3 Generation of Micromasses Using Adult Human Articular Chondrocytes

To determine whether results observed with C28/I2 chondrocyte micromasses were reflective of human primary chondrocyte cultures, primary adult human articular chondrocytes were purchased from Lonza. Cells were cultured in the recommended commercially available medium and cultured in monolayer before high-density micromass culture (Figure 2.2.12).

Cells were cultured to confluence in primary chondrocyte growth medium (growth medium; LonzaCC-3216; complete; containing 10% non heat-inactivated foetal bovine serum (FBS), 1% penstrep, insulin-like growth factor-1 (IGF-1) 0.2%, basic fibroblast growth factor (bFGF) 0.5%, transferrin 0.1%, insulin 0.2%) before subculture. Flasks were rinsed with PBS to remove any serum, and cells were detached with 0.25% warm trypsin/EDTA (Gibco, Invitrogen). The trypsin was deactivated once cells had rounded and detached by the addition of an equal volume of trypsin deactivation solution (Lonza). Cells were resuspended in 30ml complete medium (in total) and transferred to fresh flasks (10ml per flask) to achieve a 1:3 subculture. Cells were used between passage 2 and 8 for micromass culture.

Confluent monolayers (between passage 2 and 8) were detached with 0.25% trypsin-EDTA for 3 minutes at 37°C then centrifuged for 10 minutes at 400 x *g* before being resuspended in 5ml growth medium for counting. If required, cells were centrifuged a second time (400 x *g*, 10 minutes at room temperature) then resuspended to a volume of 2.5 x 10^7 cells/ml in primary chondrocyte growth medium. Micromasses were plated as in section 2.2.4.2. After the 3-hour period, peripheral cells were checked for adhesion (Figure 2.2.12F) and 2ml primary chondrocyte differentiation medium (with 10% serum, containing IGF-1 0.2%, bFGF 0.5%, Transferrin 0.1%, Insulin 0.2% and TGF-β1 0.5%; LonzaCC-3225) was added very slowly to each well, taking care not to dislodge the delicate cell pellet. After 24 hours the medium was replaced with 1ml primary chondrocyte differentiation medium (serum free, containing IGF-1 0.2%, bFGF 0.5%, transferrin 0.1%, insulin 0.2% and TGF-β1 0.5%) and cells were treated 24 hours later. Under resting conditions cells generated matrix that could be stained with Alcian blue (Figure 2.2.12G) and retained their spherical morphology throughout the culture, indicative of their chondrocytic phenotype (Figure 2.2.12H). These chondrocyte micromasses produced a lower absolute concentration of sulphated proteoglycans, reflected by a reduced Alcian blue staining intensity. Thus, a lower range of Alcian blue standards and also DNA standards were required to normalise data. In addition,

instead of 3 replicates per plate to generate n=1 as with C28/I2 chondrocyte culture, it was necessary to increase the replicates to 4 to generate less variable data.

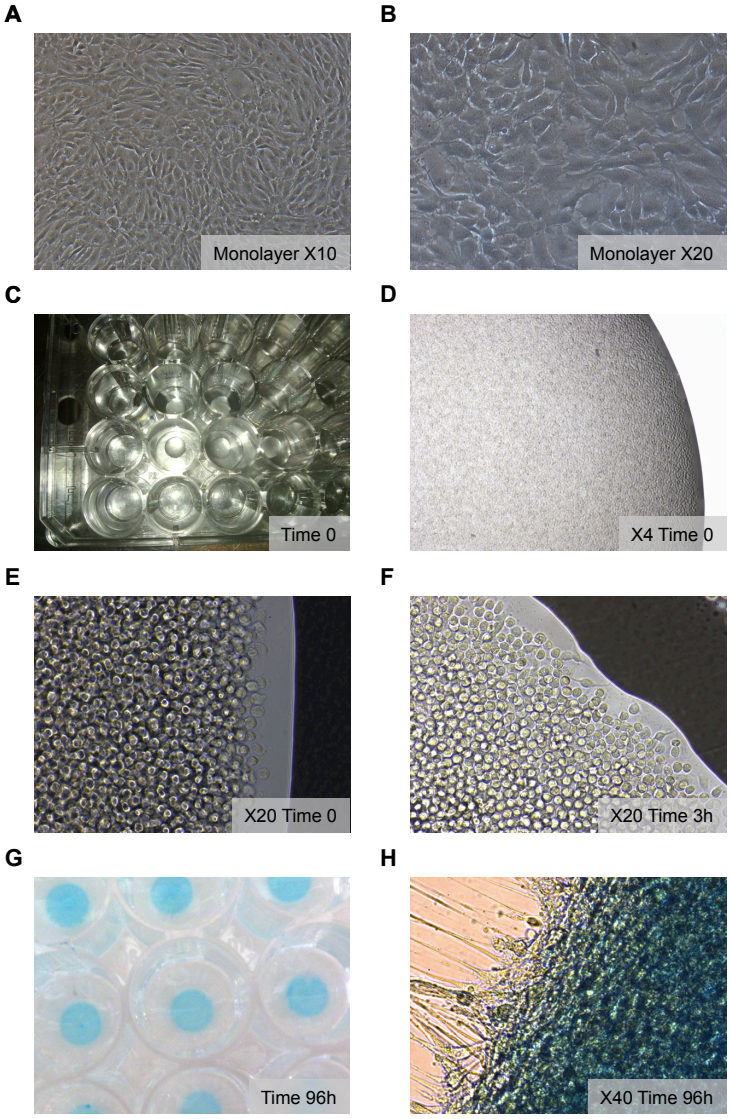

Figure 2.2.12 Generation of micromasses with adult human articular chondrocytes. (A) Chondrocytes were cultured to confluence and used between passage 1 and 5. (B) Cells appeared more complex and fibroblastic than C28/I2 chondrocytes. (C) Cells were seeded in high density (500,000 cells in 20μl), (D) formed homogenous suspensions and (E) were spherical in shape. (F) At three hours cells had adhered, and retained their spherical morphology in high-density areas. (G) By 72 hours, cells had generated matrix that stained with Alcian blue dye and (H) still retained their spherical morphology, indicating chondrocytic phenotype.

2.2.4.4 Alcian Blue Staining

For semi-quantitative analysis of cartilage-specific sulphated glycosaminoglycans (sGAGs) a method using Alcian Blue stain, optimised by De Bari et al. (2001) was employed. Alcian blue stains highly sulphated GAGs within the cartilage specifically at pH 0.2, but does not bind DNA, as this requires higher pH levels. After supernatant collection, micromasses were fixed in 4% glutaraldehyde (v/v in dH_2O) for 15 minutes at room temperature followed by acidification by rinsing with 500μl 0.1N hydrochloric acid. 400μl of Alcian Blue 8GS dye at pH 0.2 (1% Alcian Blue 8GS in 0.1N HCl) was added and micromasses incubated overnight at room temperature. Micromasses were rinsed once with 0.1N HCl and any remaining unbound dye was removed by repeated washing with PBS. Dye (and DNA) was extracted from the matrix using a 6M guanidine hydrochloride for 72 hours. The extracted dye was measured in a flat-bottomed 96-well plate at 620nm using a Multiskan Bichromatic 348 spectrophotometer (Labsystems, Finland) and the concentration was interpolated from known-concentration Alcian Blue standards (top standard 250μg/ml Alcian Blue in guanidine hydrochloride for C28/I2 micromasses, Figure 2.2.13A; top standard for primary adult human articular chondrocytes was 62.5μg/ml Alcian blue, Figure 2.2.13B).

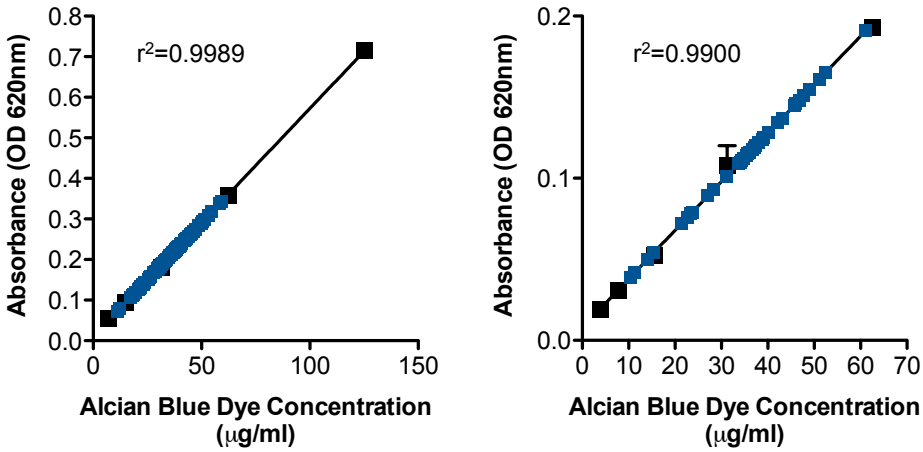

Figure 2.2.13 Alcian Blue standard curve. Alcian blue was dissolved in guanidine hydrochloride and serial dilutions were performed to generate standard curves. (A) A higher concentration range was used for determining Alcian blue dye content in C28/I2 micromasses. (B) A lower concentration range was used for determining Alcian blue dye content in primary adult human articular chondrocyte micromasses. Blue points show data interpolation from representative experiments.

2.2.4.5 Normalisation of C28/I2 Chondrocytes Micromasses

Although micromass culture of C28/I2 cells allows the reproducible assaying of chondrocyte matrix accumulation, significant variability was encountered between plates, or when serum-free or serum-supplemented medium was used. To avoid inter-plate variation, each 48-well plate (Figure 2.2.11) contained 3 wells reserved strictly for the determination of control matrix accumulation. By transforming data to percentage change from these control wells ensured that variation introduced by uncontrollable outside factors, such as humidity, temperature, surface tension of the droplet, electrostatic charge of the plate or passage number did not interfere with overall matrix content observations, especially in experiments performed over a number of weeks. Furthermore, by normalising to cell number rather than protein content, made the data more reproducibly robust. Early attempts at normalisation of chondrocyte micromasses to protein content by bicinchoninic acid (BCA) assay (Pierce) were unsuccessful, for three reasons. Firstly, the extracted dye interfered significantly with the colourimetric analysis by spectrophotometer (Figure 2.2.14), leading to inaccurate results. Second, the dye extractions were not sufficiently high in protein for the assay to determine sensitively the protein extracted and third, the 6M guanidine solution in which the dye is extracted is not recommended for BCA assay and reduced sensitivity further.

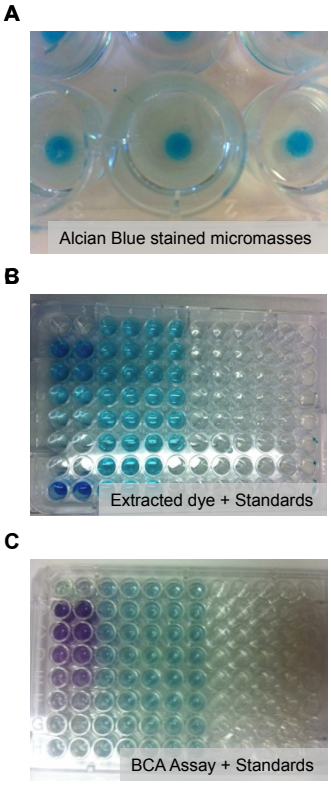

Figure 2.2.14 BCA Assay of dye/protein extractions from C28/I2 chondrocyte micromasses is affected by the inherent dye content. (A) Micromasses cultured for 72 hours were fixed and stained with Alcian blue dye. (B) Dye was extracted with 6M guanidine hydrochloride and measured spectrophotometrically. (C) Normalisation by BCA assay was not accurate due to the presence of the dye.

2.2.4.6 Normalisation of Micromass Alcian Blue Dye Content to Cell Number Using SYBRgreen Dye

The quantification of DNA was used to more accurately interpolate the approximate cell number from the guanidine dye extractions. Detection of double stranded DNA by the addition of SYBRgreen I dye (Invitrogen) is not affected by the presence of the Alcian blue and can be measured from a very small amount of dye extract. To normalise the results to cell number, 5μl of the extracted dye solution was removed and added to 1μl 100X SYBRgreen dye and 94μl Tris-EDTA. Fluorescence was measured using a TECAN M200 spectrophotometer (Tecan, Mannedorf, Switzerland) in a flat-bottomed black plate at 485/535nm and again, concentration was interpolated from a known standard curve plotted by measuring the fluorescence of genomic DNA standards. C28/I2 micromasses contained a larger amount of DNA and required a standard curve with a higher uppermost standard of 800μg (Figure 2.2.15, left panel). Standards were assayed in duplicate. Primary adult human articular chondrocyte micromasses contained a smaller amount of DNA, therefore lower standards in triplicate were assayed to generate a standard curve (Figure 2.2.15, right panel). Results were used to generate absolute sGAG concentrations, and are expressed as percentage change from control.

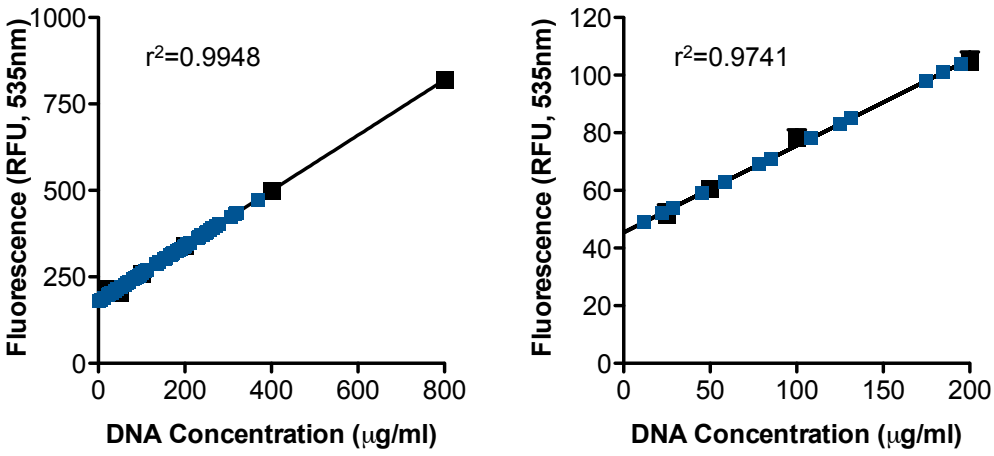

Figure 2.2.15 DNA quantification standard curve. Standard curves were generated using known concentrations of genomic DNA and quantified by SYBRgreen fluorescent dye. (A) C28/I2 C28/I2 micromass DNA was of a higher concentration and required a standard curve with a larger range with higher concentrations, performed in duplicate. (B) Primary adult human articular cartilage DNA was of a lower concentration and required a smaller range of low concentrations, which were performed in triplicate. Blue points show data interpolation from representative experiments.

2.2.5 *Ex Vivo* Cartilage Models

2.2.5.1 Generation of Rat Primary Chondrocyte Micromasses

Due to the expense and low passage capacity of human primary adult human articular chondrocytes, an alternative source for primary chondrocyte culture was explored. Rat femoral heads were collected (2 per donor), washed extensively with PBS and then minced before being placed in 50ml falcon tubes in 6ml DMEM high glucose supplemented with Collagenase type 2 (0.01%) for 18 hours in a water bath set at 37°C and equipped with a rocker. The resulting cell suspension was passed through a 70μm filter to remove cartilage pieces, and the cells were cultured in T25 culture flasks in DMEM high glucose supplemented with 10% FBS. Given the limited number of chondrocytes obtained, cells were not counted before plating, but instead allowed to expand for 3 days with half the medium changed each day. Cells had the characteristic cobblestone morphology of C28/I2 human chondrocyte cells in monolayer culture (Figure 2.2.16A). Micromasses were generated as described in section 2.2.4.2 (Figure 2.2.16).

Unfortunately, isolated rat chondrocytes did not generate sufficient matrix and did not stain intensely enough with Alcian blue to allow reproducible quantification (Figure 2.2.16H).

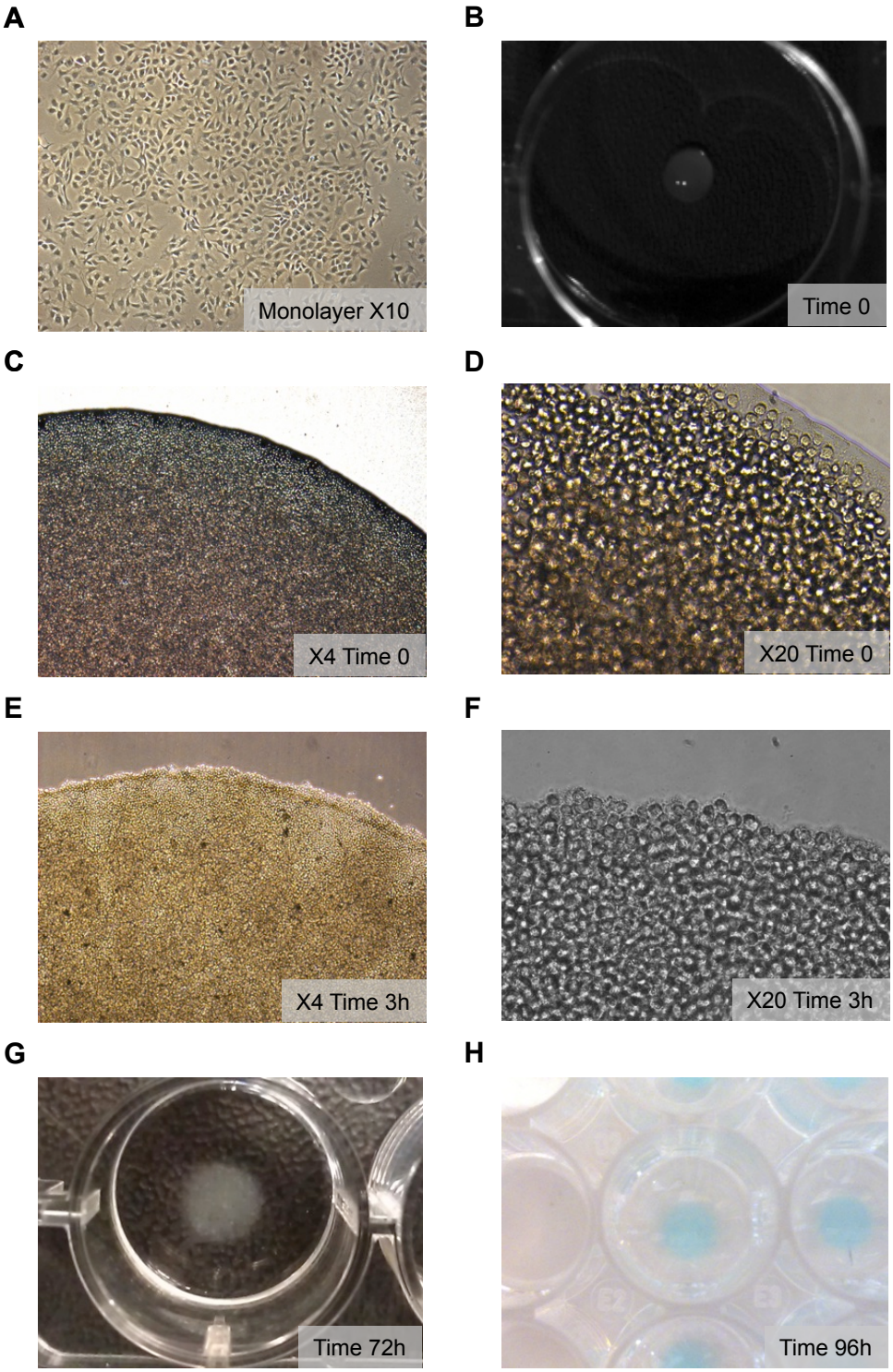

Figure 2.2.16 Generation of micromasses with isolated primary chondrocytes from rat femoral heads. (A) Isolated chondrocytes had cobblestone morphology similar to the C28/I2 cell line chondrocytes in monolayer. Cells were cultured to confluence and used between passage 1 and 5. (B) Cells were seeded in high density (5 x 10^5 cells in 20μl), (C, D) formed homogenous suspensions and were spherical in shape. (E, F) At three hours cells had adhered and in high-density areas, retained the spherical morphology. (G) By 72 hours, cells had generated a small amount of matrix (H) that stained poorly with Alcian blue dye.

2.2.5.2 Culture of Rat Femoral Head Explants as a Model of Cartilage-Native Chondrocytes

As the culture of isolated rat femoral head chondrocytes was not feasible, the explants were instead used as a model of cartilage-native chondrocyte matrix preservation. The femoral heads were ideal for this type of culture as they did not require extensive clean up to remove cells from other tissue types, unlike knee cartilage explants (Figure 2.2.17A and B). Furthermore, they could be obtained whole from the head of the femur ball without damaging the cartilage (Figure 2.2.17C), which prevented autocatalysis of the cartilage matrix by exposed chondrocytes.

Rat cartilage explants were used for experiments to investigate the entry of microparticles into cartilage. Eight-week old male Wistar rats were obtained *post-mortem* after intravital surgery, with only control or sham-operated rats used for explant collection. Tissue collection was carried out in a sterile flow cabinet under sterile conditions so that the tissue could be cultured. A paraspinal incision was made posteriorly to expose the dorsal hip joints with attaching ligaments and muscle dissected. The femurs were then dislocated and the femoral head caps detached carefully using forceps and the ligament teres removed. Femoral heads were then washed in 50ml PBS followed by agitation for one minute and replacement of PBS up to ten times. Femoral heads were incubated in 5% CO_2 for 24 hours at 37°C in 5ml serum-free DMEM-high glucose containing penicillin (200U) and streptomycin (200mg/ml) plus 1% ITS supplement before stimulation with 50ng/ml human recombinant IL-1β or vehicle (PBS) each day for 3 days.

In order to develop a method to quantify the sulphated glycosaminoglycan matrix content, the femoral heads were stained whole in the same manner as micromasses: fixed in glutaraldehyde (4%), acidified with 0.1N HCl and then stained overnight with Alcian blue. Although the femoral heads stained intensely with Alcian blue dye (Figure 2.2.17D and E), the extraction was not 100% complete, nor homogenous for the whole explant. Therefore, the femoral heads were fixed in paraformaldehyde (4%) for 18 hours before being embedded in OCT embedding medium for cryosectioning. This method was chosen over paraffin embedding as the tissue was perfectly preserved by freezing (Figure 2.2.17G) and allowed a faster throughput. Furthermore, the staining intensity with Safranin O was superior with frozen sections compared to paraffin embedded sections (Figure 2.2.17H and Figure 2.2.18).

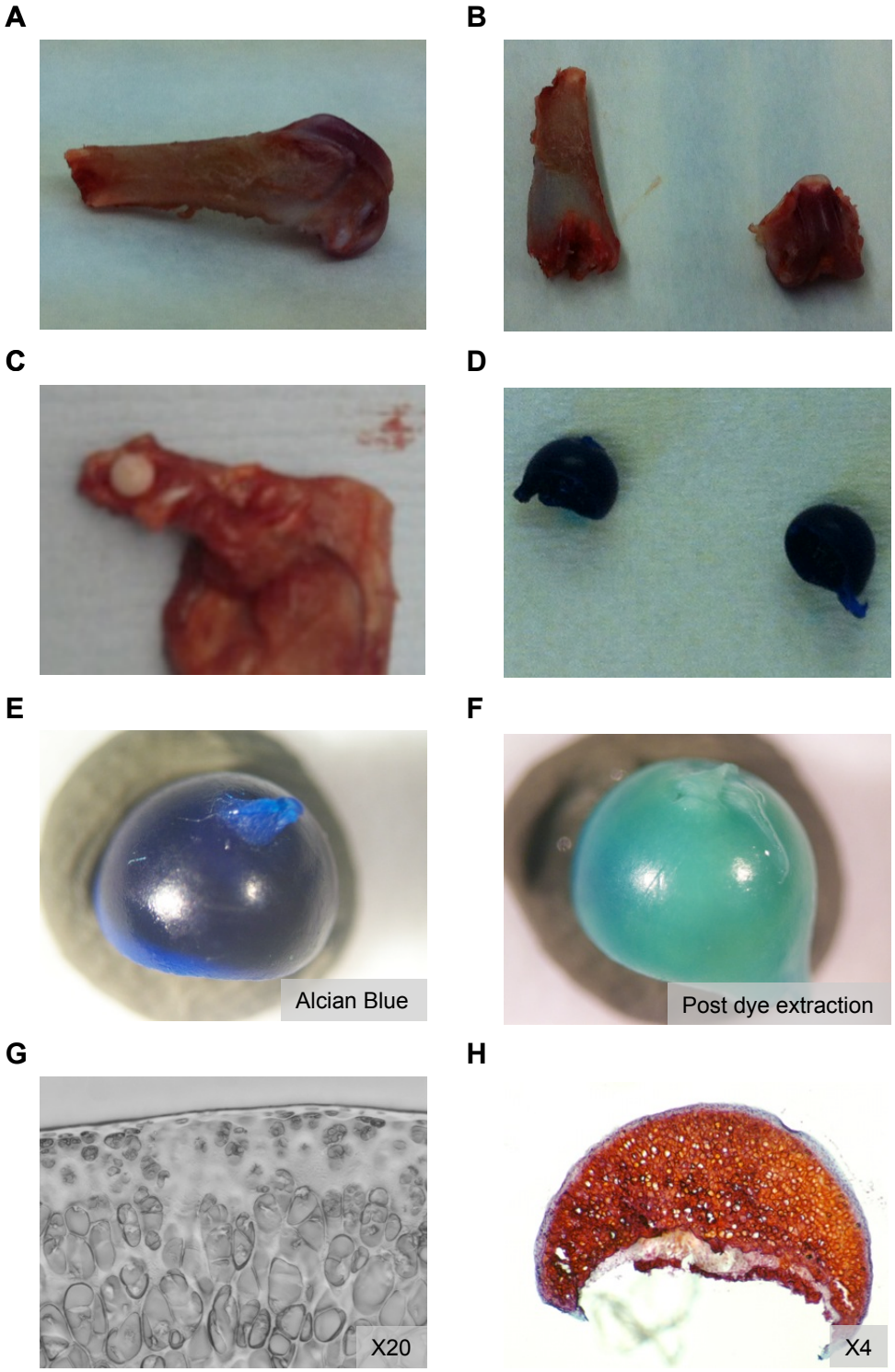

Figure 2.2.17 Rat femoral head explants as a model of cartilage-native chondrocyte matrix preservation. (A) Cartilage explants were excised from sham-operated rats post-mortem, including the knee cartilage, (B) but required extensive clean-up to remove contaminating cell types. (C) Femoral heads could be easily resected and kept intact and were free of other cell types when the ligament *teres* was removed, thus were chosen for experiments. (D and E) For quantification of sulphated glycosaminoglycans, Alcian blue was used to stain femoral heads intensely, (F) but could not be extracted fully. (G) Cryoembedding preserved the ultrastructure of the cartilage matrix and (H) Safranin O was used to quantify the sulphated proteoglycan content.

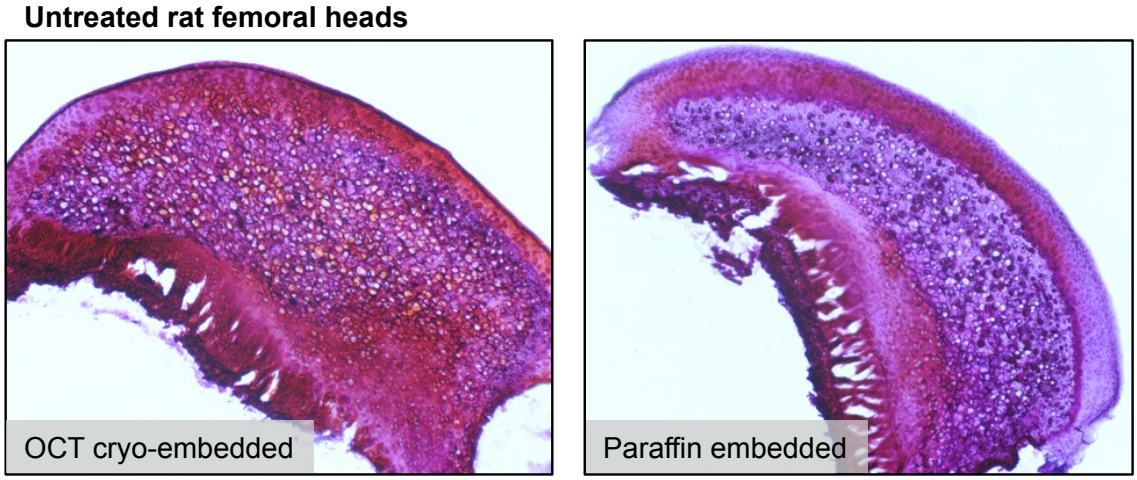

Figure 2.2.18 Superior sulphated proteoglycan staining in unstimulated rat femoral heads using Safranin O with OCT embedded explants. Rat femoral heads were collected and cultured for 3 days in supplemented DMEM high-glucose before fixation in 4% paraformaldehyde for 18 hours then either OCT embedded and frozen using dry ice before sectioning on a cryotome, or processed and paraffin embedded. Sections were then dewaxed before rehydration and staining with Safranin O. Sections at X4 magnification were captured using a standard light microscope (Olympus BH-2) with digital camera attachment (Nikon DXM1200).

2.2.5.3 Quantification of Safranin O Percentage Area Positive

Percentage area Safranin O area positive could be measured using ImageJ imaging software, allowing quantification of cartilage integrity throughout culture (Figure 2.2.19). Six images from each section, and 3 sections per femoral head were obtained using an Olympus BH-2 light microscope with Nikon DXM1200 digital camera attached. Colour images were split into their individual red/green/blue channels and the blue channel was used for quantification as it best represented the positive Safranin O areas. A positivity threshold was applied by eye using positive and negative controls from the experiment and checked against the original colour image. The threshold was applied and the area traced with the freehand tool. The threshold was the same for each batch of femoral heads sectioned. Measurements were collected and data displayed as percentage area positive for Safranin O staining.

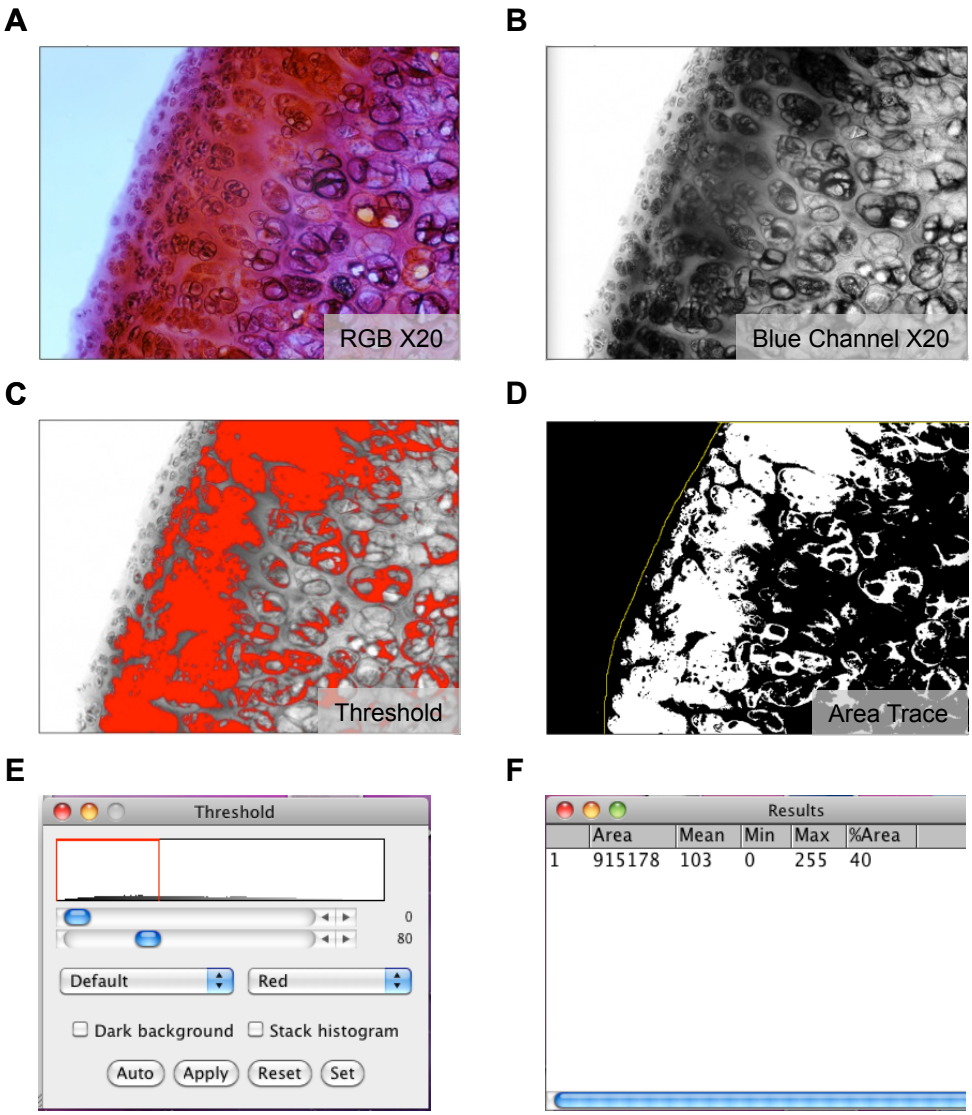

Figure 2.2.19 Sulphated proteoglycan content was quantified using ImageJ imaging software. Rat femoral heads were collected and cultured for 3 days in supplemented DMEM high-glucose before fixation in 4% paraformaldehyde for 18 hours then OCT embedded and frozen using dry ice before sectioning on a cryotome. Sections were stained with Safranin O. Sections at X4 and (A) X20 magnification were captured using an Olympus BH-2 standard light microscope with Nikon DXM1200 digital camera attachment. (B) Images were split into their individual red/green/blue channels and the blue channel was used for quantification. (C) A positivity threshold was applied by eye using positive and negative controls from the experiment and checked against the original colour image. (D) The threshold was applied and the area traced with the freehand tool. (E) The threshold was the same for each batch of femoral heads sectioned. (F) Measurements were collected and data displayed as percentage area positive for Safranin O staining.

2.2.5.4 Immunofluorescence Using Rat Femoral Heads

Cryopreservation of the cartilage explants was ideally suited for immunofluorescence analysis, and ensured that staining could be carried out without the need for antigen retrieval. Very low background staining could be achieved with anti-human antibodies, used during microparticle localisation experiments (Figure 2.2.20). Furthermore, as the processing of samples for OCT embedding is minimal, fluorescently labelled microparticles (with Bodipy-maleimide) retained their fluorescence and could be detected by both fluorescence and confocal microscopy after culture, sectioning and staining.

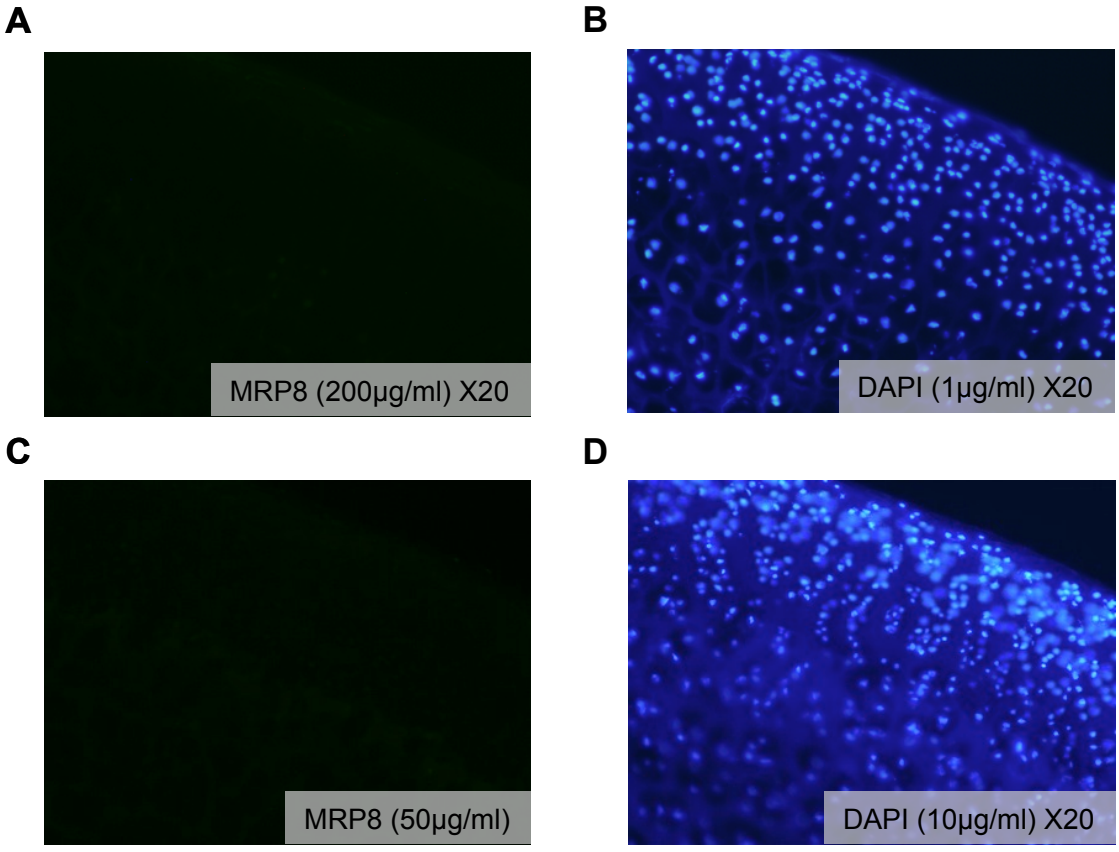

Figure 2.2.20 Rat femoral head explants did not stain positively for human MRP8. Rat femoral heads were collected and cultured for 3 days in supplemented DMEM high-glucose before being fixed in 4% paraformaldehyde for 18 hours then OCT embedded and frozen using dry ice before sectioning on a cryotome. Sections were stained with anti-human MRP8 antibodies (A 200µg/ml and C 50µg/ml) and DAPI (B 1µg/ml and D 10µg/ml) to visualise the nuclei. Sections at X4 and (A) X20 magnification were captured using a standard fluorescence microscope with digital camera attachment.

To determine entry of TMP into femoral head explants, explants were cultured phenol red-free RPMI supplemented with 1% ITS in a 24 well suspension plate for 24 hours to equilibrate. Explants were stimulated for 3 days with IL-1β (50ng/ml) or vehicle (PBS) then transferred to a 96 well suspension plate. As a control for microparticle entry, femoral head explants were treated with 100,000 synthetic fluorescent microcapsules loaded with a similar content of Annexin A1 or 100,000 Bodipy-maleimide loaded TMP. Femoral heads were washed thoroughly in PBS 18 hours later to remove any residual microparticles, fixed in PFA (4%) overnight then collected into OCT embedding medium and snap frozen. Femoral heads were cryosectioned at 10μm, placed on charged glass microscope slides to dry then stained for confocal microscopy (see section 2.3.14).

2.2.5.5 Culture of Mouse Femoral Head Explants as a Model of Cartilage-Native Chondrocytes

In later experiments, mouse femoral head cartilage was utilised as they could be genetically manipulated. Collection of mouse femoral head cartilage was carried out in the same way as for the rat femoral head isolation, but was technically challenging due to the small size of the tissue.

Mouse femoral head cartilage was collected from C57BL/6 wild type, Fpr1 or Fpr2 knockout animals (day -2) aseptically less than 40 minutes post mortem and thoroughly washed in sterile PBS before incubating for 48 hours in serum-free DMEM high glucose (4.5g/l) plus 1% ITS supplement to equilibrate. After this period (day 0), suspension culture plates were used, and medium replaced, to prevent microparticle adhesion to the plastics. Recombinant mouse IL-1β (10ng/ml) was added along with 100,000 microparticles per whole cartilage. Treatment was repeated on day 3 and 6 then collected and stained with Safranin O in the same way as rat femoral head explants.

2.2.6 *In Vivo* Delivery of Microparticles via Intra-Articular Injection

Intra-articular delivery of microparticles *in vivo* into arthritic mice was required. This technique allowed for the paired analysis of microparticle treatment in arthritic mice, reducing inter-donor variability. Damage to the cartilage during this method was avoided by repeated practice of the intra-articular injections *post mortem* in naïve C57BL/6 mice. First, the skin was resected so that the patella could be clearly visualised (Figure 2.2.21A). Intra-articular injection of Evan's blue dye was administered approximately half way up the patella. This would ensure the dose was delivered exactly within the joint space (Figure 2.2.21B). Care had to be taken not to guide the needle too far into the knee, to prevent contact with the medial and radial menisci or anterior cruciate ligament (Figure 2.2.21C). Contact with these structures causing damage to any of the matrix is liable to cause arthritis in itself. (Figure 2.2.21D) Delivery of 6μl of Evan's blue filled the entire cavity and could be seen behind the patella. (Figure 2.2.21E) Resection of intact injected knees showed that the doses had been delivered and damage to the menisci or ligaments could not be seen. For *in vivo* intra-articular injections in live mice, mice were anaesthetised with isoflurane mixed with oxygen and placed on a nose cone. The fur of the knees was then trimmed with clippers so that the patella could be visualised through the skin. A maximum of 6μl was injected into each knee.

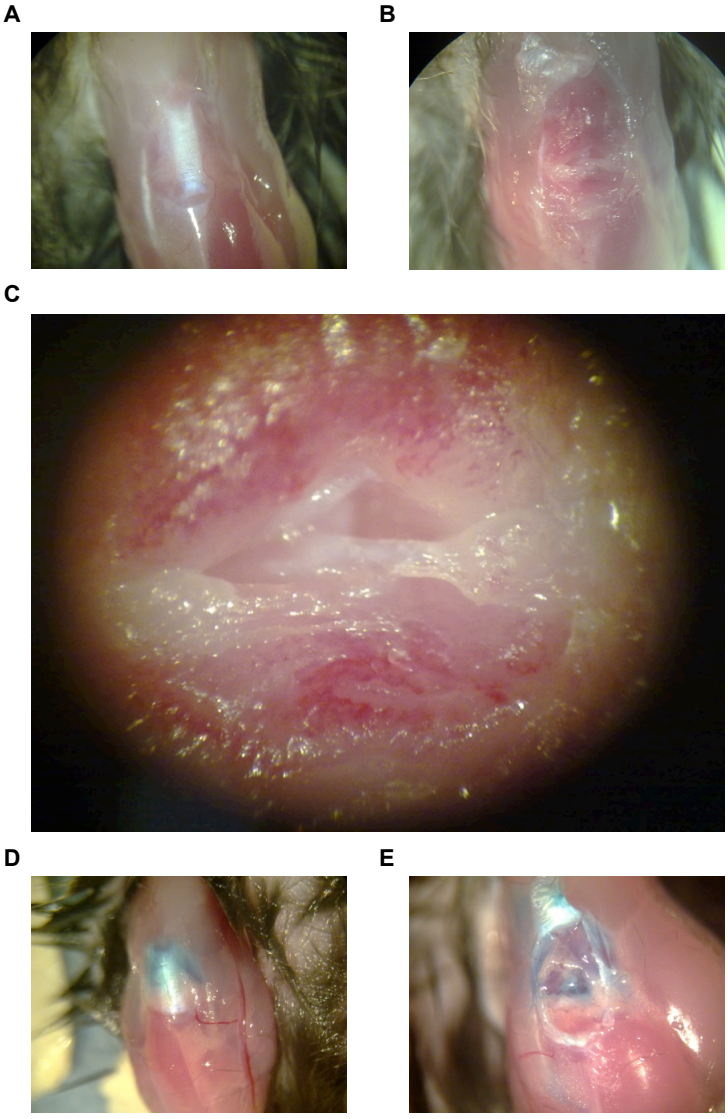

Figure 2.2.21 Accurate intra-articular injections require delivery of compounds directly to the joint space. In order to administer anti-inflammatory compounds via intra-articular injection, the injections themselves should induce no inflammation. (A) Skin was resected post-mortem so that the patella could be clearly visualised. (B) The patella was removed to expose the joint space. (C) Dissection microscopy revealed the medial and radial menisci and anterior cruciate ligament, structures that needed to be avoided when performing intra-articular injections. (D) Intra-articular injection of Evan's blue dye was administered approximately half way up the patella in intact knees. This ensured the dose was delivered exactly within the joint space. Delivery of 6μl of Evan's blue filled the entire cavity and could be seen behind the patella. (E) Resection of the intact, injected knee showed that the dose had been delivered and damage to the menisci or ligaments could not be seen.

2.3 Methods

2.3.1 Neutrophil Isolation from Peripheral Blood

Neutrophils were isolated from the peripheral blood of healthy volunteers, after providing informed consent, using the dextran sedimentation method. Blood (60ml) was drawn with a tourniquet applied using a 21-gauge butterfly needle into a 60ml syringe. Once drawn, blood was handled quickly but gently at room temperature to prevent activation of the neutrophils. The blood was immediately transferred into two 50ml falcon tubes containing 3ml 3.2% sodium citrate for anticoagulation. The falcon tubes were then gently inverted to mix, and then centrifuged at 130 x *g* for 20 minutes at room temperature to sediment the cells (Figure 2.3.1A). The platelet rich plasma was removed then 10ml PBS was carefully layered over the cell suspension, without mixing the two together. This prevents the activation of the cells by turbulence. Dextran (from *Leuconostoc,* molecular weight 450,000 to 650,000; 6% w/v, 8 ml) was gently added to the PBS. The tubes were inverted gently to mix the cell suspension with the PBS and dextran (Figure 2.3.1B).

Dextran causes red cells to form aggregates, which sink to the bottom of the tube, leaving a layer of PBS/dextran enriched in blood leukocytes that is largely depleted of red blood cells. This process takes around 20 minutes, after which the leukocyte rich layer was carefully removed without generating bubbles and layered over 10ml Histopaque 1077 in a fresh 50ml falcon tube (Figure 2.3.1C), with a maximum of 25ml of leukocyte suspension per 10ml Histopaque. Tubes were then centrifuged for 30 minutes at room temperature at 450 x *g*. Histopaque 1077 is of a specified density which allows cells to travel through only if they are of a sufficiently small density. Thus, red blood cells and granulocytes become pelleted at the bottom of the tube below the Histopaque (Figure 2.3.1D), whereas the peripheral blood mononuclear cells remain above this layer, allowing separation of the two populations of leukocytes. The mononuclear cells were then collected with every effort made to remove as many cells as possible to prevent contamination of the granulocyte population.

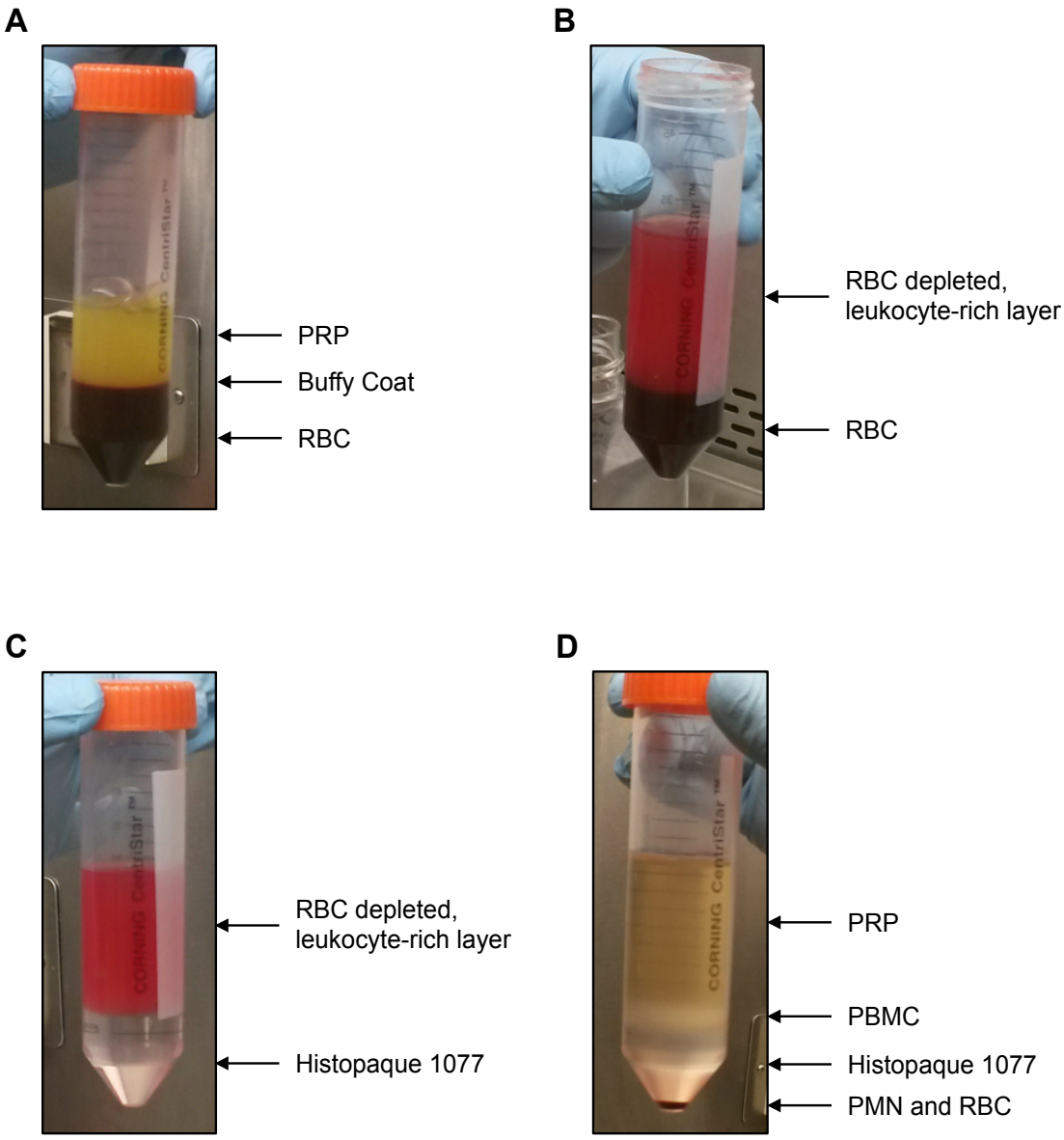

Figure 2.3.1 Neutrophil Isolation from Whole Blood via Dextran Sedimentation. (A) Platelet-rich plasma is removed from blood samples following the first centrifugation of 800 x *g* for 20 minutes, leaving the buffy coat and red cells. (B) Dextran is used to aggregate the red cells and enrich the leukocyte layer. (C) Histopaque 1077 is used to separate the populations of leukocytes, (D) which can then be collected separately. PRP, platelet-rich plasma; RBC, red blood cells; PBMC, peripheral blood mononuclear cells; PMN, polymorphonuclear cells.

The remaining plasma and Histopaque were removed, and the red blood cells were lysed through hypotonic shock with 9ml ice-cold ultrapure distilled water. Isotonicity was quickly restored (after less than 20 seconds) by drawing up the cell/water suspension and adding it to a new falcon tube containing 1ml 10x Hanks solution. New tubes were used for isotonicity restoration to prevent any mononuclear cells adherent to the plastic of the tube from being washed into the granulocyte suspension. PBS (40ml) was gently added to the cell suspension for washing, and the cells were centrifuged to pellet the cells at 300 x *g* for 10 minutes at room temperature. Once the cells were pelleted, the PBS was carefully aspirated to ensure as much as the red blood cell lysis fluid was removed as possible. The resulting neutrophil pellets were pale cream in colour, indicating full lysis of the red blood cell population. The granulocyte population was then gently but thoroughly resuspended in 3ml phenol red-free, incomplete RPMI for counting. To count, 10μl of the cell suspension was added to 490μl Turk's stain (98ml distilled H_2O, 2ml acetic acid and 2g crystal violet) in a 1.5ml eppendorf, then vortexed briefly to obtain a homogenous cell suspension with no aggregates. Cells in Turk's dye were applied to a Neubauer counting chamber with coverslip applied. The cells were visualised with an Olympus BH-2 standard light microscope with x40 objective, and cells in the 4 larger outer squares were counted (Figure 2.3.2). The average was taken and multiplied by the dilution factor to provide the number of neutrophils per ml x 10^4, and this value was multiplied by the number of millilitres the cells were resuspended in, to give the total number of cells isolated. The cell concentration was adjusted to 2 x 10^7/ml for stimulation.

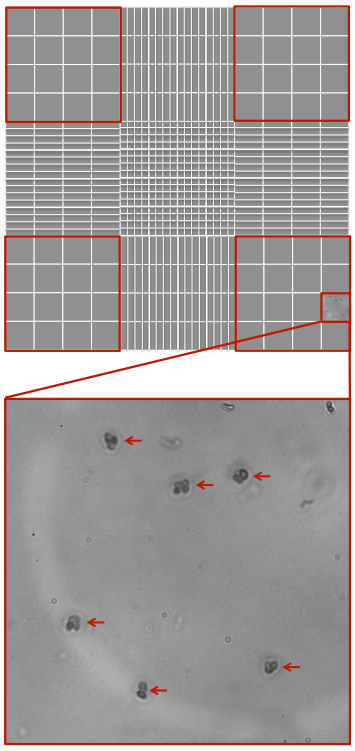

$$\frac{\text{number of cells}}{4} \times \text{dilution factor} \times 10^4 = \text{cells/ml}$$

$$\times \text{ total volume} = \text{total cells}$$

Figure 2.3.2 Counting Neutrophils using a Neubauer chamber and the formula for calculation. Neutrophils were diluted 1:50 with Turk's solution for counting and 10μl applied to the Neubauer chamber. Cells were visualised using a light microscope on X40 objective. All cells in the out four corner squares (highlighted red) were counted and divided by 4 to obtain the average. This number, multiplied by the dilution factor provides the number of cells per millilitre x 10^4. Neutrophils were counted if they had characteristic multi-lobed nuclei (red arrows).

2.3.2 Flow Cytometric Analysis of Cells

Flow cytometry is a well-characterised and useful tool for the analysis of populations of cells in suspension. By labelling cells with fluorochrome-conjugated antibody labels, the phenotype of cell populations can be determined.

2.3.2.1 Determination of Granulocyte Purity and Activation Status

Freshly isolated human neutrophils were analysed by flow cytometry to determine their purity, and their expression of activation markers, CD11b and CD62L. Cells ($5x10^5$) were added to a round-bottomed 96 well plate and pelleted by a brief spin (30 seconds at 400 x *g*, room temperature) before re-suspending in 50μl Fc block (16mg/ml) for 30 minutes on ice to prevent nonspecific binding of antibodies. Monoclonal, fluorochrome-conjugated antibodies to CD62L and CD11b were added (for concentrations, clones and catalogue numbers, see Table 2.1.1), or the relevant isotype at the same concentration, for 1 hour on ice in the dark. Cells were washed 3 times briefly with 200μl/well PBS (supplemented with 1% bovine serum albumin) and centrifuged for 30 seconds at 400 x *g*. Cells were resuspended in 200μl supplemented PBS and transferred to flow cytometry tubes for immediate acquisition. Cells were analysed using a BD FACSCalibur flow cytometer and the PMN population identified from the FSC/SSC dot plots (similar to Figure 2.2.1B). Single stains were used to determine the correct amount of compensation required, where a signal emitted from one fluorochrome appears inappropriately in two channels.

Mouse neutrophils collected from the peritoneal lavages of mice receiving 1mg zymosan from *Saccharomyces spp*. were stained with Annexin A1 polyclonal antibodies for one hour on ice in the dark, after being blocked for one hour with Fc block (16mg/ml). The cells were washed three times with PBS (supplemented with 1% BSA) followed by centrifugation briefly at 400 x *g* for 30 seconds, then the secondary anti-rabbit Alexa594 added for half an hour in the dark on ice. Ly6G antibodies were added following a second washing step, again for one hour on ice in the dark. The cells were washed three times before being resuspended in 200μl supplemented PBS and then analysed using a BD FACSCalibur.

2.3.2.2 Flow Cytometric Analysis of C28/I2 Chondrocyte Cell Line

C28/I2 cells cultured in micromass (see section 2.2.4.2) were dissociated into a single cell suspension using Accutase cell dissociation solution for 10 minutes at 37°C followed by pipetting up and down 10 times to remove any aggregates (Figure 2.3.3A). Cells were then fixed and permeabilised using a fix/perm buffer commercially available, according to manufacturer instructions (eBioscience, Figure 2.3.3B). Cells were fixed in the fix buffer (which contains blocking buffer) for 10 minutes at room temperature in the dark then permeabilised by the addition of 200μl permeabilisation buffer without removing the fixative. After 20 minutes, cells were pelleted by brief centrifugation at 400 x *g* for 30 seconds. Antibodies against FPR2/ALX, FPR1 and appropriate isotype controls were diluted to the correct concentrations (see Table 2.1.1) in permeabilisation buffer and incubated in the dark at room temperature for 30 minutes. Goat-anti-mouse Alexa594 secondary antibodies were diluted to 20μg/ml using permeabilisation buffer and added after several washes in permeabilisation buffer with brief centrifugations (30 seconds at 500 x *g*). Finally, after washing again, cells were resuspended in permeabilisation buffer and analysed using a BD FACSCalibur. 10,000 events were recorded, with fluorescence excited with the 488 laser and emission signals collected.

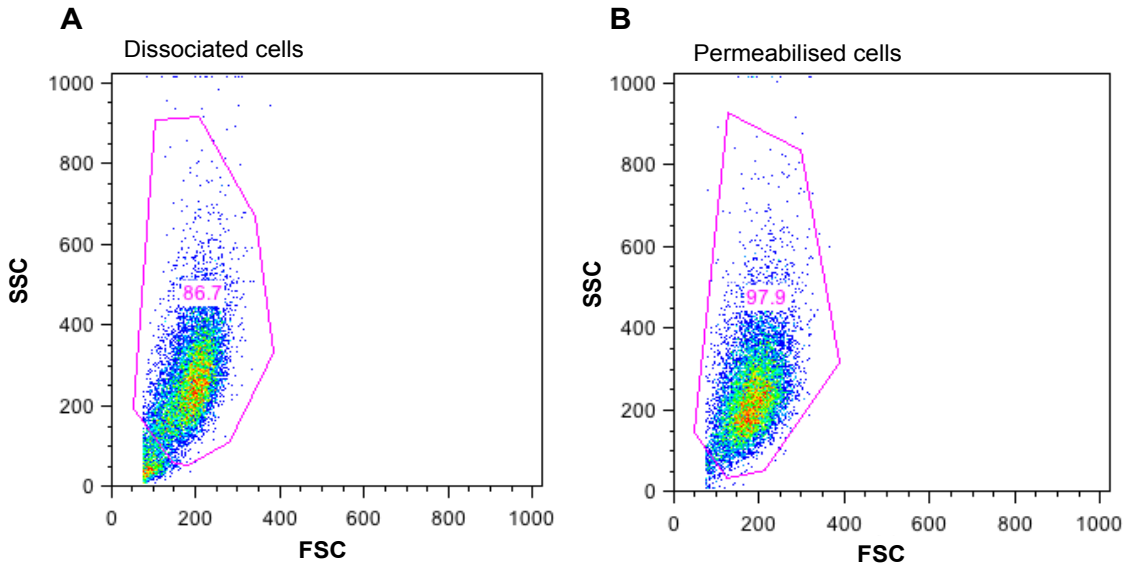

Figure 2.3.3 C28/I2 micromasses can be dissociated and permeabilised for flow cytometry. (A) Cells were dissociated by incubation in Accutase for 10 minutes at 37°C followed by pipetting to disperse clumps. (B) Cells following fixation and permeabilisation.

2.3.3 Nanoparticle Tracking Analysis

Nanoparticle tracking analysis was used to determine the absolute size of microparticles below 1μm in diameter. This method allows the absolute quantification of particle size by recording the Brownian motion of laser-illuminated particles by video microscopy. The relationship between the Brownian motion of microparticles in suspension and their size requires the diffusion coefficient and the sphere equivalent hydrodynamic radius to be calculated, which is performed by the NTA software, using the Stokes-Einstein equation. This gives the rate of diffusion of spherical particles through liquid with a low Reynolds number (i.e. with little or no turbulence). To illuminate the microparticles, a precisely focussed laser beam is introduced via a glass prism into the sample. As the laser beam is refracted at a low angle via the prism, a fine beam of laser light is generated at the interface between sample and prism. A camera is mounted perpendicularly to the sample chamber in order to collect the highest amount of light scattered by the illuminated particles. Frame-to-frame analysis of the particles' motion tracks allow their absolute size to be determined as smaller particles move more rapidly and travel a greater distance, whereas larger particles move slowly and do not travel very far. Pre-prepared, TNF-α generated microparticles were pooled from 6 donors to create a test volume of 1ml with sufficiently high microparticle numbers for analysis (around 10^7/ml). Microparticle diameters were analysed with NanoSight LM10 system with a 405nm laser (NanoSight Ltd., Amesbury, UK) at 22°C. Samples were introduced via manual syringing, and videos recorded for 90 sec using NTA software (version 2.3): blur setting, auto; detection threshold, 10; minimum expected particle size, auto; minimum track length, auto; viscosity, 0.95 cP.

2.3.4 Measurement of Apoptosis in Chondrocytes

2.3.4.1 $DIOC_6$ Staining

Early events in apoptosis, those occurring before cell shrinkage, blebbing and nuclear fragmentation, include the loss of the potential across the mitochondrial membrane (Zamzami et al., 1995). This can be measured using the cationic fluorochrome $DiOC_6$ (3,3'-dihexyloxacarbocyanine iodide), which permeates the cell membrane and accumulates within mitochondria due to the large negative membrane potential. Apoptotic cells lose this potential and the fluorescent signal subsequently decreases. It is therefore possible to distinguish $DiOC_6$-high resting cells from $DiOC_6$-low apoptotic cells using flow cytometry. To determine early apoptosis, cells were dispersed thoroughly in their wells before being incubated with $DiOC_6$ dye (40nM dissolved in 100% ethanol) for 30 minutes at 37°C in the dark. Cells were washed three times in PBS supplemented with 1% bovine serum albumin followed by brief centrifugation for 30 seconds at 400 x *g.* Cells were resuspended in 200µl supplemented PBS for sample acquisition using a BD FACSCalibur flow cytometer (see section 2.3.2.2). 10,000 events were acquired and fluorescence detected using the 488nm laser. Results are expressed as a percentage of cells $DiOC_6$ low.

Micromasses were treated with valproic acid (5mM, 10mM or 20mM) as a positive inducer of chondrocyte apoptosis for 24 hours and this was determined by $DiOC_6$ staining to induce the same level of apoptosis as IL-1β (50 or 100ng/ml) (Figure 2.3.4). Thus, IL-1β (50ng/ml) was added to micromasses with or without 100,000 CMP, TMP or IMP for 18 hours. The cells were then dissociated with Accutase for 10 minutes at 37°C and dispersed by gentle pipetting.

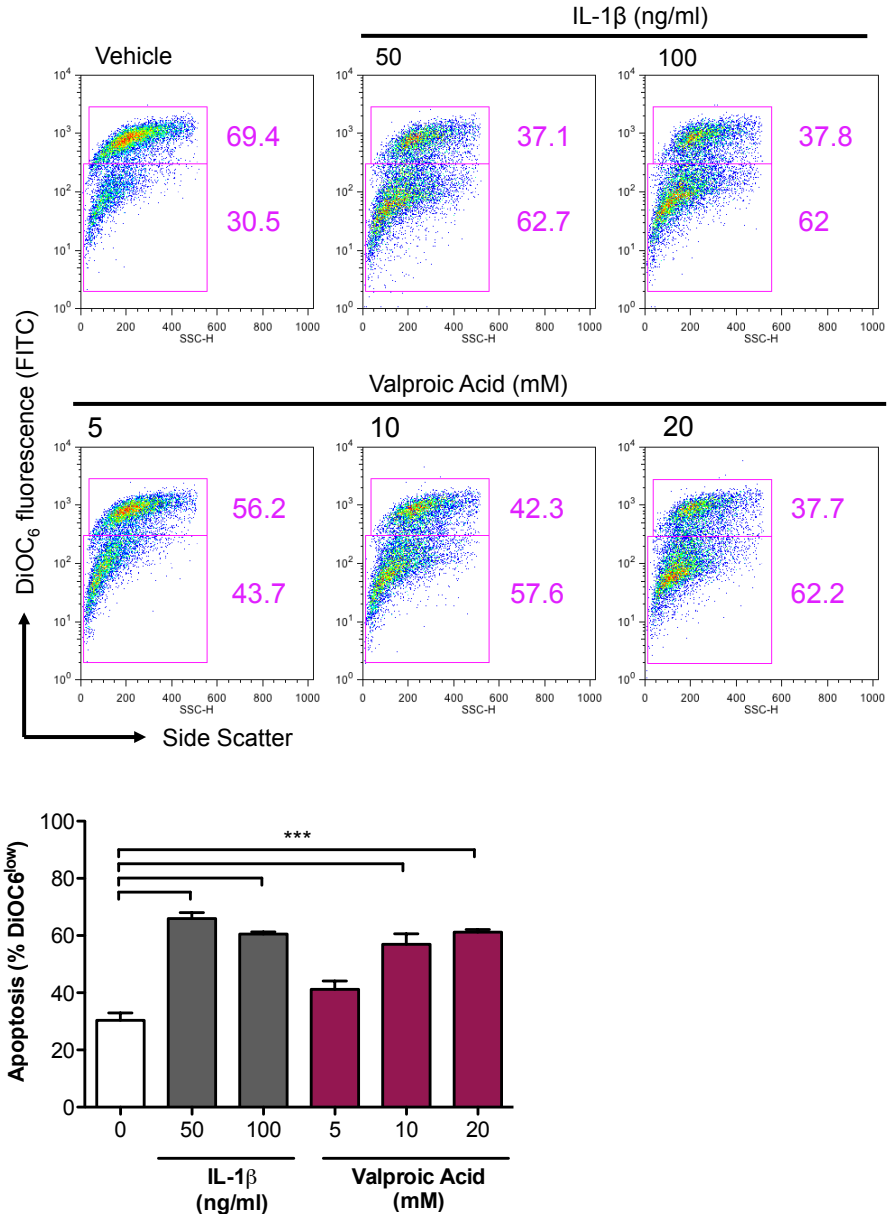

Figure 2.3.4 IL-1β is as effective at inducing apoptosis as Valproic Acid positive control. C28/I2 chondrocytes in micromass culture were stimulated for 18 hours with IL-1β (50 or 100ng/ml) or Valproic acid and apoptosis was measured using $DIOC_6$ staining. Data are expressed as mean ± SEM of 3 separate micromasses ***P<0.001 with One-way ANOVA and Bonferroni post-test. Top panels are representative plots from the experiment.

2.3.4.2 TUNEL Staining

To determine more advanced apoptosis, a TUNEL staining kit was used (Millipore ApopTag Plus Fluorescein In Situ Kit). TUNEL staining was used to detect fragmented DNA of terminally apoptotic cells. The assay is based on the incorporation of fluorescently conjugated FITC-dUTPs by the enzyme terminal deoxynucleotidyl transferase (TdT) at the 3'-OH ends of the DNA fragments.

Cells were added to charged glass microscope slides and checked using a light microscope to ensure they were at sufficiently low density for quantification. The slides were then dried and fixed in 1% paraformaldehyde (in PBS, pH 7.4) for 10 minutes. The slides were then washed twice in PBS and post-fixed and permeabilised in ethanol/acetic acid (100ml 100% ethanol containing 50ml acetic acid) for 5 minutes at -20°C. After washing twice in PBS again, 25μl equilibration buffer was added, followed by TdT enzyme (77μl reaction buffer and 33μl TdT). Slides were then incubated for 1 hour at 37°C in a humidified chamber, then dipped 3 times in Stop buffer (1ml Stop buffer in 34ml distilled water) before being incubated in Stop buffer for 10 minutes. Following another wash step, pre-warmed 25μl anti-digoxigenin conjugate was added to the slides before incubation in the dark for 30 minutes in a humidified chamber at room temperature. Slides were then washed several times more before being mounted in Mowiol containing DAPI to visualize the nucleus. Slides were visualized using an Olympus BH-2 light microscope equipped with fluorescent lamps, and images captured with a Nikon DXM1200 digital camera. Any green positive cells, as determined by applying a threshold using ImageJ were checked for obvious nuclear changes such as condensation, indicating apoptosis (Figure 2.3.5). Data are expressed as a percentage of 200 cells evaluated.

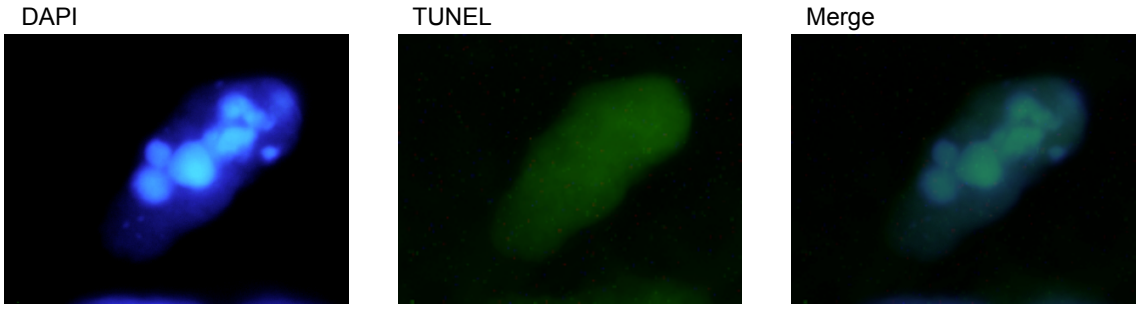

Figure 2.3.5 Apoptotic cells have condensed nuclei and stain positively with TUNEL stain. C28/I2 cells stimulated with IL-1β (50ng/ml) for 18 hours then were stained using a commercially available TUNEL kit and analysed by fluorescence microscopy for nuclear changes coinciding with TUNEL positivity.

2.3.5 1,9-Dimethylmethylene Blue Dye Binding Assay

The quantity of free sulphated glycosaminoglycans (sGAG) released into the culture medium of C28/I2 micromasses was measured by 1,9-dimethylmethylene blue dye-binding assay. For the culture supernatants to be sufficiently concentrated, micromasses were stimulated for the final 24 hours in a reaction volume of 300µl. Supernatants (100µl) were collected and digested in an equal volume of digestion buffer containing 0.5mg/ml Papain, 20mM disodium orthophosphate, 1mM EDTA and 2mM Dithiothreitol (DTT). The samples were digested for 18 hours at 65°C before 20µl was applied to the wells of a 96-well round-bottom plate in triplicate (used to aid mixing). Chondroitin-4-sulphate diluted in digestion buffer and serially diluted acted as standards at known concentrations (1mg/ml to 30µg/ml). Using a multichannel pipette, 190µl 1,9-dimethylmethylene blue dye (0.016%, 40.5mM glycine, 40.5mM NaCl, 197µl 37% HCl) was added and the plate left to equilibrate for 30 seconds. Optical density at 530nm was immediately determined using a TECAN M200 spectrophotometer. Absolute sGAG concentrations were determined from the standard curve generated by plotting known standard concentrations against absorbance (Figure 2.3.6).

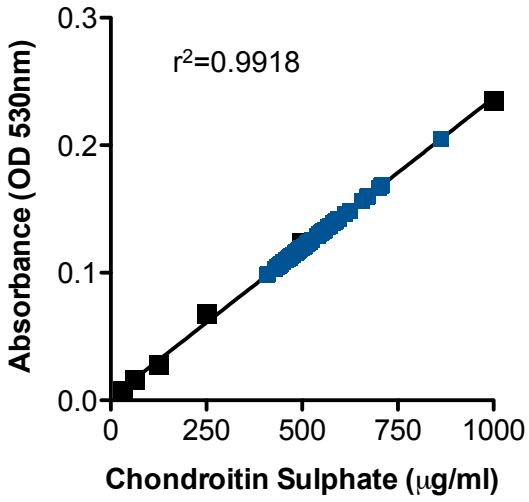

Figure 2.3.6 Standard curve for DMMB dye-binding assay. Supernatants from C28/I2 micromasses stimulated for 24 hours with or without IL-1β (30ng/ml) and 100,000 microparticles were digested overnight with papain then assayed with 1,9 dimethylmethylene blue to quantify released glycosaminoglycans. Blue points show data interpolation from a representative experiment.

2.3.6 SDS-PAGE

Sodium dodecyl sulphate-polyacrylamide gel electrophoresis (SDS-PAGE) allows analysis of proteins present within a supernatant sample or cell lysate by using gel electrophoresis to separate molecules according to size and charge then transferring them onto a polyvinylidene difluoride membrane, where proteins can be detected with specific monoclonal antibodies. The anionic detergent SDS denatures proteins by disrupting hydrogen bonds and gives the protein a negative charge by covering the polypeptide backbone of the protein in its hydrophobic tail. Consequently, the proteins migrate in the gel according to size, with the smallest proteins moving furthest through the gel. The structure of the protein is completely unfolded by the addition of DTT, which acts as a reducing agent that cleaves the disulphide bonds of the protein.

C28/I2, primary adult human articular chondrocyte or microparticle (100,000) samples were collected in boiling hot Laemmli buffer (50mM Tris-HCl (pH 6.8), 2% SDS, 10% glycerol, Sigma), before being diluted 5 parts sample to 1 part 6x SDS loading-buffer [600mM DTT, 0.6% bromophenol blue, 300mM Tris-HCl (pH 6.8), 12% SDS and 60% glycerol] and boiled for 5 minutes. Samples were loaded onto pre-prepared 4% stacking and a 10% or 12% resolving polyacrylamide gel (w/v; see Table 2.3.1 for volumes and ingredients). All reagents were combined except the APS and TEMED, which act as polymerisation catalysts, so were added immediately before casting the gels. The Hoefer casting kit and electrophoresis system were used: sandwiches of 4 gel casting cassettes were assembled by adding two T-separators to a short-plate and applying a 1.5mm front-plate (x4) and sealing the cast with clamps ensuring all rubber seals were in place. Resolving gel was poured into the cast, then overlaid with isopropanol to prevent a curved meniscus forming. Gels were left to polymerise for 20 minutes at room temperature, after which the isopropanol was poured off and the stacking gel applied. To prevent bubbles forming, the gel was poured before the 10-well combs were carefully set into each cassette. After polymerisation, the gel cassettes were placed into the electrode assembly tanks for electrophoresis. Cassettes (2 per tank) were clamped to the tank, which was filled with 200ml running buffer (25mM Tris-base, 200mM glycine and 0.1% SDS). The cavity behind the gel cassettes was then filled with running buffer from the tank using a Pasteur pipette. Combs were removed and 30μl of sample was added to each well, along with 7μl high-range rainbow molecular weight marker (GE Healthcare, Amersham) into one well, to visualise separation and sample protein size. The electrophoresis tank was run at

30mA per gel for 30 minutes to pass through the stacking gel, and then increased to 50mA per gel until the rainbow markers were separated.

Once the dye front had reached the bottom of the gel, the stacking gel from each plate was discarded, and the resolving gel placed in transfer buffer (25mM Tris-base, 192mM glycine and 20% methanol) for transfer assembly. Blotting paper (2 sheets) was placed on a sponge, the gel was placed on the blotting paper, and a methanol-activated polyvinylidene difluoride membrane was placed on top. Another layer of blotting paper was added before the sandwich was completed by the addition of the final sponge. Gel/membrane sandwiches were transferred in sample cages to Bio-Rad transfer tanks and were transferred overnight at 50V (constant current).

Table 2.3.1 Composition of 10% and 12% SDS-PAGE Resolving and 4% Stacking Gels

Composition	10% Resolving Gel	12% Resolving Gel	4% Stacking Gel
30% (w/v) Acrylamide: 0.8% Bis acrylamide stock solution (37.5:1) (Protogel) (ml)	13.32	16	3.9
Resolving Buffer: 1.5M Tris-HCl, pH 8.8, 0.4% SDS (Protogel) (ml)	10.4	10.4	
Stacking Gel Buffer: 0.5M Tris-HCl, pH 6.8, 0.4% SDS (Protogel) (ml)			7.5
dH_2O (ml)	15.84	13.16	18.3
10% (w/v) Ammonium persulfate: APS (Sigma) (μl)	400	400	150
TEMED (Sigma) (μl)	40	40	40

For the detection of proteins, membranes were blocked for 60 minutes in 5% milk in Tris-buffered saline (TBS) (150mM sodium chloride, 2mM Tris-base pH 7.4) containing 0.1% Tween 20 (Sigma) (TBST) at room temperature on a rocker. Antibodies were diluted to the correct concentration (Table 2.3.2) in either 3% non-fat dried milk in TBST for native proteins or 5% BSA for phosphorylated antigens and incubated as indicated in Table 2.3.2. Membranes were washed five times for 5 minutes each in TBST before the secondary antibody was added for 1 hour at room temperature. Membranes were washed a further 5 times before proteins were detected using a Luminata Forte HRP substrate and visualised on hyperfilm (GE Healthcare, Little Chalfont, UK) after a 2-minute exposure.

Table 2.3.2 Antibodies used for Western Blotting of proteins.

Protein of interest	Antibody	Source	Dilution	Incubation time
Annexin A1	Polyclonal rabbit anti-human	Thermo Scientific	1:250 (stock 0.7mg/ml)	4°C overnight
Sox9	Polyclonal rabbit anti-human	Abcam	140μg/ml	1 hour, room temperature
Total p38	Rabbit	Cell Signalling	1:5000	1 hour, room temperature
Total Akt	Clone C67E7	Cell Signalling	1:10,000	1 hour, room temperature
Total Hsp27	Mouse anti-human, Clone 631	Cell Signalling	1:2000	1 hour, room temperature
Total JNK	Rabbit	Cell Signalling	1:5000	1 hour, room temperature
Total ERK1/2	Rabbit	Cell Signalling	1:5000	1 hour, room temperature
Total MK2	Rabbit	Cell Signalling	1:2000	1 hour, room temperature
β Actin	Mouse anti-human, Clone AC-15	Sigma	1:15,000	1 hour, room temperature
Phospho p38	Rabbit	Cell Signalling	1:1000	Overnight, 4°C, rocking
Phospho Akt – Serine 473	Mouse anti-human, clone 587FH	Cell Signalling	1:2000	Overnight, 4°C, rocking
Phospho Hsp27 (S78)	Rabbit anti-human	Cell Signalling	1:2000	Overnight, 4°C, rocking
Phospho MK2 (T222)	Rabbit anti-human, Clone 9A7	Cell Signalling	1:2000	Overnight, 4°C, rocking
Phospho JNK	Rabbit	Cell Signalling	1:5000	Overnight, 4°C, rocking
Phospho ERK1/2	Rabbit	Cell Signalling	1:5000	Overnight, 4°C, rocking
Goat HRP	Anti-mouse IgG	Dako	1:2000	30 minutes, room temperature
Rabbit HRP	Anti-goat IgG	Dako	1:2000	30 minutes, room temperature
Rat HRP	Anti-rabbit IgG	Dako	1:2000	30 minutes, room temperature

For signaling experiments, C28/I2 cells grown in monolayer were used to detect the phosphorylation of several molecules involved in signaling pathways. Monolayers were used in preference to micromass constructs to prevent time-critical diffusion through multiple cell layers affecting the temporal modulation of the pathways. Confluent C28/I2 were serum starved for 24 hours in phenol red-free RPMI supplemented with 1% ITS. Cells were then stimulated with IL-1β (30ng/ml), microparticles, or recombinant Annexin A1 (10nM; generated in-house) for 1, 5, 10, 30, 60, 120 or 240 minutes. Some samples were pretreated with microparticles for 18 hours. Supernatants were removed by aspiration and cells lysed with boiling hot laemmli buffer containing phosphatase inhibitor b (Sigma). Wells were scraped to ensure cells were thoroughly lysed. Samples were collected and boiled for 5 minutes. Following electrophoresis, transfer and incubation with antibodies, proteins were visualised using Luminata Forte HRP substrate and imaged on x-ray film or with a FluorChem E Digital Dark Room (ProteinSimple). For normalisation, the expression of each phosphorylated antigen was normalised to its total antigen. To do this, membranes were stripped using 6M glycine at pH 2, washed thoroughly in TBST then blocked in 5% non-fat milk for 1 hour at room temperature. Membranes were then reprobed for total antigen for one hour at room temperature, and then washed thoroughly in TBST 3 times. Secondary antibodies conjugated to HRP were added for a further 2 hours at room temperature before a final thorough washing in TBST and visualisation with Luminata Forte HRP substrate. Images were captured using either Hyperfilm (GE Healthcare) x-ray film or FluorChem E Digital Darkroom (Protein Simple). Densitometry of phospho proteins was determined using ImageJ imaging software and expressed as relative intensity of total target antigen.

2.3.7 Real-Time Polymerase Chain Reaction

Real-Time PCR allows sensitive quantification of mRNA within cells by using SYBRgreen dye to visualise amplicon generation from a complimentary-DNA template. SYBRgreen dye binds to newly synthesised double-stranded DNA and emits fluorescent light in direct proportion to the number of amplicons generated in the reaction. A threshold of fluorescence detected above background was set in the exponential phase of amplification, and the cycle number at which the samples reached this level was referred to as the cycle threshold value (Ct), thus reflecting the relative abundance of the specific mRNA transcripts. To quantify the relative expression of each gene, Ct values were normalized with an endogenous housekeeping (reference) gene. Housekeeping gene was determined for C28/I2 micromasses by testing three conventional housekeeping genes to detect any modulation across stimuli. The housekeeping gene with the least modulation was selected (Figure 2.3.7), which was *RPL32*.

The comparative Ct method (Pfaffl, 2001) was used to measure gene transcription in samples. These results were expressed as relative units based on the calculation of $2^{-\Delta\Delta Ct}$, which gives the relative amount of gene normalised to the endogenous control. The control samples were averaged, used as the calibrator and given a value of 1.

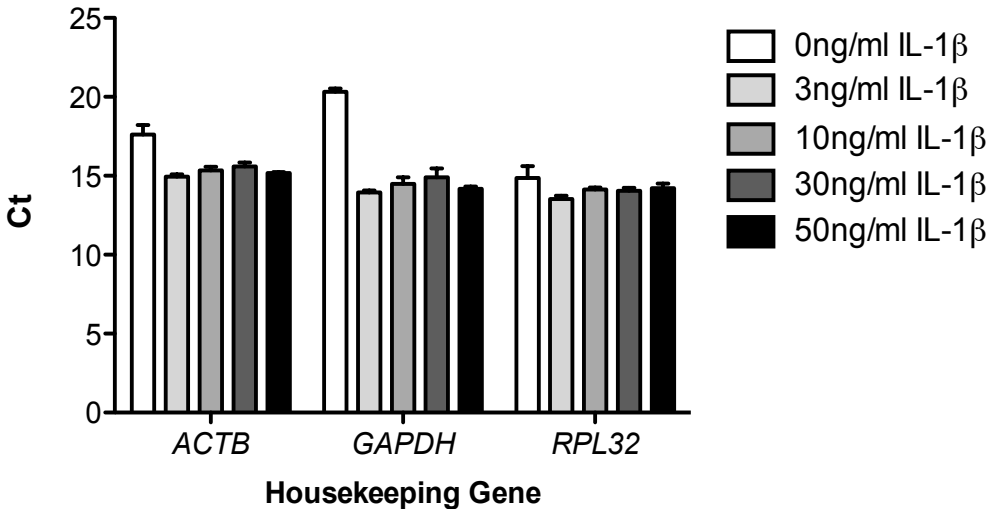

Figure 2.3.7 Housekeeping gene expression in C28/I2 micromasses with IL-1β stimulation. RPL32 was modulated the least by IL-1β stimulation and was therefore chosen as the housekeeping calibrator gene for subsequent mRNA expression studies. Ct, cycle threshold; *ACTB* beta-actin; *GAPDH,* glyceraldehyde phosphate dehydrogenase; *RPL32*, ribosomal protein L32; IL-1β, interleukin 1β.

2.3.7.1 RNA Extraction

Total RNA was extracted using a commercially available kit (Qiagen RNeasy Mini Kit) following manufacturer's guidelines. Briefly, micromass samples were lysed in 350μl RLT buffer [containing 1:100 β-mercaptoethanol] and frozen at -80°C to increase RNA yield. Samples were defrosted on ice before being homogenised by syringing 5 times through a 27.5 gauge needle. 350μl of 70% molecular biology grade ethanol was added and samples were mixed well by pipetting before transferring the entire volume to the RNeasy kit columns. Samples were centrifuged at 10,000 x *g* for 15 seconds and flow-through discarded. 700μl RW1 wash buffer was added to columns and centrifugation for a second time at 10,000 x *g* for 15 seconds followed. Flow through was discarded before the addition of 500μl RPE and a further centrifugation step. A second wash with 500μl RPE followed, and samples were centrifuged a further time at 10,000 x *g,* this time for 2 minutes. The collection tube was discarded and replaced with a new collection tube followed by a centrifugation at 12,000 x *g* for 1 minute to dry the membrane. Columns were placed into new collection eppendorfs and 30μl RNase-free water was added directly to the membrane for RNA elution. Total RNA concentrations and purity was measured using a NanoDrop spectrophotometer and ND 1000 software (NanoDrop Technologies, Wilmington, DE) at 260 and 280nm.

2.3.7.2 cDNA Synthesis

Complementary DNA (cDNA) was obtained via reverse transcription of 0.5μg of the total RNA samples, using Superscript III reverse transcriptase system (Invitrogen, Carlsbad, CA, USA). Firstly, mastermix 1 was created containing 1μl $Oligo(dT)_{15}$ primer, 1μl dNTP mix and 4μl water per sample. Mastermix 1 (6μl) was added to 0.5μg RNA sample (total 7μl volume) and incubated for 5 minutes at 65°C to denature RNA secondary structure followed by incubation on ice at 4°C to allow primer annealing. Mastermix 2 was made by adding 4μl First Strand buffer, 1μl DTT, 1μl RNase OUT and 1μl Superscript III (enough for each sample plus one) and 7μl was added to the samples. Samples were then placed in the Abgene thermal cycler and incubated for 1 hour at 55°C for cDNA extension then heated at 70°C for 15 minutes to deactivate the enzyme and stop the reaction. Negative controls were samples run without Reverse Transcriptase enzyme to exclude the possibility of human (or mouse) genomic DNA contamination.

2.3.7.3 RT-PCR

A mastermix was created for Real-Time PCR (RT-PCR): 2μl water, 5μl of 1X SYBRgreen mastermix and 1μl gene-specific primer - enough for each sample and corresponding gene. Primers were commercially available and used to probe for target mRNA. 2μl cDNA was added to the appropriate mastermixes. RT-PCR was performed using the ABI Prism 7900 real-time PCR system (Applied Biosystems Inc., CA, USA), using the following amplification profile: 2 minutes at 50°C, 15 minutes at 95° followed by 40 cycles of 94°C for 15 seconds, 55°C for 30 seconds and 72°C for 30 seconds. A dissociation step of 95°C for 15 seconds, 60°C for 15 seconds and 95°C for 15 seconds was added after the PCR reaction to confirm the absence of non-specific PCR products. mRNA data were normalised relative to *RPL32* mRNA and then used to calculate expression levels. Results are expressed as $2^{-\Delta\Delta CT}$, which gives the relative amount of target gene normalised to the endogenous constitutive control (*RPL32* RNA) and to the untreated samples (on the same 24 well plate) with the control samples set as 1. Negative controls were PCR without cDNA template.

2.3.7.4 Standard PCR

Conventional end-point PCR was performed by adding 1μl of non-diluted cDNA, 1μl GAPDH or ANXA1 primer to 10μl ThermoPrime ReddyMix PCR Mastermix (Thermo Scientific). PCR tubes were placed in an Abgene thermal cycler and the following program employed: 95°C for 5 minutes, then (95°C for 30 seconds, 55°C for 20 seconds, 72°C for 20 seconds) for 35 cycles; 72°C for 10 minutes. The resulting samples were then loaded on a 3% agarose gel containing 20μl GelRed for visualisation of bands using a FluorChem E Digital Dark Room (Protein Simple).

2.3.8 Prostaglandin E_2 Enzyme Immuno-Assay

Prostaglandin E_2 (PGE_2) enzyme immuno-assay (EIA) was carried out on micromass supernatants from cells stimulated for 24 hours with IL-1β and treated with 100,000 microparticles, Annexin A1 or ceruloplasmin. The Prostaglandin E_2 EIA is a competitive assay based on the competition between Prostaglandin E_2 and a PGE_2 tracer (Prostaglandin E_2-acetylcholinesterase) for a limited amount of the Prostaglandin E_2 monoclonal antibody. The colour change occurs when the substrate to the acetylcholinesterase is added to the wells so that it is proportional to the amount of PGE_2 tracer bound to the well and therefore inversely proportional to the amount of Prostaglandin E_2 present in the sample. The plate is set up to provide absorbance values needed in order to calculate the concentrations of Prostaglandin E_2. Blank, non-specific binding, total activity and total binding wells are required, along with known Prostaglandin E_2 standard samples for interpolation of the results (Figure 2.3.8). The plate wells were filled following Table 2.3.3.

Table 2.3.3 For PGE2 EIA, wells require different reagents to obtain absorbance values for Total Activity, Non-specific binding, total binding and blank wells.

Well	EIA buffer	Sample or standard	Tracer	Antibody
Blank				
Total Activity			5μl at development stage	
Non-specific Binding	100μl		50μl	
Maximum Binding (B_0)	50μl		50μl	50μl
Sample or standard		50μl of diluted sample or standard	50μl	50μl

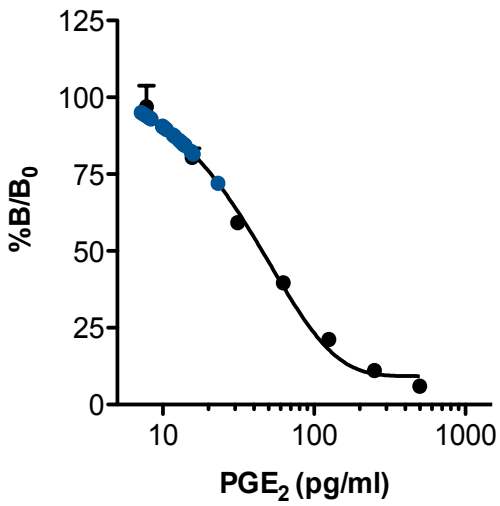

Figure 2.3.8 Prostaglandin E_2 Standard Curve. The Binding of the Standards (B) is transformed by dividing by the Corrected Maximum Binding (B_0), generated by subtracting the averaged absorbance of the non-specific binding wells from the average absorbance of the Maximum Binding wells. By multiplying by 100, the $\%B/B_0$ can then be used to generate a logistic four-parameter fit from which the samples can be interpolated after subtraction of non-specific binding. Supernatants collected from C28/I2 micromasses stimulated with or without IL-1β (3 or 30ng/ml) and 100,000 microparticles for 24 hours were assayed for Prostaglandin E_2 concentration. Blue points show data interpolation from a representative experiment.

The plate was then covered and incubated for 18 hours at 4°C before the wells were washed thoroughly 5 times with wash buffer before 200μl of Elman's development reagent was added to all wells. The plate was covered and incubated for approximately 60 minutes on a shaker at room temperature until the absorbance of the total binding well reaches >0.3 AU when measured spectrophotometrically. The plate was then measured at 420nm using a Multiskan Bichromatic 348 spectrophotometer (Labsystems). To interpolate the concentrations of the EIA, first the non-specific binding well absorbances were averaged, as were the absorbances of the Maximum Binding wells (B_0). The non-specific binding was subtracted from the entire plate, as a blank reading would be during an ELISA. The standards and sample values (denoted B) were then calculated as B/B_0. The $\%B/B_0$ can then be used to generate a logistic four-parameter fit, and the sample concentrations were interpolated.

2.3.9 Cytokine ELISA

IL-8 and IL-6 content in micromass supernatants were assayed using ready-set-go! ELISA kits (eBioscience). Corning Costar 9018 96-well plates were coated with 100μl capture antibody prepared in coating buffer, covered with parafilm and incubated overnight at 4°C. Wells were washed 3 times using 250μl wash buffer (PBS containing 0.05% Tween-20; 1 minute incubation between each wash) before blotting dry on paper towels. Wells were blocked with 200μl 1X assay diluent (diluted in deionized water) for 1 hour at room temperature. Standards were generated by diluting recombinant IL-8 or IL-6 to achieve a top standard or 250pg/ml for IL-8 and 200pg/ml for IL-6 and serially diluted down to 3.125pg/ml. After washing, 100μl of each standard was added to two columns of the 96-well plate, including two blank wells, which included only phenol-red and serum-free RPMI, the same medium the micromasses were stimulated in. The plate was then sealed and incubated at room temperature for 2 hours. The plate was washed three times as before, then 1X detection antibody was diluted in assay diluent and 100μl added to each well. The plate was incubated for 1 hour at room temperature before another 3 washes, with 2-minute incubations to ensure any excess detection antibody was removed. 100μl of substrate solution was added to each well and the plate incubated at room temperature for 15 minutes before 50μl stop solution (2N H_2SO_4) was added. The plate was then read at 450nm with 570nm wavelength subtraction using a Multiskan Bichromatic 348 spectrophotometer (Labsystems, Finland). Sample concentrations were then interpolated from the standard curve (Figure 2.3.9).

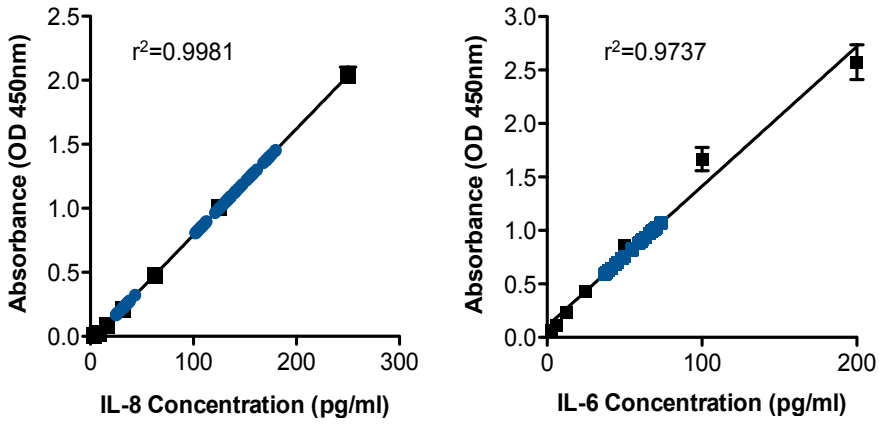

Figure 2.3.9 Standard Curve for IL-8 or IL-6 ELISA. C28/I2 micromasses were stimulated with or without IL-1β (3ng/ml and 30ng/ml) and 100,000 microparticles for 24 hours. Supernatants were collected and assayed for IL-6 and IL-8 concentration. Blue points show data interpolation from a representative experiment.

2.3.10 Cytokine Bead Array for TGF-β

Transforming growth factor beta 1 (TGF-β) concentrations were measured in the supernatants of micromasses using a BD Cytometric Bead Array. Supernatants from micromasses cultured in 300μl serum free differentiation medium were assayed for TGF-β content following acidification to remove the latency-associated protein. To do this, samples (300μl) were acidified to pH 3.0 with 60μl 1N HCl, mixed thoroughly and incubated at room temperature for 10 minutes. Samples were neutralised to pH 7.2 with 60μl of 1.2N NaOH/0.5M HEPES. Once the latency-associated protein was removed, the immunoreactive TGF-β could then be assayed.

The cytokine bead array system uses particles with discrete fluorescence intensities to test low concentration analytes such as cytokines. The TGF-β is captured by antibody-coated beads of a known size and fluorescence, and is detected by PE-conjugated detection antibodies, allowing determination of the concentration of the sandwich complexes by flow cytometry. It is the PE intensity from which the concentration can be inferred.

Firstly, standards are generated for inferring the unknown sample concentrations, which are reconstituted and serially diluted to give a range of 10ng/ml to 39pg/ml plus a 0ng/ml blank sample. The capture beads are then diluted 1:50 in capture bead diluent, vortexed for 15 minutes then 50μl added to each undiluted sample (50μl acidified/neutralised sample). Samples were incubated for 1 hour at room temperature. The PE detection reagent was then diluted 1:50 in detection reagent diluent, mixed well, then 50μl was added to each sample. Tubes were incubated for 2 hours in the dark at room temperature. 1ml of wash buffer was added to each sample and eppendorfs centrifuged for 5 minutes at 200 x *g*, supernatant discarded and pellets resuspended in 300μl wash buffer for sample collection using a BD LSRFortessa flow cytometer. During sample acquisition, standards were acquired with blank first, then increasing concentrations from lowest to highest. Samples were acquired on high and analysed using FCAP Array software downloaded from the BD website. Sample concentration was interpolated from the standard curve after fitting with a 5 parameter logistic (which resulted in the best curve fit, with a higher R^2 (>0.98) value than 4 parameter logistic). Sample concentrations were then multiplied by a 1.4 dilution factor to account for the acidification/neutralisation step.

2.3.11 Griess Assay

Conditioned supernatants (phenol-red free RPMI supplemented with ITS 1%) from the culture of rat femoral heads were snap frozen and stored at -80°C before Griess assay. Nitric oxide levels in biological fluids can be inferred from the concentration of one of the stable breakdown products, nitrite (NO_2-), measured by the Griess assay. The Griess reagent system (cat. G2930, Promega) uses sulphanilamide and *N*-1-napthylethylenediamine dihydrochloride (NED; added sequentially to increase sensitivity) which react with NO_2- producing an Azo compound under acidic conditions. To measure the nitrite concentration in femoral head cultures, 50μl was added in triplicate to a 96-well plate. A nitrite standard reference curve was generated in the first three columns of the 96 well plate: 1ml of a 100μM nitrite solution was made by diluting 0.1M nitrite standard 1:1000 in supplemented RPMI (the same buffer used for femoral head culture). 100μl of the top concentration standard was added to three wells and a serial dilution performed by taking 50μl from the first well and added to 50μl supplemented RPMI and so on, to generate 7 standards of decreasing concentration, from 100μM, 50μM, 25μM, 12.5μM, 6.25μM, 3.125μM and 1.56μM. Supplemented RPMI only was added to the final well to create a blank reading. Using a multichannel pipette, 50μl room temperature sulphanilamide solution (1% in 5% phosphoric acid) was added to every well and incubated for 10 minutes at room temperature in the dark. Then, 50μl of NED (0.1% in water) was added to every well. The plate was incubated at room temperature in the dark until the standard curve had developed a magenta colour, which took around 5 minutes. The plate was then analysed using a spectrophotometer at 530nm. The standard curve was generated by plotting the average absorbance of each standard against the nitrite concentration (Figure 2.3.10).

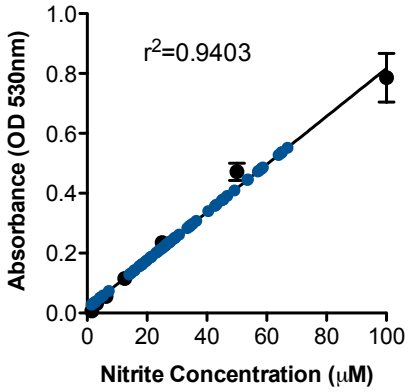

Figure 2.3.10 Standard Curve used in Griess Assay. Supernatants collected from the culture of rat femoral heads stimulated with or without IL-1β (10ng/ml) and 100,000 microparticles every two days for 7 days, then assayed for nitrite concentration. Blue points show data interpolation from representative experiments.

2.3.12 *In Vivo* Experiments

All experiments were approved and performed under the guidelines of the Ethical Committee for the Use of Animals, Barts and The London School of Medicine and Home Office regulations (Scientific Procedures Act, 1986). C57BL/6 mice were purchased from Charles River. Fpr1, Fpr2/3 and Anxa1 null mice were generated in-house on the C57BL/6 background. In all experiments age and sex-matched controls were used. Mice were fed standard laboratory chow and water *ad libitum* and were maintained on a 12 hour light-dark cycle under specific pathogen-free conditions. All experiments strictly followed UK Home Office regulations (Guidance on the Operation of Animals, Scientific Procedures Act, 1986).

2.3.12.1 K/BxN Serum Arthritis

K/BxN serum transfer arthritis was used to recapitulate the neutrophil-rich flare-phase of human RA. This model is adaptive immune cell-independent; instead the deposition of glucose-6-phosphate isomerase antibodies from the arthritogenic serum onto the surface of the cartilage initiates an innate immune response mainly mediated by leukotriene B_4 recruiting neutrophils and mast cells (Chou et al., 2010). K/BxN serum transfer arthritis is an acute, aggressive polyarthritis with high disease penetrance, which resolves over 28 days. Eight-week old male C57BL/6 mice were injected intraperitoneally with 100μl arthritogenic serum (generated in-house and diluted in 100μl PBS) on day 0 and day 2. Arthritic parameters were recorded everyday including clinical score, where any digits, wrists, ankles or pads on each limb were swollen, for a total score out of a possible twelve (Figure 2.3.11); weight loss (cachexia) and water displacement plethysmometry performed to determine paw volume. In addition, mice injected intra-articularly had their knee widths measured using digital calipers daily.

In the first set of arthritis experiments, K/BxN mice received 100,000 TMP intravenously, or 100μl saline as a vehicle control, at the peak of disease on day 5, with joints collected on day 8 for histological analysis.

0 – No signs of arthritis

1 – A single swollen digit, wrist, ankle or pad

2 – a combination of two swollen areas. Multiple digits count as a score of 1.

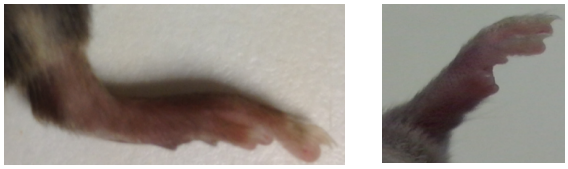

3 – Swollen wrist or ankle AND pad AND any digit

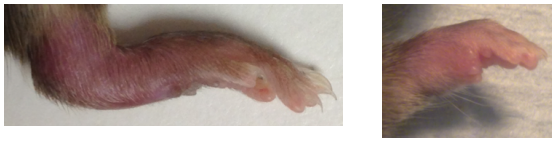

Figure 2.3.11 Arthritis scoring procedure. Arthritis scoring was carried out as follows: each limb was inspected for signs of swelling and given a score based on the part of the paw which was swollen. Any swollen digit (one, or more than one) was given a score of one, as was a swollen pad, wrist or ankle. Any of these in combination could be observed to give a total score out of three. This scoring system was used for both K/BxN K/BxN arthritis and collagen-induced arthritis, and was used to monitor the progression of the disease throughout the experiment.

In further experiments where microparticles were delivered locally, mice were injected on day 3, intra-articularly into the knees with 6μl buffer using a 31.5-gauge needle attached to a 10μl gas-tight Hamilton syringe for increased accuracy. The buffer contained either vehicle (sterile saline), TMP (10,000 or 30,000) with or without WRW_4 (10μM) or WRW_4 alone. Both wild type and Fpr2/3 mice were used. Some mice had their arthritis evaluated by in vivo bioluminescence imaging (see section 2.3.12.2). Joints were collected on day 5 for histological analysis.

2.3.12.2 Adoptive Transfer of Bodipy-maleimide Labelled Mouse Neutrophils into K/BxN Mice

Wild type C57BL/6 donor mice were injected with zymosan (1mg/mouse, i.p.) to induce neutrophilic peritonitis (Figure 2.3.12). Exudated neutrophils were collected 4 hours later by peritoneal lavage with PBS and the cells were labelled with Bodipy-maleimide dye (2.5μM) and analysed by flow cytometry. Labelled neutrophils (1 x 10^6 per mouse) were adoptively transferred to wild type mice on day 3 of K/BxN serum-induced arthritis via tail vein injection. Wrists were collected 24 hours later into OCT medium and sectioned using diamond blades on a cryotome. Sections were processed for confocal microscopy. Sections were stained with rat anti-mouse MRP14/S100A9 antibodies and DAPI to visualise the nuclei (see section 2.3.14).

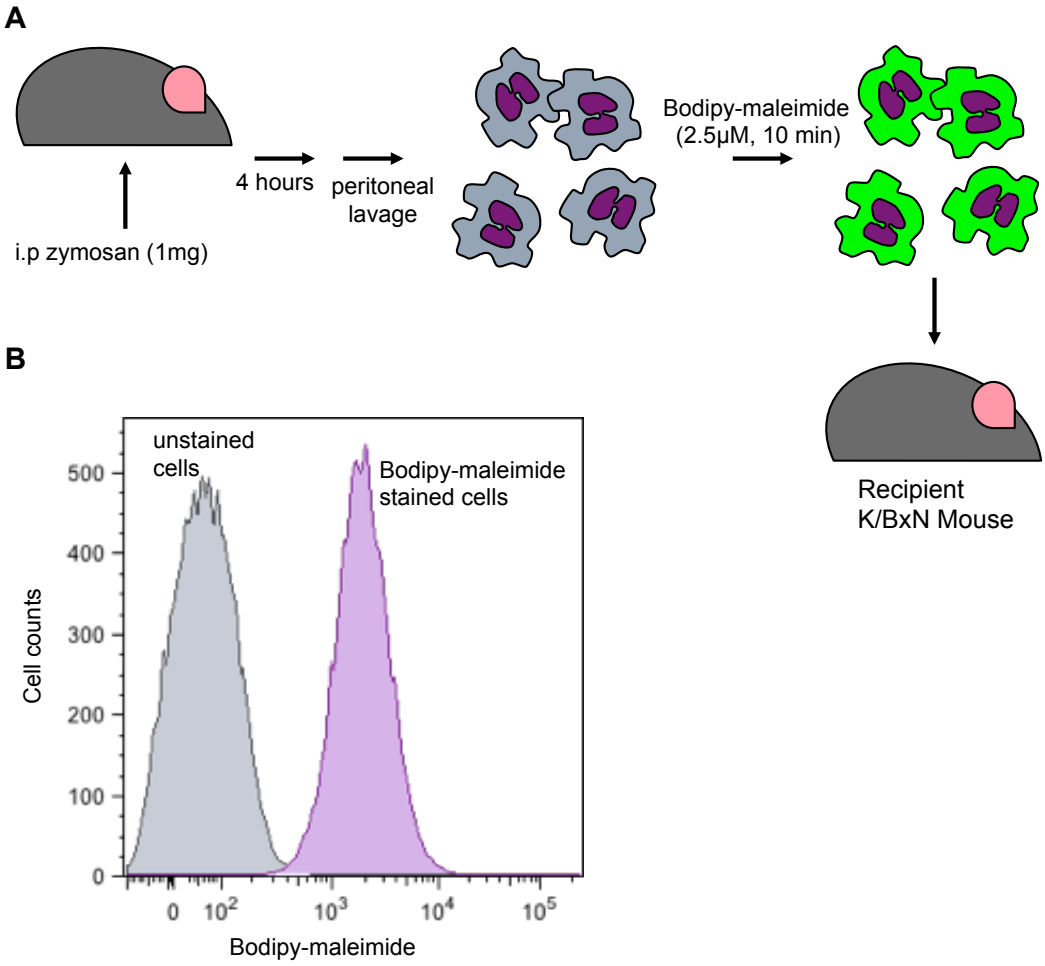

Figure 2.3.12. Generation of Bodipy-maleimide labelled neutrophils for adoptive transfer into K/BxN mice. (A) Schematic of experimental procedure. (B) All cells stained with Bodipy-maleimide when analysed by flow cytometry.

2.3.12.3 IVIS Bioluminescence Imaging

On day 5, anaesthetised (isoflurane mixed with oxygen) mice undergoing K/BxN arthritis were imaged using an IVIS bioluminescence imager to detect inflammation (Gross et al., 2009). The mice were injected with 50mg/kg luminol sodium salt (Sigma) in PBS 10 minutes prior to imaging with the IVIS 200 system (Caliper, Hopkinton, MA). Extracellular myeloperoxidase, a product of neutrophil primary granule release and therefore indicative of acute or neutrophillic inflammation, cleaves luminol into a luminescent compound allowing detection by bioluminescent imaging. For photon quantification, a region of interest was manually selected and kept constant throughout (f/stop 1, no optical filter). Photons emitted from live mice were acquired as photons per s/cm^2 per steradian, using Living Imaging 3.0 (Caliper). By creating regions of interest (ROIs), the photon emission per second can be determined and background luminescence subtracted by placing an ROI on a non-inflamed part of the body, in this case the abdomen or chest of each mouse (Figure 2.3.13).

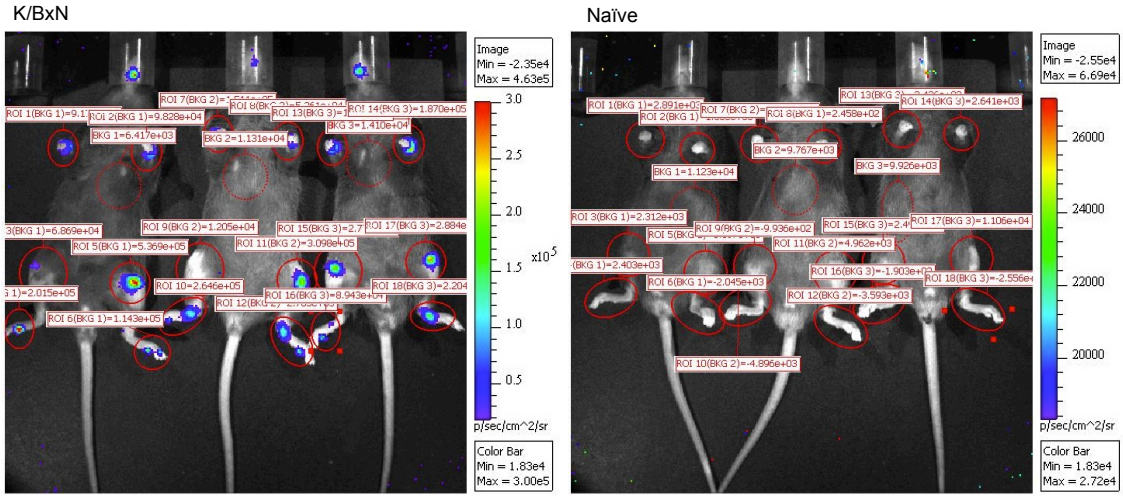

Figure 2.3.13 Interrogation of Regions of Interest (ROI) during IVIS Bioluminescence Imaging. Mice were injected with 50mg/kg Luminol salt for 10 minutes before imaging. Regions of interest were generated using Living Imaging 3.0 and photons per second analysed after subtracting the background signal from the abdomen or chest of each mouse.

2.3.13 Histological Staining and Analysis

Joints were collected on day 8 or day 5 for K/BxN experiments. The entire hind limbs with skin removed were fixed for 48 hours in neutral buffered formalin (40X the volume of the limb, around 50ml each; 10% neutral buffered formalin containing 0.4% sodium phosphate, monobasic and 0.65% sodium phosphate dibasic) before decalcification in 10% formic acid for 24 to 48 hours. To determine full decalcification, a fine needle was used to test the softness of the bones. Once decalcification was complete, tissues were dissected into knee tissues and paw tissues and placed in labeled tissue cassettes for embedding separately. Cassettes were placed in running tap water for one hour, then left in tap water overnight to help remove the formic acid. Samples were then placed in 70% ethanol and processed for wax infusion in a Leica Tissue Processor. Finally, knee samples were embedded in molten paraffin wax using small molds. Knees were embedded coronally, so that the knee joint faced the front of the block with the femur and tibia perpendicular to each other. Embedded sample blocks were left to harden on a cold plate (-4°C) before being removed from their molds. Blocks were then kept at -20°C degrees to harden for cutting. Sections (10μm) were cut using a Leica microtome, and placed on lukewarm water to remove wrinkles. Sections were transferred to charged glass microscope slides and left to dry.

Before staining, dried slides were placed in a 65°C oven to soften the wax, which was removed by two 5-minute incubations of histoclear (xylene replacement). Sections were rehydrated by moving from 100% ethanol for 5 minutes to 95% ethanol for 5 minutes followed by distilled water for 2 minutes before proceeding to staining.

2.3.13.1 Toluidine Blue Staining

Toluidine blue is superior to Safranin O in delineating differences in metachromasy between pericellular and interterritorial regions of articular cartilage. The reproducibility of staining between serial sections relies on section thickness: sections thinner than 8μm show modest to significant variability in metachromatic staining, whereas those cut at 8-10μm achieve superior reproducibility and staining intensity (Getzy, 1982).

Slides were placed in 1% toluidine blue dye for 10 minutes before being washed with tap water for 5 minutes (or until the water was clear). Slides were air dried before mounting in DPX slide mountant (Sigma) and left to harden for 24 hours.

2.3.13.2 Toluidine Blue Percentage Area Positive Quantification

The quantification of percentage area toluidine blue positive was carried out in a similar manner to that of Safranin O quantification (2.2.5.3). Slides were viewed using an Olympus BH-2 standard light microscope and Nikon DXM1200 digital camera. Acquired images were opened in ImageJ and split into individual RGB channels. The hue of the toluidine blue dye is dependent on the pH, thus, the channel which best represented the positive and negative staining was not necessarily the same for each experiment, and had to be selected at the time of analysis. The selected channel then had a threshold masked over the top and the area of the cartilage traced. The threshold mask was then measured over the selected area.

2.3.13.3 Safranin O Staining

Rat femoral head cartilage explants were collected and fixed overnight in paraformaldehyde (4%) before embedding in OCT and sectioned at 10μm. Slides were counterstained in fast green (0.1% dye in distilled water) or haematoxylin for 5 minutes then dipped 10 times in 0.1% acetic acid. Slides were incubated for 20 minutes in Safranin O (0.1% in acetate acid buffer; 0.1M acetic acid-sodium acetate buffer at pH 5.0; 0.8% sodium acetate in 0.1M acetic acid) before washing in gently running tap water for 5 minutes. Slides were then air dried, mounted with DPX and left to harden for 24 hours. Sections were imaged using a standard light microscope (Olympus BH-2) and Nikon DXM1200 digital camera. Percentage area Safranin O positive staining was calculated using a threshold applied using ImageJ imaging software (see section 2.2.5.3).

2.3.13.4 Haematoxylin and Eosin Staining

Dewaxed and rehydrated slides were incubated in haematoxylin for 2 minutes then rinsed in tap water for 5 minutes to remove excess stain but also to blue the nuclei by introducing a more alkali pH. Slides were then stained for 30 seconds to 1 minute in eosin before another wash in tap water. Slides were then dehydrated with 5 minutes each in graded ethanol (70%, 90% and 100% ethanol, five minutes each) followed by clearing twice in Histoclear for 5 minutes. Slides were left to dry completely before mounting in DPX mounting medium and left to harden for 24 hours. Images were captured using an Olympus BH-2 microscope (Tokyo, Japan) with fluorescent filters and Nikon DXM1200 digital camera (Melville, NY).

2.3.14 Fluorescence and Confocal Microscopy

2.3.14.1 Sample Preparation

Freshly isolated neutrophils ($1x10^5$) were seeded onto positively charged glass microscope slides and checked to ensure even distribution of the cells using a light microscope. Cells were left to dry at room temperature. Once dried, slides were either mounted immediately using ProLong immunogold antifade reagent containing DAPI for visualisation of the nucleus, or permeabilised in ice-cold acetone for ten minutes. Once dry, a wax ring was applied using a Dako wax pen and slides placed in a humidified chamber for staining. Cells were blocked for 1 hour at room temperature using 10% fetal bovine serum in Tris-buffered saline (FBS/TBS). MRP8 antibody or isotype antibodies at the same concentration diluted in 10% FBS/TBS (50µl) were added directly on top of the blocking solution and incubated for 1 hour in the dark at room temperature. Slides were then rinsed three times in 1% FBS/TBS followed by a brief dip in double-distilled ultrapure water to dissolve any remaining salts. Slides were then dried in the dark and mounted in ProLong immunogold antifade reagent containing DAPI to stain the nuclei.

Pre-labelled microparticles were applied to charged glass microscope slides and allowed to dry. Slides were dipped briefly into double distilled ultra-pure water to dissolve any salts in the buffer before being allowed to dry again. Microparticles were mounted with ProLong immunogold antifade reagent.

Rat femoral heads were cryosectioned to 10µm, applied to charged glass microscope slides and allowed to dry. To determine whether any background staining from MRP8 antibodies occurred, MRP8 antibodies were tested at two concentrations. Sections were permeabilised in ice-cold acetone for 10 minutes and once dry, a wax ring was applied using a Dako wax pen and slides placed in a humidified chamber for staining. Sections were blocked for 1 hour at room temperature using 10% fetal bovine serum in Tris-buffered saline. MRP8 antibody or isotype antibodies at the same concentration diluted in 10% FBS/TBS (50µl) was added directly on top of the blocking solution and incubated for 1 hour in the dark at room temperature. Slides were then rinsed three times in 1% FBS/TBS. DAPI nuclear stain was tested at two concentrations, diluted in TBS and incubated for 10 minutes in the dark followed by a brief dip in double-distilled ultrapure water to dissolve any remaining salts. Sections were left to dry then mounted with ProLong immunogold antifade reagent.

Alternatively, rat femoral head explants treated with human microparticles were stained to determine the localization of human antigen. After ringing with a Dako wax pen, sections were blocked using 10% fetal bovine serum in Tris buffered saline (FBS/TBS) for one hour in a humidified chamber. Sections were either stained with Annexin A1 purified monoclonal antibody for one hour in the dark at room temperature followed by washing 3 times in 1% FBS/TBS before the secondary antibodies were added, or stained with anti-human MRP8 conjugated antibody. Slides were then washed 3 times in 1% FBS/TBS. The matrix was visualised by staining with wheat germ agglutinin conjugated to AlexaFluor633 (1:500 diluted in 1% FBS/TBS) for 10 minutes in the dark at room temperature followed by a further 3 washes in FBS/TBS. Slides were dipped briefly into double distilled water to dissolve any salts and sections left to dry. Slides were mounted using ProLong immunogold antifade reagent containing 4,6-diamidino-2-phenylindole (DAPI).

2.3.14.2 Fluorescence Microscopy

Slides were analysed by fluorescence microscopy using an Olympus BH-2 microscope connected to a Nikon DXM1200 digital camera. Image capture was carried out using Lucia imaging software. DAPI staining was visualised on the UV channel (excitation wavelength 360-370 nm), Alexa488 FL1 channel (excitation wavelength 460-490 nm) and Alexa555 FL2 channel (excitation wavelength 530-560 nm).

2.3.14.3 Fluorescence Time-Lapse Imaging

For fluorescence microscopy time-lapse imaging, freshly isolated neutrophils resuspended at 1 x 10^6 cells/ml in phenol red-free RPMI were added to a 12-well suspension culture plate following labelling with Bodipy-maleimide dye (2.5μM). Cells were visualised with an EVOS fluorescence microscope (Invitrogen) with a X60 long working-range objective. TNF-α (50ng/ml) was added once the cells had settled and a budding neutrophil visualised. Following 5-minute stimulation, time-lapse images were captured once every minute using a GFP LED cube. Images were cropped using Microsoft Office PowerPoint but no further adjustments made.

2.3.14.4 Confocal Microscopy

Confocal microscopy was carried out using a Zeiss LSM 510 laser scanning confocal microscope with supplied Zeiss imaging software. The following excitation/emission conditions were used in separate channels with either the X40 or X63 oil immersion objective: DAPI 364/475–525 nm, Bodipy-maleimide or 488/505–530 nm, and AlexaFluor546 at 543/560 – 600 nm.

2.3.14.5 Analysis of Images for Microparticle Penetration

Images acquired with the Zeiss LSM scanning confocal microscope were analysed for the distance travelled by microparticles co-cultured in Rat femoral heads using ImageJ imaging software. Micrographs were checked for microparticle positivity by eye: distinct double-stained puncta, positive for MRP8 and Bodipy-maleimide fluorescence, or Annexin A1 and Bodipy-maleimide fluorescence; or diffusely double-positive chondrocytes which had taken up and dismantled microparticles were measured. Using the ImageJ measurement tool, the distance from the centre of the microparticle or cell to the articular surface was measured. The metadata from the file ensured correct pixel/absolute size calibration, and this was double-checked by measuring the scale bar in each image. All microparticle positivity was measured in each micrograph (in total 140 microparticles from control femoral heads and 166 microparticles in IL-1β treated femoral heads) and 6 micrographs from each treatment were measured (maximum 2 micrographs from each cartilage donor). Each of the measurements was then manually binned in GraphPad Prism software to generate histograms. The data was then displayed as Box and Whisker plots with Tukey's whiskers to demonstrate outliers.

2.3.15 Preparation of Samples for Electron Microscopy

C28/I2 and primary adult human articular chondrocyte micromasses were collected 24 hours after stimulation with IL-1β (30ng/ml) and were fixed in 4% paraformaldehyde, 0.5% glutaraldehyde and 0.1M sodium cacodylate buffer (pH 7.4) for 24 hours at 4°C. The micromasses were then transferred to 10% fixative solution (diluted in sodium cacodylate buffer) at 4°C and transported to São José do Rio Preto, Immunomorphology laboratory department. Samples were kindly processed by Dr Cristiane Damas Gil.

2.3.16 RNA Extraction From Formalin-Fixed, Paraffin Embedded Sections.

In order to determine mRNA expression profiles from K/BxN mice injected intra articularly with microparticles on day 3 of 5, total mRNA was extracted from formalin-fixed, paraffin embedded sections using a commercially available kit (PureLink FFPE Total RNA Isolation Kit, Invitrogen). Sections (8 x 10μm) at the region of interest (cut far in to the joint enough to create sections where the menisci form triangles) were collected into sterile, RNase free eppendorfs before 300μl Melting Buffer was added. Eppendorfs were centrifuged for 20 seconds at 10,000 x *g* then incubated for 10 minutes at 72°C using a heating block, to melt the paraffin. Proteinase K (20μl, for genomic DNA removeal) was then added to each sample, and the tubes incubated at 60°C for 1 hour before gentle mixing. The samples were then incubated for a further 30 minutes, so that the lysis was complete. The samples were immediately transferred to a microfuge and centrifuged for 1 minute at 10,000 x *g* so that the paraffin separated from the sample lysate. The lysate was then collected by piercing the paraffin meniscus with a pipette tip and aspirating the lysate. This was placed in a fresh sterile eppendorf and 400μl Binding Buffer and 800μl 100% molecular biology grade ethanol added. The solution was mixed well, then 700μl transferred to a Spin Cartridge mounted on a Collection Tube. The sample was centrifuged at 800 x *g* for 1 minute, flow-through discarded, and the remaining sample added to the Spin Cartridge to ensure all RNA was collected. The tube was spun again at 800 x *g* for 1 minute. The flow-through was discarded and the Spin Cartridge placed into a clean Wash Tube. Wash solution was made by adding 80ml 100% molecular biology grade ethanol to 20ml Wash Buffer and mixing well. 500μl Wash solution was added to each Spin Cartridge and samples centrifuged at 10,000 x *g* for 1 minute. This wash step was repeated 3 times, with flow-through discarded each time. The Spin Cartridge was spun once more at 10,000 x *g* without adding wash solution to remove any excess ethanol and dry the membrane. For elution of the RNA, Spin Cartridges were mounted onto a clean Recovery Tube then 50μl of RNase-free water, heated to 65°C, was added to the center of the cartridge membrane. After 1 minute, the samples were centrifuged for 1 minute at 10,000 x *g*. The elution step was repeated once more to increase RNA yield. Samples were then analysed for concentration and purity using a NanoDrop spectrophotometer. Total RNA was reversed transcribed as described (section 2.3.7) and used for RT-PCR analysis as described (section 2.3.7), using mouse primers (see Table 2.1.2).

2.3.17 Statistical Analysis

Statistical analysis was assessed using GraphPad Prism 4 (San Diego) software, SPSS software or GraphPad Prism software. Data are expressed as mean ± standard error of the mean (SEM) of n experiments for parametric data, and median, interquartile range (IQR) and range for non-parametric data. All data were tested for normal distribution and statistical differences were analysed using the tests outline in Table 2.3.4. A *P* value of <0.05 was considered significant to reject the null hypothesis and differences were considered significant. All tests performed used a two-tailed significance value unless specifically stated. One-tailed significance cut-offs were chosen *a priori*.

Table 2.3.4 Statistical tests used during this project and when they were applied.

Statistical Test	Data used	Parametric/non parametric
Paired t-test	Two groups within the same animal, e.g. paired knee analysis of proteoglycan content	Parametric
Mann-Whitney t-test	Two groups with non-Gaussian distribution, such as the distance of microparticle penetration measured in IL-1β-treated or resting cartilage	Non-Parametric
Kruskall-Wallis test with Dunn's multiple comparison post-test	Nonparametric data generated with $2^{-\Delta\Delta CT}$ values, three or more groups tested	Non-parametric
One-way ANOVA with Bonferroni post-test	Three or more groups tested, with normal, homogenous data such as proteoglycan release into the medium of micromass cultures measured by DMMB assay	Parametric
Two-way ANOVA with Bonferroni post-test	Three or more groups tested with two variables. Used for testing differences both within and between groups and determining differences in mRNA expression from RT-PCR on Logged data.	Parametric
Matched Two-way	Three or more groups tested with two	Parametric

ANOVA with Bonferroni post-test	variables. Used for testing differences within groups over a period of days, such as with mouse body weight during arthritis, or for data paired for individual mice, for example intra articular injections of TMP in one knee, and vehicle in the contralateral knee.	
Mixed Model ANOVA with Bonferroni post-test	Used for matched (in vivo) data of more than two groups, with more than one variable (e.g. genotype) where the group sizes are not necessarily equal.	Parametric

Non-parametric data which required Two-way ANOVA analysis were normalized by logging the data before performing Two-way ANOVA statistical analysis. Data is displayed in the graphs as unnormalised.

CHAPTER 3: CHARACTERISATION OF HEALTHY NEUTROPHIL-DERIVED MICROPARTICLES

3.1 Characterisation of Neutrophil Microparticles

Microparticles derived from various cell-types have been shown to be abundant in the rheumatoid synovium (Berckmans et al., 2005, Berckmans et al., 2002, Boilard et al., 2010, Cloutier et al., 2013), and yet microparticle phenotype (and function) reflects the phenotype of the parent cell (Timar et al. 2013). For example, Dalli et al. (2013) showed that neutrophils stimulated in suspension produce proteomically distinct microparticles from those adhered to endothelial cells. Additionally, Timar et al. (2013) demonstrated that differential stimulation of neutrophils leads to different numbers of microparticles being generated. Neutrophils exposed to opsonised *Staphylococcus aureus* bacteria generated the highest number of microparticles, followed by phorbol esters and TNF-α. In contrast, resting neutrophils generated more microparticles than those stimulated with stromal-derived factor (SDF-1 also known as CXCL12), lipopolysaccharide (LPS) and formyl-methionyl-leucyl-phenylalanine (fMLP). Therefore it was important to characterise the function of microparticles not only derived from a single cell type (in this case the neutrophil) but also to demonstrate that a neutrophil microparticle derived from a resting cell may be phenotypically dissimilar to one shed by a stimulated cell.

Furthermore, as microparticles are known to be abundant within the rheumatoid synovium, I wanted to generate neutrophil microparticles *in vitro* to use as a surrogate model. In order to induce microparticle shedding in a manner relevant to rheumatoid arthritis, I selected TNF-α and IL-8 to stimulate the neutrophils. In addition to these cytokines present within the rheumatoid joint are a multitude of other cytokines, chemokines and proinflammatory mediators, but these are the most potent cytokine stimulators of neutrophil degranulation, and induce neutrophil activation in a manner representative of this autoimmune disease, rather than say, bacterial infection or cell injury (such as LPS or formylated peptides). Of note, IL-1β is known to have important functions in rheumatoid pathogenesis, however its actions are more indirect in terms of neutrophil activation, instead inducing stromal cells to produce activation and survival signals (Prince et al., 2004).

Thus, TNF-α, an important cytokine involved in the pathogenesis of rheumatoid arthritis was chosen as the stimulus for microparticle generation in preliminary studies, and compared to those generated by IL-8 (CXCL8) stimulation, a potent neutrophil chemoattractant, which had not previously been tested.

3.1.1 Characterisation of Neutrophil Microparticles by Size and Number

The sizing and enumeration of microparticles from biological fluids or culture supernatants is not simple, and no gold standard exists for the accurate measurement of microparticle parameters. Traditionally, flow cytometry has been used as the mainstay of microparticle analysis, however this technique has major drawbacks in terms of detecting microparticle size, and differentiating the true microparticle signal from noise. Thus a variety of methods must be used to corroborate data, including the use of cutting edge imaging technologies, such as the ImageStream^{x}, and re-appropriating analysers used for quality control in industrial chemical applications, such as with Nanoparticle Tracking Analysis.

To confirm the purity of isolated neutrophils from healthy volunteers, they were first characterised by flow cytometry (Figure 3.1.1). From forward scatter/side scatter plots the isolated cell population was 98% polymorphonuclear cells, with 2% contaminating lymphocytes, with no visible contaminating monocytes when nuclei were fluorescently stained (Figure 3.1.1A and B). To determine whether the cells were activated by TNF-α (50ng/ml) and IL-8 (50ng/ml), the cells were stained for the activation markers CD11b and CD62L (Figure 3.1.1C and D). TNF-α induced CD11b up-regulation and near-complete shedding of CD62L, which is a typical profile for activated neutrophils. IL-8, a potent chemotactic stimulus, did not induce full CD62L shedding nor CD11b up-regulation to the same extent, which was expected. Therefore the cells had not released their secretory granules to the same extent when exposed to this stimulus.

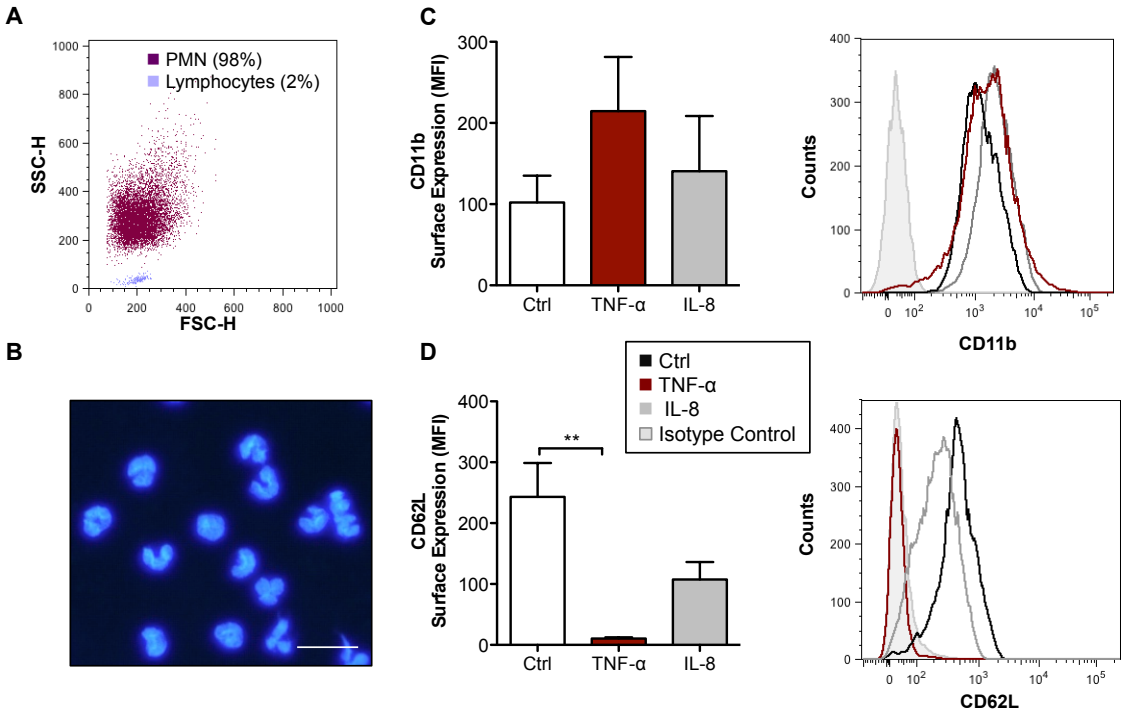

Figure 3.1.1 Characterisation of neutrophils used to generate microparticles. Neutrophils (2 x 10^7/ml) were isolated from healthy donors, stimulated with TNF-α (50ng/ml), IL-8 (50ng/ml) or Ctrl (vehicle; PBS) for 20 minutes at 37°C and analysed by flow cytometry for activation markers. (A) Purity of isolated neutrophil (polymorphonuclear cells; PMN) population as shown by representative FSC/SSC plot. (B) Fluorescent micrograph of freshly isolated neutrophils stained with DAPI to demonstrate characteristic nuclei. Scale bar denotes 25μm. (C) Expression of neutrophil activation markers CD11b and (D) CD62L. Data are shown as mean ± SEM of mean fluorescence intensity (MFI; arbitrary units) of 3 different blood donors. $^{**}P<0.01$ using One-way ANOVA with Bonferroni post-test. Right-hand panels show representative histograms.

Microparticle production however was significantly up-regulated by both TNF-α and IL-8 as measured by flow cytometry (Figure 3.1.2A). TNF-α stimulation of 1 x 10^7 neutrophils (total; at 2 x 10^7/ml) induced more than double the number of microparticles (referred to as TMP) shed in 20 minutes at 37°C compared to control (referred to as CMP; 9.1 ± 1.3 vs. 3.9 ± 0.3 x10^7/ml, *P*<0.01 with One-way ANOVA), and IL-8 induced double the amount of microparticle shedding (IMP; 8 ± 1.1 vs. 3.9 ± 0.3 x10^7/ml, *P*<0.05). The offspring microparticles appeared below 1μm calibration beads (shown in purple) on the forward/side scatter plots set to log scale, when gated from their fluorescence versus side-scatter signal following loading with Bodipy-maleimide dye (Figure 3.1.2B).

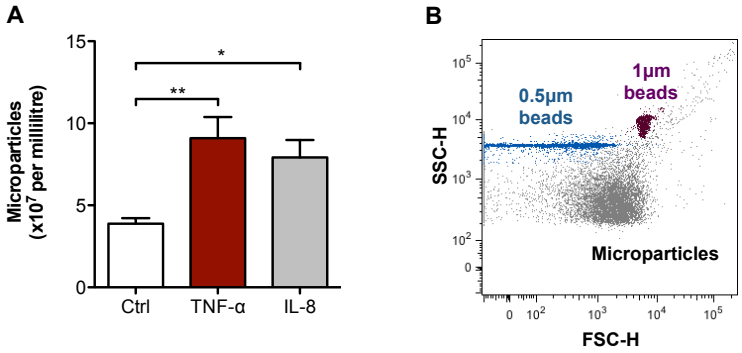

Figure 3.1.2 Stimulation of neutrophils increases microparticle generation. Neutrophils (1 x 10^7) were stimulated with TNF-α (50ng/ml), IL-8 (50ng/ml) or vehicle (PBS) for 20 minutes at 37°C to induce microparticle release. (A) Microparticle numbers were quantified by flow cytometry after loading with Bodipy-maleimide dye (2.5μM) and by measuring the number of events double positive for neutrophil marker expression (CD66b) and Bodipy-maleimide versus flow rate. Data are shown as mean ± SEM of 5 different blood donors. **P*<0.05 and ***P*<0.01 using One-way ANOVA with Bonferroni post-test. (B) Representative FSC/SSC plot showing microparticles (grey) with 1μm (purple) and 0.5μm (blue) comparison beads.

Flow cytometry is a largely inaccurate method for sizing and enumeration of microparticles, so a new technology, in the form of ImageStream^{x} analysis was employed to further analyse neutrophil microparticles. This analyser is part high-sensitivity flow cytometer, part high-resolution microscope, which uses a syringe pump to drive the sample and can therefore calculate the absolute concentration from the volume consumed during analysis, allowing for accurate derivation of the sample concentration without the need for calibration beads. Also, unlike a flow cytometer, the smallest object that can be detected is a function of its brightness, so fluorescently labelled samples as small as 50nm can be assessed (see section 2.3.3).

Using this method it was found that the number of TMP produced from 5 x 10^6 TNF-α-stimulated neutrophils (total; at 2 x 10^7/ml) is over double that of resting cells (3.6 ± 0.9 vs. 1.2 ± 0.3 x10^7 microparticles/ml, P<0.05 with paired t test), although around two times lower than that calculated by flow cytometry (Figure 3.1.3). It is also possible to get some idea of the size of the microparticles using this technology. It was found that microparticles appeared to be more than 1μm in diameter, have a perimeter between 4 and 5μm and a volume of around 2μm^3 (calculated from the diameter), regardless of stimulus. This data is calculated from the bright field images generated during sample collection, which, as can be seen in Figure 3.1.3E, does not always correlate with the fluorescence image generated by the higher-sensitivity fluorescence detector. Analysis from the fluorescence channel is possible, however significant haloing occurs around each microparticle due to the brightness of the Bodipy-maleimide dye they are loaded with. Therefore, any size measurements performed using this technique are likely to be an over-estimation of the true microparticle size and volume. Thus, further analysis of microparticle size is required using nanoparticle tracking analysis technology.

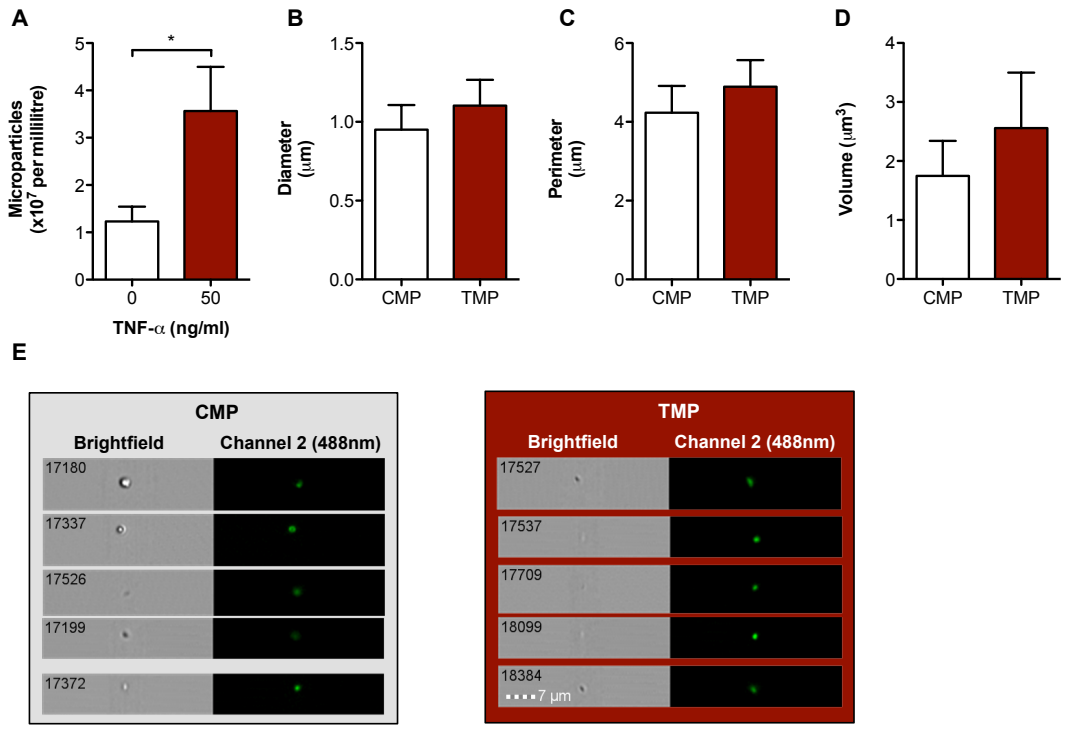

Figure 3.1.3 Stimulation of neutrophils increases microparticle production but does not alter the size of the offspring microparticles. Microparticles generated from resting neutrophils (5 x 10^6, total; at 2 x 10^7/ml; CMP) and following stimulation with TNF-α (50ng/ml; TMP) were analysed using ImageStream^X after loading with Bodipy-maleimide dye (2.5μM). (A) Accurate quantification of microparticle numbers performed using IDEAS software. Analysis of microparticle (B) diameter and (C) perimeter from bright field channel images. (D) Spherical volume of microparticles calculated from diameter values. (E) Representative images of the two microparticle subsets from ImageStream^X Analysis gallery. Data are shown as mean ± SEM of 6 blood donors. *P<0.05 using paired t test.

Nanoparticle tracking analysis allows the absolute quantification of particle size. This technique uses the Brownian motion of laser-illuminated particles recorded by a microscope with attached video camera to determine the size of a heterogeneous particle population, such as the case with microparticles. Frame-to-frame analysis of the particles' motion tracks allow their absolute size to be determined as smaller particles move more rapidly and travel a greater distance, whereas larger particles move slowly and do not travel very far (see section 2.3.3).

Neutrophil microparticles generated from 6 separate donors and pooled to ensure sufficient sample volume (1ml of approximately 1 x 10^7 objects/ml are required) were analysed using this technology (Figure 3.1.4). Representative histogram and relative intensity plots show that microparticle sizes are largely homogenous, with CMP observed to be larger than TMP (Table 3.1.1). The main caveat to this technique is that particles above 1μm in size are completely excluded from analysis as their movement is below the limit of observable Brownian motion; thus tracks cannot be generated, and size and concentration cannot be calculated. Thus, the true distribution of CMP and TMP sizes cannot be generated without such skewing towards smaller particles.

Stimulation of neutrophils with TNF-α led to double the number of microparticles shed compared to resting cells. The pooled samples were generated from 40 million neutrophils per donor and were interpolated to find the number of microparticles generated per million neutrophils. Resting neutrophils (10^6) basally produced approximately 2.5 x 10^6 microparticles over 20 minutes at 37°C following isolation from the circulation. Upon stimulation with TNF-α neutrophils (10^6) produced approximately 4.2 x 10^6 microparticles (Figure 3.1.4). It is not possible to produce enough microparticles from a single donor for individual analyses.

Small particle skewing in NTA and large particle bias in flow cytometry and ImageStream^x analysis makes sizing the entire populations of biologically diverse microparticles extremely difficult.

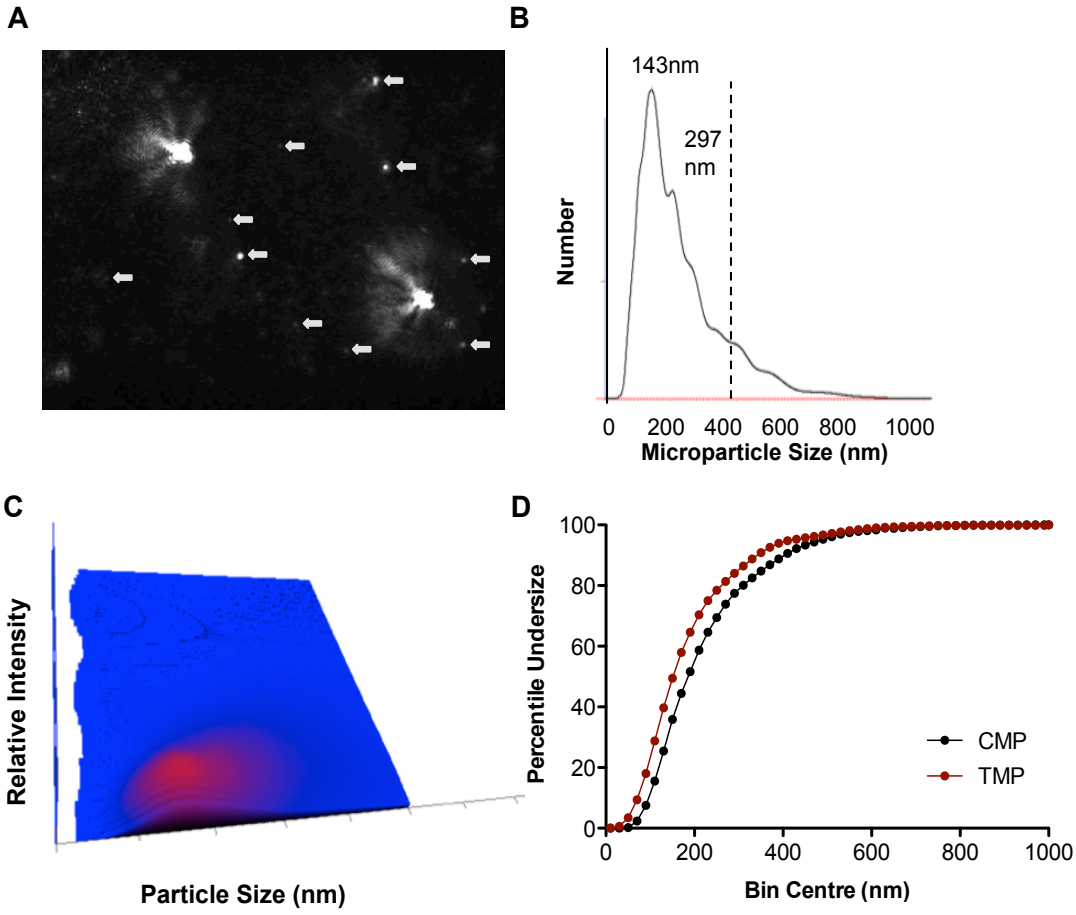

Figure 3.1.4 Nanoparticle Tracking Analysis of microparticles. Microparticles generated from 6 pooled donors' (4 x 10^7 per donor; isolated and resuspended to 200µl/donor) resting neutrophils (CMP) and following stimulation with TNF-α (50ng/ml; TMP) were analysed using nanoparticle tracking analysis. (A) A single frame from a nanoparticle tracking analysis video. White arrows denote microparticles. (B) Representative histogram of microparticle size distribution (CMP). Dotted line represents 90% of microparticles appear below 412nm. The majority of microparticles are 143nm followed by 297nm. (C) The population distribution of microparticles in terms of size and scattering intensity. (D) Percentile of microparticle population appearing below each size.

Table 3.1.1 Data generated from Nanoparticle Tracking Analysis. Microparticles generated from 6 pooled donors' (4 x 10^7 per donor; isolated and resuspended to 200μl/donor) resting neutrophils (CMP) and following stimulation with TNF-α (50ng/ml; TMP) were analysed using Nanoparticle tracking analysis. D10, D50 and D90 percentile sizes are given for each population along with pooled counts.

Parameter	CMP	TMP
Mean (nm)	231	195
Mode (nm)	143	118
D10 (nm)	106	81
D50 (nm)	195	161
D90 (nm)	412	351
Absolute sample counts (10^8)	4.93	8.39
Interpolated count per million neutrophils (approximate value, 10^6)	2.465	4.195

Finally, it was important to determine for future imaging studies whether microparticles loaded with Bodipy-maleimide dye could be visualised using fluorescence microscopy. Although X60 or X40 magnification is sufficient for microparticle analysis, the resolution of conventional light microscopes is not great enough to visualise unstained microparticles unless they are around 1μm apart from each other, and have a difference in size that is a function of their surface area. However, it is possible, using a bright dye such as Bodipy-maleimide, to take advantage of the significant haloing that occurs in these small particles. In this way, single particles may be distinguished by eye and the heterogeneity of the size of the microparticle population may be observed. TMP and IMP appeared to have a greater spread of microparticle sizes from very small to very large, compared to CMP, which had fewer large particles (Figure 3.1.5). Although fluorescent micrographs of isolated microparticles are not information-rich, the fact that microparticles could be visualised at X60 magnification ensured that imaging studies with pre-loaded microparticles was feasible.

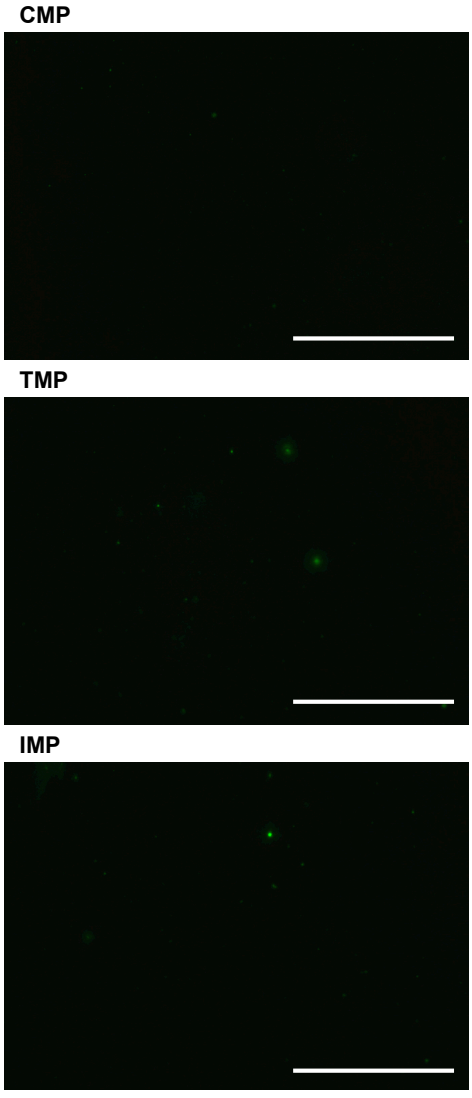

Figure 3.1.5 A proportion of fluorescently labelled microparticles are visible by standard fluorescence microscopy. Microparticles generated from resting neutrophils (CMP) and following stimulation with TNF-α (50ng/ml; TMP) and IL-8 (50ng/ml; IMP) were loaded with Bodipy-maleimide dye (2.5μM) before being applied to positively charged glass microscope slides. Visualisation using oil immersion objectives and integrated fluorescence/light microscope with FL1 channel (excitation wavelength 460-490 nm) connected to a digital camera. Representative photographs of microparticles generated from 4 donors. Scale bar denotes 50μm. CMP, control microparticles, TMP, TNF-α generated microparticles, IMP, IL-8 generated microparticles.

Together, these results demonstrate that stimulation of neutrophils leads to increased microparticle shedding, and the offspring microparticles are around 150nm in size. Importantly, it is possible to detect microparticles by flow cytometry, ImageStream analysis, Nanoparticle Tracking Analysis and fluorescence microscopy. I wanted to determine the temporal kinetics of microparticle release along with investigating what regulated this increase in microparticle shedding. Furthermore, I wanted to investigate whether these offspring microparticles had an altered phenotype.

3.1.2 Kinetics and Regulation of Microparticle Formation

It was next important to determine the temporal regulation of the process of microparticle shedding. To determine the kinetics of microparticle production, time-lapse video fluorescent microscopy of neutrophils loaded with Bodipy-maleimide dye (2.5μM) immediately following isolation (Figure 3.1.6) was carried out. Cells stimulated with TNF-α at 5 minutes prior to image capture could be seen shedding microparticles from approximately 10 minutes post-TNFα stimulation. This method of microparticle kinetics analysis proved to be extremely intensive and time-consuming, thus only a small number of samples were analysed, and only one representative cell shown.

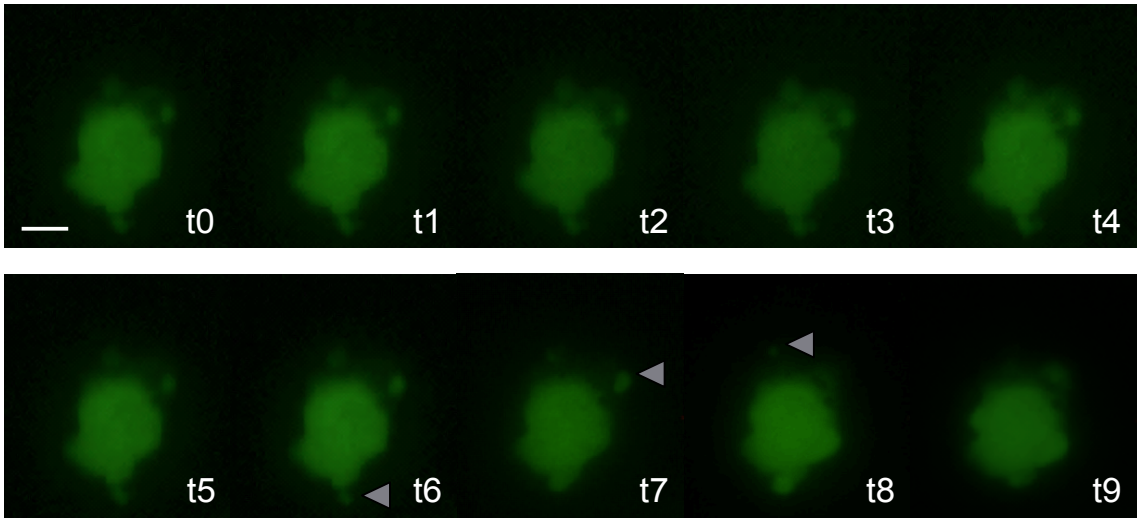

Figure 3.1.6 Time-lapse video recording of a TNF-α stimulated neutrophil releasing several microparticles over a period of 10 minutes. Freshly isolated neutrophils were loaded with Bodipy-maleimide dye (2.5μM) and visualised using an integrated fluorescence/light microscope with FL1 channel (excitation wavelength 460-490nm) connected to a digital camera. TNF-α (50ng/ml) was added 5 minutes prior to imaging (t-5), and one image acquired each minute from time 0 (t0) at X60 magnification with oil immersion objective. Scale bar denotes 5μm, t denotes time in minutes. Grey arrowheads depict fully formed microparticles prior to dislocation from the cell.

To generate meaningful data, the ImageStream^X was instead used to enumerate microparticle generation over time. Uniquely among analytical instruments used for microparticle testing, this analyser allows parallel analysis of both parent neutrophils and offspring microparticles in the same sample collection, thus making it a powerful tool for assessing the kinetics of microparticle formation. ImageStream^X analysis of neutrophils immediately visualised following isolation showed that the rate of neutrophil microparticle production was much higher when the cells were stimulated with TNF-α (50ng/ml) than that of resting cells over a 45-minute period (Figure 3.1.7). Although a plateau of neutrophil microparticle production with TNF-α was not reached after 45 minutes, analysis of a longer time point was limited by the size of the data files produced, and therefore would require a different sampling technique over time.

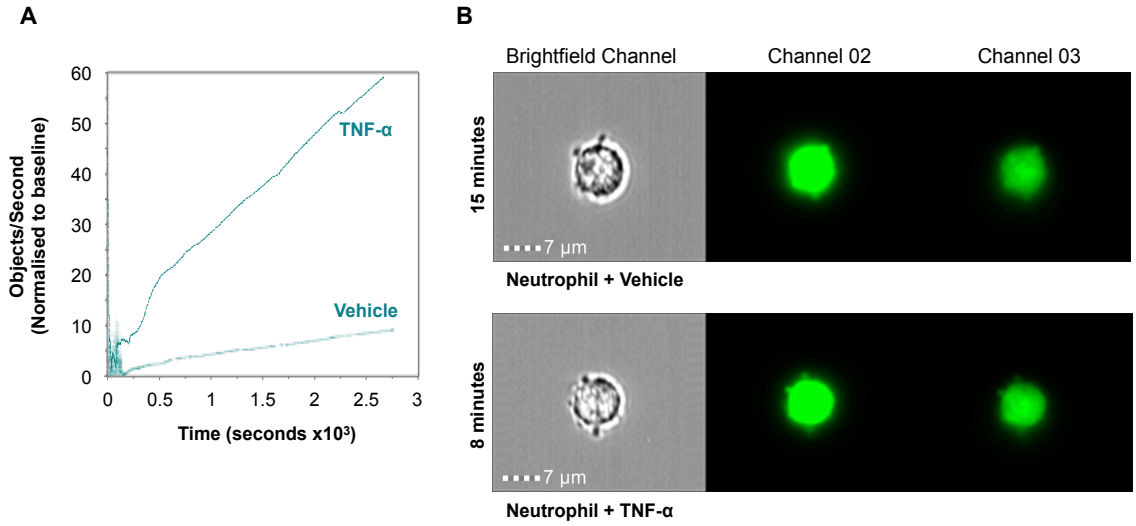

Figure 3.1.7 Microparticle production kinetics. Freshly isolated neutrophils were loaded with Bodipy-maleimide dye (2.5μM) and stimulated with TNF-α (50ng/ml) immediately prior to ImageStream^X analysis. Samples were acquired constantly for 45 minutes collecting only microparticle events. Objects per second were determined using IDEAS software by adding the feature to the features list and applying it to the microparticle gate. (A) Representative plot of paired neutrophils stimulated with TNF-α (50ng/ml) or vehicle (PBS) from n=4 separate neutrophil donors. (B) Representative ImageStream^X gallery images of neutrophils budding at the times indicated.

Microparticle shedding is known to involve the rearrangement of the cytoskeleton, and as microparticles are known to contain cytoskeletal proteins (Dalli et al., 2013), I wanted to determine whether the presence of filamental actin could be detected within neutrophil microparticles. Interestingly, all subsets of microparticles displayed positivity for phalloidin staining, as shown by flow cytometry. This could have implications for microparticle generation and motility, which requires cytoskeletal components including a cortical actin network (Figure 3.1.8).

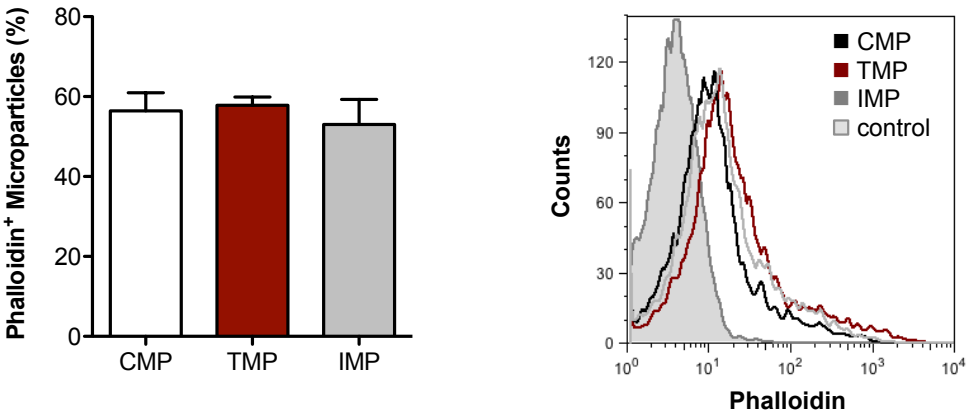

Figure 3.1.8 Neutrophil microparticles contain filamental actin. Microparticles generated from resting neutrophils (CMP) or following stimulation with TNF-α (50ng/ml; TMP) or IL-8 (50ng/ml; IMP) were analysed by flow cytometry for phalloidin positivity indicating the presence of filamental actin. Right-hand panel shows representative histogram. Data are expressed as percentage of Bodipy-maleimide/CD66b double-positive population and shown as mean ± SEM of 3 blood donors, not significant with One-way ANOVA and Bonferroni post-test.

As the presence of filamental actin had been detected, I next wanted to determine the involvement of cytoskeletal rearrangement during microparticle generation. Firstly, Trypan blue dye exclusion was used to determine if the cytoskeletal inhibitors or calcium chelator tested had detrimental effects on the viability of isolated neutrophils (Figure 3.1.9).

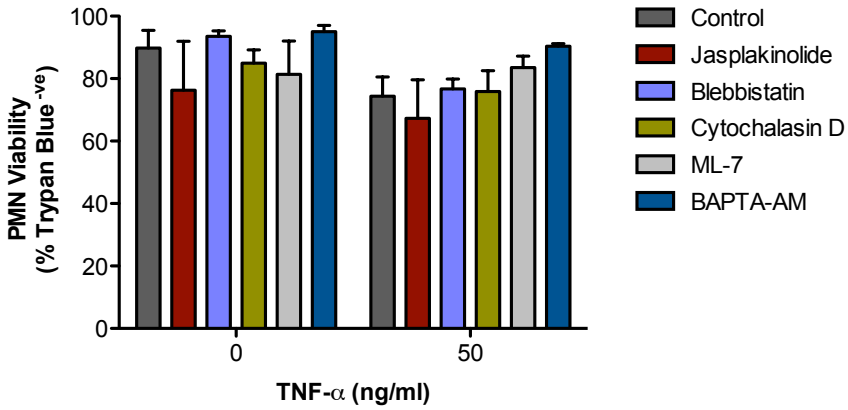

Figure 3.1.9 Drugs affecting microparticle production do not impair neutrophil viability. Neutrophils were treated with Jasplakinolide (1μM), Blebbistatin (10μM), Cytochalasin D (2μM), ML-7 (20μM) or BAPTA-AM (20μM) for 10 minutes then TNF-α (50ng/ml) for 20 minutes. Viability was assessed by Trypan blue dye exclusion. Data are shown as mean ± SEM of 4 donors, not significant with Two-way ANOVA and Bonferroni post-test.

As neutrophil viability was not significantly affected, the offspring microparticles were loaded with Bodipy-maleimide dye and quantified using ImageStream^x analysis. Jasplakinolide, which inhibits actin depolymerisation and cytochalasin D, which inhibits actin polymerisation, both had significant effects on the number of microparticles produced by neutrophils without altering the size or shape of the microparticles generated (Figure 3.1.10). Jasplakinolide significantly inhibited microparticle production induced by TNF-α stimulation (0.9 ± 0.3 vs. 1.9 ± 0.5 x10^7 microparticles/ml, P<0.05 with Two-way ANOVA and Bonferroni post-test) whereas cytochalasin D increased microparticle production in unstimulated (2.6 ± 0.2 vs. 0.8 ± 0.3 x10^7 microparticles/ml, P<0.01 with Two-way ANOVA and Bonferroni post-test) as well as TNF-α stimulated neutrophils (3.0 ± 0.1 vs. 1.9 ± 0.5 x10^7 microparticles/ml, P<0.05 with Two-way ANOVA and Bonferroni post-test), and induced the highest amount of microparticle shedding of all the drugs tested. These data implicate the actin cytoskeleton in the regulation of microparticle production, as enhanced actin polymerisation inhibits microparticle shedding and disruption of the cortical actin network enhances the number of microparticles generated.

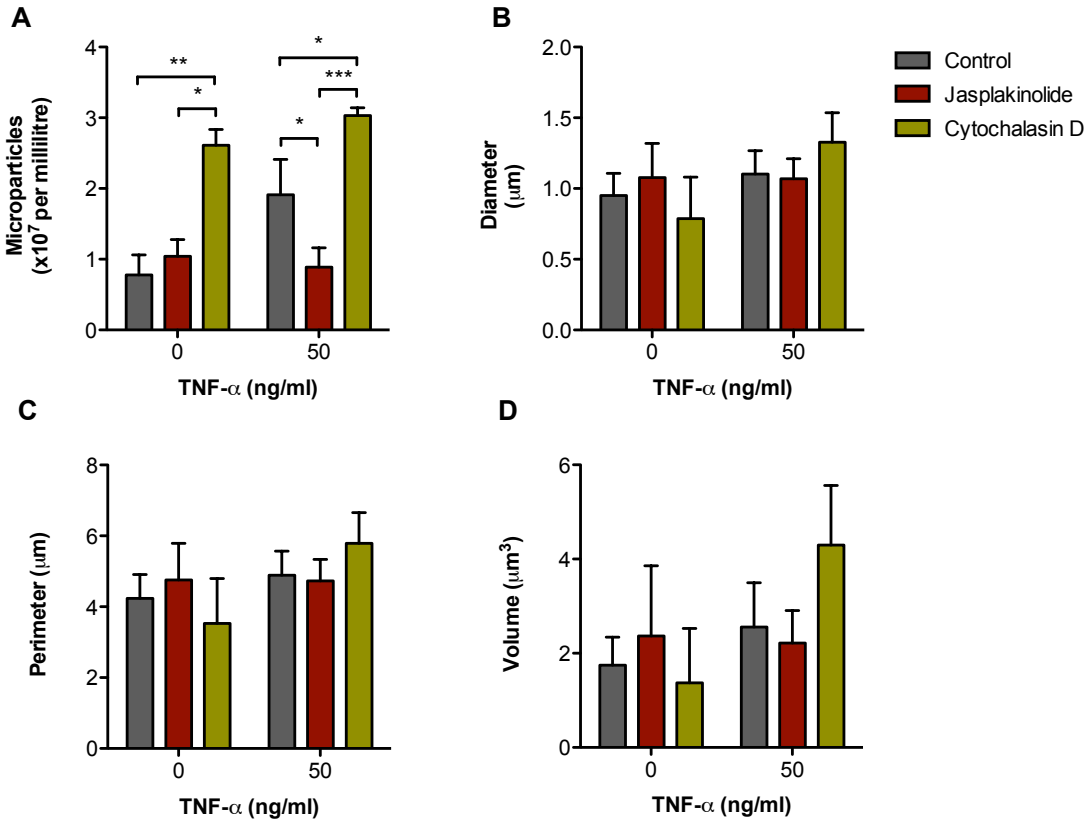

Figure 3.1.10 Microparticle formation involves regulation of the actin cytoskeleton. Neutrophils were treated with Jasplakinolide (1μM) or Cytochalasin D (2μM) for 10 minutes then TNF-α (50ng/ml) for 20 minutes and supernatant microparticles analysed using ImageStream^X after loading with Bodipy-maleimide dye (2.5μM). (A) Microparticles were accurately enumerated by ImageStream IDEAS software. Analysis of microparticle (B) diameter and (C) perimeter from bright field channel images. (D) Spherical volume of microparticles calculated from diameter values. Data are shown as mean ± SEM of 3-6 blood donors. **P*<0.05, ***P*<0.01 and ****P*<0.001 using Two-way ANOVA with Bonferroni post-test.

In contrast, the number of microparticles produced during treatment with drugs that inhibit myosin activity did not reach statistical significance, even when repeated with seven blood donors (Figure 3.1.11). The size of the microparticles was also not altered. This suggests that formation of focal adhesions between the actin and myosin cytoskeleton, processes inhibited by Blebbistatin and ML-7, are not necessary in these settings for microparticle formation.

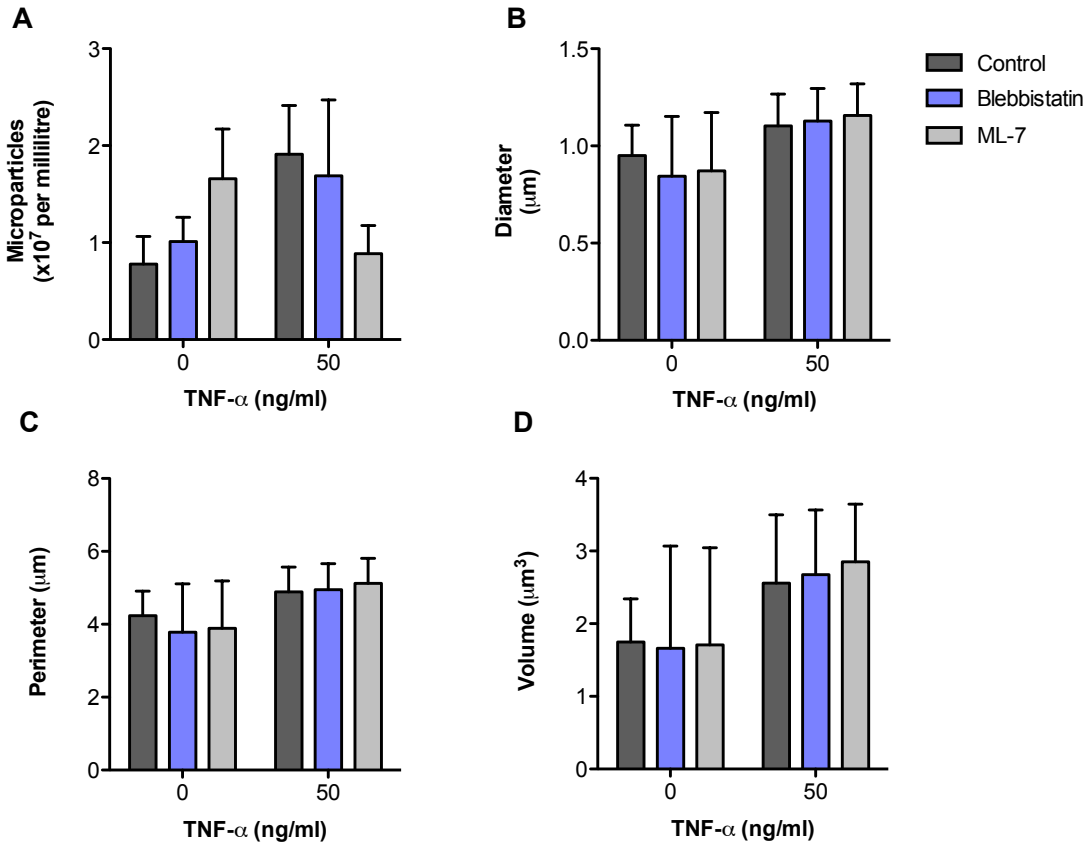

Figure 3.1.11 Microparticle formation is not myosin/actin focal adhesion dependent. Neutrophils were treated with Blebbistatin (10μM) or ML-7 (20μM) for 10 minutes then TNF-α (50ng/ml) for 20 minutes and supernatant microparticles analysed using ImageStream^X after loading with Bodipy-maleimide dye (2.5μM). (A) Microparticles were accurately enumerated by ImageStream IDEAS software. Analysis of microparticle (B) diameter and (C) perimeter from bright field channel images. (D) Spherical volume of microparticles calculated from diameter values. Data are shown as mean ± SEM of 7 blood donors, not significant with Two-way ANOVA and Bonferroni post-test.

Intracellular fluxes of calcium are known to be heavily involved in the events surrounding microparticle formation and shedding from initial receptor ligation up to the rearrangement of cytoskeletal components and phospholipid reorganisation. Calcium fluxes also recruit annexins to the plasma membrane to achieve membrane cleavage and microparticle release (Potez et al., 2011). Intracellular calcium chelation using BAPTA-AM significantly inhibited microparticle production compared to stimulation with TNF-α (0.3 ± 0.2 vs. 1.9 ± 0.5 x10^7 microparticles/ml, P<0.05 with Two-way ANOVA and Bonferroni post-test) as expected (Figure 3.1.12).

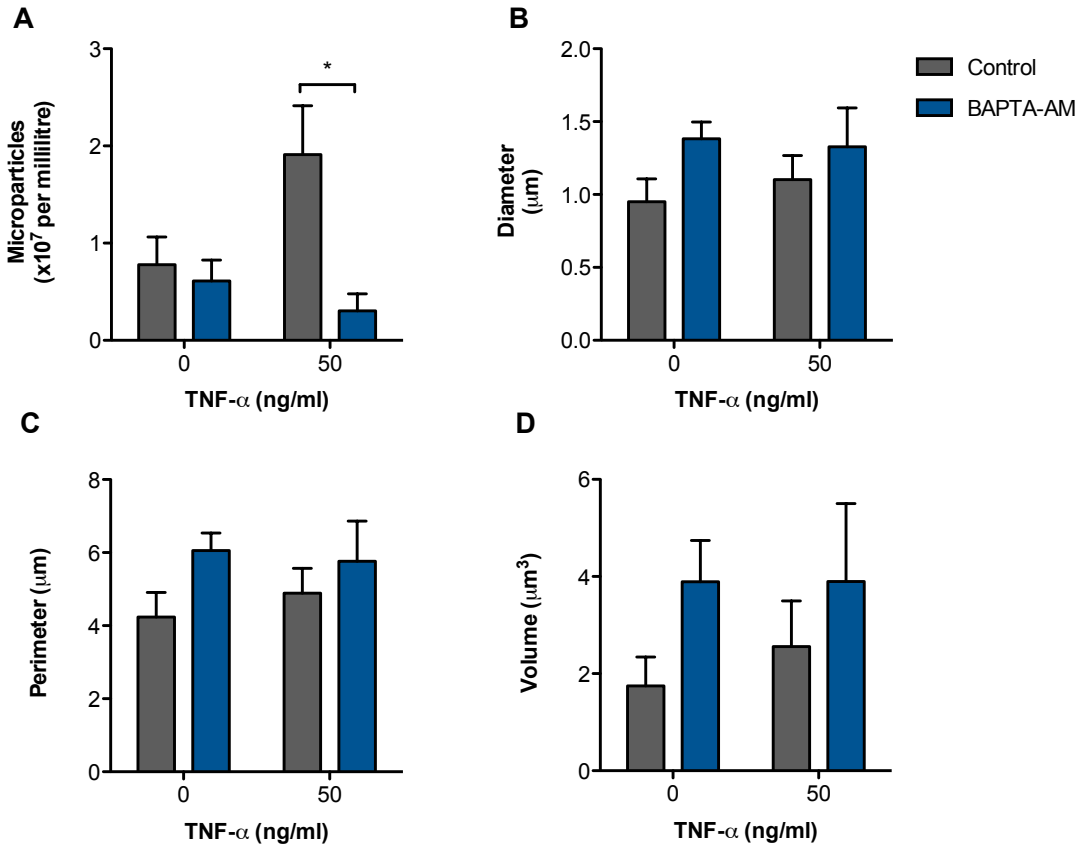

Figure 3.1.12 TNF-α-induced Microparticle formation requires intracellular calcium. Neutrophils were treated with BAPTA-AM (20μM) for 10 minutes then TNF-α (50ng/ml) for 20 minutes and supernatant microparticles analysed using ImageStream^X after loading with Bodipy-maleimide dye (2.5μM). (A) Microparticles were accurately enumerated by ImageStream IDEAS software. Analysis of microparticle (B) diameter and (C) perimeter from bright field channel images. (D) Spherical volume of microparticles calculated from diameter values. Data are shown as mean ± SEM of 3 blood donors. **P*<0.05 using Two-way ANOVA with Bonferroni post-test.

Thus, microparticle shedding is a rapidly occurring event that requires intracellular calcium and the coordinated rearrangement of the actin cytoskeleton. The requirement of polymerisable and de-polymerisable actin was especially evident upon TNF-α stimulation, compared to resting cells, suggesting that differential processes may be inducing microparticle production. Therefore, it seemed likely that the content of these microparticles may also differ if the machinery involved in their production was different depending on the activation state of the parent cell.

3.1.3 Neutrophil Microparticles Contain Functional Proteins

I next wanted to explore the potential cargo of these microparticles and whether their proteome was influence by the stimulus inducing their release, as previously reported (Dalli et al., 2013), (Timar et al., 2013). To characterise the expression of several markers associated with neutrophil microparticle formation, flow cytometric analysis was employed. Approximately 75% of microparticles expressed the neutrophil-surface marker CD66b, regardless of stimulus (Figure 3.1.13A). The majority could also bind Annexin V, a marker for phosphatidylserine exposure, an event thought to be key to microparticle formation and release (Figure 3.1.13B).

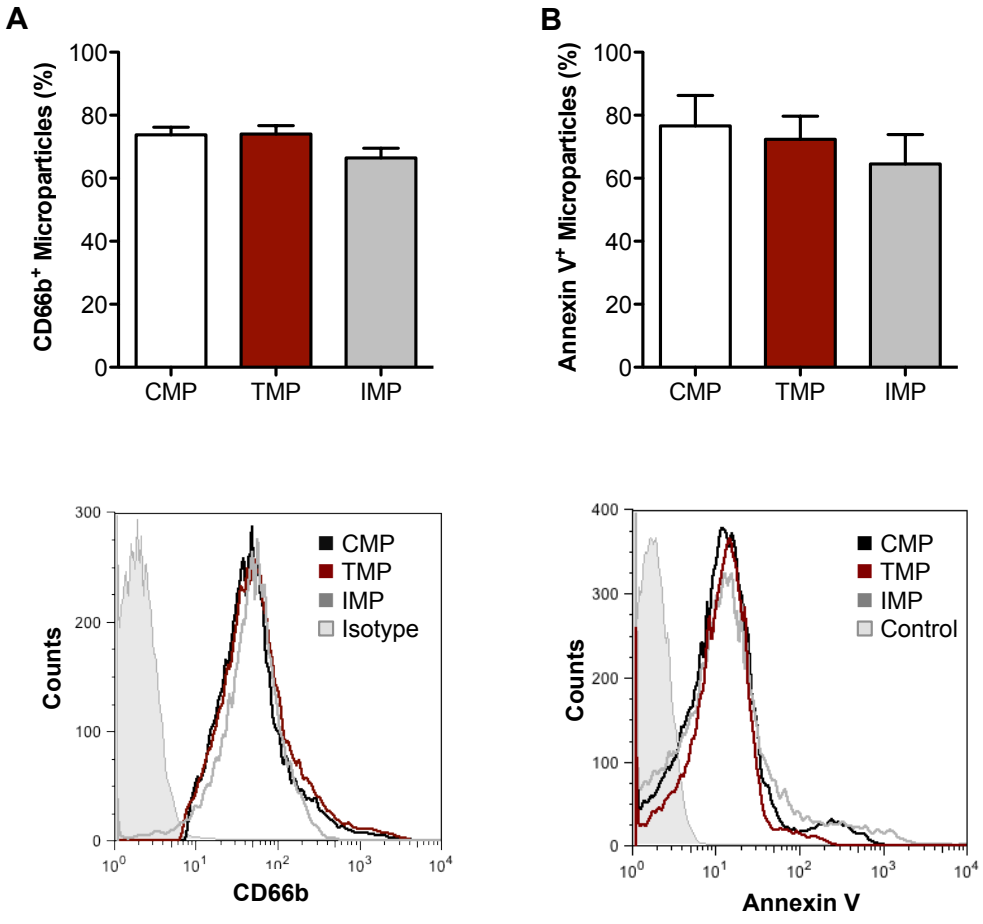

Figure 3.1.13 Neutrophil microparticles express CD66b and Phosphatidylserine. Microparticles generated from resting neutrophils (CMP) or following stimulation with TNF-α (50ng/ml; TMP) or IL-8 (50ng/ml; IMP) were analysed by flow cytometry for (A) CD66b neutrophil marker expression and (B) Annexin V binding to indicate phosphatidylserine exposure. Bottom panels show representative histograms. Data are expressed as percentage of Bodipy-maleimide positive population and shown as mean ± SEM of 3 blood donors, not significant with One-way ANOVA and Bonferroni post-test.

I then wanted to determine if any of the other cytoplasmic constituents present in the neutrophil were also present within microparticles. Myeloid-related protein 8 (MRP8, also known as S100A8) constitutes more than 40% of the total cytoplasmic neutrophil protein content, and isolated human neutrophils stain intensely for this protein (Figure 3.1.14).

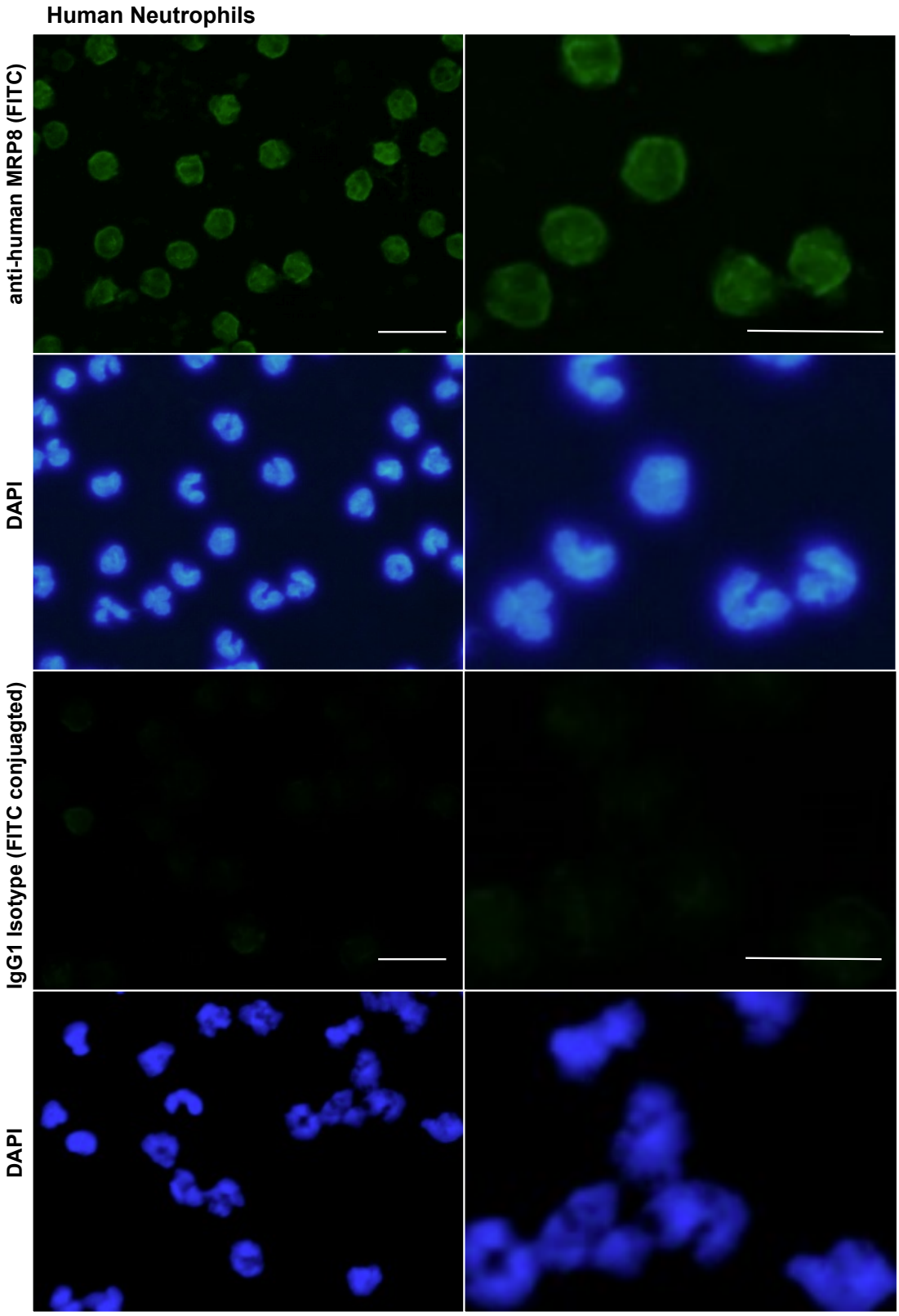

Figure 3.1.14 Neutrophils express myeloid-related protein 8. Freshly isolated neutrophils were stained with FITC-conjugated monoclonal myeloid-related protein 8 (MRP8) antibody or isotype at the same concentration and visualised using an integrated fluorescence/light microscope with FL1 channel (excitation wavelength 460-490nm) and DAPI channel (excitation wavelength 360-370nm) connected to a digital camera. Images were captured at X20 magnification. Scale bar denotes 25μm. Representative images, and right-hand panels show digital magnification for detail inspection.

It was therefore not surprising that more than 80% of each microparticle subset was positive for this protein (Figure 3.1.15A). MRP8 is also a protein specific to neutrophils, and could be used as a marker for microparticles of neutrophil origin. Physiologically, MRP8 is usually found with its binding and stabilising partner, MRP14 (also known as S100A9), though a lower percentage of microparticles expressed this protein on their surface (Figure 3.1.15B).

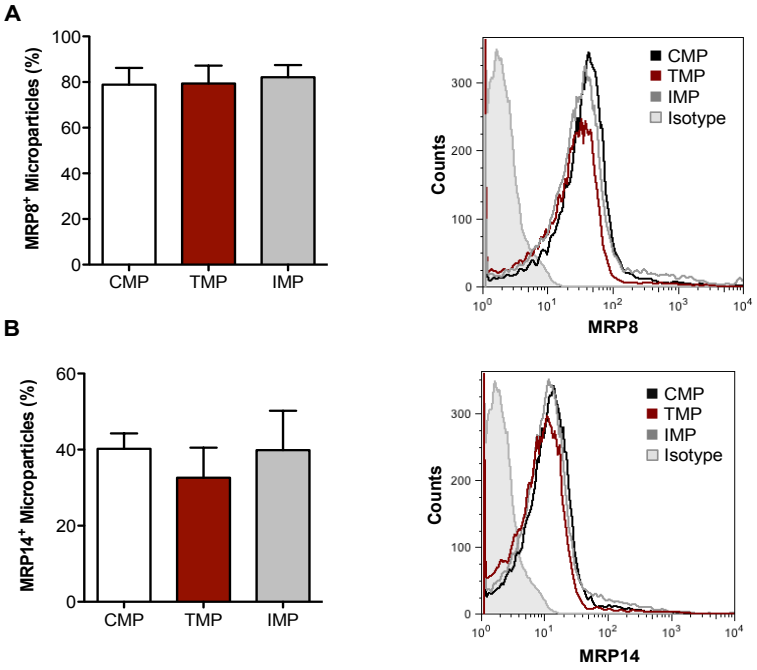

Figure 3.1.15 Neutrophil microparticles express Myeloid Related Protein 8 and 14. Microparticles generated from resting neutrophils (CMP) or following stimulation with TNF-α (50ng/ml; TMP) or IL-8 (50ng/ml; IMP) were analysed by flow cytometry for (A) MRP8 and (B) MRP14 positivity. Right-hand panels show representative histograms. Data are expressed as percentage of Bodipy-maleimide/CD66b double-positive population and shown as mean ± SEM of 3 blood donors, not significant with One-way ANOVA and Bonferroni post-test.

Previous data from our laboratory showed that microparticles express over 300 proteins when analysed by tandem LC/MS/MS (Dalli et al., 2013). It was therefore important to determine whether the expression of some of these proteins with potential immune-regulating functions was modulated by the differential stimuli applied to generate microparticles from neutrophils. Using flow cytometric analysis it was found that the number of microparticles expressing α_2-Macroglobulin was significantly increased upon TNF-α stimulation compared to control (31.1 ± 3.9 vs. 13.7 ± 2.7%, $P<0.01$ with One-way ANOVA and Bonferroni post-test), while the per-microparticle surface expression remained similar across stimuli (Figure 3.1.16). Similarly, the percentage of microparticles positive for ceruloplasmin staining was significantly increased in TMP compared to CMP subsets (33.6 ± 3.2 vs. 23.5 ± 0.2%, $P<0.05$ with One-way ANOVA and Bonferroni post-test, Figure 3.1.16C) whilst the per-microparticle surface expression remained unchanged across stimuli (Figure 3.1.16D). In contrast, heat shock protein 70 expression was not modulated by stimulation in terms of percentage positive, or on a per-microparticle basis (Figure 3.1.16E,F). Both α_2-Macroglobulin and ceruloplasmin have anti-inflammatory functions and could predict immune-modulatory properties for neutrophil microparticles.

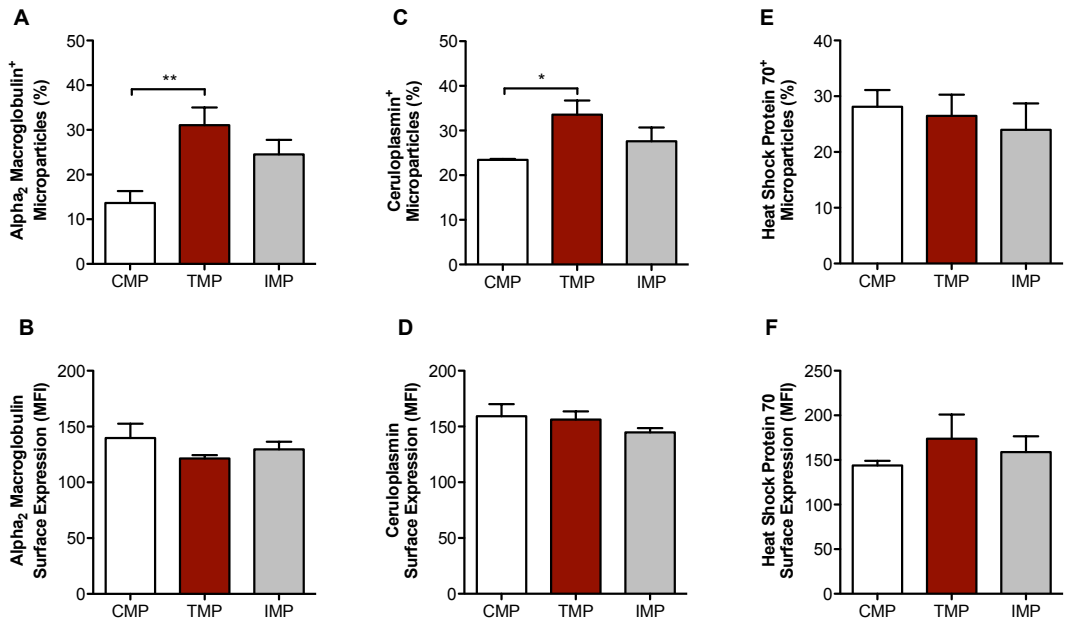

Figure 3.1.16 Neutrophil microparticles express proteins with immunological functions. Microparticles generated from resting neutrophils (CMP) or following stimulation with TNF-α (50ng/ml; TMP) or IL-8 (50ng/ml; IMP) were analysed by flow cytometry for (A) Alpha$_2$ macroglobulin positivity and (B) surface expression, (C) ceruloplasmin positivity and (D) surface expression and (E) heat shock protein 70 positivity and (F) surface expression. Data are expressed as percentage of Bodipy-maleimide/CD66b double-positive population or mean fluorescence intensity (MFI, arbitrary units) of this population and shown as mean ± SEM of 4 blood donors. *P<0.05 and **P<0.01 using One-way ANOVA with Bonferroni post-test.

Neutrophil microparticles contain a potent anti-inflammatory and pro-resolving protein, Annexin A1 (Dalli et al., 2008), which has important functions in the resolution phase of inflammation (Perretti and D'Acquisto, 2009). Neutrophils are an abundant source of this protein, and aside from its inherent anti-inflammatory functions, Annexin A1 is involved in the resealing of the plasma membrane following injury (Potez et al., 2011), and could therefore have important implications in the release of microparticles. Upon stimulation with TNF-α, neutrophils released a larger percentage of microparticles positive for Annexin A1 compared to resting cells (21.7 ± 1.5 vs. 10.0 ± 0.7%, P<0.01 with One-way ANOVA and Bonferroni post-test; Figure 3.1.17). An even greater percentage of IMP was positive for Annexin A1 compared to CMP (24.8 ± 2.5 vs. 10.0 ± 0.7%, P<0.001 with One-way ANOVA and Bonferroni post-test). Furthermore, the surface expression of Annexin A1 per microparticle was increased in both TMP and IMP subsets compared to CMP (142 ± 9.9 and 165 ± 22.4 vs. 88.0 ± 7.3 arbitrary units of mean fluorescence intensity, both P<0.05 with One-way ANOVA and Bonferroni post-test).

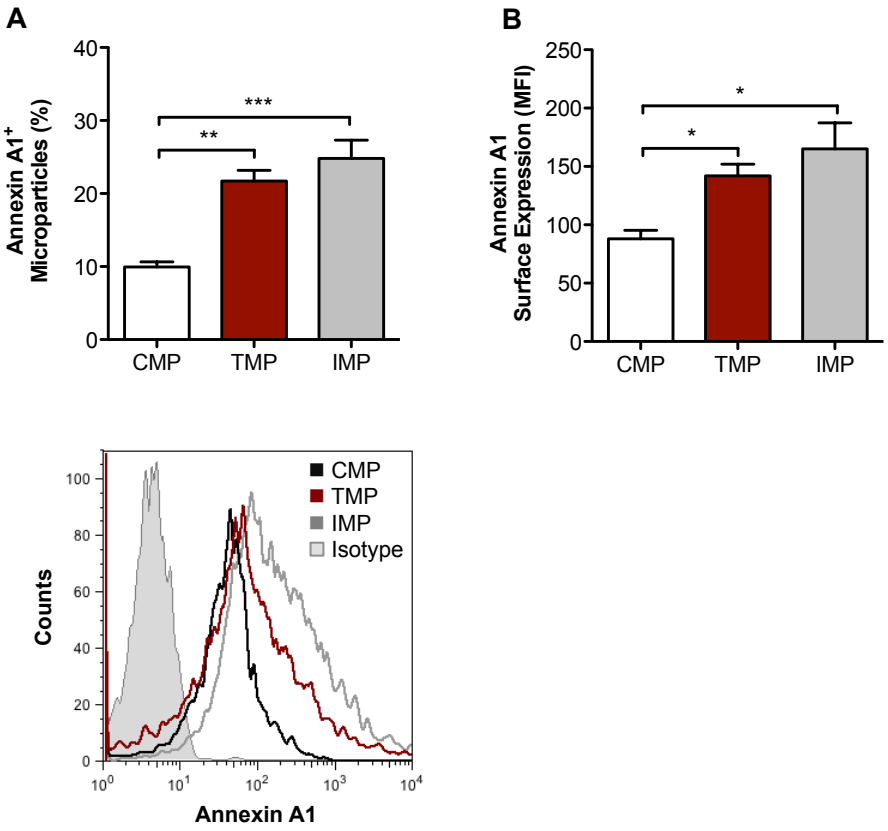

Figure 3.1.17 Neutrophil microparticles express anti-inflammatory protein Annexin A1. Microparticles generated from resting neutrophils (CMP) or following stimulation with TNF-α (50ng/ml; TMP) or IL-8 (50ng/ml; IMP) were analysed by flow cytometry for (A) Annexin A1 positivity and (B) surface expression. Bottom panel shows a representative histogram. Data are expressed as percentage of CD66b/ Bodipy-maleimide double-positive population or mean fluorescence intensity (MFI, arbitrary units) of this population and shown as mean ± SEM of 4 blood donors. **P*<0.05, ***P*<0.01 and ****P*<0.001 using One-way ANOVA with Bonferroni post-test.

As it is not possible to determine the internal content of microparticles by flow cytometry (as permeabilisation of these small structures is not feasible), the Annexin A1 total protein expression was determined by Western blotting. The total Annexin A1 content in TMP is much higher than CMP and IMP, suggesting that internal Annexin A1 protein contributes significantly to the total Annexin A1 content (Figure 3.1.18). To determine the approximate amount of Annexin A1, CMP and TMP at various microparticle counts were loaded alongside known amounts of recombinant human Annexin A1. From this blot it is possible to tell that 5ng of Annexin A1 provides a similar signal intensity to that of 30,000 TMP and 100,000 CMP, suggesting that TMP are loaded with approximately three times the amount of Annexin A1 compared to CMP, which may have important consequences for microparticle function.

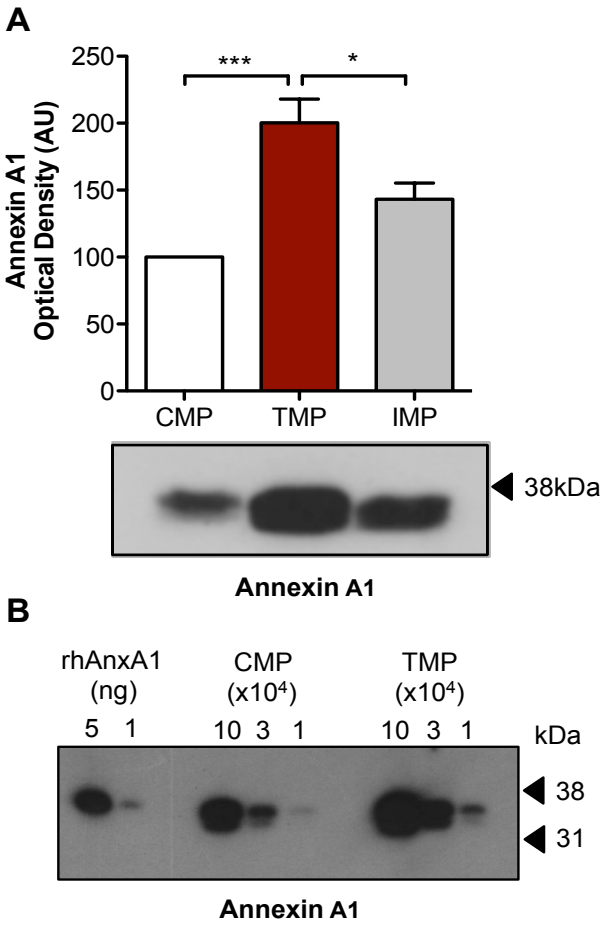

Figure 3.1.18 Neutrophil microparticles contain anti-inflammatory protein Annexin A1. Microparticles generated from resting neutrophils (CMP) or following stimulation with TNF-α (50ng/ml; TMP) or IL-8 (50ng/ml; IMP) were analysed by Western blotting for Annexin A1 protein expression. (A) Densitometry of N=5 individual donor blots. Bands are normalised to 100,000 microparticles; data are shown as mean ± SEM. **P*<0.05 and ****P*<0.001 using One-way ANOVA and Bonferroni post-test (B) Representative blot showing comparison of different dilutions of CMP and TMP with known amounts of recombinant Annexin A1.

Together, these results demonstrate that neutrophil microparticles contain a variety of putative anti-inflammatory proteins, the concentration of which was sometimes dependent on the stimulus that led to microparticle release. In particular, Annexin A1 was shown to be highly abundant in microparticles, especially if they were derived from TNF-α stimulated neutrophils. Some of the proteins levels were not changed upon stimulation, such as MRP8 and MRP14, and could represent a further neutrophil microparticle marker.

CHAPTER 4: EXAMINING THE ROLE OF NEUTROPHIL MICROPARTICLES IN *IN VITRO* MODELS OF CARTILAGE TURNOVER

4.1 Neutrophil Microparticles Protect Chondrocytes *In Vitro*

The role of neutrophil microparticles in rheumatoid arthritis has not been studied. Previous reports have demonstrated an unexpected role for platelet microparticles, which deliver IL-1β to arthritic joints, contributing to the pathogenesis of the disease (Boilard et al., 2010). As the effect of microparticles on the aberrant synovial fibroblasts is an active area of research, I decided instead to turn my attention to the effect of neutrophil microparticles on chondrocyte and cartilage biology, an area which has never been studied before. Furthermore, if neutrophil microparticles had pathogenic effects on cartilage, this would broaden the repertoire of neutrophil microparticle functions, which have been previously reported to be anti-inflammatory (Dalli et al., 2008, Gasser and Schifferli, 2004, Eken et al., 2008, Eken et al., 2010).

4.1.1 Characterisation of the Effect of Microparticles on Extracellular Matrix Accumulation *In Vitro*

To investigate the potential effects of neutrophil microparticles in the context of rheumatoid arthritis, it was important to characterise an *in vitro* model of cartilage matrix synthesis. By culturing the chondrocyte cell line C28/I2 at high density, the cells retain their spherical morphology and generate matrix rich in sulphated proteoglycans, reflecting physiological matrix generation. This matrix can be specifically stained with Alcian blue dye at pH 0.2, which after extraction can be quantified spectrophotometrically. This system allows for medium-throughput cartilage matrix assaying for the investigation of various catabolic (degradative) and anabolic (accumulative) stimuli. Importantly, this assay does not allow the determination of increased matrix synthesis or increased matrix degradation by enzymes, but can provide a good global measure of the net extracellular matrix content, hence matrix accumulation.

It was necessary to identify a stimulus that reduced chondrocyte extracellular matrix accumulation in the micromass culture system, to determine whether microparticles had any contribution to the cartilage integrity loss characteristic of rheumatoid arthritis. The cytokines that contribute most significantly to cartilage integrity loss in human rheumatoid arthritis are primarily IL-1β and TNF-α, which are increased in the synovial fluid of patients (Wright et al., 2012).

IL-1β at increasing concentrations reduced matrix accumulation as shown by Alcian blue staining, with low concentrations, such as 3ng/ml inducing significant reduction compared to control (-23.8 ± 3.3 vs. 0.0 ± 4.6% P<0.01 with One-way ANOVA and Bonferroni post-test; Figure 4.1.1A). The sensitivity of this assay to small concentrations of IL-1β allows subtle changes in matrix accumulation to be monitored and provides a range of working concentrations for a variety of assays, up to 30ng/ml (-68.5 ± 2.3 vs. 0.0 ± 4.6% P<0.001 with One-way ANOVA and Bonferroni post test). In contrast, TNF-α stimulation did not induce a significant reduction in matrix accumulation until concentrations reached 30ng/ml (-26.2 ± 6.4 vs. 0.0 ± 4.2% P<0.01 with One-way ANOVA and Bonferroni post-test), providing a less sensitive assay for changes in matrix accumulation (Figure 4.1.1B).

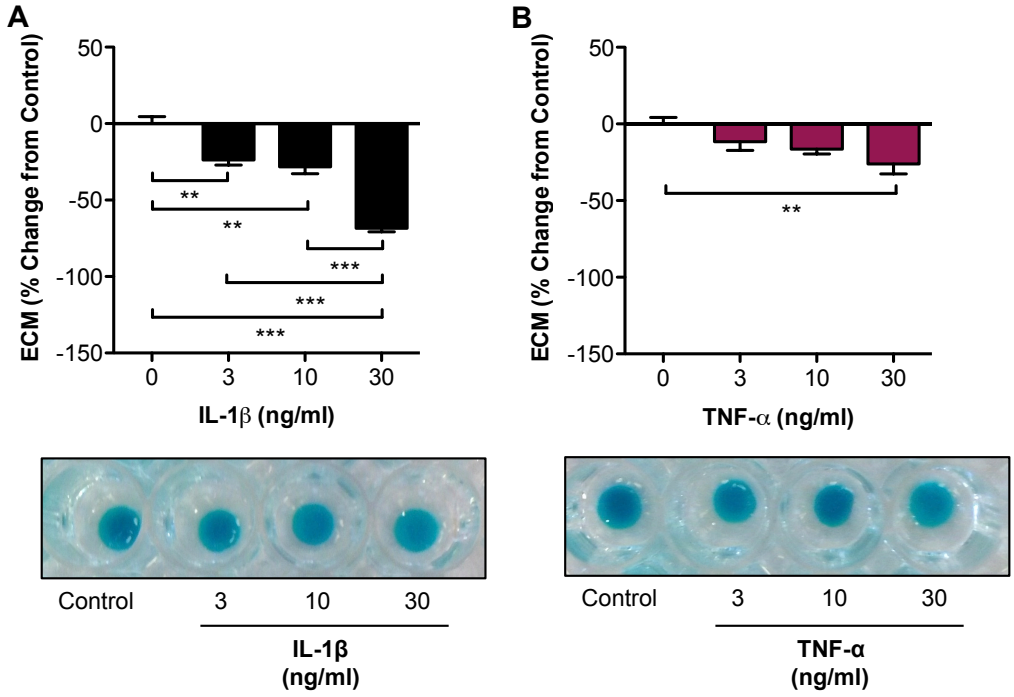

Figure 4.1.1 IL-1β and TNF-α reduce C28/I2 chondrocyte micromass extracellular matrix accumulation. Chondrocyte micromasses were treated with increasing concentrations of (A) IL-1β and (B) TNF-α for 24 hours before extracellular matrix accumulation was quantified with Alcian blue staining. Below are representative photographs of micromasses before dye extraction. Data are shown as mean ± SEM of 6 separate micromass preparations. $**P$<0.01 and $***P$<0.001 using One-way ANOVA and Bonferroni post-test. ECM, extracellular matrix.

As TNF-α induced more subtle degradative effects in the C28/I2 chondrocytes, this cytokine was dispensed with as a model cytokine in these assays. Although microparticles generated using TNF-α were being profiled for functionality in terms of the best activator of neutrophils, it made more sense to also select a stimulus of chondrocytes best suited to chondrocyte “activation”, providing more reproducible read-outs.

Treatment of chondrocyte micromasses with IL-1β also significantly reduced the mRNA expression of *ACAN* at concentrations of 30ng/ml (0.4 IQR 0.2-0.6 vs. 1 IQR 0.9-1.1; *P*<0.01 with Kruskal-Wallis test and Dunn's multiple comparison post-test) and 50ng/ml (0.3 IQR 0.2-0.5 vs. 1 IQR 0.9-1.1; *P*<0.05 with Kruskal-Wallis test and Dunn's multiple comparison post-test; Figure 4.1.2A). *COL2A1* expression was also down regulated by treatment with IL-1β (30ng/ml) compared to control (0.4 IQR 0.3-1 vs. 1 IQR 0.8-1.2; *P*<0.01 with Kruskal-Wallis test and Dunn's multiple comparison post-test; Figure 4.1.2B). These two genes are key to matrix production. At a 6-hour time point however, TNF-α did not significantly suppress *ACAN* expression (0.4 IQR 0.3-1 vs. 1 IQR 0.9-1.1) or *COL2A1* expression (1.1 IQR 1.1-1.4 vs. 1 IQR 0.8-1.2) compared to untreated micromasses (Figure 4.1.2C and D). The expression profile of *COL2A1* induced by TNF-α stimulation was significantly different to that induced by IL-1β (3ng/ml) treatment (0.7 IQR 0.4-0.9 vs. 1.1 IQR 1.1-1.4; *P*<0.05 with Kruskal-Wallis test and Dunn's multiple comparison post-test) or IL-1β (30ng/ml) treatment (0.4 IQR 0.3-0.6 vs. 1.1 IQR 1.1-1.4; *P*<0.01 with Kruskal-Wallis test and Dunn's multiple comparison post-test).

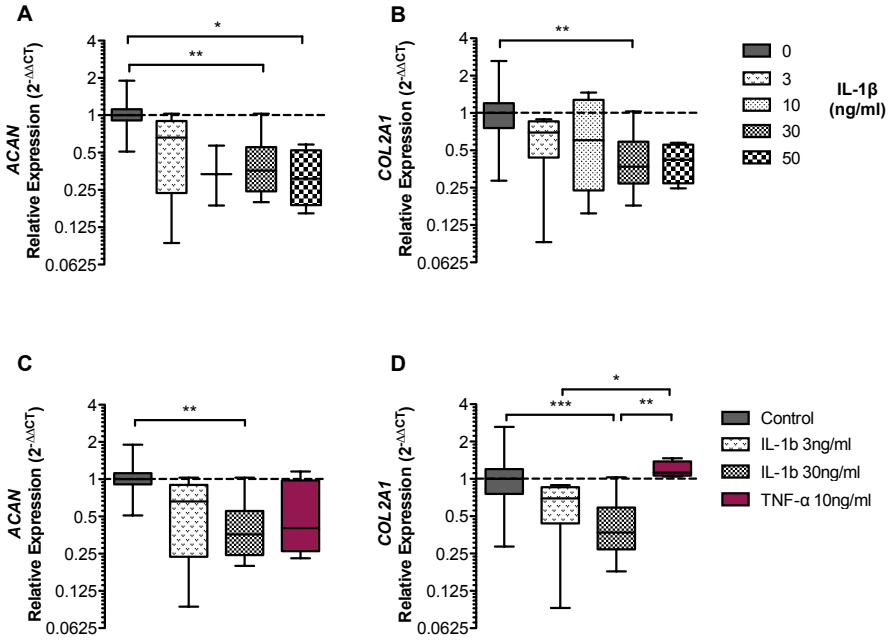

Figure 4.1.2 IL-1β, but not TNF-α treatment of chondrocyte micromasses induces down-regulation of key matrix production genes. Chondrocyte micromasses were treated with increasing concentrations of IL-1β (3ng/ml-50ng/ml) or TNF-α (10ng/ml) for 6 hours before mRNA extraction and RT-PCR. (A) Relative expression of *ACAN* and (B) *COL2A1* following IL-1β treatment. (C) Relative expression of *ACAN* and (D) *COL2A1* following IL-1β and TNF-α treatment. Data shown are $2^{-\Delta\Delta CT}$ with untreated as calibrator and *RPL32* as housekeeping gene. Data expressed as median, interquartile range and range 5 and 3 separate micromass preparations. **P*<0.05, ***P*<0.01 and ****P*<0.001 using Kruskal-Wallis test and Dunn's multiple comparison post-test.

Thus, microparticles were co-cultured with micromasses stimulated with IL-1β and TNF-α, to determine whether any effects in extracellular matrix accumulation could be observed. Interestingly, co-culture of chondrocyte micromasses with each subset of microparticles increased matrix accumulation during concomitant IL-1β stimulation (Figure 4.1.3A). No significant changes in matrix accumulation were observed during microparticle treatment alone (CMP -1.7 ± 0.4, TMP -2.2 ± 0.4 and IMP -1.7 ± 0.4 vs. 0.0 ± 3.5%). However, in chondrocyte micromasses stimulated with IL-1β (3ng/ml), CMP, TMP and most significantly IMP increased extracellular matrix accumulation above that even of untreated control micromasses (CMP 78.5 ± 30.4, TMP 128.1 ± 29.8 and IMP 228.0 ± 44.6 vs. control 0.0 ± 3.5% $P<0.001$ with Two-way ANOVA and Bonferroni post-test). IMP treatment achieved the greatest matrix accumulation of each of the microparticle subsets, significantly higher than TMP or CMP at 3ng/ml IL-1β (228 ± 44.6 vs. TMP 128.1 ± 29.8 or CMP 78.5 ± 30.4% $P<0.001$ with Two-way ANOVA and Bonferroni post-test). Strikingly, microparticle treatment with concomitant IL-1β (30ng/ml) stimulation also induced significant matrix accumulation (CMP 57.3 ± 1.4, TMP 64.9 ± 1.5 and IMP 24.1 ± 6.0 vs. -67.3 ± 2.4% $P<0.001$ with Two-way ANOVA and Bonferroni post-test), which was clearly visible in Alcian blue stained micromasses before dye extraction. This significant increase in matrix accumulation was also observed when TMP were co-cultured with TNF-α (30ng/ml) stimulated chondrocyte micromasses (72.9 ± 23.0 vs. -16.5 ± 3.1% $P<0.01$ with Two-way ANOVA and Bonferroni post-test; Figure 4.1.3B). Again, no increase in matrix accumulation was observed without the concomitant stimulation with TNFα (3.5 ± 27.5 vs. 0 ± 4.2%).

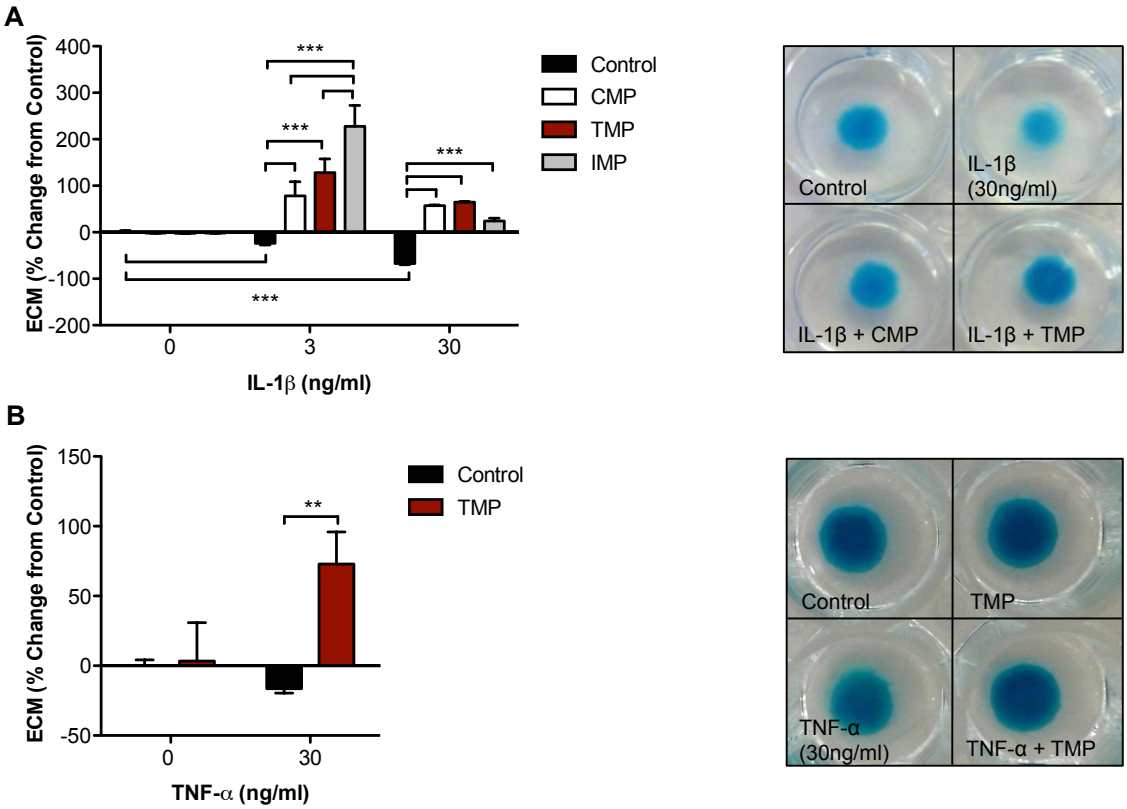

Figure 4.1.3 Microparticles reverse the effect of IL-1β and TNF-α to increase extracellular matrix accumulation. Chondrocyte micromasses were treated with (A) IL-1β or (B) TNF-α and 100,000 CMP, TMP or IMP for 24 hours before extracellular matrix accumulation was quantified by Alcian blue staining. Right are representative photographs of micromasses before dye extraction. Data are shown as mean ± SEM of 6 separate microparticle donors. ***P*<0.01 and ****P*<0.001 using Two-way ANOVA and Bonferroni post-test. CMP, control microparticles; TMP, TNF-α generated microparticles; IMP, IL-8 generated microparticles; ECM, extracellular matrix.

The accumulation of matrix induced by microparticle co-culture was dose-dependent (Figure 4.1.4). With IL-1β (3ng/ml) as a stimulus, a concentration of 100,000 TMP significantly increased matrix accumulation above IL-1β alone (128 ± 29.8 vs. -21.8 ± 3.9% P<0.001 with Two-way ANOVA and Bonferroni post-test). This concentration was more effective than lower concentrations of TMP (128 ± 29.8 vs. 10,000 TMP 13.4 ± 13.4 and 50,000 TMP 2.1 ± 20% P<0.001 with Two-way ANOVA and Bonferroni post-test). In contrast, all concentrations of TMP induced significant matrix accumulation compared to IL-1β (30ng/ml) alone (10,000 TMP 12.8 ± 12.1, 50,000 TMP 10.6 ± 20.1 and 100,000 TMP 64.9 ± 1.5 vs. -66.8 ± 2.8% P<0.001 with Two-way ANOVA and Bonferroni post-test). 100,000 TMP induced significantly greater matrix accumulation compared to the two lower concentrations of TMP using 30ng/ml IL-1β (100,000 TMP 64.9 ± 1.5 vs. 10,000 TMP 12.8 ± 12.1 and 50,000 TMP 10.6 ± 20.1 P<0.05 with Two-way ANOVA and Bonferroni post-test). A similar effect was observed with CMP plus IL-1β stimulation, but a lower concentration of 50,000 CMP induced significant matrix accumulation compared to IL-1β (3ng/ml) alone (30.7 ± 7.3 vs. -23.83 ± 3.3% P<0.05 with Two-way ANOVA and Bonferroni post-test) as well as 100,000 CMP (78.5 ± 30.4 vs. -23.83 ± 3.3% P<0.001 with Two-way ANOVA and Bonferroni post-test). Similarly, all microparticle concentrations produced significant matrix accumulation compared to IL-1β (30ng/ml) (10,000 CMP 24.5 ± 14.9, 50,000 CMP 45.9 ± 14.7 and 100,000 CMP 57.3 ± 1.4 vs. -67.3 ± 2.4% P<0.001 with Two-way ANOVA and Bonferroni post-test), with 100,000 CMP at 30ng/ml IL-1β yielding the most significant difference (57.3 ± 1.4 vs. 24.5 ± 14.9% *P*<0.05 with Two-way ANOVA and Bonferroni post-test).

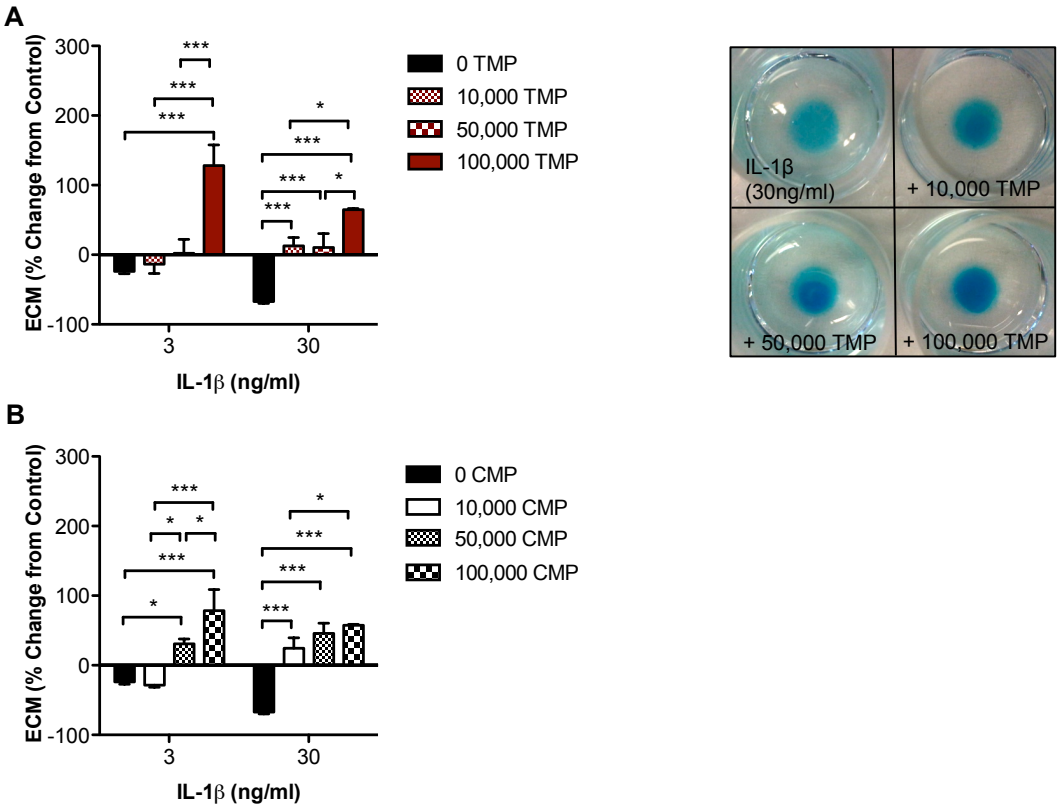

Figure 4.1.4 Microparticles increase extracellular matrix accumulation in a concentration dependent manner. Chondrocyte micromasses were treated with increasing concentrations of IL-1β and 10,000, 50,000 or 100,000 (A) TMP or (B) CMP for 24 hours before extracellular matrix accumulation was quantified by Alcian blue staining. Right are representative photographs of micromasses before dye extraction. Data are shown as mean ± SEM of 6 separate microparticle donors. **P*<0.05, ***P*<0.01 and ****P*<0.001 using Two-way ANOVA and Bonferroni post-test. CMP, control microparticles; TMP, TNF-α generated microparticles; ECM, extracellular matrix.

To determine whether this observed increase in extracellular matrix accumulation induced by microparticles was unique to the of C28/I2 chondrocyte cell line, primary adult human articular chondrocytes were cultured in micromasses and stimulated with IL-1β (3 and 30ng/ml) with concomitant microparticle treatment (Figure 4.1.5). Microparticle treatment (100,000 TMP) alone had no effect (-1.4 ± 2.0 vs. 0.0 ± 10%), but significantly increased matrix accumulation compared to IL-1β at 3ng/ml (23.9 ± 8.1 vs. -15.1 ± 9.2% $P<0.05$ with Two-way ANOVA and Bonferroni post-test) and 30ng/ml concentrations (33.0 ± 10.1 vs. -25.7 ± 5.0% $P<0.001$ with Two-way ANOVA and Bonferroni post-test).

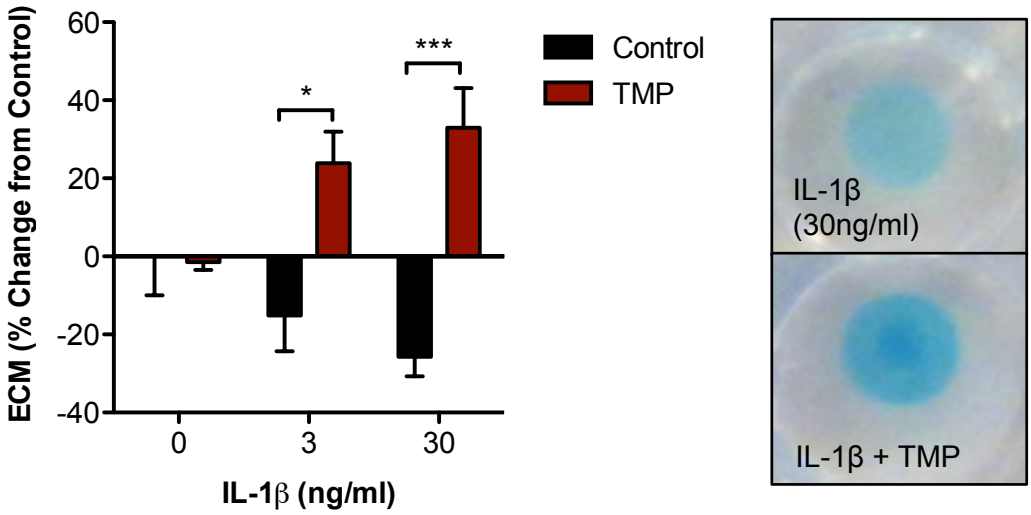

Figure 4.1.5 Microparticles increase extracellular matrix accumulation in primary adult human articular chondrocyte micromasses. Primary human chondrocyte micromasses were treated with increasing 3ng/ml or 30ng/ml IL-1β and 100,000 TMP for 24 hours before extracellular matrix accumulation was quantified by Alcian blue staining. Right are representative photographs of micromasses before dye extraction. Data are shown as mean ± SEM of 4 separate microparticle donors. **P*<0.05 and ****P*<0.001 using Two-way ANOVA and Bonferroni post-test. TMP, TNF-α generated microparticles; ECM, extracellular matrix.

To investigate whether the increase in matrix accumulation observed during microparticle treatment was due to changes in the enzymatic degradation induced by IL-1β, a 1,9 dimethylmethylene blue dye-binding assay was performed on chondrocyte micromass supernatants. This assay allows quantification of free (and therefore enzymatically cleaved) proteoglycans released from chondrocyte micromasses during culture with IL-1β (Figure 4.1.6). IL-1β (3ng/ml) stimulation induced significant matrix degradation compared to control micromasses (6.9 ± 0.5 vs. 4.3 ± 0.5μg/ml *P*<0.05 with One-way ANOVA and Bonferroni post-test). Concomitant IL-1β (3ng/ml) and microparticle treatment was not significantly changed from control (CMP 4.9 ± 1.1 and TMP 5.0 ± 0.5 vs. 4.3 ± 0.5μg/ml, not significant with One-way ANOVA and Bonferroni post-test). In contrast, IL-1β (30ng/ml) induced considerable matrix degradation (19.9 ± 3.7 vs. 5.3 ± 0.2μg/ml *P*<0.001 with One-way ANOVA and Bonferroni post-test), which was inhibited significantly by microparticle treatment (CMP 7.0 ± 0.5 and TMP 4.4 ± 0.8 vs. 19.9 ± 3.7μg/ml *P*<0.001 with One-way ANOVA and Bonferroni post-test).

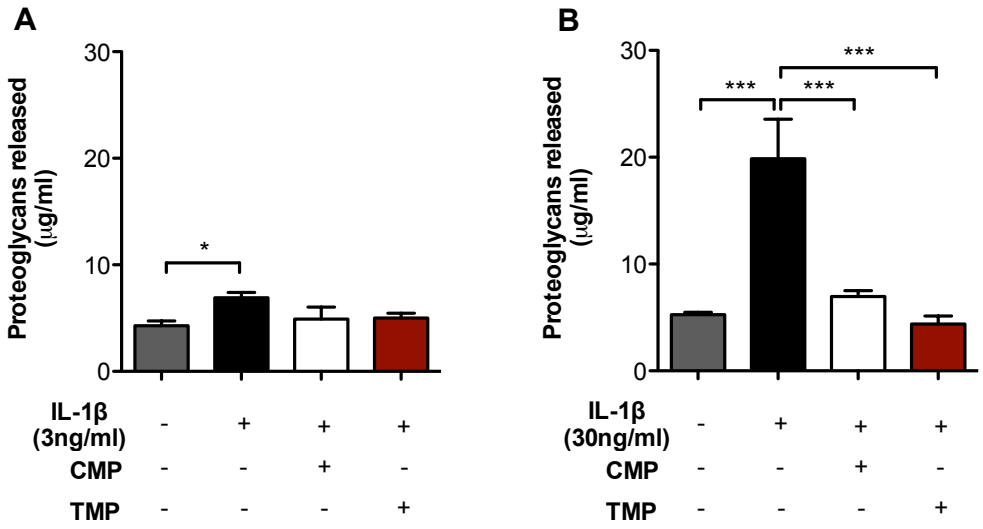

Figure 4.1.6 Microparticles prevent extracellular matrix degradation induced by IL-1β treatment. Chondrocyte micromasses were treated with (A) IL-1β (3ng/ml) or (B) (30ng/ml) and 100,000 CMP or TMP for 24 hours before released sulphated proteoglycans were quantified in supernatants by 1,9 dimethylmethylene blue dye binding assay. Data are shown as mean ± SEM of 3 or 5 separate microparticle donors. **P*<0.05 and ****P*<0.001 using One-way ANOVA and Bonferroni post-test. CMP, control microparticles; TMP, TNF-α generated microparticles.

These results indicate that the reduced matrix accumulation observed in chondrocyte micromasses stimulated with IL-1β (30ng/ml) is a consequence of enzymatic degradation, and that microparticles may inhibit this process. It was also therefore imperative to determine whether microparticles could induce matrix accumulation via its biosynthesis.

4.1.2 Neutrophil Microparticles Modulate Chondrocyte Gene Expression to Increase Extracellular Matrix and Prevent Chondrocyte Apoptosis.

To determine whether microparticle treatment was inhibiting extracellular matrix production, the gene expression of matrix-metalloproteinases *MMP13* and *ADAMTS5*, two enzymes induced by IL-1β stimulation and responsible for cartilage degradation in rheumatoid arthritis, was measured in C28/I2 chondrocyte micromasses stimulated with IL-1β and treated with 100,000 microparticles for 6 hours (Figure 4.1.7). The relative expression of *MMP13* was significantly increased upon stimulation with IL-1β (30ng/ml) compared to control (10 IQR 8.3-15.3 vs. 1 IQR 1-1.1; $P<0.001$ with Kruskal-Wallis test and Dunn's multiple comparison post-test; Figure 4.1.7A). This was also the case for concomitant IL-1β (30ng/ml) treatment and CMP (6.3 IQR 4-11.2 vs. 10 IQR 8.3-15.3; $P<0.001$ with Kruskal-Wallis test and Dunn's multiple comparison post-test), and less significantly with TMP (5.3 IQR 3.6-6 vs. 10 IQR 8.3-15.3; $P<0.001$ with Kruskal-Wallis test and Dunn's multiple comparison post-test). Whereas IL-1β did not significantly induce expression of *ADAMTS5* mRNA at this time point (0.6 IQR 0.4-2.9 vs. 1 IQR 0.8-1) and gene expression was not significantly altered upon microparticle treatment (CMP 1.4 IQR 1-2.7 and TMP 1 IQR 0.7-2.5 vs. 0.6 IQR 0.4-2.9; Figure 4.1.7B). It is plausible that microparticles may be involved in events that occur post-transcriptionally, such as the competitive inhibition of matrix degrading enzymes rather than modulating the transcription of the genes themselves at 6 hours.

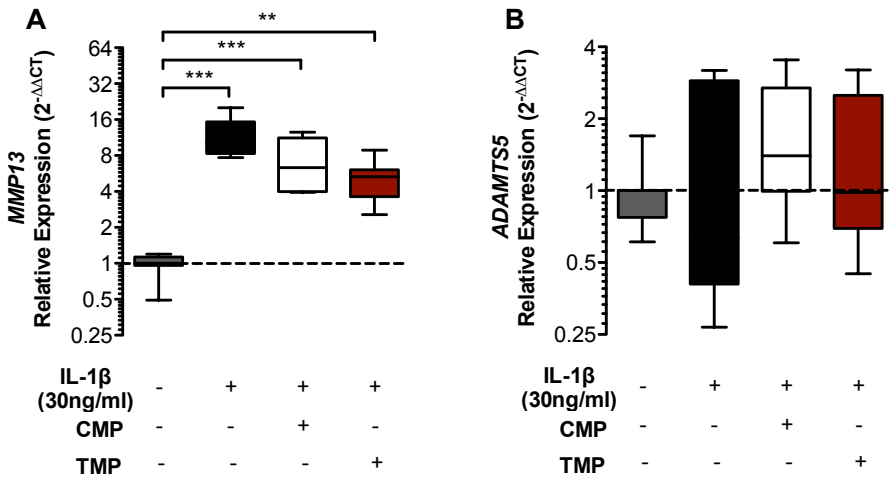

Figure 4.1.7 Microparticles do not significantly affect mRNA levels of matrix metalloproteinases associated with extracellular matrix degradation. Chondrocyte micromasses were treated with IL-1β (30ng/ml) and 100,000 CMP or TMP for 6 hours before mRNA extraction and RT-PCR. (A) Relative expression of *MMP13* and (B) *ADAMTS5.* Data shown are $2^{-\Delta\Delta CT}$ with untreated as calibrator and *RPL32* as housekeeping gene. Data expressed as median, interquartile range and range of 5 and 3 separate microparticle donors. $^{**}P<0.01$ and $^{***}P<0.001$ using Kruskal-Wallis test and Dunn's multiple comparison post-test. CMP, control microparticles; TMP, TNF-α generated microparticles.

The expression of genes associated with matrix accumulation, aggrecan and type II collagen, was next investigated in chondrocyte micromasses stimulated with IL-1β and treated with microparticles (Figure 4.1.8). The expression of *ACAN* mRNA upon IL-1β (3ng/ml) stimulation and TMP treatment was significantly different compared to IL-1β alone (1.2 IQR 0.8-1.5 vs. 0.7 IQR 0.2-0.9; $P<0.05$ with Kruskal-Wallis test and Dunn's multiple comparison post-test), but IL-1β treatment was not significantly different from control (Figure 4.1.8A; 0.7 IQR 0.2-0.9 vs. 1 IQR 0.9-1.1). In contrast, IL-1β (30ng/ml) significantly reduced relative expression of *ACAN* mRNA compared to control (0.4 IQR 0.2-0.6 vs. 1 IQR 0.9-1.1; $P<0.01$ with Kruskal-Wallis test and Dunn's multiple comparison post-test; Figure 4.1.8B), but microparticle treatment was not significantly different to control or IL-1β (30ng/ml) (CMP 0.5 IQR 0.4-0.8 and TMP 0.5 IQR 0.3-1 vs. control 1 IQR 0.9-1.1 or IL-1β 0.4 IQR 0.2-0.6).

Treatment of micromasses with CMP or TMP significantly reversed the down-regulation of *COL2A1* mRNA induced by IL-1β (3ng/ml) (1.4 IQR 1-2 and 1.1 IQR 0.9-1.5 vs. 0.7 IQR 0.4-0.9; *P*<0.01 with Kruskal-Wallis test and Dunn's multiple comparison post-test; Figure 4.1.8C). At 30ng/ml IL-1β, *COL2A1* expression was significantly down-regulated compared to control (0.4 IQR 0.3-0.6 vs. 1 IQR 0.8-1.1; *P*<0.05 with Kruskal-Wallis test and Dunn's multiple comparison post-test) which was inhibited by CMP treatment (1.1 IQR 1-1.3 vs. 0.4 IQR 0.3-0.6; *P*<0.01 with Kruskal-Wallis test and Dunn's multiple comparison post-test) and TMP treatment (1.1 IQR 1-1.5 vs. 0.4 IQR 0.3-0.6; *P*<0.05 with Kruskal-Wallis test and Dunn's multiple comparison post-test; Figure 4.1.8D). Taken together, these data suggest microparticles have gene-modulating functions in stimulated chondrocyte micromasses as measured at the 6-hour time point.

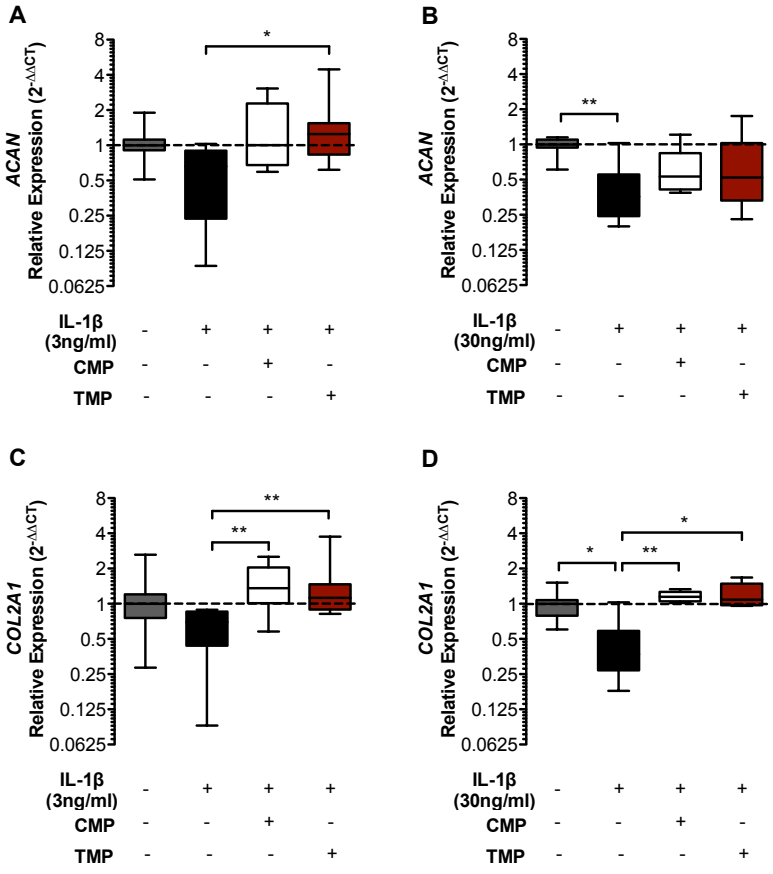

Figure 4.1.8 Microparticles reverse the down-regulation of mRNA expression associated with extracellular matrix generation induced by IL-1β. Chondrocyte micromasses were treated with IL-1β (3ng/ml or 30ng/ml) and 100,000 CMP or TMP for 6 hours before mRNA extraction and RT-PCR. (A, B) Relative expression of *ACAN* and (C, D) *COL2A1.* Data shown are $2^{-\Delta\Delta CT}$ with untreated as calibrator and *RPL32* as housekeeping gene. Data expressed as median, interquartile range and range of 5 and 3 separate microparticle donors. **P*<0.05 and ***P*<0.01 using Kruskal-Wallis test and Dunn's multiple comparison post-test. CMP, control microparticles; TMP, TNF-α generated microparticles.

The transcription of *COL2A1* and *ACAN* mRNA is governed by the chondrocyte-specific transcription factor *SOX9*; therefore the effect of microparticles on the relative expression of *SOX9* was investigated (Figure 4.1.9). There was no significant alteration of *SOX9* expression in chondrocyte micromasses stimulated with IL-1β (3ng/ml) for 6 hours, however, at 30ng/ml IL-1β, *SOX9* expression was significantly down-regulated compared to control (0.3 IQR 0.3-0.4 vs. 1 IQR 0.9-1.1; $P<0.05$ with Kruskal-Wallis test and Dunn's multiple comparison post-test). Furthermore, concomitant treatment with TMP reversed this down-regulation (1 IQR 0.6-1.3 vs. 0.3 IQR 0.3-0.4; $P<0.05$ with Kruskal-Wallis test and Dunn's multiple comparison post-test).

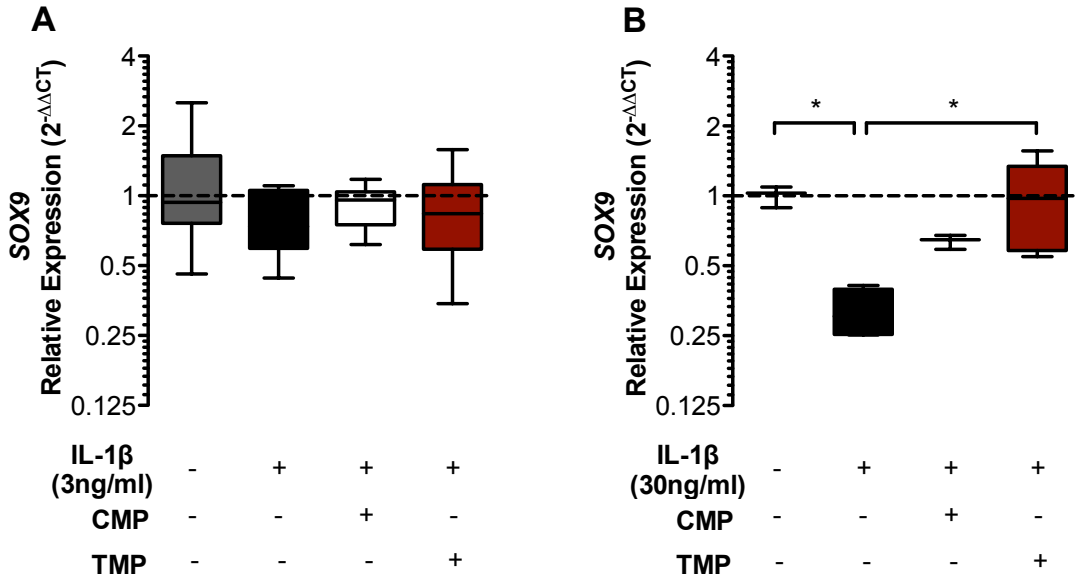

Figure 4.1.9 Microparticles induce *SOX9* transcription factor mRNA expression associated with extracellular matrix generation. Chondrocyte micromasses were treated with (A) IL-1β (3ng/ml) (B) or (30ng/ml) and 100,000 CMP or TMP for 6 hours before mRNA extraction and RT-PCR. Data shown are $2^{-\Delta\Delta CT}$ with untreated as calibrator and *RPL32* as housekeeping gene. Data expressed as median, interquartile range and range of 5 separate microparticle donors. $*P<0.05$ and $**P<0.01$ using Kruskal-Wallis test and Dunn's multiple comparison post-test. CMP, control microparticles; TMP, TNF-α generated microparticles.

This increased relative expression of *SOX9* transcription factor mRNA was mirrored by an increase in SOX9 protein at 24 hours post microparticle treatment as seen by Western blotting (Figure 4.1.10). The concomitant treatment of chondrocyte micromasses with IL-1β (30ng/ml) and microparticles led to a reversal of the down-regulation induced by IL-1β alone (CMP 149 ± 53.6 and TMP 116.2 ± 30 vs. 62.2 ± 14.5). Furthermore, microparticle treatment led to the appearance of further bands of a larger molecular weight (up to 100kDa) than IL-1β alone or control. The identity of these extra bands is unknown, but could represent IgG present within the microparticle fraction, although on reducing gels these usually appear at 25kDa and 50kDa. Alternatively, these extra bands could represent various splice variants and could account for some of the increased matrix accumulation seen in micromasses treated with both IL-1β and microparticles. Further identification of these bands would be interesting, even just to exclude endogenous IgG in the microparticle fraction.

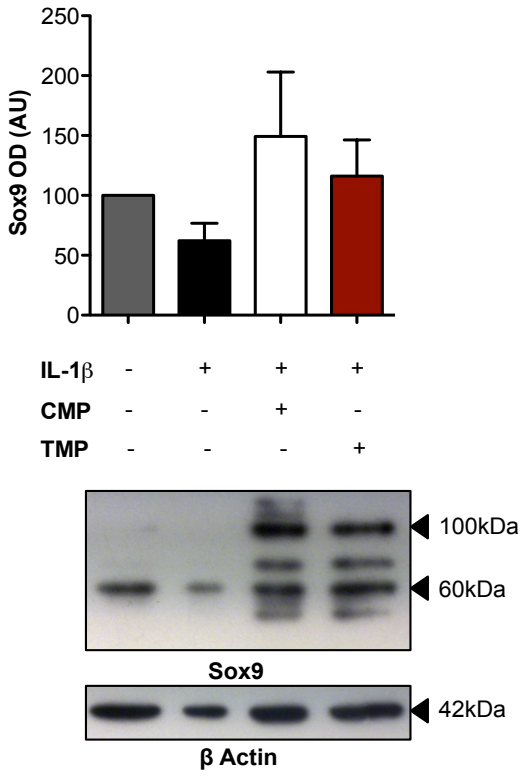

Figure 4.1.10 Microparticles induce Sox9 transcription factor protein expression. Chondrocyte micromasses treated with IL-1β (30ng/ml) and 100,000 CMP or TMP for 24 hours were analysed by Western blotting for Sox9 protein expression. Expected band size 56kDa. Bands appearing at other molecular weights are unidentified. Data are shown as mean ± SEM of 4 separate microparticle donors and blots and expressed as percentage-change from 100% control after normalisation to β Actin. CMP, control microparticles; TMP, TNF-α generated microparticles. Not significant with One-way ANOVA and Bonferroni post-test.

SOX9 is an important regulator in chondrocytes, controlling not only matrix-associated gene transcription, but also protects these cells from apoptosis. Thus, apoptosis in chondrocyte micromasses stimulated with high levels of IL-1β (50ng/ml) was measured after 18 hours using an indicator of early apoptosis, $DiOC_6$ dye (Figure 4.1.11). Approximately 40% of chondrocytes stimulated with IL-1β (50ng/ml) in micromass cultured entered early apoptosis by 18 hours and appeared as $DiOC_6$-fluorescence low compared to non-apoptotic cells. This was significantly higher than baseline (45.4 ± 0.5 vs. 26.3 ± 2.4% $P<0.001$ with One-way ANOVA and Bonferroni post-test). In order to analyse the cells using a flow cytometer, they must first be dissociated by gentle pipetting to create a single-cell suspension, which may account for the high baseline apoptosis. Regardless, concomitant CMP treatment significantly reduced the number of apoptotic chondrocytes compared to IL-1β treatment alone (35.3 ± 0.6 vs. 45.4 ± 0.5% $P<0.01$ with One-way ANOVA and Bonferroni post-test), as did TMP treatment (37.4 ± 1.7 vs. 45.4 ± 0.5% $P<0.05$ with One-way ANOVA and Bonferroni post-test). However, both microparticle treatments in combination with IL-1β still induced significantly greater levels of apoptosis compared to untreated chondrocytes (CMP 35.3 ± 0.6 and TMP 37.4 ± 1.7 vs. 26.3 ± 2.4% $P<0.01$ with One-way ANOVA and Bonferroni post-test).

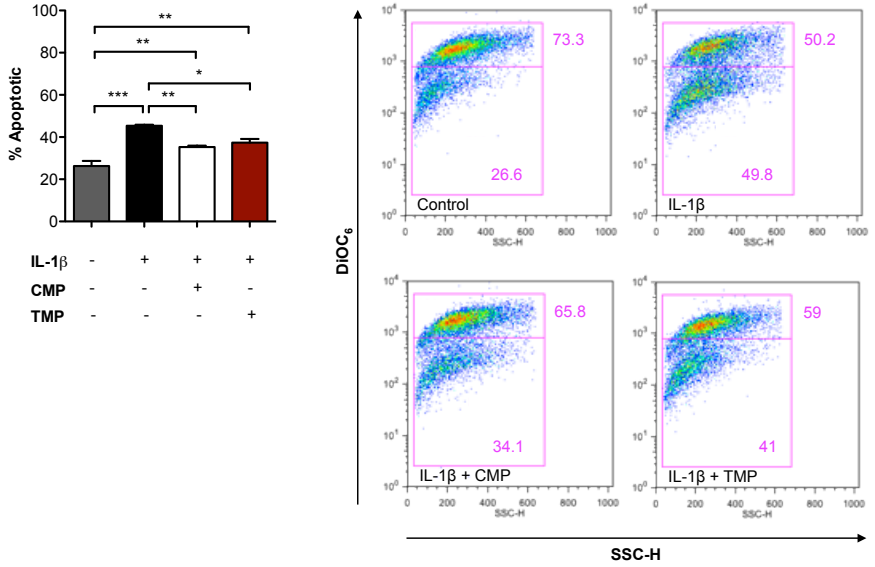

Figure 4.1.11 Microparticles generated by resting neutrophils (CMP) inhibit chondrocyte apoptosis induced by high doses of IL-1β. Chondrocyte micromasses were treated with IL-1β (50ng/ml) and 100,000 CMP or TMP for 18 hours before apoptosis was quantified by $DiOC_6$ staining and flow cytometry. Right are representative dot plots of chondrocytes disassociated from micromasses. Data are shown as mean ± SEM of 4 separate microparticle donors. $*P<0.05$, $**P<0.01$ and $***P<0.001$ using One-way ANOVA and Bonferroni post-test. CMP, control microparticles; TMP, TNF-α generated microparticles.

Late apoptosis was next quantified using TUNEL staining (Figure 4.1.12). Again, IL-1β induced significant levels of apoptosis compared to control (27.5 ± 2.2 vs. 15.9 ± 2.4% $P<0.05$ with One-way ANOVA and Bonferroni post-test) at 18 hours. In this case, only CMP treatment could significantly suppress IL-1β-induced apoptosis in C28/I2 micromasses (15.8 ± 1.5 vs. 27.5 ± 2.2% $P<0.05$ with One-way ANOVA and Bonferroni post-test) to a degree similar to that of untreated micromasses (15.8 ± 1.5 vs. 15.9 ± 2.4%). In the TMP treatment group, large variation was encountered as only a small number of samples were tested (n=3 individual microparticle donors). IMP treatment did not significantly reduce IL-1β-induced chondrocyte apoptosis.

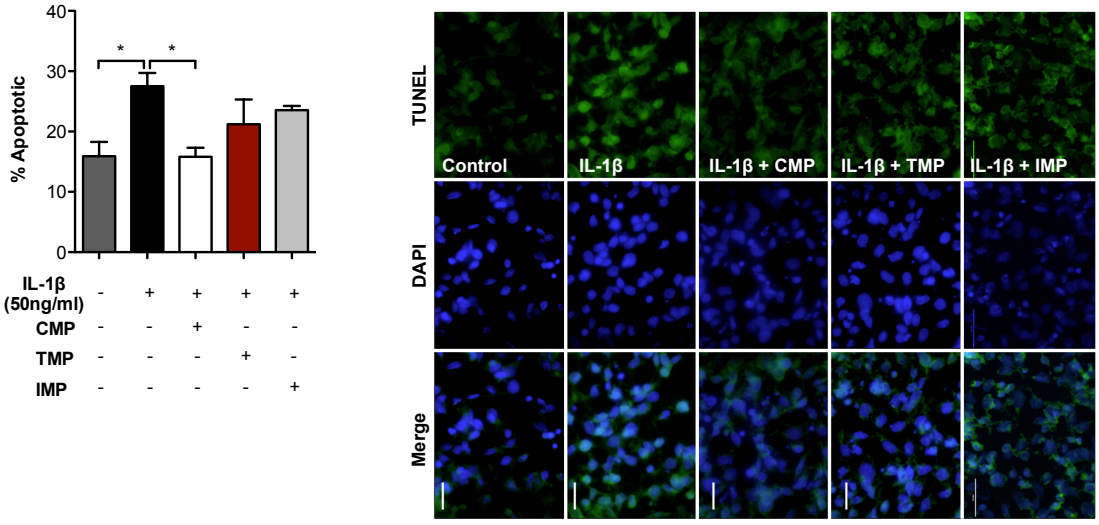

Figure 4.1.12 Microparticles generated by resting neutrophils (CMP) inhibit chondrocyte apoptosis induced by high doses of IL-1β. Chondrocyte micromasses were treated with IL-1β (50ng/ml) and 100,000 CMP, TMP or IMP for 18 hours before apoptosis was quantified by TUNEL staining using ImageJ imaging software. Right are representative fluorescent micrographs of chondrocytes disassociated from micromasses then stained. Data are shown as mean ± SEM of 4 separate microparticle donors. *$P<0.05$ using One-way ANOVA and Bonferroni post-test. CMP, control microparticles; TMP, TNF-α microparticles; IMP, IL-8 generated microparticles.

Therefore, microparticle treatment is able to reverse some of the catabolic effects induced by IL-1β stimulation, including the transcription of MMP13, the suppression of ACAN and COL2A1 gene transcription, and the induction of apoptosis. Microparticle treatment also alters the expression of Sox9 protein, leading to the appearance of bands with different weights.

4.1.3 Neutrophil Microparticles Modulate the Expression of Pro-Inflammatory Cytokines

Cartilage metabolism can be governed in 3 ways: by the regulation of anabolic and catabolic gene expression, by enzymatic remodelling and finally by the induction of degradative pathways by proinflammatory cytokines. Rheumatoid arthritis is not only characterised by a loss of cartilage matrix, but also by a dysregulated inflammatory response that does not resolve in a timely manner. The infiltration of immune cells into the joint usually occurs in response to chemoattractant signals, of which IL-8 is important in chondrocyte physiology. Therefore, the production of IL-8 by chondrocyte micromasses was investigated by ELISA (Figure 4.1.13). Microparticle treatment alone did not induce IL-8 production above baseline at 24 hours (CMP 1.6 ± 0.5 and TMP 0.41 ± 0 vs. 0.6 ± 0.0ng/ml), however IL-1β (30ng/ml) induced a 20-fold increase in IL-8 production (9.6 ± 0.9 vs. 0.6 ± 0ng/ml) which CMP and TMP both inhibited significantly (CMP 6.6 ± 0.4 and TMP 6.8 ± 0.3 vs. 9.6 ± 0.9ng/ml $P<0.001$ with Two-way ANOVA and Bonferroni post-test) at the same time point.

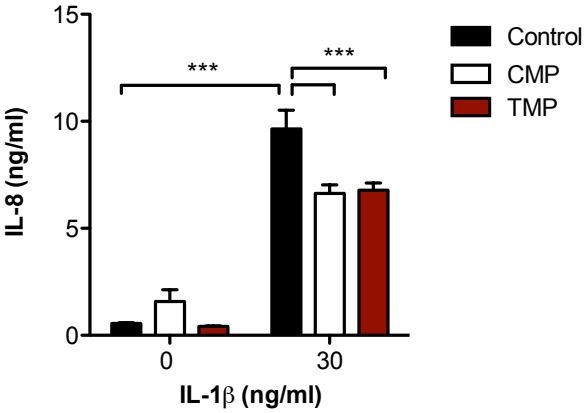

Figure 4.1.13 Microparticles inhibit chondrocyte IL-8 production induced by IL-1β. Chondrocyte micromasses were treated with IL-1β (30ng/ml) and 100,000 CMP or TMP for 24 hours before IL-8 production was quantified by ELISA. Data are shown as mean ± SEM of 6 separate microparticle donors. ***$P<0.001$ using Two-way ANOVA and Bonferroni post-test. CMP, control microparticles; TMP, TNF-α generated microparticles.

Joint pain is also a significant burden in rheumatoid arthritis, and high levels of prostaglandin E_2, associated with pain, and is detected in patient synovial fluid during flares of the disease. However, lower concentrations of prostaglandin E_2 are thought to have protective effects on cartilage matrix and native chondrocytes, but these data remain controversial. However, high concentrations are known to directly suppress matrix production and influence the expression of cartilage-degrading enzymes. Thus, prostaglandin E_2 levels were measured in chondrocyte micromass cultures (Figure 4.1.14). Surprisingly, CMP treatment alone induced significant prostaglandin E_2 production in unstimulated micromasses compared to untreated micromasses (176.9 ± 70.9 vs. 64.0 ± 6.0pg/ml $P<0.05$ with Two-way ANOVA and Bonferroni post-test). This level was significantly higher than that produced by TMP-treated unstimulated micromasses (176.9 ± 70.9 vs. 26.4 ± 6.3pg/ml $P<0.01$ with Two-way ANOVA and Bonferroni post-test) or IMP-treated unstimulated micromasses (176.9 ± 70.9 vs. 44.2 ± 3.2pg/ml $P<0.05$ with Two-way ANOVA and Bonferroni post-test). It is possible that this result is a reflection of donor variation, but equally, CMP-induced PGE_2 production could represent a caveat preventing *in vivo* microparticle testing. In contrast, CMP treatment as well as TMP treatment significantly reduced the levels of IL-1β-induced prostaglandin E_2 in stimulated micromasses (CMP 197.2 ± 15.4 and TMP 165.6 ± 8.6 vs. 746.5 ± 51.8pg/ml $P<0.001$ with Two-way ANOVA and Bonferroni post-test) representing a 4.5-fold decrease in prostaglandin E_2 production. IMP reduced the amount of prostaglandin E_2 produced upon IL-1β stimulation (592.0 ± 58.5 vs. 746 ± 51.8pg/ml $P<0.05$ with Two-way ANOVA and Bonferroni post-test), but this was significantly different from CMP or TMP treatments (592.0 ± 58.5 vs. CMP 197.2 ± 15.4 and TMP 165.6 ± 8.6pg/ml $P<0.001$ with Two-way ANOVA and Bonferroni post-test).

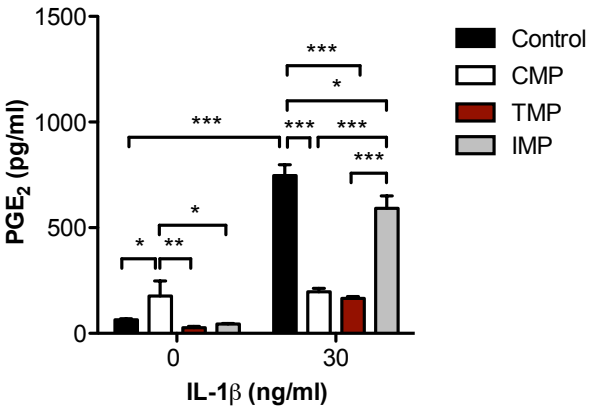

Figure 4.1.14 Microparticles inhibit chondrocyte Prostaglandin E_2 production induced by IL-1β. Chondrocyte micromasses were treated with IL-1β (30ng/ml) and 100,000 CMP, TMP or IMP for 24 hours before PGE_2 production was quantified by EIA. Data are shown as mean ± SEM of 6 separate microparticle donors. $*P<0.05$, $**P<0.01$ and $***P<0.001$ using Two-way ANOVA and Bonferroni post-test. CMP, control microparticles; TMP, TNF-α generated microparticles; IMP, IL-8 generated microparticles; PGE_2, prostaglandin E_2.

Although the role of IL-6 as a pro-inflammatory cytokine in acute inflammatory events is well defined, IL-6 is known to have homeostatic effects on chondrocytes, and even high levels of expression are not known to induce significant cartilage integrity loss. However, IL-6 does affect the tissues surrounding cartilage within the joint. For example, synovial fibroblasts are sensitive to IL-6 and produce a host of inflammatory cytokines in response to IL-6 stimulation, which recruits immune cells in arthritis. Chondrocyte micromass IL-6 production was measured following stimulation with IL-1β and treatment with microparticles (Figure 4.1.15). Microparticle treatment alone in unstimulated micromasses did not induce any IL-6 production above control (CMP 0.0 ± 0 and TMP 0.1 ± 0 vs. 0.1 ± 0ng/ml). Treatment with CMP significantly altered the production of IL-6 by IL-1β-stimulated micromasses (1.4 ± 0.1 vs. 2.4 ± 0.01ng/ml $P<0.001$ with Two-way ANOVA and Bonferroni post-test), as did TMP treatment (1.3 vs. 0.1 vs. 2.4 ± 0.01ng/ml $P<0.001$ with Two-way ANOVA and Bonferroni post-test) when compared to IL-1β alone.

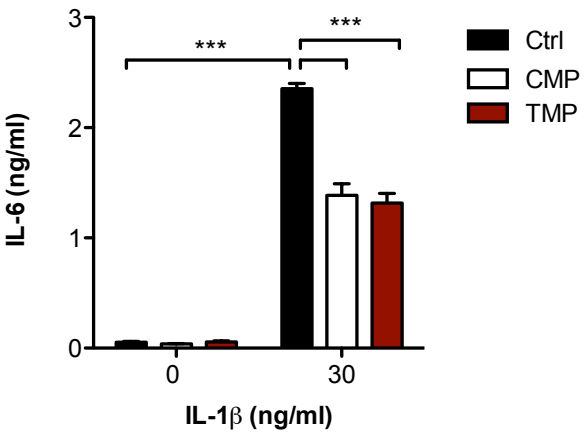

Figure 4.1.15 Microparticles reduce chondrocyte IL-6 production induced by IL-1β. Chondrocyte micromasses were treated with IL-1β (30ng/ml) and 100,000 CMP or TMP for 24 hours before IL-6 production was quantified by ELISA. Data are shown as mean ± SEM of 6 separate microparticle donors. ***$P<0.001$ with Two-way ANOVA and Bonferroni post-test. CMP, control microparticles; TMP, TNF-α generated microparticles.

Interestingly, microparticles seem to influence the production of inflammatory mediators by chondrocytes stimulated with IL-1β. Taken with the previous data, this suggests that microparticles are acting in a variety of ways to protect the chondrocytes *in vitro.* Firstly, by inducing matrix accumulation, in part by preventing its enzymatic degradation, and also by the regulation of gene transcription involved with both matrix production and matrix degradation by matrix metalloproteinases. In addition, the microparticles also reduce the release of IL-8, Prostaglandin E_2 and IL-6.

4.1.4 Neutrophil Microparticles, Not Neutrophils, are Responsible for Microparticle-Induced Chondroprotection

The pathogenic roles of neutrophils in rheumatoid arthritis are known, and the aberrant recruitment of these cells to the synovial joints during flares contributes to tissue damage. However, for neutrophil-derived microparticles to be functionally protective *in vivo* and in physiological settings, the spatial regulation of the protective process must allow for chondrocyte protection to occur. Therefore an experiment was devised to recapitulate the cartilage barrier separating neutrophils from chondrocytes to explore the spatial separation that inhibits direct contact between these cells physiologically in the joint, using transwells of varying pore sizes.

Surprisingly, TNF-α stimulated neutrophils only significantly reduced matrix accumulation within chondrocyte micromasses when the pore size of the transwell was large enough to allow neutrophils to transmigrate (8000nm pore size -32.5 ± 14.2 vs. 400nm pore size 5.6 ±11.2 and 200nm pore size -0.1 ± 17.7% $P<0.01$ with Two-way ANOVA and Bonferroni post-test; Figure 4.1.16). Strikingly, neutrophils separated by transwells with a pore size of 200nm or 400nm significantly increased matrix accumulation in micromasses stimulated with IL-1β (30ng/ml) compared to IL-1β treatment alone (400nm 60 ± 18.5 and 200nm 42.3 ± 8 vs. -43.8 ± 8% $P<0.001$ with Two-way ANOVA and Bonferroni post-test). In contrast, neutrophils separated by transwells with an 8μm pore size, large enough to allow neutrophils to pass through, significantly reduced matrix accumulation compared to IL-1β alone (-911.3 ± 529 vs. -43.8 ± 8% $P<0.001$ with Two-way ANOVA and Bonferroni post-test). This suggests that the matrix accumulation was reduced by direct neutrophil-chondrocyte contact. With this large pore size, some micromasses lifted from the bottom of the wells, indicating necrotic cell death, with destruction of the micromass structure. In samples that weren't completely degraded by direct neutrophil contact in combination with IL-1β, the matrix staining intensity was visibly drastically reduced. Thus, the spatial separation of neutrophils from chondrocytes is key to allowing neutrophil microparticles to perform their protective functions.

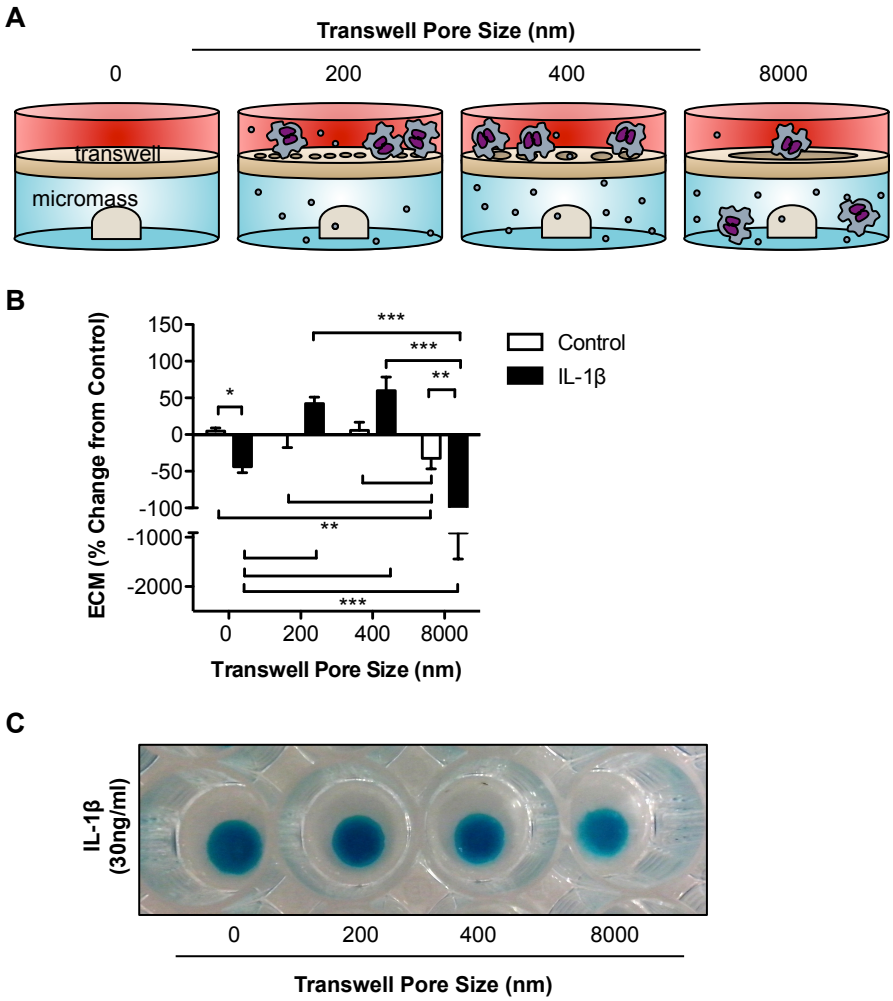

Figure 4.1.16 Neutrophils induce extracellular matrix accumulation in C28/I2 chondrocytes only when separated from direct cell-to-cell contact by transwells. Chondrocyte micromasses were treated with IL-1β (30ng/ml) before application of transwells with various sized pores containing 1x10^6 freshly isolated, TNF-α-stimulated (50ng/ml; 10 minutes followed by washing) human neutrophils for 4 hours. (A) Schematic of experimental procedure. (B) Extracellular matrix accumulation was quantified by Alcian blue staining at 24 hours. (C) Representative photographs of micromasses before dye extraction. Data are shown as mean ± SEM of 6 separate neutrophil donors. *P<0.05, **P<0.01 and ***P<0.001 using Two-way ANOVA and Bonferroni post-test. ECM, extracellular matrix.

It was therefore pertinent to determine whether modulating microparticle release by neutrophils would still confer protection to IL-1β-stimulated micromasses. Thus, neutrophils were placed on 400nm transwells and treated with cytoskeletal-affecting drugs to modulate microparticle formation (Figure 4.1.17). Treatment of neutrophils with jasplakinolide, which inhibits actin depolymerisation and stiffens the cytoskeleton inhibiting microparticle release, and cytochalasin D, which prevents actin polymerisation leading to increased cytoskeletal fluidity and increased microparticle shedding, did not protect from IL-1β-induced matrix loss (-134 ± 27.3 and -123.9 ± 31.1 vs. -70.5 ± 32.6%) compared with untreated neutrophils (60 ± 18.5 vs. -70.5 ± 32.6% P<0.001 with Two-way ANOVA and Bonferroni post-test).

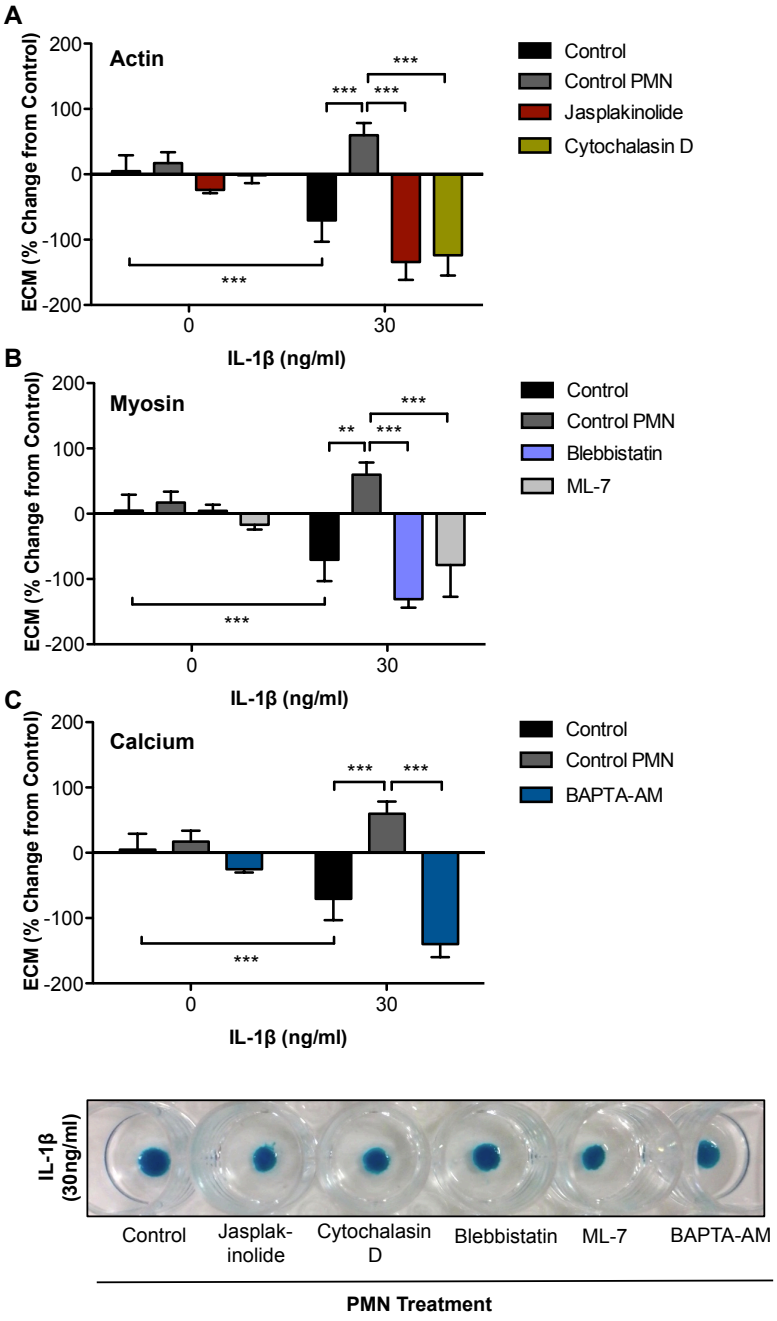

Figure 4.1.17 Neutrophil microparticle protection is lost upon disruption of the actin and myosin cytoskeleton, or chelation of intracellular neutrophil calcium. Chondrocyte micromasses were treated with IL-1β (30ng/ml) before application of transwells (400nm pore size) containing 1x10^6 freshly isolated human neutrophils treated with (A) Jasplakinolide (1μM; increases cell rigidity), Cytochalasin D (2μM; increases cell cytoskeleton fluidity), (B) Blebbistatin (10μM, inhibits focal adhesion formation), ML-7 (20μM; inhibits cell contractility) or (C) BAPTA-AM (20μM; chelates intracellular calcium) for 10 minutes then TNF-α (50ng/ml) for 20 minutes. Transwells were removed after 4 hours. Extracellular matrix accumulation was quantified by Alcian blue staining at 24 hours. Below are representative photographs of micromasses before dye extraction. Data are shown as mean ± SEM of 6 separate neutrophil donors. $^{**}P<0.01$ and $^{***}P<0.001$ using Two-way ANOVA and Bonferroni post-test. ECM, extracellular matrix; PMN, polymorphonuclear cells.

Thus, manipulating microparticle formation attenuates protection. Furthermore, these data suggest that the neutrophil actin cytoskeleton is required for the formation of microparticles with chondroprotective effects, as protein loading is likely dependent on a functioning cytoskeleton. Similarly, treatment of neutrophils with Blebbistatin, which binds and inhibits myosin II in an actin detached state, and therefore inhibits the formation of actomyosin, making the cell less rigid (Kovacs et al., 2004); or ML-7 a selective myosin light-chain inhibitor which prevents contraction of the cell necessary for blebbing (Shin et al., 2010) also prevented chondroprotection (-130.8 ± 13.1 and -78.4 ± 48.8 vs. 60 ± 18.5% $P<0.001$ with Two-way ANOVA and Bonferroni post-test). This suggests that the loss of cellular contractility prevents the formation of functional chondroprotective microparticles. Furthermore, treatment of neutrophils with BAPTA-AM, which chelates intracellular calcium, limiting microparticle formation, completely blocked chondroprotection (-139.8 ± 20.1 vs. 60 ± 18.5% $P<0.001$ with Two-way ANOVA and Bonferroni post-test). This indicates that limiting microparticle formation without affecting the cytoskeleton of the neutrophil also prevents chondroprotection in this co-culture model.

Next, we assessed the contribution of phosphatidylserine to the protective effects of microparticles (Figure 4.1.18). The expression of phosphatidylserine has been linked with the resolution of inflammation, by inducing the release of TGFβ1 in macrophages that have ingested apoptotic cells (Huynh et al., 2002). Incubation of microparticles with an excess of Annexin V led to approximately 80% positivity (Figure 4.1.18A). In micromass co-culture, Annexin V alone, used as a control, together with annexin V coated microparticles did not alter matrix accumulation in unstimulated micromasses as expected (13 ± 6.6 and 21.2 ± 5.3 vs. 4.3 ± 2.8%; Figure 4.1.18B). Annexin V treatment also did not affect the suppression of matrix accumulation induced by IL-1β (30ng/ml; -28.1 ± 2.3 vs. -18.2 ± 3.4%). However, treatment of IL-1β stimulated micromasses with Annexin V coated microparticles did induce significant matrix accumulation compared to IL-1β alone (23 ± 6.3 vs. -18.2 ± 3.4% *P*<0.001 with Two-way ANOVA and Bonferroni post-test). Interestingly, Annexin V coated microparticle treatment induced significantly less matrix accumulation compared to uncoated microparticles (23 ± 6.3 vs. 50 ± 7.9% *P*<0.01 with Two-way ANOVA and Bonferroni post-test) in IL-1β stimulated micromasses, suggesting a partial inhibition of microparticle function by Annexin V shielding of exposed phosphatidylserine.

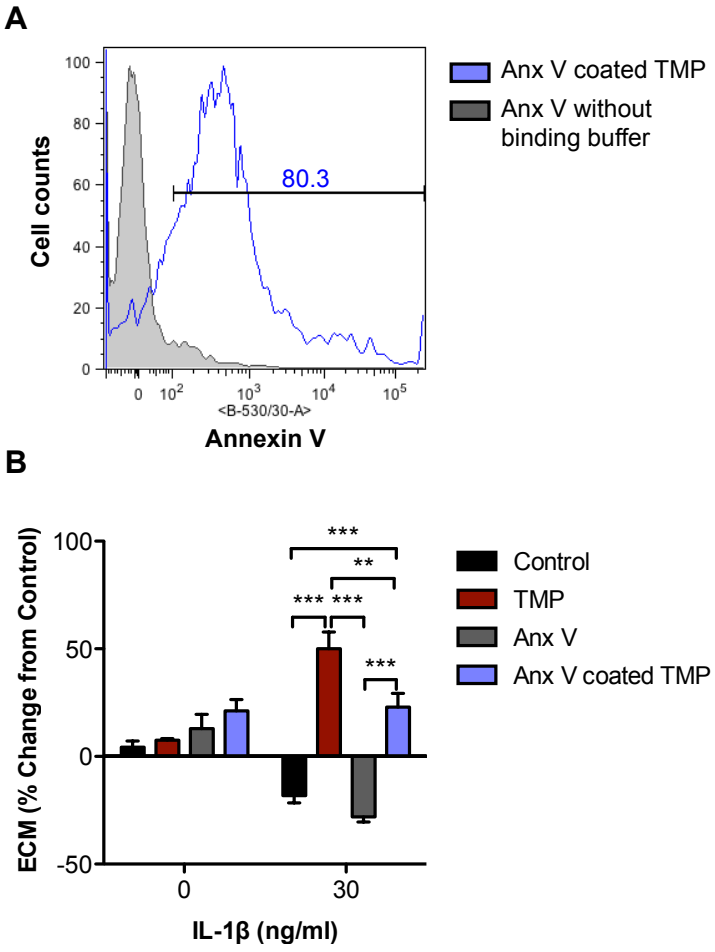

Figure 4.1.18 Coating microparticles with Annexin V partially reverses their protective effects on extracellular matrix accumulation. (A) TMP were coated in Annexin V (1mg in 100μl) for 20 minutes at room temperature in the presence of calcium binding buffer then analysed by flow cytometry. (B) Chondrocyte micromasses were treated with IL-1β (30ng/ml) and 100,000 annexin V-coated TMP for 24 hours before extracellular matrix accumulation was quantified by Alcian blue staining. Data are shown as mean ± SEM of 4 separate microparticle donors. ***P*<0.01 and ****P*<0.001 using Two-way ANOVA and Bonferroni post-test. TMP, TNF-α generated microparticles; ECM, extracellular matrix; Anx V, Annexin V.

4.2 Microparticle Mediators Responsible for Chondroprotection

The surprising finding that neutrophil microparticles protected chondrocytes in *in vitro* arthritic conditions merited further investigation to determine the molecules and mechanism responsible for these effects. From several hundred proteins found in neutrophil microparticles by mass spectrometry, candidates with known inflammation-modulating functions were screened for functional microparticle effects.

4.2.1 Is Annexin A1 Responsible for the Chondroprotection Observed with Microparticle Treatment? Characterisation of the Function of Annexin A1 in Chondrocyte Biology

The first protein screened for chondroprotection was Annexin A1, which displays potent anti-inflammatory effects and drives the resolution of inflammation (D'Acquisto et al., 2008). Firstly, the effect of Annexin A1 on chondrocyte micromass matrix accumulation was tested (Figure 4.2.1). Annexin A1, in low nanomolar concentrations significantly increased matrix accumulation in unstimulated micromasses compared to control (1nM 113.8 ± 23.9 and 10nM 72.5 ± 18.1 vs. 0 ± 3.5% $P<0.001$ with Two-way ANOVA and Bonferroni post-test). This effect was lost at a higher concentration (30nM; 25.4 ± 17 vs. control 0 ± 3.5%), and 1nM Annexin A1 (113.8 ± 23.9 vs. 25.4 ± 17% $P<0.001$ with Two-way ANOVA and Bonferroni post-test). Annexin A1 reversed the loss in matrix accumulation induced by IL-1β (3ng/ml) at concentrations of 10nM (57.3 ± 14.8 vs. -23.8 ± 3.3% $P<0.001$ with Two-way ANOVA and Bonferroni post-test) and most notably 30nM (130.4 ± 26.8 vs. -23.8 ± 3.3% $P<0.001$ with Two-way ANOVA and Bonferroni post-test). The optimal concentration of Annexin A1 to reverse the effects of a high concentration of IL-1β (30ng/ml) was 10nM, although all three concentrations of Annexin A1 gave protection (1nM 6.8 ± 10.1, 10nM 75 ± 38.7 and 30nM 23.8 ± 24 vs. -67.3 ± 2.4% $P<0.001$ with Two-way ANOVA and Bonferroni post-test).

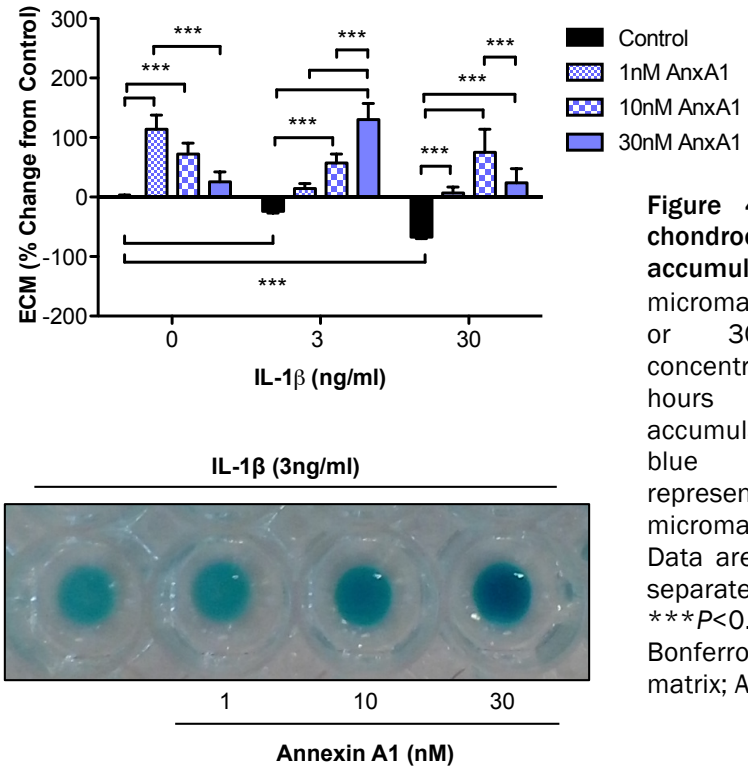

Figure 4.2.1 Annexin A1 increases chondrocyte extracellular matrix accumulation in vitro. Chondrocyte micromasses were treated with IL-1β (3 or 30ng/ml) and increasing concentrations of Annexin A1 for 24 hours before extracellular matrix accumulation was quantified by Alcian blue staining. Bottom is a representative photograph of micromasses before dye extraction. Data are shown as mean ± SEM of 6 separate micromass preparations. ***P<0.001 using Two-way ANOVA and Bonferroni post-test. ECM, extracellular matrix; AnxA1, Annexin A1.

To decipher the mechanism of ECM protection afforded by Annexin A1 treatment, the modulation of cartilage matrix-producing genes was first investigated (Figure 4.2.2). Surprisingly, Annexin A1 treatment across all concentrations significantly down-regulated *ACAN* mRNA expression in resting chondrocyte micromasses (-0.4 ± 0.1 for each concentration vs. 0 ± 0.05 Figure 4.2.2A). No other significant effects were seen in either the expression of *ACAN* mRNA or *COL2A1* mRNA, whether the micromasses had been stimulated with IL-1β or not (Figure 4.2.2A and B).

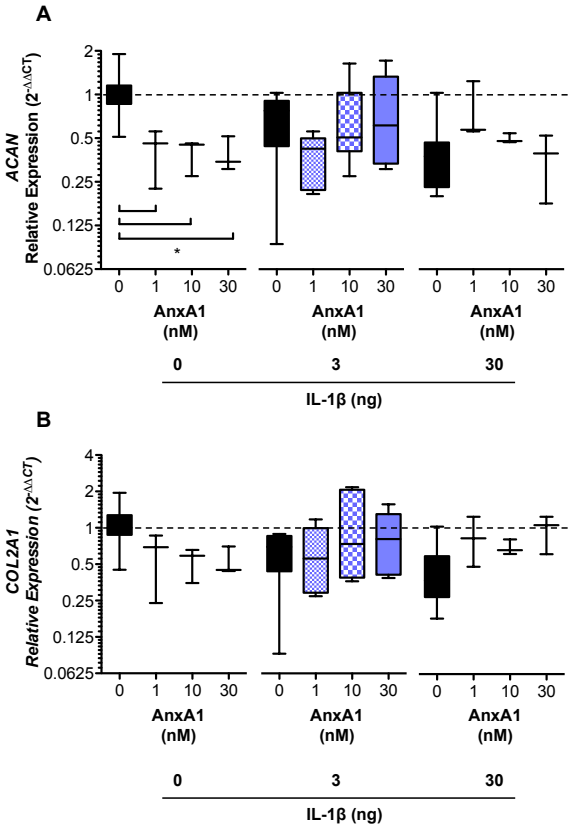

Figure 4.2.2 Annexin A1 does not significantly reverse IL-1β-induced down regulation of cartilage matrix-producing genes. Chondrocyte micromasses were treated with IL-1β (3ng/ml or 30ng/ml) and increasing concentrations of Annexin A1 for 6 hours before mRNA extraction and RT-PCR. (A) Relative expression of *ACAN* and (B) *COL2A1.* Data shown are $2^{-\Delta\Delta CT}$ with untreated as calibrator and *RPL32* as housekeeping gene. Data expressed as median, interquartile range and range of at least 3 separate micromass preparations. **P*<0.05 using Two-way ANOVA with Bonferroni post-test performed on the logged data. AnxA1, Annexin A1.

Microparticles inhibited the production of IL-8 and Prostaglandin E_2 in IL-1β stimulated micromasses, so the effect of Annexin A1 treatment on production of these pro-inflammatory mediators was investigated. Annexin A1 treatment did not induce the production of IL-8 in unstimulated micromasses (1nM 0.4 ± 0, 10nM 0.9 ± 0.1, 30nM 1 ± 0.1 vs. 0.6 ± 0) nor suppress the production of IL-8 from IL-1β stimulated chondrocytes (Figure 4.2.3; 1nM 9.1 ± 0.4, 10nM 8.1 ± 0.6, 30nM 10.3 ± 1.6 vs. 9.6 ± 0.9).

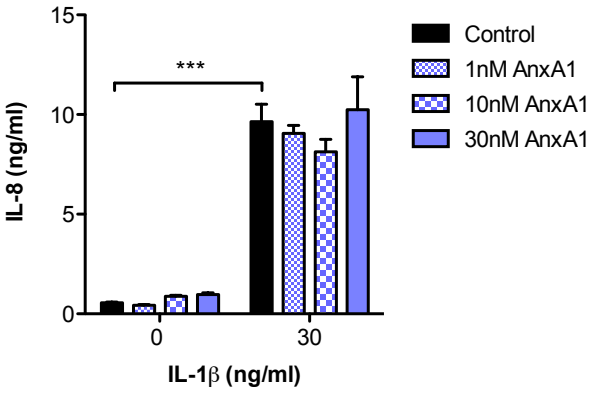

Figure 4.2.3 Annexin A1 does not block chondrocyte IL-8 production induced by IL-1β. Chondrocyte micromasses were treated with IL-1β (30ng/ml) and increasing concentrations of Annexin A1 for 24 hours before IL-8 production was quantified by ELISA. Data are shown as mean ± SEM of 3 separate micromass preparations, ***P<0.001 with Two-way ANOVA and Bonferroni post-test. AnxA1, Annexin A1.

Annexin A1 treatment did not induce prostaglandin E_2 synthesis in unstimulated micromasses (Figure 4.2.4; 1nM 52.4 ± 3.1, 10nM 85.5 ± 21.4, 30nM 77 ± 3.2 vs. 64 ± 6) or but did significantly reduce prostaglandin E_2 generation at a concentration of 10nM compared to IL-1β (30ng/ml) alone (10nM 466.1 ± 106 vs. 746.5 ± 51.8 P<0.001 with Two-way ANOVA and Bonferroni post-test). With treatment of 30nM Annexin A1, this protection was lost (667.9 ± 12.2 vs. 466.1 ± 106 P<0.05 with Two-way ANOVA and Bonferroni post-test). Together, these results suggest that although Annexin A1 significantly increases matrix accumulation in chondrocyte micromasses, and can reverse the down-regulation of matrix accumulation induced by IL-1β stimulation, Annexin A1 is not solely responsible for the anti-inflammatory properties observed in microparticle co-culture with chondrocytes.

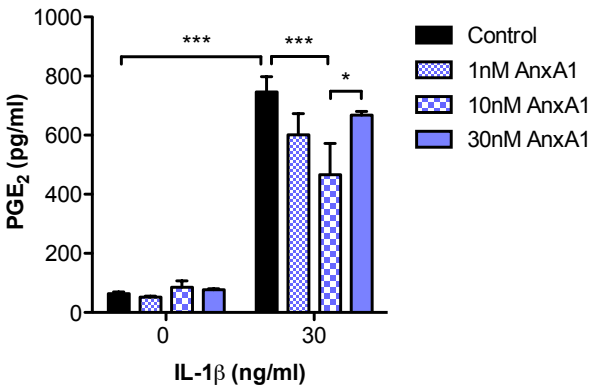

Figure 4.2.4 Annexin A1 does not efficiently inhibit chondrocyte PGE_2 production induced by IL-1β. Chondrocyte micromasses were treated with IL-1β (30ng/ml) and increasing concentrations of Annexin A1 for 24 hours before Prostaglandin E_2 production was quantified by EIA. Data are shown as mean ± SEM of 3 separate micromass preparations. **P*<0.05 and ****P*<0.001 with Two-way ANOVA and Bonferroni post-test using Two-way ANOVA and Bonferroni post-test. AnxA1, Annexin A1; PGE_2, prostaglandin E_2.

To determine whether microparticle Annexin A1 was responsible for the increases in ECM accumulation seen during IL-1β stimulation of chondrocyte micromasses, an experiment was designed to test whether microparticles generated from *Anxa1* knockout mice could increase matrix accumulation compared to those from wild type mice. Murine Annexin A1 is 78% homologous to human Annexin A1 and displays anti-inflammatory effects *in vitro* with human cells. To obtain sufficient neutrophils, a peritonitis model was utilised, as the number of circulating neutrophils in mice is low. Furthermore, neutrophil isolation and purification techniques performed on mouse blood often have a very low yield. The increased purity in these samples would be advantageous, however to isolate enough neutrophils to obtain microparticles would involve a large number of mice being pooled. Instead, neutrophils were collected from the peritoneum of mice treated with 1mg/ml zymosan A to induce high levels of neutrophil recruitment at 4 hours. As expected, Annexin A1 null mice had an increased level of neutrophil recruitment to the peritoneum (WT 3.6 ± 0.4 vs. 5.95 ± 0.4 x 10^6 cells/mouse *P*<0.01 with unpaired, two-tailed t-test), as had been previously published (Chatterjee et al., 2005) and were more than 75% positive for the neutrophil marker LY6G when characterised by flow cytometry (Figure 4.2.5B and C). As expected, mouse neutrophils obtained from Annexin A1 null mice did not stain for Annexin A1 whilst wild type neutrophils were positive (Figure 4.2.5D). Following stimulation with recombinant mouse TNF-α (50ng/ml; 2x10^6 cells/ml), both genotypes of neutrophil shed similar numbers of microparticles, as counted by flow cytometry (2.5 ± 0.8 vs. 1.6 ± 0.7; Figure 4.2.5E).

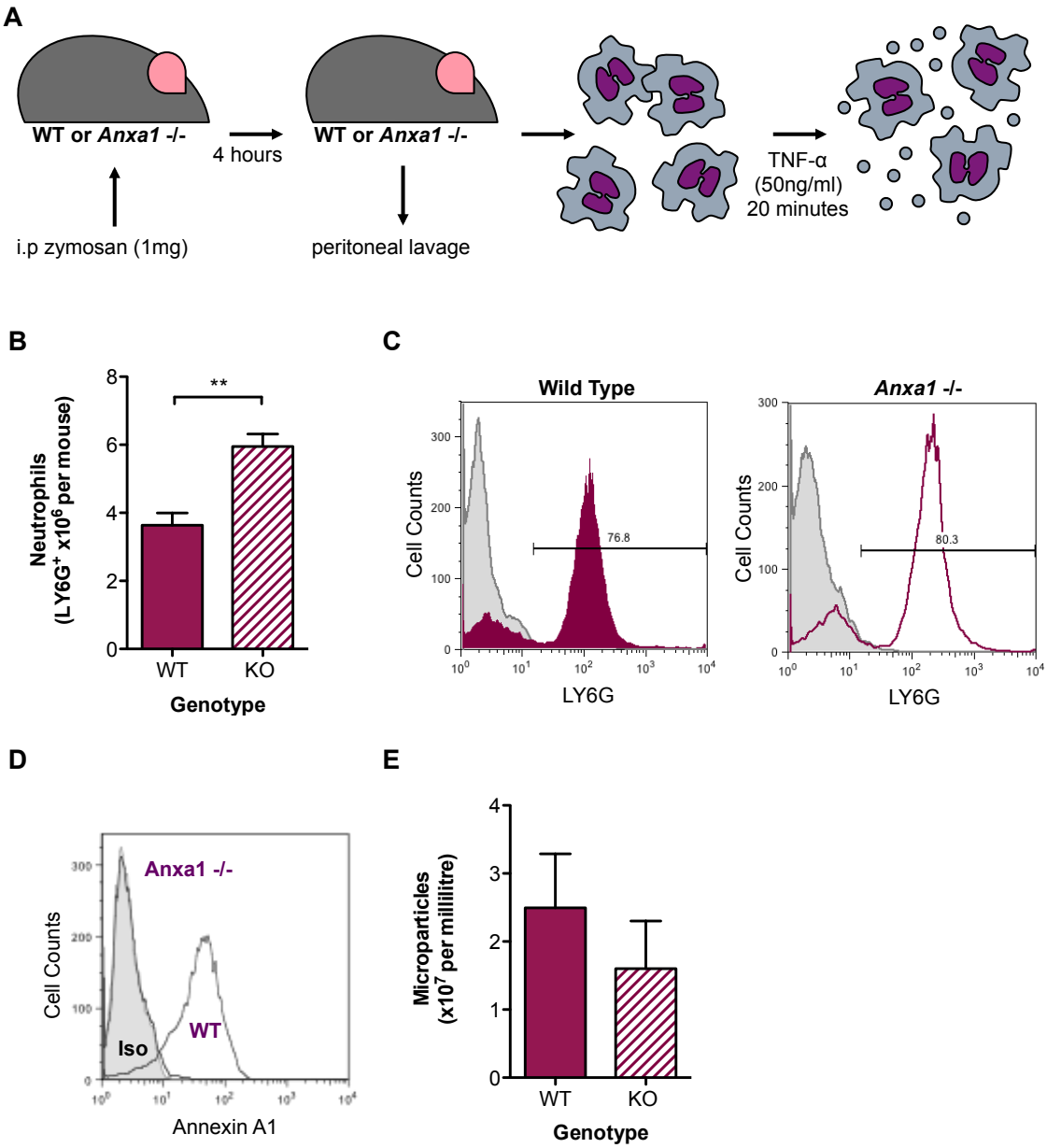

Figure 4.2.5 Characterisation of neutrophil microparticles generated from wild type or Annexin A1 null mice. (A) Wild type or *Anxa1*$^{-/-}$ C57BL/6 mice received an intraperitoneal injection of 1mg/mouse zymosan A to induce neutrophil recruitment. Cells were collected 4 hours post injection, (B) counted and characterised by staining with (C) LY6G and (D) Annexin A1 polyclonal antibodies and analysed by flow cytometry $^{**}P<0.01$ with unpaired t-test. (E) Cells were stimulated with recombinant TNF-α (50ng/ml) and offspring microparticles counted by flow cytometry following loading with BODIPY dye (2.5μM). Not significant with unpaired t-test. AnxA1, Annexin A1; WT, wild type; KO, Annexin A1 knockout; i.p., intraperitoneal.

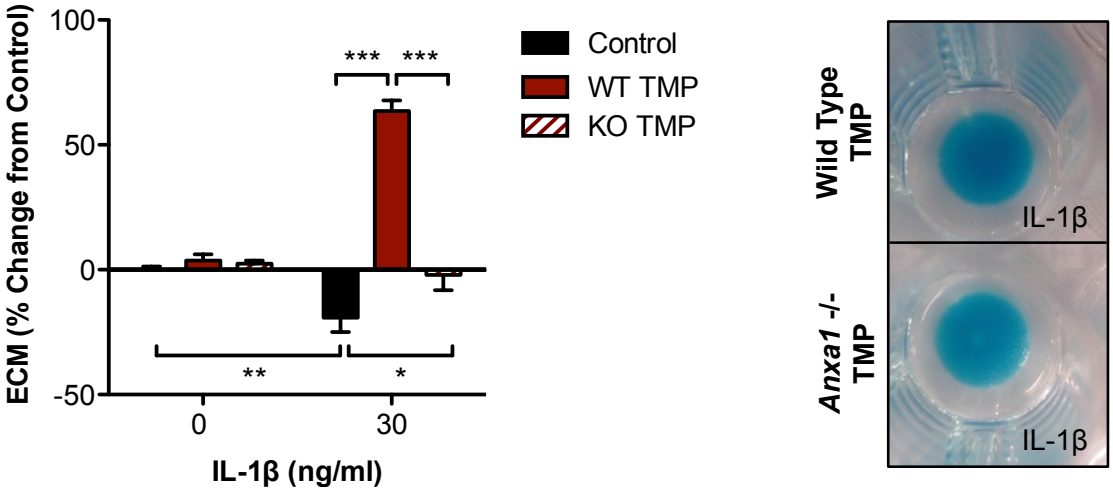

Figure 4.2.6 Annexin A1 null microparticles are anti-catabolic, but do not induce increased extracellular matrix accumulation to the same extent as wild type microparticles. Chondrocyte micromasses were treated with IL-1β (30ng/ml) and 100,000 wild type or *Anxa1*$^{-/-}$ TMP for 24 hours before extracellular matrix accumulation was quantified by Alcian blue staining. Right are representative photographs of micromasses before dye extraction. Data are shown as mean ± SEM of 4 pooled microparticle preparations from each genotype and 5 separate micromass preparations. *P<0.05, **P<0.01 and ***P<0.001 using Two-way ANOVA and Bonferroni post-test. TMP, TNF-α-treatment generated neutrophil microparticles; AnxA1, Annexin A1; ECM, extracellular matrix; WT, wild type; KO, Annexin A1 knockout.

Microparticles generated from either wild type or Annexin A1 knockout mouse neutrophils did not affect matrix accumulation in unstimulated micromasses (WT 3.7 ± 2.5, *Anxa1*$^{-/-}$ 2.4 ± 1.2 vs. 0 ± 1.3%; Figure 4.2.6). Wild type microparticles significantly increased matrix accumulation in IL-1β-stimulated micromasses compared to IL-1β treatment (63.5 ± 4.2 vs. -19.2 ± 5.7% P<0.001 with Two-way ANOVA and Bonferroni post-test). Interestingly, Annexin A1 knockout microparticles prevented IL-1β-induced ECM reduction stimulated micromasses compared to IL-1β treatment alone (-2 ± 6.1 vs. -19.2 ± 5.7% P<0.05 with Two-way ANOVA and Bonferroni post-test). However, Annexin A1 null microparticles did not cause an increase in ECM above basal levels as observed with wild type microparticles (-2 ± 6.1 vs. 63.5 ± 4.2% P<0.001 with Two-way ANOVA and Bonferroni post-test).

These data suggest that although Annexin A1 treatment resembles some aspects of microparticle chondroprotection, it is clear that Annexin A1 is only partially responsible for chondroprotection *in vitro.* Other endogenous microparticle constituents may contribute to the suppression of cytokine release and control of gene transcription.

4.2.2 The Annexin A1 Receptor FPR2/ALX is Required for Microparticle-Induced Chondrocyte Matrix Accumulation

To investigate whether Annexin A1-induced matrix accumulation was receptor dependent, it was first important to assess expression levels of the receptors on chondrocytes. The expression of FPR2/ALX, and its orthologue, FPR1, was determined using flow cytometry, as the expression of either G-protein coupled receptor has not previously been reported in chondrocytes. Chondrocytes expressed FPR2/ALX as well as FPR1 (Figure 4.2.7).

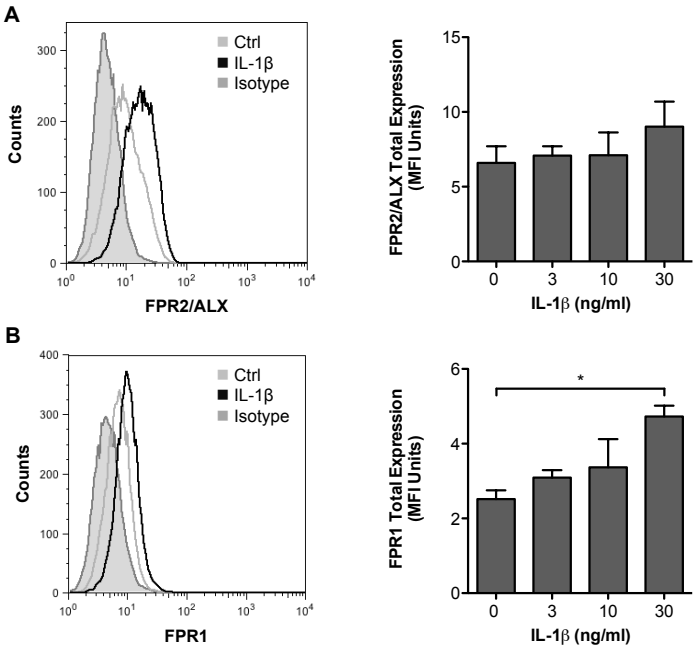

Figure 4.2.7 C28/I2 chondrocytes express the Annexin A1 receptor, FPR2/ALX, and its orthologue FPR1. Chondrocytes were treated with increasing concentrations of IL-1β for 24 hours before dissociation and analysis by flow cytometry for (A) FPR2/ALX and (B) FPR1 mean fluorescence intensity (MFI, arbitrary units). Right hand panels show representative histograms. Data are shown as mean ± SEM of 3 separate micromass preparations. **P*<0.05 using One-way ANOVA and Bonferroni post-test.

Upon 24-hour stimulation with IL-1β (30ng/ml), FPR2 expression remained unchanged (3ng/ml 7.1 ± 0.6, 10ng/ml 7.1 ± 1.5, 30ng/ml 9.0 ± 1.7 vs. 6.6 ± 1.1) whereas FPR1 expression was significantly increased (4.7 ± 0.3 vs. 2.5 ± 0.2 $P<0.05$ with One-way ANOVA and Bonferroni post-test). Modulation of *FPR2* (Figure 4.2.8A; 1 IQR 0.8-1.4 vs. 1.3 IQR 1.2-1.4) or *FPR1* (Figure 4.2.8B; 1 IQR 0.9-1.7 vs. 0.5 IQR 0.5-1.6) gene expression by IL-1β (30ng/ml) at 6 hours was not seen, possibly because of the particular time-point chosen or because the transcriptional control of these receptors involves rapid degradation and transcriptional repression (Karoor et al., 1996, Mandal et al., 2005), thus it would be interesting to explore the kinetics of receptor regulation in these cells further.

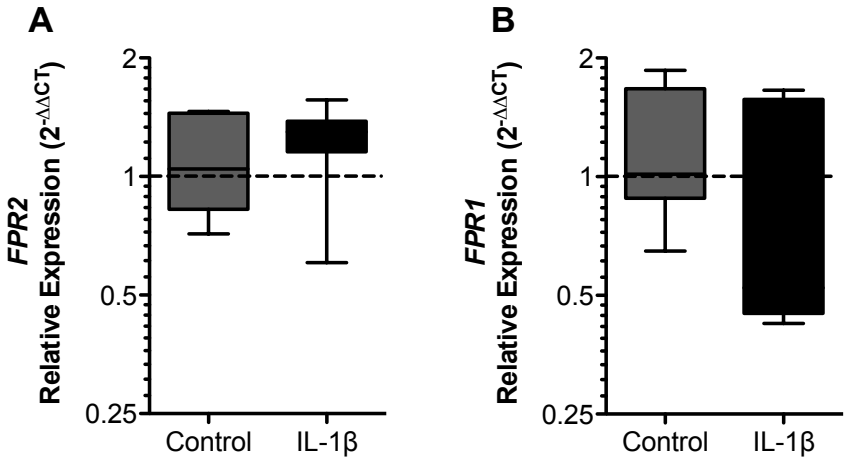

Figure 4.2.8 C28/I2 chondrocyte *FPR2* and *FPR1* mRNA levels are not significantly modulated by IL-1β treatment. Chondrocyte micromasses were treated with IL-1β (30ng/ml) for 6 hours before mRNA extraction and RT-PCR. (A) Relative expression of *FPR2* and (B) *FPR1.* Data shown are $2^{-\Delta\Delta CT}$ with untreated as calibrator and *RPL32* as housekeeping gene. Data expressed as median, interquartile range and range of 6 separate micromass preparations, not significant by Mann-Whitney t-test.

To elucidate whether microparticle-Annexin A1 contributes to matrix accumulation by a receptor dependent mechanism, rather than direct binding to phospholipids on the chondrocyte cell membrane, pharmacological inhibitors WRW_4 and cyclosporin H that antagonise FPR2/ALX and FPR1 were used (Figure 4.2.9). WRW_4 treatment did not affect matrix accumulation in unstimulated micromasses (18.9 ± 13.5 vs. 0 ± 12%), or TMP-treated unstimulated micromasses (13.4 ± 19.4 vs. -1.9 ± 3.4%) and had no effect on IL-1β (30ng/ml) treatment alone (-65.7 ± 9.8 vs. -65.8 ± 3.4%). However, FPR2/ALX antagonism abrogated the microparticle-induced increase in matrix accumulation following IL-1β-stimulation (-51.5 ± 10.6 vs. 57.3 ± 1.4% $P<0.01$ with Two-way ANOVA and Bonferroni post-test), suggesting that FPR2/ALX is important for microparticle protection. Cyclosporin H treatment did not affect ECM in unstimulated micromasses yet reverted the effects of IL-1β (-11.4 ± 22.4 vs. -65.8 ± 3.4%), so the contribution of FPR1 to microparticle-induced matrix accumulation could not be determined.

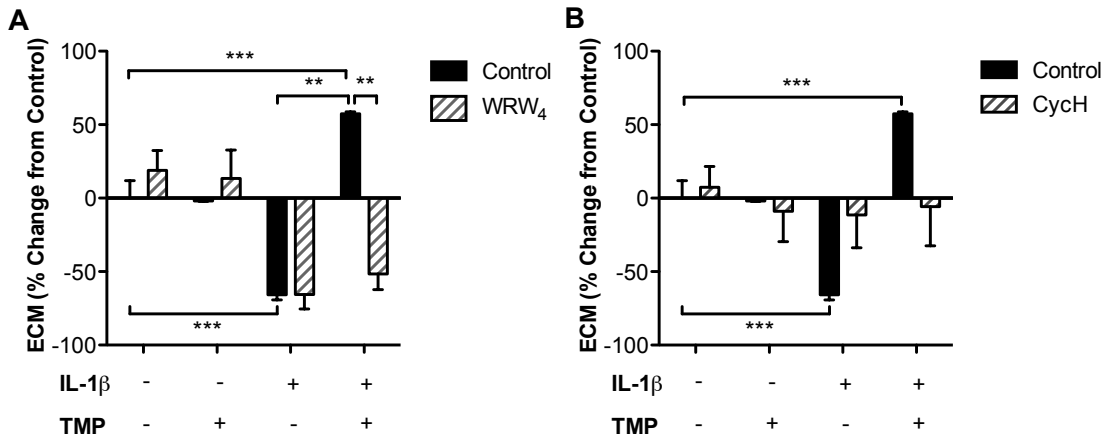

Figure 4.2.9 Antagonism of FPR2/ALX significantly inhibits microparticle induced extracellular matrix accumulation. Chondrocyte micromasses were treated with (A) an FPR2/ALX antagonist, WRW_4 (10μM) or (B) Cyclosporin H (CycH; 2.5μM), an FPR1 antagonist for 10 minutes followed by IL-1β (30ng/ml) and 100,000 TMP for 24 hours before extracellular matrix accumulation was quantified by Alcian blue staining. Data are shown as mean ± SEM of 4 microparticle donors. $^{**}P<0.01$ and $^{***}P<0.001$ using Two-way ANOVA and Bonferroni post-test. TMP, TNF-α-treatment generated microparticles; ECM, extracellular matrix.

It was therefore important to assess whether Annexin A1-induced matrix accumulation in unstimulated micromasses was receptor-dependent (Figure 4.2.10). The FPR2/ALX antagonist WRW_4 was able to partially reverse the ECM accumulation observed with Annexin A1 treatment, although this did not reach statistical significance (34.3 ± 21.9 vs. 91 ± 35.7%). Interestingly, in the case of Annexin A1 free protein (and not microparticle-associated), matrix accumulation was significantly inhibited upon FPR1 antagonism with cyclosporin H (2.0 ± 13.1 vs. 91 ± 35.7% $P<0.01$ with Two-way ANOVA and Bonferroni post-test.

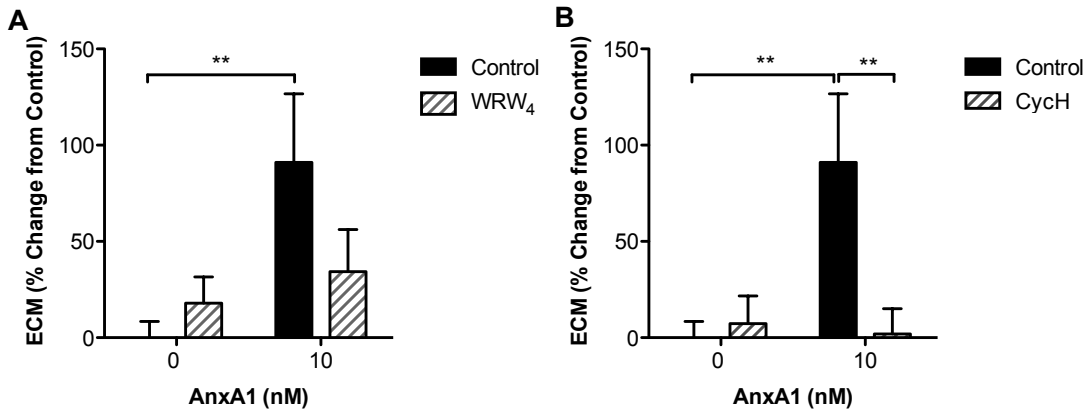

Figure 4.2.10 Annexin A1 induces extracellular matrix accumulation via FPR1 in unstimulated micromasses. Chondrocyte micromasses were treated with (A) WRW_4 (10μM) or (B) Cyclosporin H (CycH; 2.5μM) for 10 minutes followed by Annexin A1 (10nM) for 24 hours before extracellular matrix accumulation was quantified by Alcian blue staining. Data are shown as mean ± SEM of 5 separate micromass preparations. $^{**}P<0.01$ using Two-way ANOVA and Bonferroni post-test. AnxA1, Annexin A1; ECM, extracellular matrix.

Taken together, these results suggest that Annexin A1 in suspension acts upon chondrocytes to increase extracellular matrix accumulation via both FPR2/ALX and FPR1 and microparticle-associated Annexin A1 (plus other molecules) increase matrix accumulation via FPR2/ALX, but the contribution of FPR1 remains to be determined.

4.2.3 Endogenous Annexin A1 Expression by C28/I2 Chondrocytes

The expression of Annexin A1 and its physiological relevance in chondrocyte biology has not been reported. Therefore, the expression of Annexin A1 mRNA and protein were monitored in C28/I2 and primary adult human articular chondrocytes, and its cellular localisation was assessed by electron microscopy together with its receptor FPR2/ALX and orthologue, FPR1. C28/I2 chondrocytes express Annexin A1 gene products as confirmed by standard PCR and Western Blotting (Figure 4.2.11).

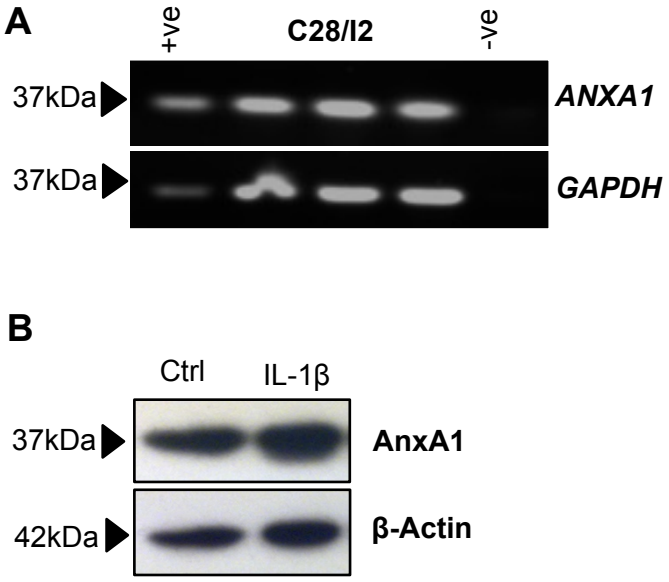

Figure 4.2.11 C28/I2 chondrocytes express *ANXA1* mRNA and Annexin A1 protein endogenously. (A) Chondrocytes micromasses were collected for mRNA extraction and standard PCR and gel electrophoresis. Gene expression was compared to neutrophil mRNA (positive control) and *GAPDH* as loading control. Negative control was molecular biology-grade water. Representative photograph of 3 separate micromass preparations. (B) Chondrocyte micromasses were treated with IL-1β (30ng/ml) for 24 hours before Western blotting for Annexin A1 protein. Representative blot shown, β-actin used as loading control. +ve, positive control; -ve, negative control; AnxA1, Annexin A1.

The subcellular location of Annexin A1 in C28/I2 and primary chondrocytes cultured in micromass was next interrogated by immunogold staining and transmission electron microscopy following IL-1β (30ng/ml) treatment for 24 hours. Annexin A1 expression was detected relatively uniformly, though sparsely, in both the nucleus and cytoplasm, and was also associated with electron-dense vesicles and mitochondria of C28/I2 cells (Figure 4.2.12). The distribution of Annexin A1 did not seem to be concentrated to the plasma membrane or nuclear envelope in either control or IL-1β stimulated cells in these micrographs.

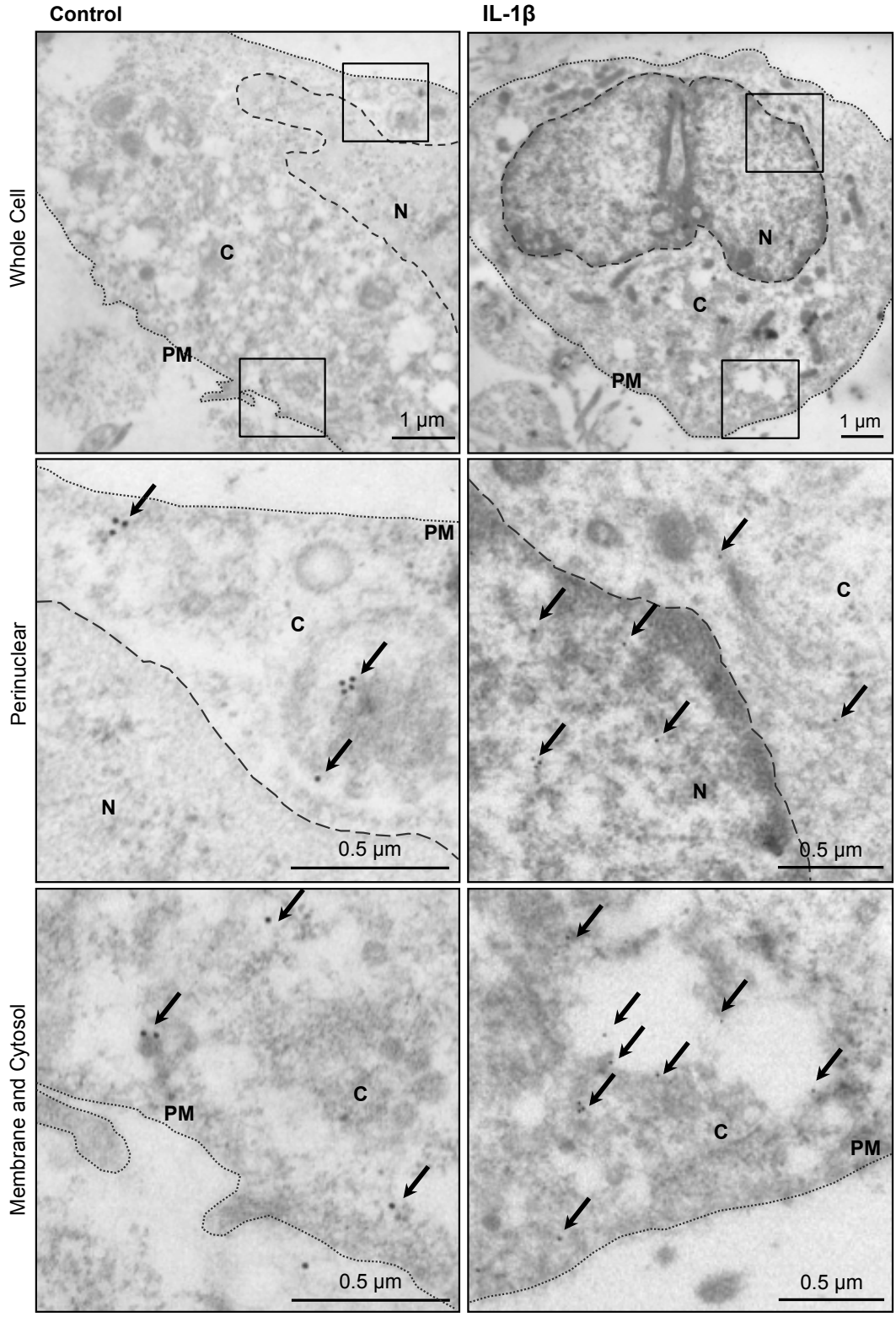

Figure 4.2.12 C28/I2 chondrocytes express Annexin A1 endogenously. C28/I2 chondrocytes cultured in micromass were treated with IL-1β (30ng/ml; right-hand panels) or vehicle (PBS, control; left-hand panels) for 24 hours before fixing for immunogold staining. Annexin A1 was labelled with antibodies conjugated to 20nm gold beads (arrows). Black boxes indicate panels magnified below. Dotted line indicates plasma membrane, dashed line indicates nuclear envelope. PM, plasma membrane; C, cytoplasm; N, nucleus. Scale bars as indicated. With special thanks to Professor Sonia Oliani and Dr Cristiane Damas Gil for electron microscopy and immunogold labelling.

FPR2/ALX expression was detectable in C28/I2 chondrocytes and co-localised with Annexin A1 in resting and IL-1β-stimulated cells (Figure 4.2.13 and Figure 4.2.15). In control cells, Annexin A1 and FPR2/ALX appeared more rarely in the nucleus as a pair than in the cytoplasm (Figure 4.2.13, left-hand panels). Conversely, upon IL-1β (30ng/ml) stimulation, Annexin A1 and FPR2/ALX clustered next to the nuclear envelope (Figure 4.2.13, right-hand middle panel; arrows and arrowheads), whereas FPR2/ALX is cytoplasmic (Figure 4.2.13, right-hand panels; arrowheads).

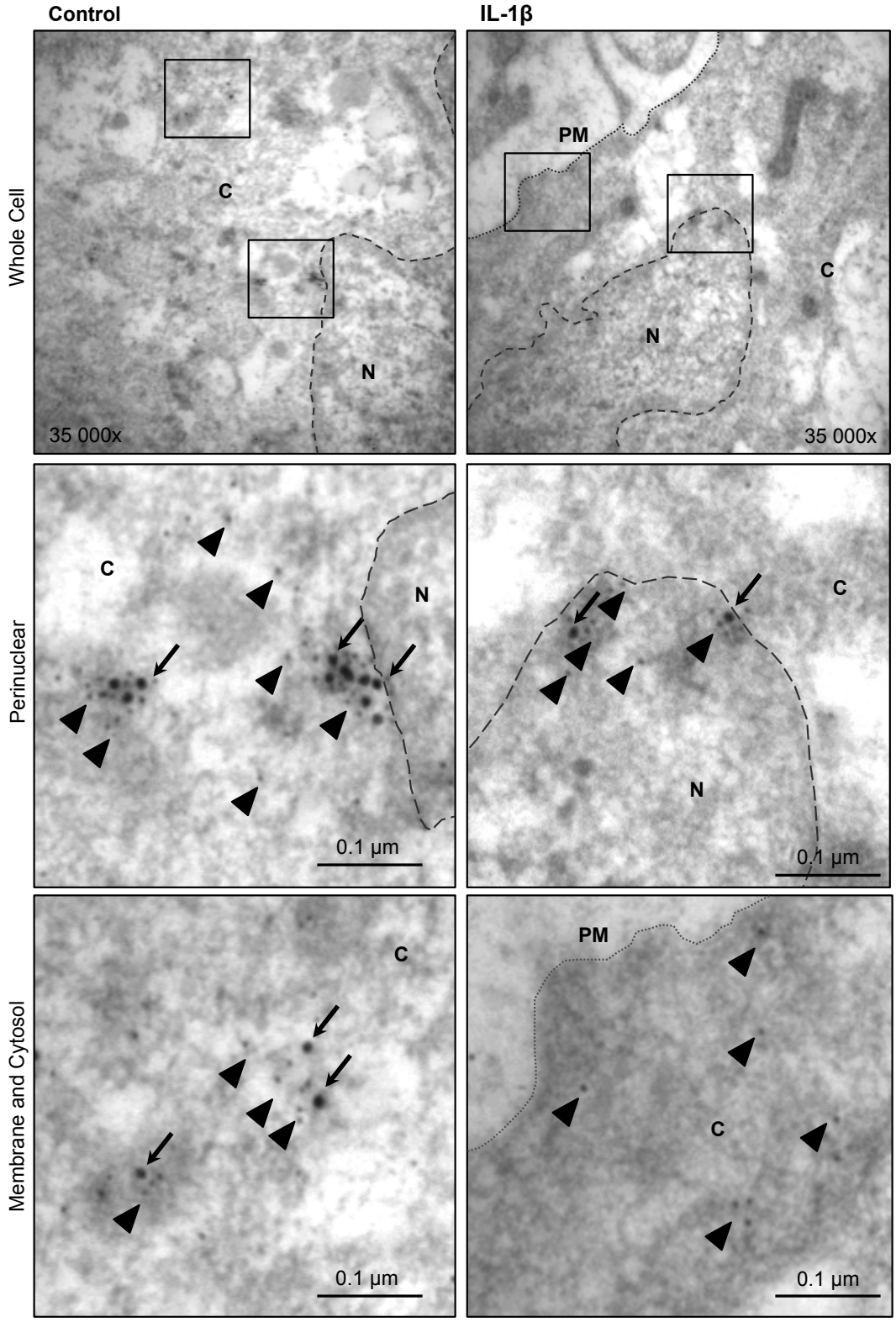

Figure 4.2.13. C28/I2 chondrocytes express Annexin A1 and FPR2/ALX. C28/I2 chondrocytes cultured in micromass were treated with IL-1β (30ng/ml; right-hand panels) or vehicle (PBS, control; left-hand panels) for 24 hours before fixing for immunogold staining. Annexin A1 was labelled with antibodies conjugated to 20nm gold beads (arrows); FPR2/ALX was labelled with antibodies conjugated to 10nm gold beads (arrow heads). Black boxes indicate panels magnified below. Dotted line indicates plasma membrane, dashed line indicates nuclear envelope. PM, plasma membrane; C, cytoplasm; N, nucleus. Scale bars as indicated. With special thanks to Professor Sonia Oliani and Dr Cristiane Damas Gil for electron microscopy and immunogold labelling.

In contrast to FPR2/ALX, FPR1 staining did not co-localise with Annexin A1 expression in either resting (left-hand panels) or IL-1β-stimulated cells (right-hand panels; Figure 4.2.14). FPR1 expression was diffuse and sparse throughout the cytoplasm and nucleus. Bottom right-hand panel shows an example of Annexin A1 expression associated with an electron-dense vesicle. These electron micrographs collectively indicate that Annexin A1 interacts with FPR2/ALX in the cytoplasm under resting conditions, which then translocates to the nucleus upon IL-1β stimulation. Endogenous Annexin A1 does not appear to co-localise with FPR1 under resting conditions or upon stimulation.

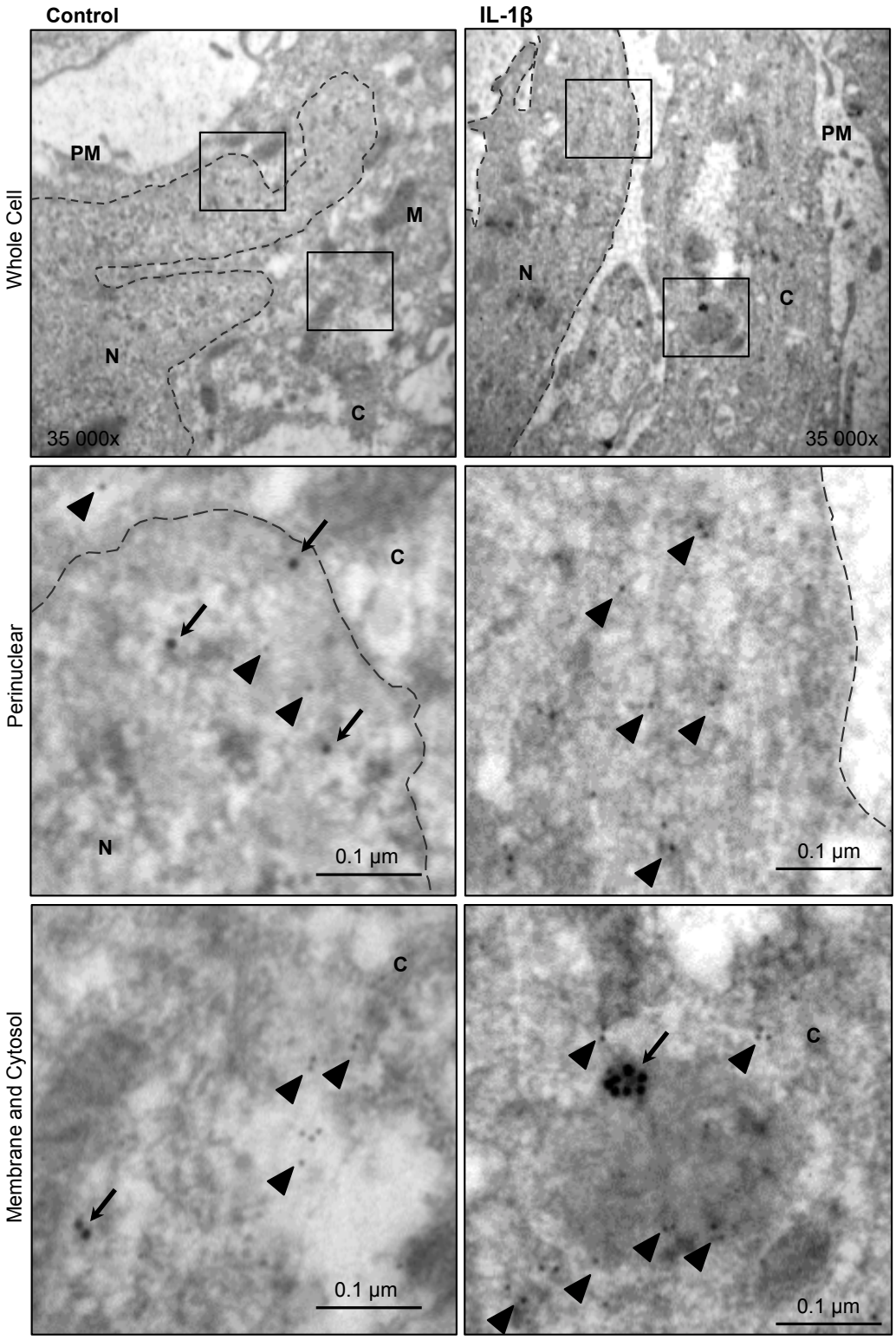

Figure 4.2.14 C28/I2 chondrocytes express Annexin A1 and FPR1 endogenously, but they do not co-localise. C28/I2 chondrocytes cultured in micromass were treated with IL-1β (30ng/ml; right-hand panels) or vehicle (PBS, control; left-hand panels) for 24 hours before fixing for immunogold staining. Annexin A1 was labelled with antibodies conjugated to 20nm gold beads (arrows); FPR1 was labelled with antibodies conjugated to 10nm gold beads (arrow heads). Black boxes indicate panels magnified below. Dotted line indicates plasma membrane, dashed line indicates nuclear envelope. PM, plasma membrane; C, cytoplasm; N, nucleus; M, mitochondrion. Scale bars as indicated. With special thanks to Professor Sonia Oliani and Dr Cristiane Damas Gil for electron microscopy and immunogold labelling.

Annexin A1 and FPR2/ALX were also detected in primary adult human articular chondrocytes cultured in micromasses (Figure 4.2.15). Annexin A1 and FPR2/ALX appear in close proximity within the cell, localised mainly within the cytoplasm.

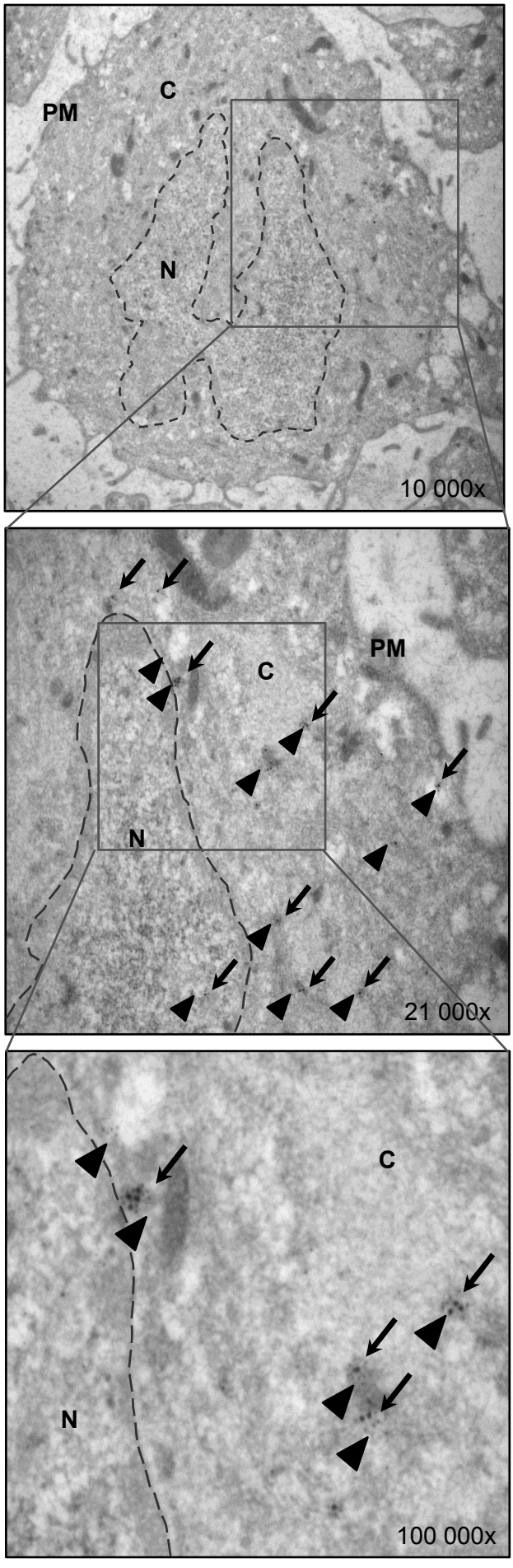

Figure 4.2.15 FPR2/ALX and Annexin A1 are found in close proximity within primary adult human articular chondrocytes. Primary human chondrocytes were fixed for immunogold staining. Annexin A1 was labelled with 20nm gold beads (arrows); FPR2/ALX was labelled with 10nm gold beads (arrow heads). Grey boxes represent areas magnified to the right, dotted line represents nuclear envelope. N, nucleus; C, cytoplasm; PM, plasma membrane. With special thanks to Professor Sonia Oliani and Dr Cristiane Damas Gil who performed transmission electron microscopy and immunogold labelling.

These data demonstrate the presence of Annexin A1, and its receptor, FPR2/ALX in human primary and C28/I2 chondrocytes, along with the orthologue receptor FPR1. Importantly, Annexin A1 and FPR2/ALX co-localisation indicate that this pair interacts under resting condition and with IL-1β-stimulation.

4.2.4 Is Ceruloplasmin Responsible for the Chondroprotection Observed with Microparticle Treatment? Characterisation of the Effect of Exogenous Ceruloplasmin in Chondrocyte Biology

Experiments performed using recombinant Annexin A1 indicated that Annexin A1 does not solely account for the chondroprotective functions of microparticles. Furthermore, Annexin A1 null microparticles still exert anti-catabolic effects on chondrocyte micromass matrix accumulation, reversing the effects of IL-1β at a concentration of 30ng/ml. Thus, a second protein identified during previous proteomic analysis, namely ceruloplasmin, a plasma copper-transporting enzyme with putative anti-inflammatory functions was investigated.

Exogenous addition of ceruloplasmin to micromass cultures exerted similar effects to those observed with Annexin A1 (Figure 4.2.16). Unlike microparticles, ceruloplasmin treatment alone significantly increased matrix accumulation in unstimulated micromasses at concentrations of 1nM (49.7 ± 9 vs. 0 ± 3.5% P<0.001 with Two-way ANOVA and Bonferroni post-test) and 30nM (61.0 ± 14.6 vs. 0 ± 3.5% P<0.001 with Two-way ANOVA and Bonferroni post-test). In micromasses stimulated with IL-1β (3ng/ml), ceruloplasmin treatment induced matrix accumulation with a similar concentration response as that seen with Annexin A1, where lower concentrations of ceruloplasmin induce significantly higher matrix accumulation compared to higher concentrations. In this case, only 1nM (74.9 ± 16.5 vs. -23.8 ± 3.3% P<0.001 with Two-way ANOVA and Bonferroni post-test) and 10nM (21.2 ± 9.6 vs. -23.8 ± 3.3% P<0.001 with Two-way ANOVA and Bonferroni post-test) ceruloplasmin concentrations induced higher matrix accumulation than IL-1β 3ng/ml alone. Again, similarly to Annexin A1, ceruloplasmin treatment at all concentrations in micromasses stimulated with IL-1β (30ng/ml) significantly increased matrix accumulation compared to IL-1β (30ng/ml) treatment alone (1nM -1.9 ± 13, 10nM -11.9 ± 10.7, 30nM 34 ± 14 vs. -67.3 ± 2.4% P<0.001 with Two-way ANOVA and Bonferroni post-test).

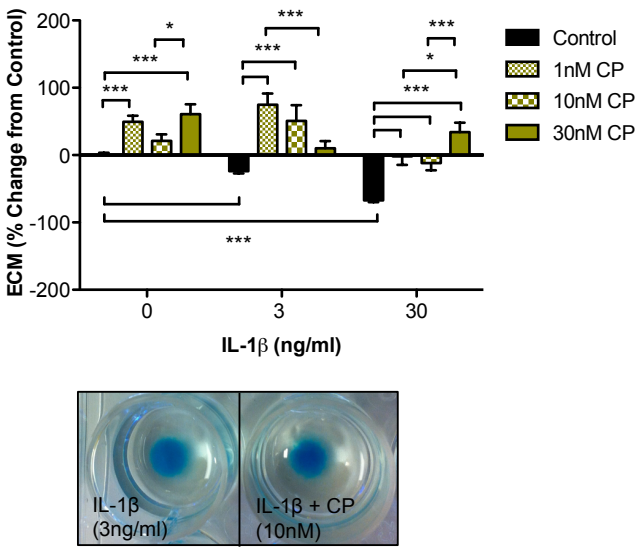

Figure 4.2.16 Ceruloplasmin increases chondrocyte extracellular matrix accumulation in vitro. Chondrocyte micromasses were treated with IL-1β (3 or 30ng/ml) and increasing concentrations of ceruloplasmin (CP) for 24 hours before extracellular matrix accumulation was quantified by Alcian blue staining. Bottom are representative photographs of micromasses before dye extraction. Data are shown as mean ± SEM of 6 separate micromass preparations. **P*<0.05 and ****P*<0.001 using Two-way ANOVA and Bonferroni post-test. ECM, extracellular matrix.

Ceruloplasmin treatment of IL-1β stimulated chondrocyte micromasses did not reverse the down-regulation of *ACAN* (1nM 0.8 IQR 0.5-0.9 or 10nM 0.5 IQR 0.5-0.7 vs. 0.4 IQR 0.3-0.5) or *COL2A1* (1nM 0.8 IQR 0.6-0.9 or 10nM 0.6 IQR 0.5-0.6 vs. 0.4 IQR 0.3-0.5) mRNA induced by IL-1β stimulation (Figure 4.2.17). However, significant IL-1β-induced MMP13 mRNA up-regulation (10 IQR 8.7-13.6 vs. 1 IQR 1-1.1; *P*<0.05 with Kruskal-Wallis test and Dunn's multiple comparison post-test) was counter-regulated by ceruloplasmin treatment (1nM 0.7 IQR 0.4-1 vs. 10 IQR 8.7-13.6 *P*<0.05 and 10nM 0.7 IQR 0.5-0.8 vs. 10 IQR 8.7-13.6; *P*<0.01 with Kruskal-Wallis test and Dunn's multiple comparison post-test). *ADAMTS5* gene expression was not significantly altered by IL-1β treatment (0.8 IQR 0.5-2.8 vs. 1 IQR 0.8-1) or ceruloplasmin treatment (1nM 0.9 IQR 0.7-1 or 10nM 0.7 IQR 0.5-0.9 vs. 0.8 IQR 0.5-2.8).

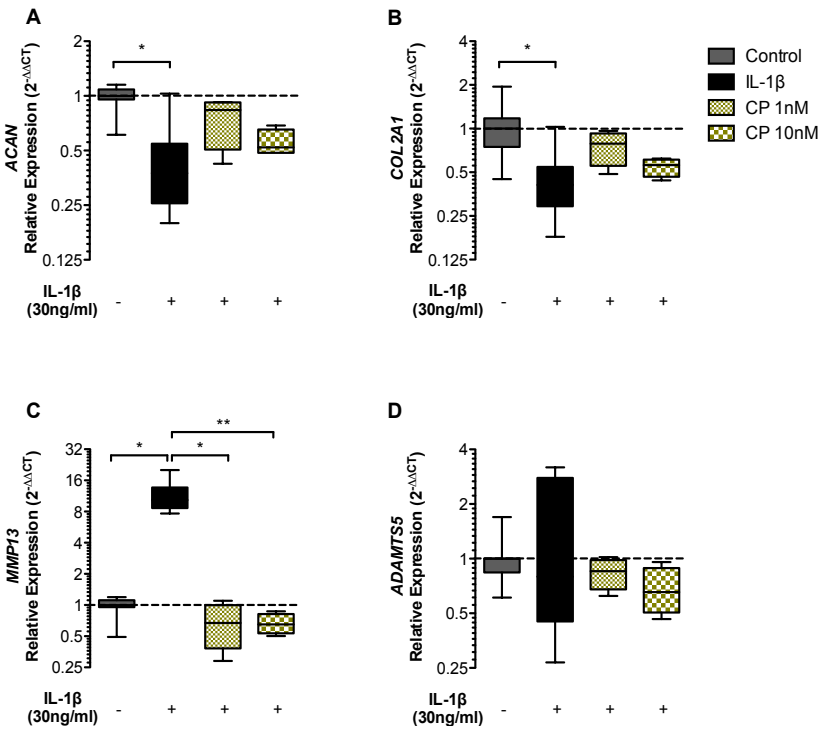

Figure 4.2.17 Ceruloplasmin counter-regulates *MMP13* induction by IL-1β but does not reverse the down regulation of cartilage matrix-producing gene mRNA. Chondrocyte micromasses were treated with IL-1β (30ng/ml) and increasing concentrations of ceruloplasmin (CP) for 6 hours before mRNA extraction and RT-PCR. (A) Relative expression of *ACAN,* (B) *COL2A1*, (C) *MMP13* and (D) *ADAMTS5.* Data shown are $2^{-\Delta\Delta CT}$ with untreated as calibrator and *RPL32* as housekeeping gene. Data expressed as median, interquartile range and range of 4 separate micromass preparations. **P*<0.05 and **P<0.01 using Kruskal-Wallis test and Dunn's multiple comparison post-test.

Ceruloplasmin did not significantly induce IL-8 production in resting chondrocyte micromasses (1nM 1.8 ± 0, 10nM 1.8 ± 0 and 30nM 1.7 ± 0 vs. 0.6 ± 0ng/ml), nor alter the production levels of IL-8 in chondrocyte micromasses stimulated with IL-1β (30ng/ml) (1nM 8.8 ± 0, 10nM 9.7 ± 0.8 and 30nM 9.6 ± 1.2 vs. 9.6 ± 0.1ng/ml; Figure 4.2.18).

Figure 4.2.18 Ceruloplasmin does not inhibit chondrocyte IL-8 production induced by IL-1β. Chondrocyte micromasses were treated with IL-1β (30ng/ml) and increasing concentrations of ceruloplasmin (CP) for 24 hours before IL-8 production was quantified by ELISA. Data are shown as mean ± SEM of 3 separate micromass preparations, ***P<0.001 with Two-way ANOVA and Bonferroni post-test.

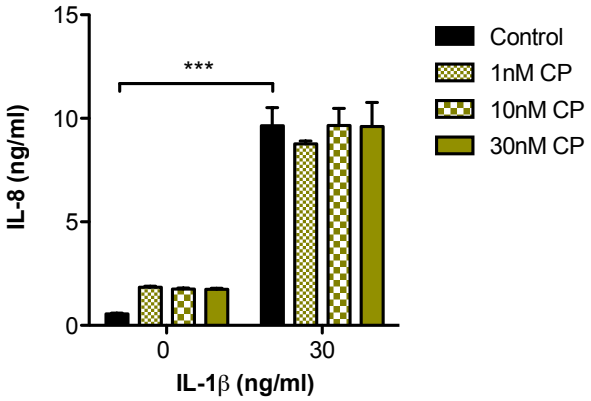

In contrast, although ceruloplasmin did not alter prostaglandin E_2 production in resting chondrocyte micromasses (1nM 171.6 ± 19.3, 10nM 123.9 ± 14.9 and 30nM 138.4 ± 7.5 vs. 122.5 ± 24.2ng/ml), prostaglandin E_2 levels were significantly increased at 1nM ceruloplasmin treatment in IL-1β stimulated micromasses compared with IL-1β (30ng/ml) (1027 ± 182.1 vs. 746.5 ± 51.8ng/ml P<0.05 with Two-way ANOVA and Bonferroni post-test; Figure 4.2.19). Comparatively, Ceruloplasmin (30nM) treatment partially reduced (25%) IL-1β-induced prostaglandin E_2 levels (552.7 ± 81.1 vs. 746.5 ± 51.8ng/ml P<0.05 with Two-way ANOVA and Bonferroni post-test). These effects were modest compared to the 75% reduction seen with microparticle treatment (Figure 4.1.14).

Figure 4.2.19 Ceruloplasmin enhances IL-1β-induced chondrocyte Prostaglandin E_2 biosynthesis at lower concentrations, but suppresses it at higher concentrations. Chondrocyte micromasses were treated with IL-1β (30ng/ml) and increasing concentrations of ceruloplasmin (CP) for 24 hours before supernatant Prostaglandin E_2 (PGE_2) generation was quantified by EIA. Data are shown as mean ± SEM of 3 separate micromass preparations. **P*<0.05 and ***P<0.001 using Two-way ANOVA and Bonferroni post-test.

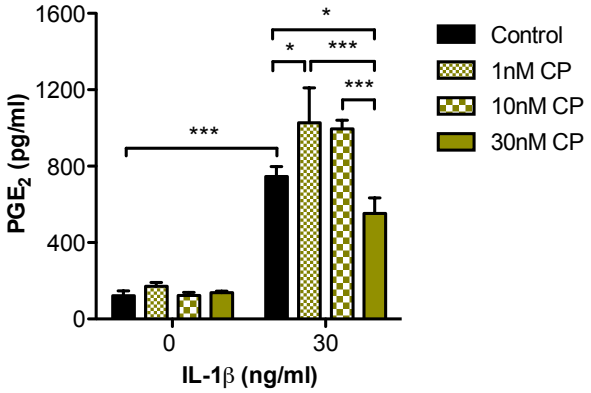

Finally, the effect of lactoferrin was also explored in extracellular matrix accumulation in chondrocytes. Previous reports have suggested both an anti-inflammatory role in arthritis (Guillen et al., 2000) and a pro-proliferative role for lactoferrin in primary human chondrocytes, whose receptor is LRP-1 (Brandl et al., 2010). In C28/I2 micromasses however, lactoferrin did not modulate extracellular matrix accumulation in resting (-1.6 ± 2 vs. -13.1%) or IL-1β-stimulated micromasses (-23 ± 6 vs. -37.5 ± 8.4%) nor increase the DNA content of resting (271.9 ± 20.2 vs. 224.4 ± 18.5μg/micromass) or stimulated micromasses (222.3 ± 22.3 vs. 206.7 ± 30μg/micromass), a crude measure of cell number (Figure 4.2.20).

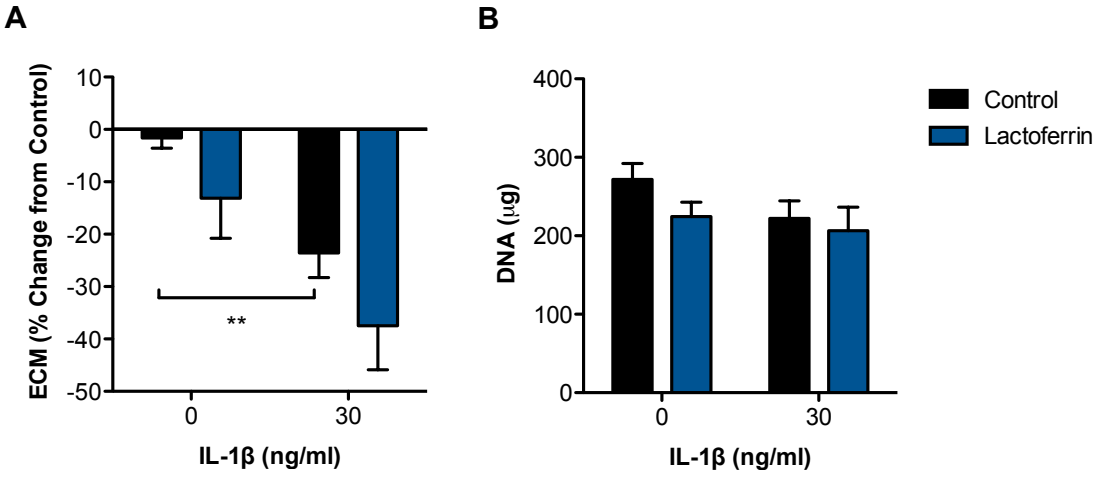

Figure 4.2.20 Lactoferrin does not modulate extracellular matrix accumulation in vitro, or induce cellular proliferation. Chondrocyte micromasses were treated with IL-1β (30ng/ml) and Lactoferrin (10μg/ml) for 24 hours before (A) extracellular matrix accumulation was quantified by Alcian blue staining and (B) DNA was quantified using SYBRGreen I dye. Data are shown as mean ± SEM of 4 separate micromass preparations. ***P*<0.01 using Two-way ANOVA and Bonferroni post-test. ECM, extracellular matrix.

Taken together, these results suggest that ceruloplasmin may contribute to the matrix accumulation seen during microparticle co-culture, but that ceruloplasmin has little, if any, capacity to reduce pro-inflammatory mediators produced by chondrocytes during IL-1β stimulation. Interestingly, ceruloplasmin did dramatically inhibit the transcription of MMP13 by the chondrocytes stimulated with IL-1β, but without the use of ceruloplasmin null mice to corroborate this data, the full role of this protein will remain unclear. Lactoferrin, a putative anti-oxidant with pro-proliferative properties did not alter chondrocytes matrix accumulation or proliferation, suggesting little contribution of this protein to chondroprotection *in vitro*.

4.2.5 Pro-Resolving Lipid Mediators

Microparticles are known to be vectors for not only functional protein cargo, but also are also highly involved in bioactive lipid transfer as their main constituents are the plasma membrane and its derivatives. Pro-resolving lipid mediators, for example Resolvin D1, are also highly involved in the resolution of inflammation and could therefore have important bearings on the anti-inflammatory properties. Neutrophil-derived microparticles contain the precursors of pro-resolving lipid mediators (Norling et al., 2011), which, when delivered to cells, can be utilised to generate protective lipid mediators such as Resolvin D1 (Dalli and Serhan, 2012). Therefore the actions of Resolvin D1 were assessed in C28/I2 chondrocyte micromasses (Figure 4.2.21).

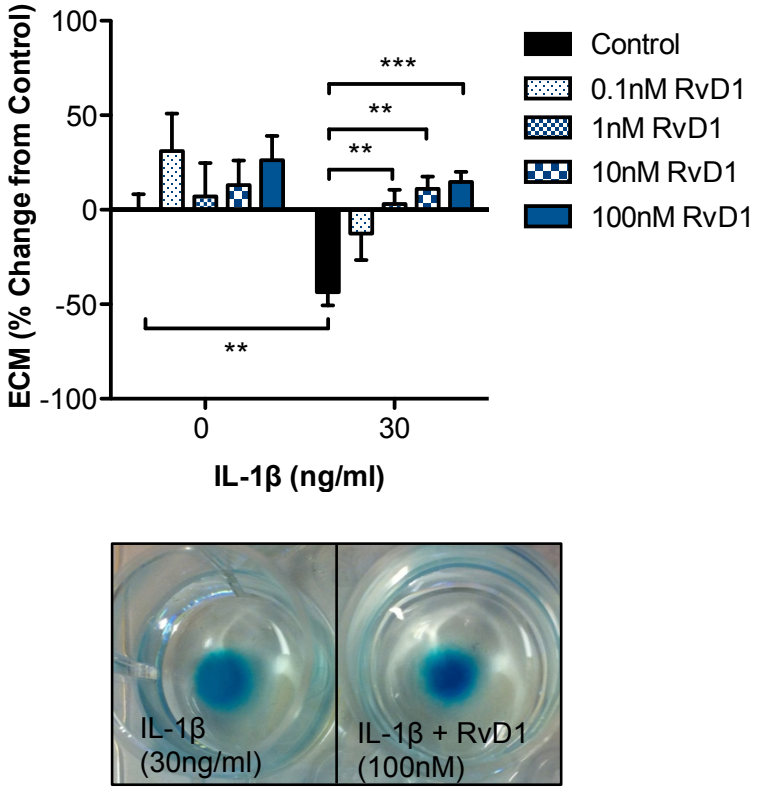

Figure 4.2.21 Pro-resolving lipid mediator Resolvin D1 increases extracellular matrix accumulation in vitro. Chondrocyte micromasses were treated with IL-1β (30ng/ml) and increasing concentrations of Resolvin D1 (RvD1) for 24 hours before extracellular matrix accumulation was quantified by Alcian blue staining. Bottom are representative photographs of micromasses before dye extraction. Data are shown as mean ± SEM of 6 separate micromass preparations. $^{**}P<0.01$ and $^{***}P<0.001$ using Two-way ANOVA and Bonferroni post-test. ECM, extracellular matrix.

Resolvin D1 did not modulate matrix accumulation in resting chondrocyte micromasses compared to control (0.1nM 31 ± 19.8, 1nM 7.2 ± 17.6, 10nM 13.1 ± 13, 100nM 26.3 ± 12.8 vs. 0 ± 8.3%). However, in micromasses stimulated with IL-1β (30ng/ml), Resolvin D1 at concentrations of 1nM (3.1 ± 7.5 vs. -43.6 ± 7% $P<0.01$ with Two-way ANOVA and Bonferroni post-test), 10nM (11.1 ± 6.5 vs. -43.6 ± 7% $P<0.01$ with Two-way ANOVA and Bonferroni post-test) and 100nM (14.8 ± 5.3 vs. -43.6 ± 7% $P<0.001$ with Two-way ANOVA and Bonferroni post-test) was able to counter-regulate IL-1β-induced reduction in matrix accumulation.

As FPR2/ALX is a high-affinity receptor for Resolvin D1 (Krishnamoorthy et al., 2010), the receptor dependence was tested using the FPR2/ALX-specific antagonist, WRW_4. As before, treatment with WRW_4 had no adverse effect on matrix accumulation in unstimulated micromasses yet pre-treatment prior to Resolvin D1 addition to IL-1β-stimulated micromasses blocked the matrix-accumulating effects observed with Resolvin D1 (-19.1 ± 2.2 vs. 35.8 ± 9% $P<0.001$ with Two-way ANOVA and Bonferroni post-test; Figure 4.2.22). As Annexin A1 knockout microparticles still exhibited anti-catabolic effects in IL-1β-stimulated micromasses, whereas FPR2/ALX pharmacological inhibition completely blocked microparticle-induced matrix accumulation, the current data suggests that Resolvin D1 bioactive lipid mediator, as well as Annexin A1 pro-resolving protein might both contribute to the accumulation of matrix induced by microparticle treatment.

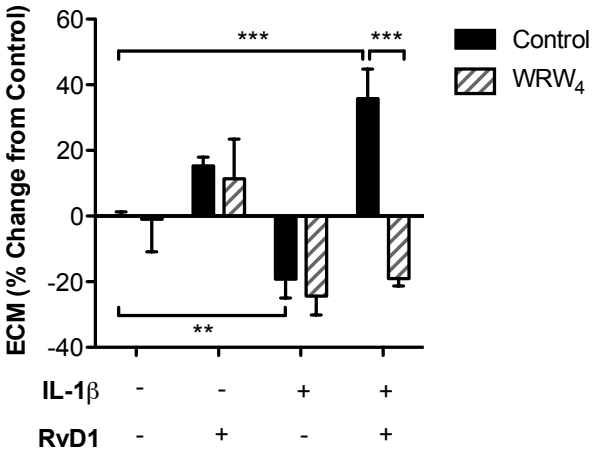

Figure 4.2.22 Antagonism of FPR2/ALX reverses Resolvin D1 induced extracellular matrix accumulation. Chondrocyte micromasses were treated with 10μM WRW_4 (10μM) for 10 minutes followed by IL-1β (30ng/ml) and Resolvin D1 (RvD1; 10nM) for 24 hours before extracellular matrix accumulation was quantified by Alcian blue staining. Data are shown as mean ± SEM of 4 micromass preparations. $**P<0.01$ and $***P<0.001$ using Two-way ANOVA and Bonferroni post-test. ECM, extracellular matrix.

4.3 Chondroprotective Circuits Initiated by Microparticles

As some of the effects noted during microparticle co-culture seemed to be Annexin A1-mediated, it was next determined whether these effects were due to receptor ligation of FPR2/ALX on the surface of the chondrocyte. The downstream signalling pathways that follow FPR2/ALX ligation in immune cells is beginning to emerge (Cooray et al., 2013, Bena et al., 2012b, Renshaw et al., 2010, Pupjalis et al., 2011), yet have never been explored in chondrocytes. Furthermore, the signalling induced by microparticle treatment, which results in extracellular matrix accumulation with IL-1β (or TNF-α) stimulated micromasses, is also unknown.

4.3.1 Modulation of Signalling Molecule Phosphorylation by Microparticle and Annexin A1 Treatment

As the signalling events surrounding microparticle treatment in chondrocytes has not been reported, a range of inflammatory signalling pathways were profiled for their phosphorylation status following IL-1β stimulation, microparticle treatment and, as a comparison, Annexin A1 treatment. Monolayer, rather than micromasses were used as the timing of the phosphorylation profiles of signalling molecules are key to elucidating their mechanism, and diffusion through multiple layers of cells combined with generated matrix could not be controlled for temporally.

Firstly, p38 phosphorylation was investigated in C28/I2 chondrocytes seeded in monolayer and stimulated with IL-1β with or without microparticles (Figure 4.3.1). The activation of p38 regulates pro-inflammatory cytokine production and downstream targets of this signalling molecule, among many, are enzymes such as MMP13 and COX-2. Relevantly, MMP13 and the COX-2 product Prostaglandin E_2 were both reduced upon microparticle treatment. The phosphorylation of p38 was not altered above baseline by microparticle treatment alone in resting chondrocytes (0.07 ± 0 vs. 0.05 ± 0) or by Annexin A1 treatment (-0.24 ± 0.3 vs. 0.05 ± 0; used as a negative control as it did not induce reductions in prostaglandin E_2 production) at 1 hour. IL-1β stimulation induced p38 phosphorylation at one hour as expected (0.55 ± 0.1 vs. 0.05 ± 0 (Lin et al., 2008)).

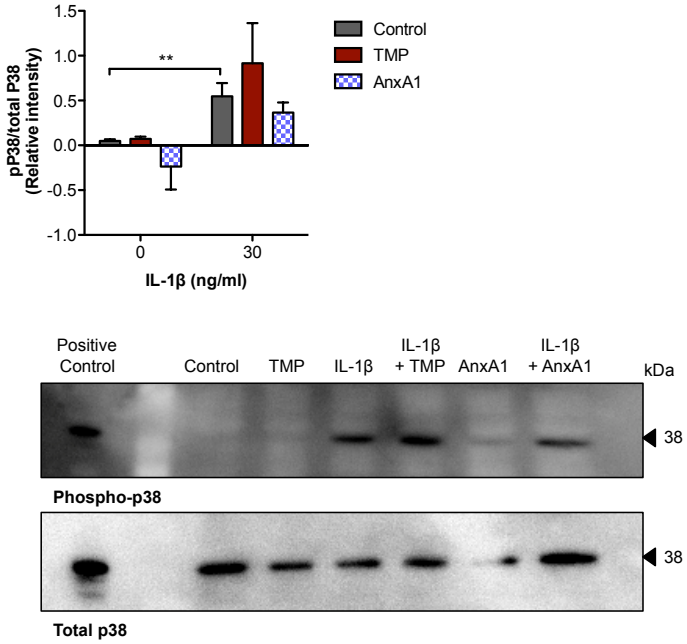

Figure 4.3.1 Microparticles do not modulate chondrocyte p38 phosphorylation induced by IL-1β at one hour. C28/I2 chondrocytes in monolayer were treated with IL-1β (30ng/ml) and 100,000 TMP or Annexin A1 (10nM) for 1 hour before blotting for phospho-p38 and total p38 protein. Positive control is human neutrophils stimulated for 10 minutes with TNF-α. Data are shown as mean ± SEM of 4 separate microparticle donors and blots and expressed as relative intensity after normalisation to total p38. $^{**}P<0.01$ with Two-way ANOVA and Bonferroni post-test. TMP, TNF-α-treatment generated microparticles.

Concomitant treatment with microparticles slightly increased the phosphorylation of p38 above IL-1β alone (0.92 ± 0.4 vs. 0.55 ± 0.1), whereas Annexin A1 caused a slight reduction (0.37 ± 0.1 vs. 0.55 ± 0.1). As microparticle treatment did not have a striking effect at one hour, a time course of p38 phosphorylation was carried out to determine whether microparticles temporally modulated p38 phosphorylation or alternatively modulated the duration of the IL-1β signal.

Under basal resting conditions, no phosphorylation of p38 was observed in C28/I2 chondrocyte monolayers and this was not modulated upon co-administration of 100,000 TMP across any of the time points tested (Figure 4.3.2). In contrast, IL-1β induced phosphorylation of p38 by 30 minutes, which peaked at 1 hour and reduced down to baseline at 4 hours. The bands obtained from microparticle-treated IL-1β stimulated chondrocytes showed a less intense signal than IL-1β alone at 30 minutes, but at 1 hour both the microparticle and IL-1β signal were roughly similar. By 2 hours, microparticle treatment induced greater phosphorylation than IL-1β alone, but returned to baseline by 4 hours. This delay in phosphorylation of p38 is interesting, but its relevance requires further investigation.

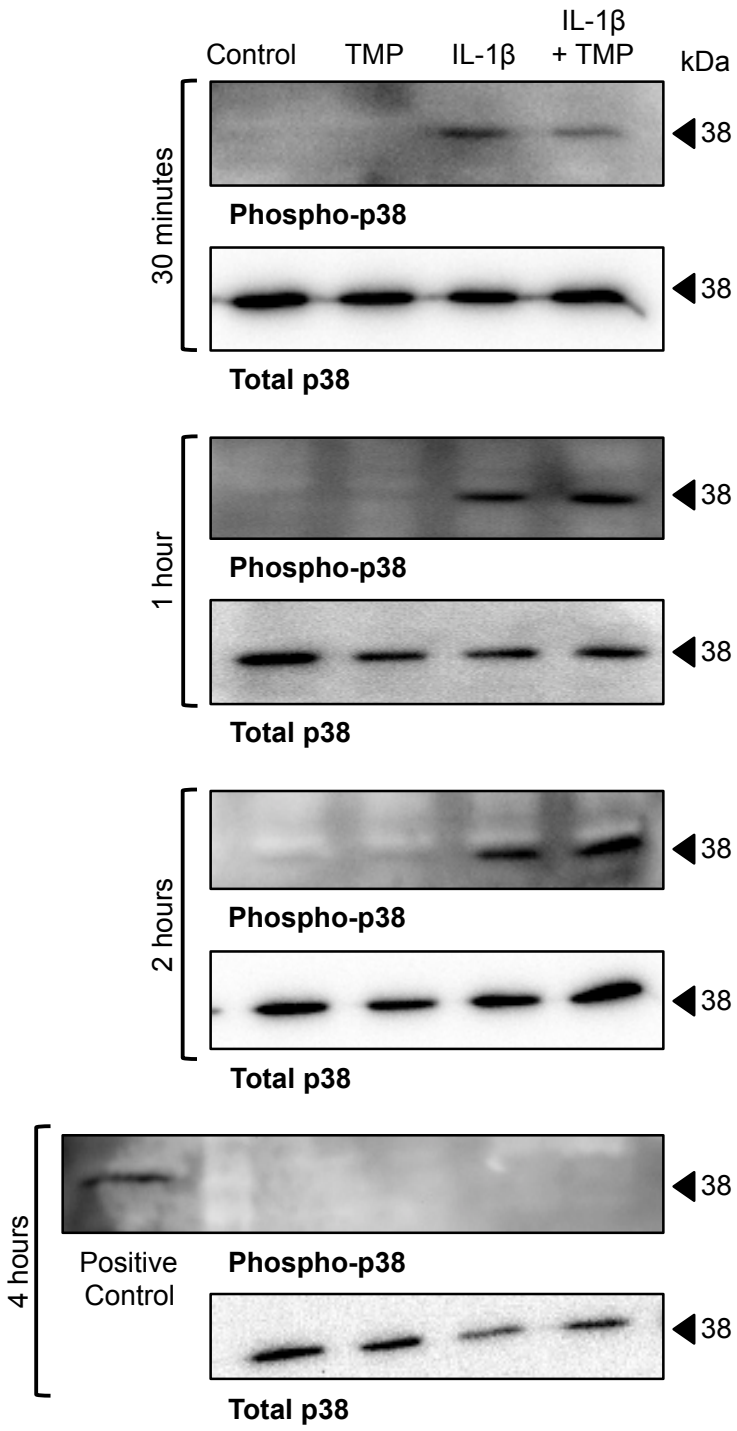

Figure 4.3.2 Microparticles do not significantly modulate p38 phosphorylation in IL-1β-stimulated micromasses. C28/I2 chondrocytes in monolayer were treated with IL-1β (30ng/ml) and 100,000 TMP or Annexin A1 (10nM) before blotting for phospho-p38 protein. Data are shown are examples of 4 separate microparticle donors and blots. Negative expression at 4 hours shows positive control (10 minute, TNF-α-stimulated neutrophils) for validation.

Downstream of p38 phosphorylation is MAPKAPK2, which modulates the translation of pro-inflammatory mRNA via stabilisation. Phosphorylation of MAPKAPK2 is maximal at 30 minutes following IL-1β stimulation (Jones et al., 2009), thus this time point was selected. Phosphorylation of MAPKAPK2 was not observed under basal conditions, but was significantly up-regulated by IL-1β as expected (1 ± 0.4 vs. -0.1 ± 0.1, $P<0.001$ with Two-way ANOVA and Bonferroni post-test). At 30 minutes, phosphorylation of MAPKAPK2 was not altered by treatment with microparticles in either unstimulated (0.1 ± 0 vs. -0.1 ± 0.1) or IL-1β-stimulated chondrocytes (0.8 ± 0.3 vs. 1 ± 0.4; Figure 4.3.3).

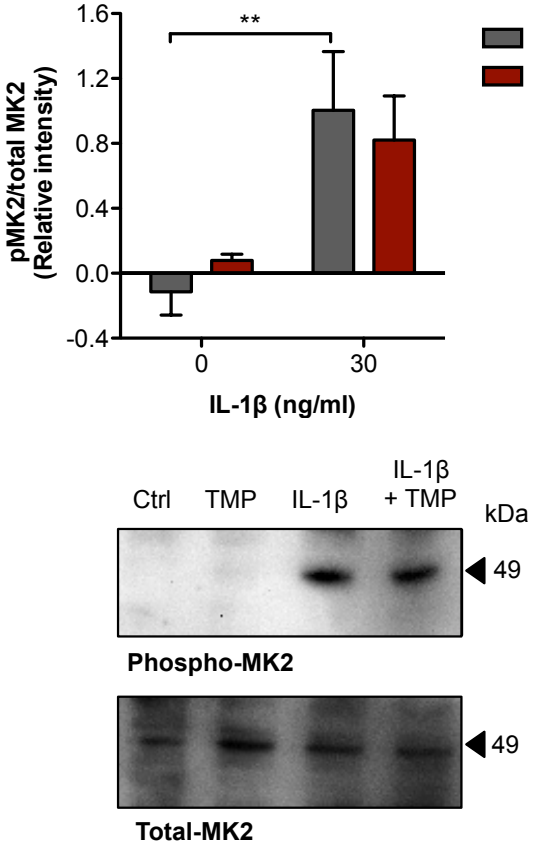

Figure 4.3.3 Microparticles do not modulate chondrocyte MAPKAPK2 phosphorylation induced by IL-1β. C28/I2 chondrocytes in monolayer were treated with IL-1β (30ng/ml) and 100,000 TMP for 30 minutes before blotting for phospho-MAPKAPK2 (MK2) protein. Data are shown as mean ± SEM of 4 separate microparticle donors and blots and expressed as relative intensity after normalisation to total MK2. $**P<0.01$ with Two-way ANOVA and Bonferroni post-test. TMP, TNF-α generated microparticles.

As prostaglandin E_2, IL-6 and IL-8 synthesis was affected by microparticle addition, a further downstream target of p38 and MAPKAPK2, phosphorylation of heat-shock protein (Hsp) 27 was investigated (Figure 4.3.4). Surprisingly, phosphorylation of Hsp27 was completely inhibited at 10 minutes by microparticle co-administration with IL-1β (0.08 ± 0 vs. 0.4 ± 0.1 P<0.001 with Two-way ANOVA and Bonferroni post-test). Unphosphorylated Hsp27 exists as large oligomeric structures, and upon phosphorylation is released to form dimers. These dimers stabilise the mRNA of target genes such as *COX2*, *TNFA1*, *IL6* and *IL8* (Lasa et al., 2000). Thus, microparticles may act directly at this step in the p38 MAPK pathway to prevent Hsp27 phosphorylation directly and prevent its release from its oligomeric homopolymer, allowing the degradation of the unstable mRNAs encoding IL-8, IL-6 and COX-2. This would account for the reduction of these cytokines and prostaglandin E_2 in the supernatants of chondrocyte micromasses stimulated with IL-1β and treated with microparticles.

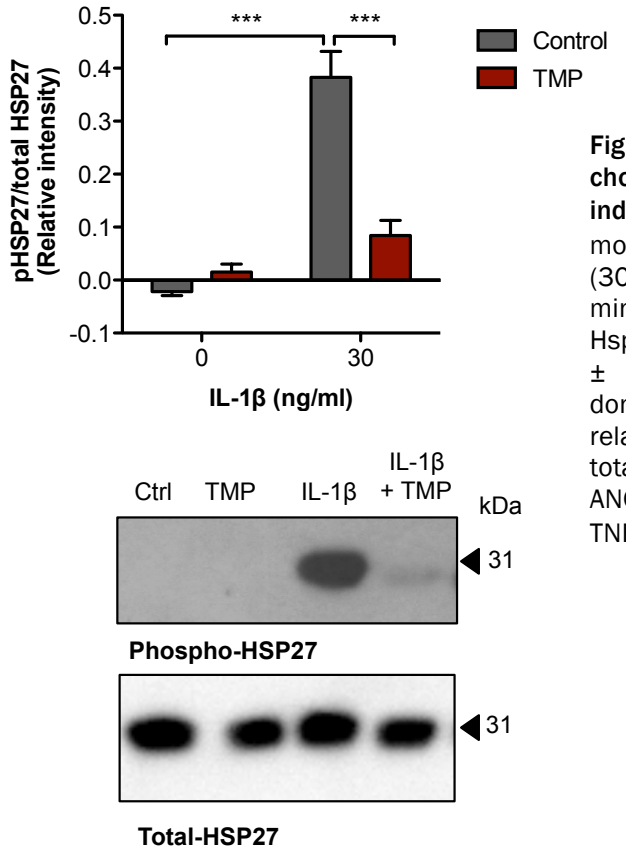

Figure 4.3.4 Microparticles reduce chondrocyte Hsp27 phosphorylation induced by IL-1β. C28/I2 chondrocytes in monolayer were treated with IL-1β (30ng/ml) and 100,000 TMP for 10 minutes before blotting for phospho-Hsp27 protein. Data are shown as mean ± SEM of 4 separate microparticle donors and blots and expressed as relative intensity after normalisation to total Hsp27, ***P<0.001 with Two-way ANOVA and Bonferroni post-test. TMP, TNF-α generated microparticles.

Other signalling pathways are also initiated downstream of IL-1β in chondrocytes (Lin et al., 2008). Indeed, phosphorylation of c-Jun N-terminal kinase (JNK) regulates cytokine production and matrix metalloproteinase expression in chondrocytes (Beier and Loeser, 2010). Intriguingly, IL-1β-induced MMP13 expression requires phosphorylation of both p38 and JNK; whereas inhibition of MMP13 requires blockade of only one of these signalling pathways. Microparticle treatment inhibited JNK phosphorylation in both resting (0.1 ± 0 vs. 0.2 ± 0.1) and IL-1β (30ng/ml) stimulated C28/I2 chondrocytes (0.3 ± 0.1 vs. 0.2 ± 0.1; Figure 4.3.5). This could account for the microparticle-induced down-regulation of proteoglycan cleavage and release into the medium seen by DMMB dye-binding assay.

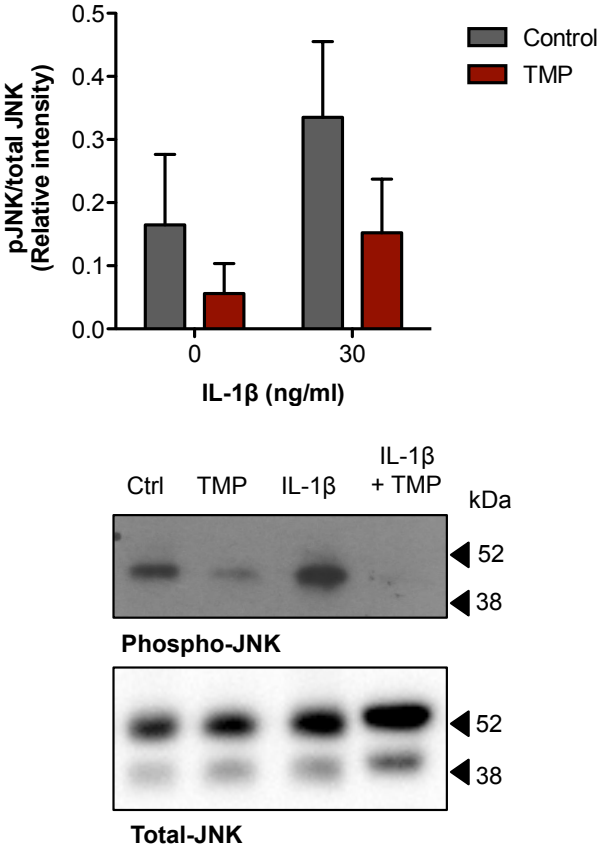

Figure 4.3.5 Microparticles reduce chondrocyte JNK phosphorylation induced by IL-1β. C28/I2 chondrocytes in monolayer were treated with IL-1β (30ng/ml) and 100,000 TMP for 10 minutes before blotting for phospho-JNK protein. Data are shown as mean ± SEM of 4 separate microparticle donors and blots and expressed as relative intensity after normalisation to total JNK, not significant with Two-way ANOVA and Bonferroni post-test. TMP, TNF-α generated microparticles.

Akt phosphorylation in cartilage is associated with the regulation of mRNA translation and protein synthesis via the activation of mammalian Target of Rapamycin (mTOR) and factors such as p70S6K, and 4E-BP-1 (eIF-4E-binding protein) (Yin et al., 2009). 10-minute microparticle treatment alone in resting primary adult human articular chondrocytes induced significant Akt phosphorylation compared to resting chondrocytes alone (0.7 ± 0.2 vs. 0.2 ± 0, $P<0.05$ with Two-way ANOVA and Bonferroni post-test) and microparticle pre-treatment (18 hours; 0.7 ± 0.2 vs. 0.2 ± 0.1, $P<0.05$ with Two-way ANOVA and Bonferroni post-test; Figure 4.3.6). This was lost upon stimulation with IL-1β for 10 minutes (TMP 0.3 ± 0.1 vs. IL-1β 0.4 ± 0.2). After 40 minutes, the phosphorylation of Akt had decreased and was no longer significant in resting chondrocytes (0.5 ± 0.2 vs. 0.4 ± 0.1) but had increased in IL-1β stimulated chondrocytes, although the level of phosphorylation did not vary between IL-1β-stimulated groups (IL-1β 0.7 ± 0.1, TMP pre-treatment 0.8 ± 0.1 and IL-1β plus TMP 0.6 ± 0.2).

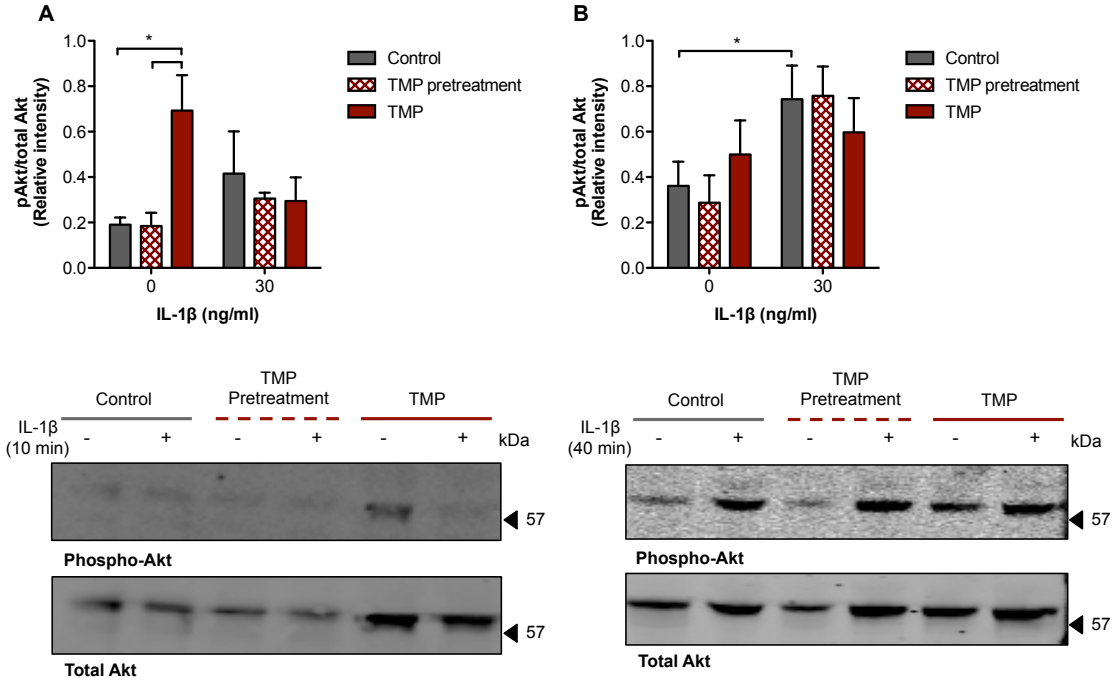

Figure 4.3.6 Microparticles modulate primary adult human articular chondrocyte Akt phosphorylation temporally. Primary adult human articular chondrocytes in monolayer were either pre-treated with 100,000 TMP for 16 hours or treated with IL-1β (30ng/ml) and 100,000 TMP for (A) 10 minutes or (B) 40 minutes, before blotting for phospho-Akt protein. Data are shown as mean ± SEM of 4 separate microparticle donors and blots and expressed as relative intensity after normalisation to total Akt, *$P<0.05$ with Two-way ANOVA and Bonferroni post-test. TMP, TNF-α-treatment generated microparticles. With thanks to Dr Sadani Cooray for performing this western.

Phosphorylated ERK1/2 on the other hand induces the phosphorylation and activation of other kinases and several other factors promoting cell proliferation and/or gene transcription in cartilage (Yin et al., 2009). ERK1/2 phosphorylation was not significantly altered upon IL-1β stimulation at 10 minutes (1.2 ± 0.3 vs. 1 ± 0.3) or 40 minutes (1.3 ± 0.2 vs. 1.1 ± 0.4) or concurrent microparticle treatment at 10 minutes (1.1 ± 0.1 vs. 1.2 ± 0.3) or 40 minutes (1.1 ± 0.1 vs. 1.3 ± 0.2; Figure 4.3.7).

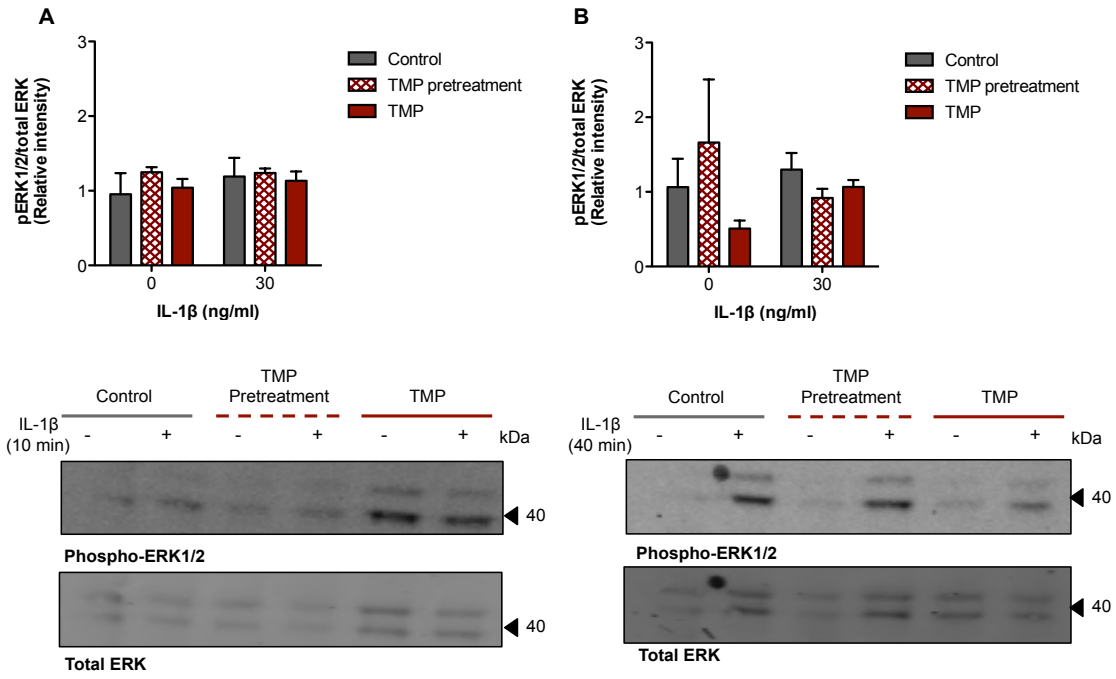

Figure 4.3.7 Microparticles modulate primary adult human articular chondrocyte ERK1/2 phosphorylation temporally. Primary adult human articular chondrocytes in monolayer were either pre-treated with 100,000 TMP for 16 hours or treated with IL-1β (30ng/ml) and 100,000 TMP for (A) 10 minutes or (B) 40 minutes, before blotting for phospho-Akt protein. Data are shown as mean ± SEM of 4 separate microparticle donors and blots and expressed as relative intensity after normalisation to total ERK, not significant with Two-way ANOVA and Bonferroni post-test. TMP, TNF-α-treatment generated microparticles. With thanks to Dr Sadani Cooray for performing this western.

Collectively, these results suggest microparticles influence several signalling pathways in a diverse and temporally orchestrated manner. Given the number of proteins (and other components such as lipids) present within microparticle populations, it is difficult to identify one single pathway responsible for all the chondroprotective effects seen in microparticle and IL-1β co-culture. However, the strong indication that Hsp27 phosphorylation is inhibited rapidly upon microparticle treatment deserves further investigation to determine whether it is this event that leads to the down-regulation of inflammatory cytokine production by chondrocytes.

4.3.2 FPR2 Downstream Transcriptional Target Modulation by Microparticles

Next, the modulation of *FPR2* mRNA by microparticle-associated FPR2 agonists and Annexin A1 was investigated, as the feed-forward regulation of FPR2 by its agonists is largely unknown (Figure 4.3.8). *FPR2* mRNA levels were not significantly altered by IL-1β stimulation at either 3ng/ml (1.3 ± 0.1 vs. 1 ± 0.1) or 30ng/ml (1.1 ± 0.2 vs. 1 ± 0.1) compared to control or by concomitant CMP treatment (CMP + IL-1β 3ng/ml 1.4 ± 0.4 or 30ng/ml 0.7 ± 0.1 vs. 1 ± 0.1) or TMP treatment (TMP + IL-1β 3ng/ml 1.4 ± 0.4 or 30ng/ml 0.9 ± 0.1 vs. 1 ± 0.1). Annexin A1 treatment (30nM) induced a trend of up-regulation of *FPR2* mRNA in micromasses stimulated with IL-1β (3ng/ml) compared to IL-1β stimulation alone (2.4 ± 0.7 vs. 1.3 ± 0.1) but this did not reach statistical significance.

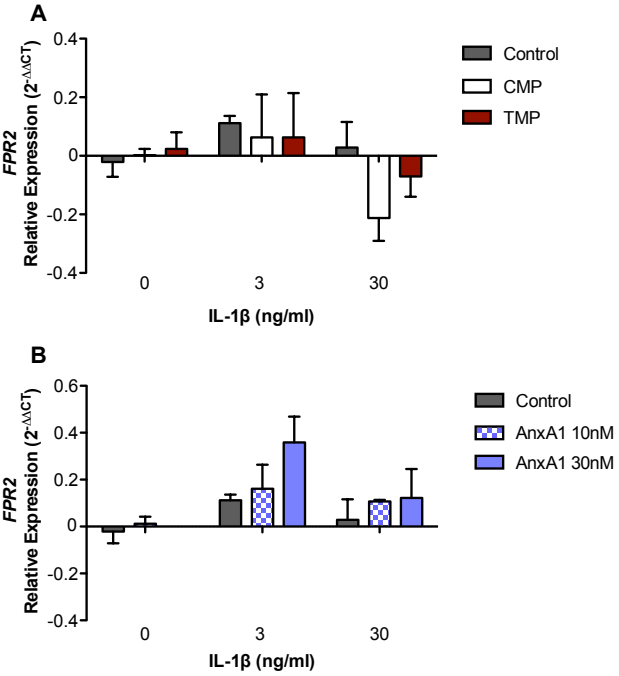

Figure 4.3.8 Transcriptional regulation of *FPR2* by agonists. Chondrocyte micromasses were treated with IL-1β (3ng/ml or 30ng/ml) and (A) 100,000 CMP or TMP or (B) increasing concentrations of Annexin A1 for 6 hours before mRNA extraction and RT-PCR for relative expression of *FPR2.* Data shown are $2^{-\Delta\Delta CT}$ with untreated as calibrator and *RPL32* as housekeeping gene. Data expressed as mean ± SEM of 4 microparticle donors or 3 separate micromass preparations, not significant with Two-way ANOVA and Bonferroni post-test of logged data. CMP, control microparticles, TMP, TMP, TNF-α-treatment generated microparticles. With Special Thanks to Dr Trinidad Montero-Melendez for performing this assay.

Downstream transcriptional targets up-regulated by FPR2 ligation (Renshaw et al., 2010) were investigated in C28/I2 chondrocyte micromasses stimulated with IL-1β, microparticles and Annexin A1. Firstly, *SGPP2* mRNA, which encodes sphingosine 1-phosphate phosphatase expression was analysed (Figure 4.3.9). In chondrocytes, *SGPP2* expression induced by IL-1β stimulation was significantly down-regulated by concurrent microparticle treatment (TMP 1.4 ± 0.6 vs. 2.9 ± 0.1 $P<0.05$ with Kruskal-Wallis test and Dunn's multiple comparison post-test), especially by CMP (0.9 ± 0.1 vs. 2.9 ± 0.1 $P<0.01$ with Kruskal-Wallis test and Dunn's multiple comparison post-test; Figure 4.3.9A). In contrast, Annexin A1 treatment did not alter *SGPP2* expression in either resting (1.5 ± 0.6 vs. 1.2 ± 0.5) or IL-1β-stimulated chondrocytes (2.3 ± 0 vs. 2.9 ± 0.1; Figure 4.3.9B). Accumulating evidence suggests Sphingosine 1-phosphate is plays a role in inflammation, and its downstream phosphatase, sphingosine 1-phosphate phosphatase, or SPP2 (encoded by *SGPP2*) is highly up-regulated in inflammatory settings. Mechtcheriakova et al. (2007) found a predicted NFκB binding site in the promoter of the *SGPP2* gene, suggesting that its transcription is NFκB-dependent. Furthermore, the production of several pro-inflammatory cytokines requires SPP2 and silencing with siRNA reduced IL-8 production induced by TNF-α stimulation in endothelial cells.

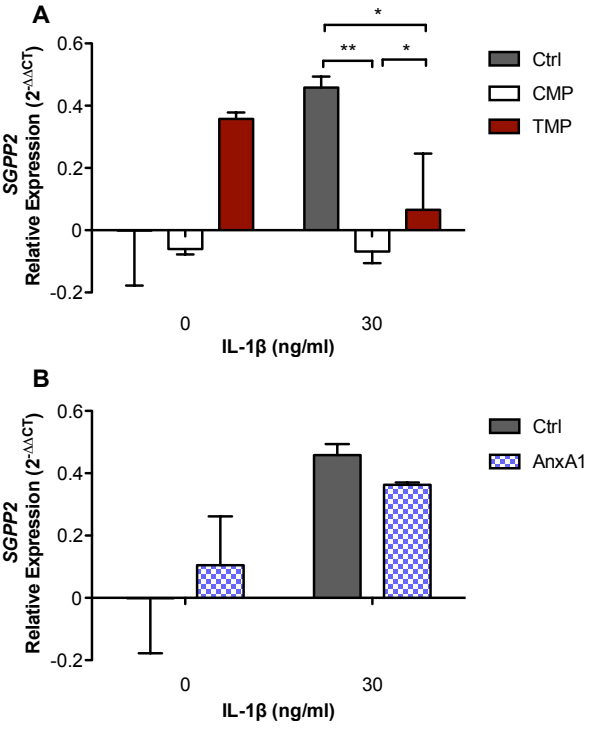

Figure 4.3.9 *SGPP2*, a downstream transcriptional target of FPR2 signalling, is modulated by microparticle treatment. Chondrocyte micromasses were treated with IL-1β (30ng/ml) and (A) 100,000 CMP or TMP or (B) Annexin A1 (10nM) for 6 hours before mRNA extraction and RT-PCR for relative expression of *SGPP2*. Data shown are $2^{-\Delta\Delta CT}$ with untreated as calibrator and *RPL32* as housekeeping gene. Data expressed as mean ± SEM of 3 microparticle donors or 3 separate micromass preparations, $*P<0.05$ and $**P<0.01$ using Two-way ANOVA and Bonferroni post-test of logged data. CMP, control microparticles, TMP, TNF-α-treatment generated microparticles. With Special Thanks to Dr Trinidad Montero-Melendez for performing this assay.

Other targets, such as *JAG1, JAM3, IKBK* and *SP1* were not significantly altered in these settings and require further investigation (Figure 4.3.10).

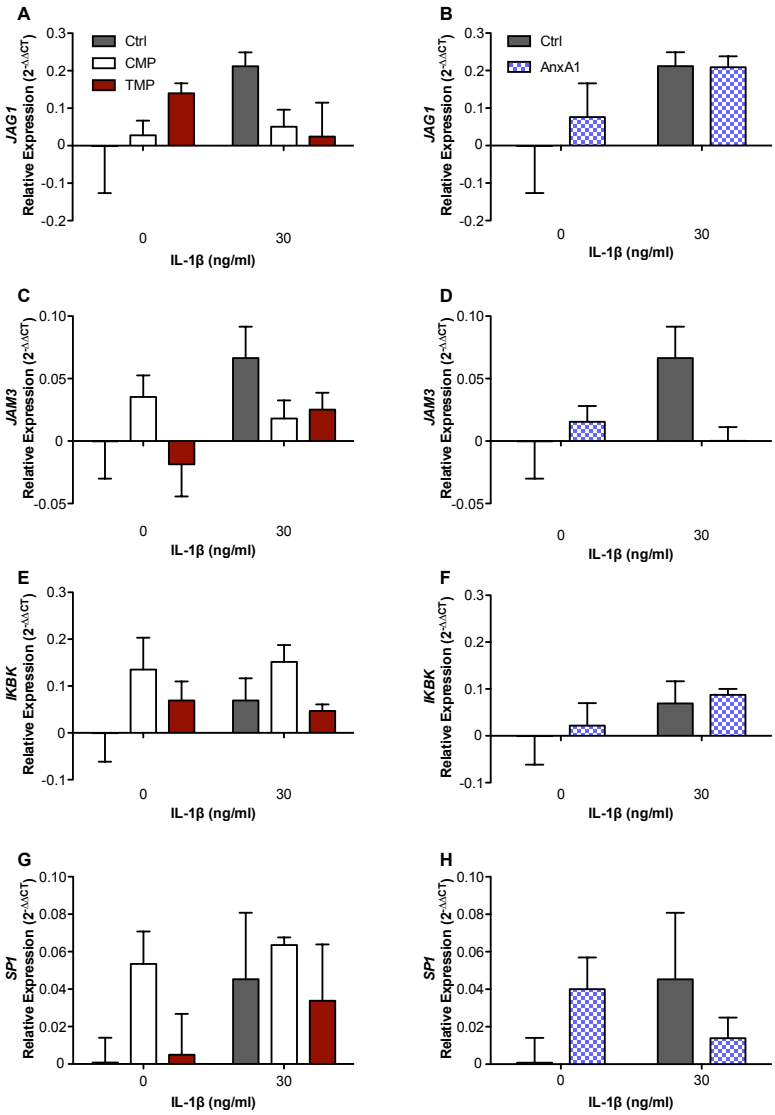

Figure 4.3.10 *JAG1*, *JAM3, IKBK* and *SP1*, downstream transcriptional targets of FPR2 signalling, are not modulated by microparticle or Annexin A1 treatment. Chondrocyte micromasses were treated with IL-1β (30ng/ml) and (A, C, E, G) 100,000 CMP or TMP or (B, D, F, H) Annexin A1 (10nM) for 6 hours before mRNA extraction and RT-PCR for relative expression of *JAG1, JAM3, IKBK* or *SP1.* Data shown are $2^{-\Delta\Delta CT}$ with untreated as calibrator and *RPL32* as housekeeping gene. Data expressed as mean ± SEM of 4 microparticle donors or 3 separate micromass preparations, not significant with Two-way ANOVA and Bonferroni post-test of logged data. CMP, control microparticles, TMP, TNF-α-treatment generated microparticles. With Special Thanks to Dr Trinidad Montero-Melendez for performing this assay.

Thus, these data are interesting, as they confirm that the effects mediated by microparticle interaction with chondrocytes is not wholly dependent on Annexin A1, and that other anti-inflammatory pathways are being induced in this setting. Collectively, these data suggest that the chondroprotection induced by microparticle co-culture is the sum of several anti-inflammatory pathways and events. Hsp27 phosphorylation functions to stabilise the mRNA of pro-inflammatory cytokines and this was inhibited by microparticle treatment. SGPP2 transcription is also associated with the further up-regulation of pro-inflammatory cytokines such as IL-8, and this too was inhibited by microparticle treatment.

4.3.3 Microparticle Treatment Induces Chondrocyte TGF-β Production

Previous reports have demonstrated the role of TGF-β in microparticle-induced anti-inflammatory effects (Gasser and Schifferli, 2004). Therefore it was pertinent to investigate the production of TGF-β1 by C28/I2 chondrocytes cultured in micromass constructs. Co-culture of IL-1β stimulated micromasses with TMP significantly elevated *TGFβ1* mRNA expression compared to IL-1β treatment alone (Figure 4.3.11A, 2.3 ± 0.2 vs. 0.48 ± 0.2 P=0.023 with Kruskal-Wallis test and Dunn's multiple comparison post-test). Treatment with CMP trended towards this effect but did not reach statistical significance (2.3 ± 1 vs. 0.48 ± 0.2). This suggests that microparticle treatment induces *de novo* production of TGF-β1.

In addition, TGF-β1 protein levels were measured in micromass supernatants using a cytokine bead array kit, a highly sensitive sandwich immunoassay analysed using flow cytometry to detect fluorescence intensity that is proportional to the concentration of the analyte (Figure 4.3.11). TGF-β1 possesses potent anti-inflammatory and anabolic effects on chondrocytes. Microparticle culture with resting chondrocytes induced significant TGF-β1 production (31.4 ± 3.7 vs. 0 ± 8.9% P<0.05 with Two-way ANOVA and Bonferroni post-test; Figure 4.3.11A). Furthermore, microparticle co-culture with chondrocyte micromasses stimulated with IL-1β reversed the down-regulation of TGF-β1 production (44.6 ± 6.2 vs. -8.7 ± 11.8% P<0.001 with Two-way ANOVA and Bonferroni post-test).

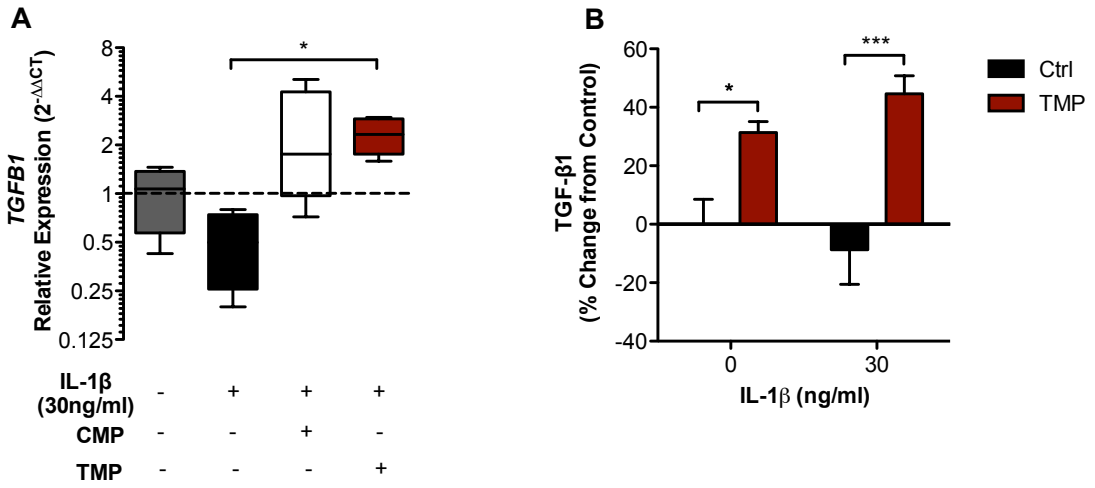

Figure 4.3.11 Microparticles induce TGF-β mRNA and protein expression. Chondrocyte micromasses were treated with IL-1β (30ng/ml) and 100,000 CMP or TMP for 24 or 6 hours before supernatant collection and mRNA extraction for RT-PCR. (A) Relative expression of *TGFβ1* after 6 hours. Data shown are $2^{-\Delta\Delta CT}$ with untreated as calibrator and *RPL32* as housekeeping gene. Data expressed as median, interquartile range and range of 4 separate microparticle donors. (B) Total TGF-β1 protein content in supernatants were quantified by cytokine bead array. Data are shown as mean ± SEM of 8 separate microparticle donors. **P*<0.05 and ****P*<0.001 with Two-way ANOVA and Bonferroni post-test. **P*<0.05 and using Kruskal-Wallis test and Dunn's multiple comparison post-test. CMP, control microparticles, TMP, TNF-α-treatment generated microparticles. With Special Thanks to Mr Hefin Rhys Jones for performing the CBA assay.

The contribution of TGFβ1 to matrix accumulation was next assessed using TGFβ neutralising antibodies (Figure 4.3.12). As expected, TMP reversed the reduction in matrix accumulation induced by IL-1β (30ng/ml) treatment (41.7 ± 1.9 vs. -19 ± 4.6%, *P*<0.001 with Two-way ANOVA and Bonferroni post-test). Treatment of micromasses with TGFβ neutralising antibodies had no effect in either resting (-4.6 ± 5.8 vs. 3.1 ± 1.4%, not significant) or IL-1β stimulated micromasses (-24 ± 3 vs. -19 ± 4.6%, not significant). In contrast, the combination of microparticle treatment with TGFβ neutralising antibodies significantly down-regulated chondroprotection in IL-1β stimulated chondrocytes (6.5 ± 6.5 vs. 41.7 ± 1.9%, *P*<0.01 with Two-way ANOVA and Bonferroni post test) without modulating matrix production in resting chondrocytes (-6.6 ± 14 vs. 3.1 ± 1.4%, not significant). This suggests that chondrocyte TGFβ production induced by microparticle treatment is at least partially responsible for microparticle protection.

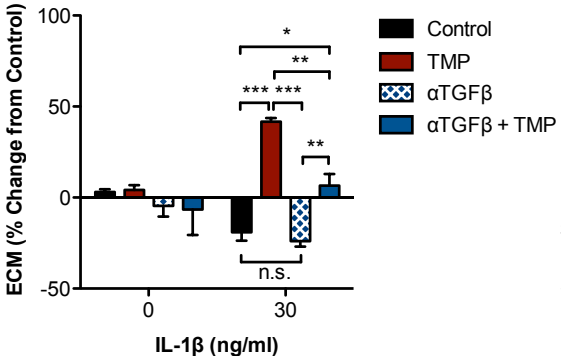

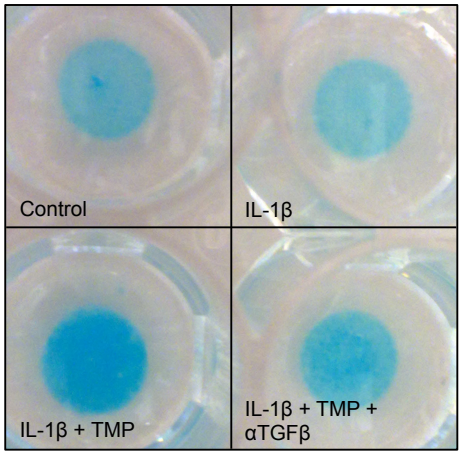

Figure 4.3.12 TGF-β neutralising antibodies significantly inhibit microparticle-induced chondroprotection. Chondrocyte micromasses were treated with IL-1β (30ng/ml) and 100,000 TMP with or without TGF-β neutralising antibodies (10μg/ml) for 24 hours before extracellular matrix accumulation was quantified by Alcian blue staining. Data are shown as mean ± SEM of 3 separate microparticle donors. **P*<0.05, ***P*<0.01 and ****P*<0.001 using Two-way ANOVA and Bonferroni post-test. TMP, TNF-α generated microparticles; ECM, extracellular matrix; αTGFβ, Transforming growth factor β neutralising antibodies.

Therefore, the production of TGF-β1, a protective growth factor for chondrocytes, was induced by co-culture with microparticles, and neutralisation of TGF-β reversed chondroprotection. This suggests that the downstream programme induced by microparticles involves the induction of TGF-β.

4.4 Microparticles Protect Cartilage-Native Chondrocytes *Ex Vivo*

As microparticle treatment of arthritic chondrocytes *in vitro* led to an unexpected increase in cartilage matrix accumulation and supressed the generation of inflammatory cytokines, it was critical to understand whether microparticles could elicit similar protective effects in whole cartilage explants. This would provide more physiologically relevant details about microparticle-chondrocyte interaction when spatially divided by cartilage matrix.

4.4.1 Microparticles Penetrate Cartilage Matrix

To investigate any potential protective effects of microparticles on cartilage explants, a culture system using whole rat femoral cartilage explants was devised. Removal of the entire cartilage femoral head cap ensured that auto-degradation of the matrix was minimised, as mechanically damaging the cartilage by cutting induces a defective repair programme, inducing the expression of matrix metalloproteinases by chondrocytes. In the first instance, rat tissue rather than mouse tissue was utilised due to the technical challenge of removing intact murine femoral heads.

Firstly, the loss of matrix integrity, measured by Safranin O staining in rat femoral head explants, was determined after culturing with IL-1β for a period of 14 days (Figure 4.4.1). By day 4, IL-1β treatment (10ng/ml) had induced significant cartilage proteoglycan loss compared to day 0 (41.4 ± 2.9 vs. 83.5 ± 3.5% $P<0.001$ with Two-way ANOVA and Bonferroni post-test), a reduction of 50%. By day 7, control cartilage had lost a proportion of its integrity compared to day 0 and day 4 (53 ± 2.7 vs. day 4 71.6 ± 3.9 and day 0 83.5 ± 3.5%), but this was significantly increased in IL-1β treated femoral heads (22.8 ± 2.9 vs. 53 ± 2.7% $P<0.001$ with Two-way ANOVA and Bonferroni post-test). Proteoglycan loss after this time-point plateaued, and further loss was not seen in either control (52.3 ± 3.1 vs. 53 ± 2.7%) or IL-1β-treated femoral heads (18.9 ± 2 vs. 22.8 ± 29). Thus, a 7-day time point was chosen for further experiments.

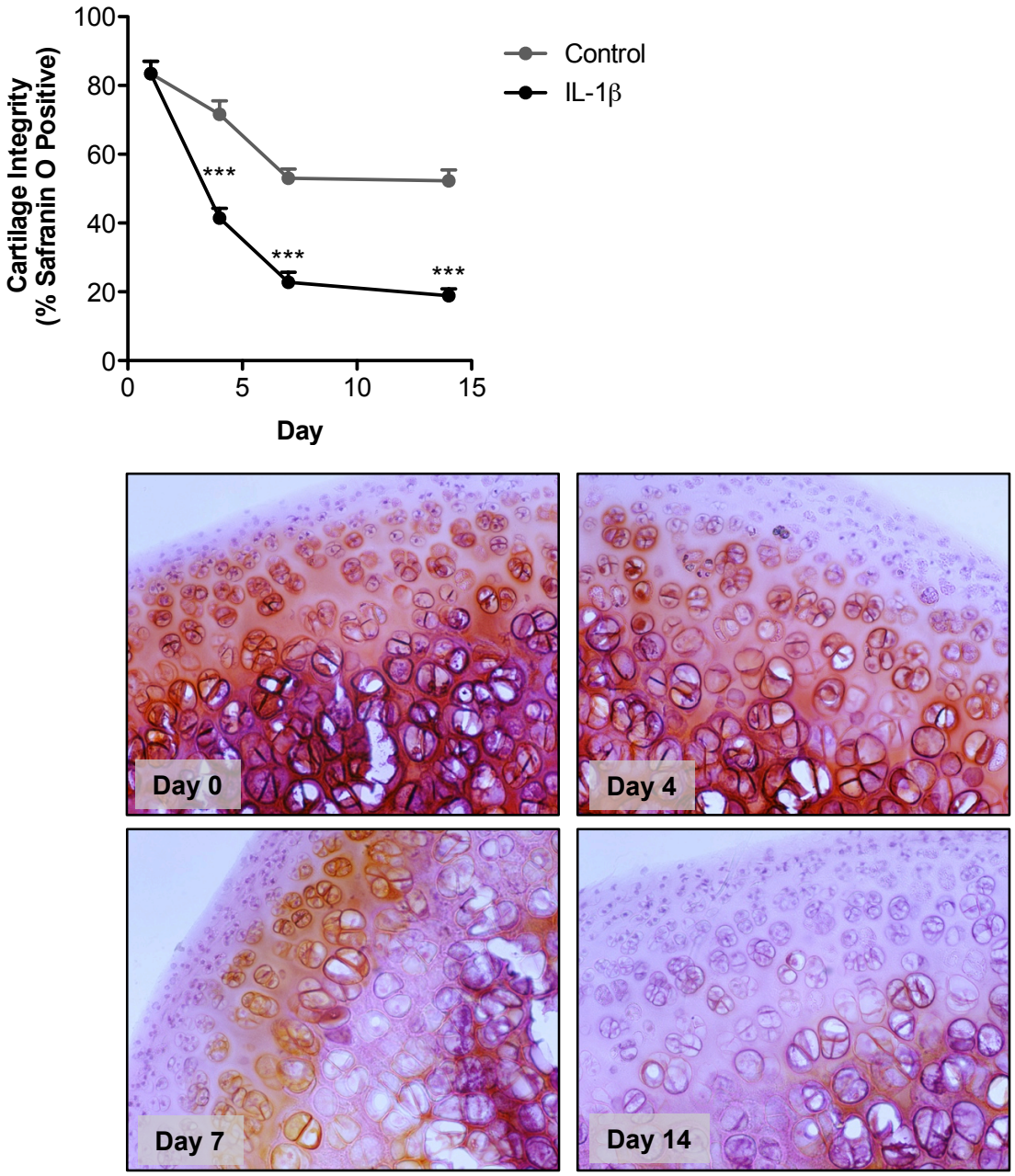

Figure 4.4.1 IL-1β reduces rat femoral head cartilage integrity over 4 to 14 days. Rat femoral head cartilage explants were treated with IL-1β (10ng/ml) every two days for 14 days and stained with Safranin O on days 0, 4, 7 and 14. Data are expressed as percentage area Safranin O positive and shown as mean ± SEM of 4 separate rats. ***P<0.001 using Two-way ANOVA with Bonferroni post-test.

As predicted, IL-1β treated femoral heads had reduced matrix integrity compared to control (22.8 ± 2.9 vs. 53 ± 2.7% *P*<0.001 with Two-way ANOVA and Bonferroni post-test, Figure 4.4.2). Concurrent microparticle treatment with IL-1β (10ng/ml) stimulation every two days protected from IL-1β-induced loss in cartilage integrity (CMP 46.2 ± 8.7 and IMP 46.9 ± 9.8 vs. 22.8 ± 2.9% *P*<0.01 and TMP 51.5 ± 5 vs. 22.8 ± 2.9% *P*<0.001 with Two-way ANOVA and Bonferroni post-test), indicating that microparticles can exert effects in whole tissue explants as well a during micromass co-culture.

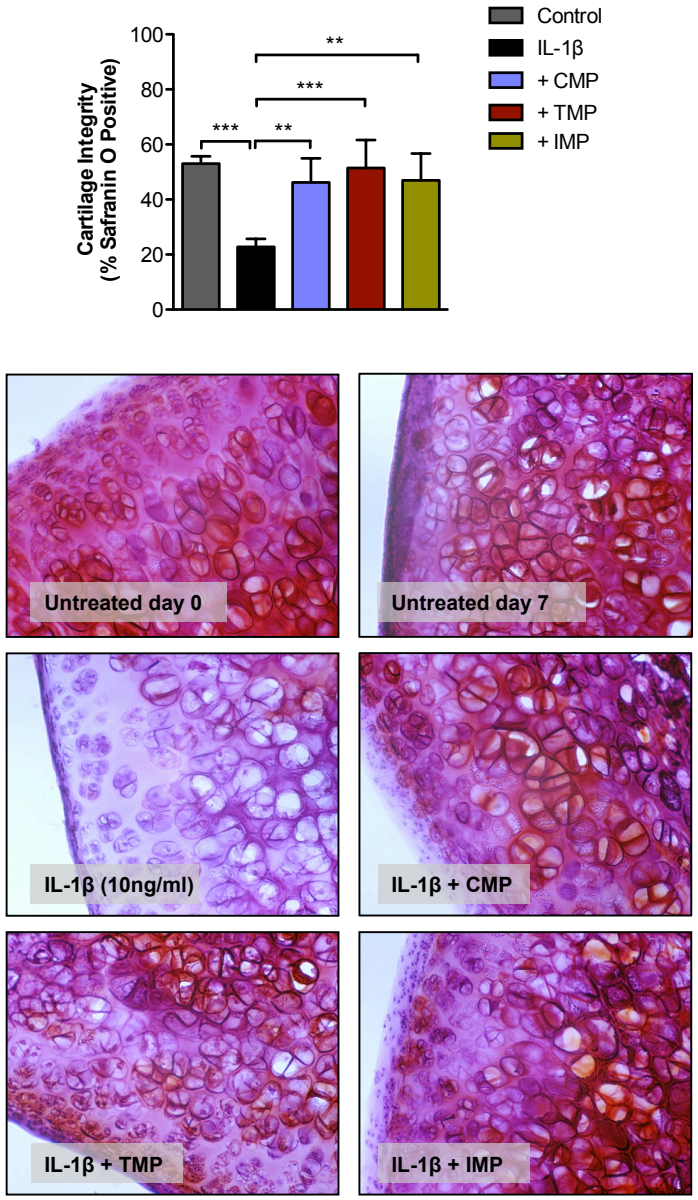

Figure 4.4.2 Microparticles protect from IL-1β-induced cartilage integrity loss at 7 days. Rat femoral head cartilage explants were treated with IL-1β (10ng/ml) and 100,000 CMP, TMP or IMP every two days for 7 days and stained with Safranin O on day 7. Data are expressed as percentage area Safranin O positive and shown as mean ± SEM of 4 separate microparticle donors and 4 separate cartilage donors. ***P*<0.01 and ****P*<0.001 using Two-way ANOVA with Bonferroni post-test. CMP, control microparticles; TMP, TNF-α-treatment generated microparticles; IMP, IL-8-treatment generated microparticles.

To determine whether protection of the cartilage matrix was accompanied by alterations in proinflammatory mediator production, Prostaglandin E_2 and nitric oxide were measured in the culture supernatants. By day 7 significant proteoglycan loss was observed in the IL-1β-treated cartilage explants, and the production of prostaglandin E_2 into the supernatant was significantly higher than that of control femoral heads (0.08 ± 0.1 vs. 4.1 ± 1.6ng/ml $P<0.05$ with Two-way ANOVA and Bonferroni post-test; Figure 4.4.3). Prostaglandin E_2 production was not reduced by concurrent treatment with CMP, TMP or IMP compared to IL-1β alone (1.5 ± 0.6, 2.8 ± 1.2 and 3.2 ± 1.5 vs. 4.1 ± 1.6ng/ml) even though protection from proteoglycan loss was observed.

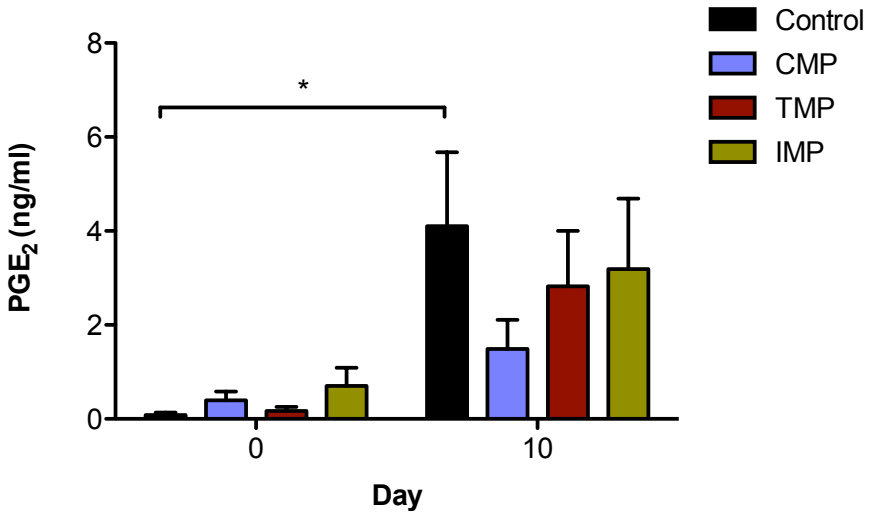

Figure 4.4.3 Microparticles do not affect prostaglandin E_2 production induced by IL-1β on day 7. Rat femoral head cartilage explants were treated with or without IL-1β (10ng/ml) and 100,000 CMP, TMP or IMP every two days for 7 days. Supernatants were assayed for prostaglandin E_2 by EIA. Data are shown as mean ± SEM of 4 separate microparticle donors and 4 separate cartilage donors. *$P<0.05$ using Two-way ANOVA with Bonferroni post-test. CMP, control microparticles; TMP, TNF-α-treatment generated microparticles; IMP, IL-8-treatment generated microparticles; PGE_2, prostaglandin E_2.

In contrast, nitric oxide metabolism was increased by TMP and IMP treatment of resting femoral head explants on day 7 (TMP 18.1 ± 4.4 and IMP 17.8 ± 3.6 vs. 5.6 ± 1.2μM $P<0.05$ with Two-way ANOVA and Bonferroni post-test; Figure 4.4.4). This was not the case for femoral heads stimulated with IL-1β and then treated with microparticles (19.7 ± 1.2 vs. CMP 29.3 ± 2.2, TMP 23.8 ± 2.8 or IMP 25 ± 1.2μM). This suggests that, at least *in vitro*, microparticles are not as effective at reducing proinflammatory mediator production, but can still protect from cartilage degradation in this chimeric rat tissue/human microparticle model.

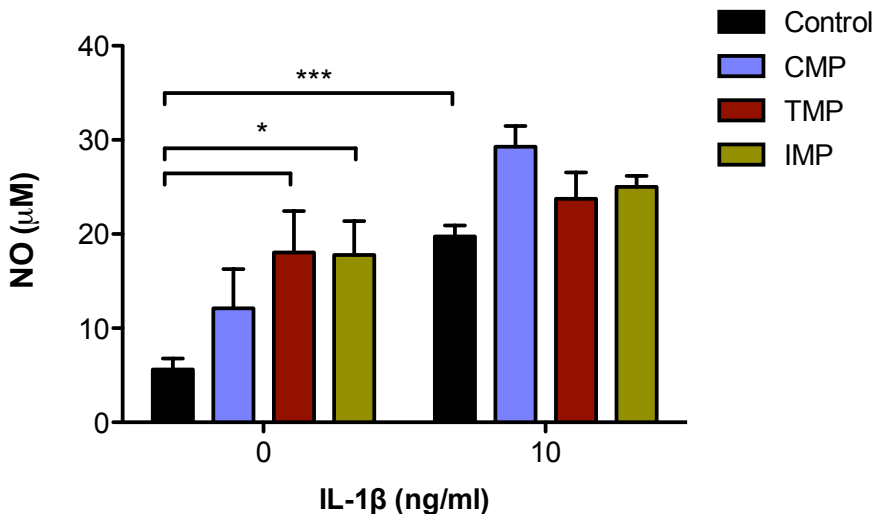

Figure 4.4.4 Microparticles increase nitric oxide production in resting cartilage explants. Rat femoral head cartilage explants were treated with IL-1β (10ng/ml) and 100,000 CMP, TMP or IMP every two days for 7 days. Supernatants were assayed for Nitric oxide metabolism by Griess Assay. Data are shown as mean ± SEM of 4 separate microparticle donors and 4 separate cartilage donors. *$P<0.05$ and ***$P<0.001$ using Two-way ANOVA with Bonferroni post-test. CMP, control microparticles; TMP, TNF-α-treatment generated microparticles; IMP, IL-8-treatment generated microparticles.

Next it was determined whether Annexin A1 treatment had any effect on cartilage matrix integrity as observed during *in vitro* experiments. Annexin A1 treatment of control rat femoral head explants did not induce any significant changes in proteoglycan retention at day 7 (50.9 ± 4.7 vs. 52.1 ± 8.8%; Figure 4.4.5). However, concomitant treatment with IL-1β protected cartilage matrix integrity at day 7 compared to IL-1β alone (55 ± 3.8 vs. 20.2 ± 1.6% $P<0.01$ with Two-way ANOVA and Bonferroni post-test), with levels of Safranin O staining similar to those observed in untreated femoral heads (55 ± 3.8 vs. 52.1 ± 8.8%). These data suggest that *ex vivo* treatment of cartilage explants with microparticles induces protection of the cartilage matrix integrity with Annexin A1 being a likely molecule responsible for this protection.

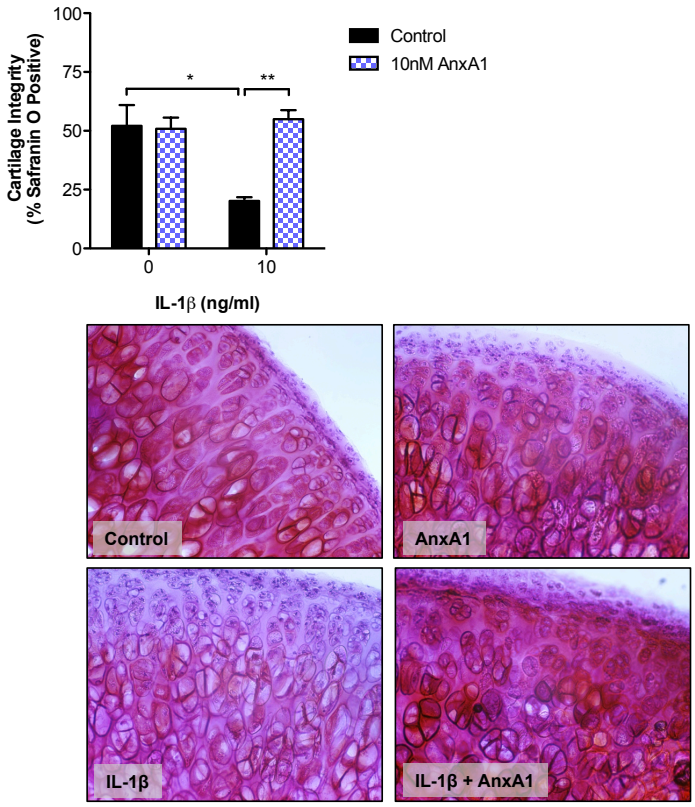

Figure 4.4.5 Annexin A1 protects from IL-1β-induced cartilage integrity loss. Rat femoral head cartilage explants were treated with IL-1β (10ng/ml) and recombinant human Annexin A1 (10nM) every two days for 7 days before Safranin O staining. Data are expressed as percentage area Safranin O positive and shown as mean ± SEM of 4 separate rats. **P*<0.05 and ***P*<0.01 using Two-way ANOVA with Bonferroni post-test. AnxA1, Annexin A1.

To determine whether the Annexin A1 G-protein coupled receptors (GPCRs) were involved in the retention of proteoglycans, cartilage explants were obtained from mice with genetic knockout of *Fpr1* and *Fpr2/3*. Wild type mouse femoral head cultures treated with IL-1β for 7 days with concurrent microparticle treatment led to a greater retention of proteoglycans compared to IL-1β treatment alone in both wild-type (64.4 ± 1.3 vs. 40.8 ± 5.5% $P<0.05$ woth Two-way ANOVA and Bonferroni post-test) and *Fpr1*$^{-/-}$ (75.6 ± 1.7 vs. 52.5 ± 3.3% $P<0.001$ with Two-way ANOVA and Bonferroni post-test) femoral heads at day 7, at levels similar to those of untreated femoral heads (wild type 64.4 ± 1.3 vs. 67.3 ± 4.1% and *Fpr1*$^{-/-}$ 75.6 ± 1.7 vs. 84.1 ± 1.1%; Figure 4.4.6). In contrast, microparticle treatment of *Fpr2/3*$^{-/-}$ femoral head explants (the murine orthologue of human FPR2) did not induce any retention of proteoglycans compared to IL-1β alone (60.7 ± 2.4 vs. 64.3 ± 3% not significant with Two-way ANOVA and Bonferroni post-test).

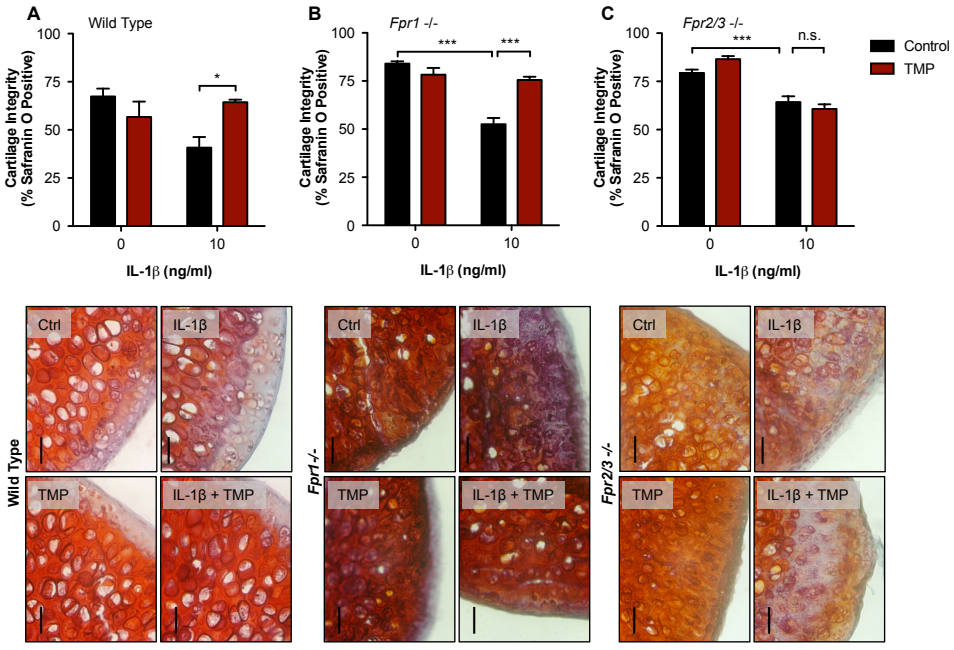

Figure 4.4.6 Microparticles protect from IL-1β-induced cartilage integrity loss in wild type and *Fpr1*$^{-/-}$ but not *Fpr2/3*$^{-/-}$ mouse femoral head cartilage. (A) Wild type, (B) *Fpr1* null and (C) *Fpr2/3* null femoral head cartilage explants were treated with IL-1β (10ng/ml) and 100,000 TMP every two days for 7 days before Safranin O staining. Data are expressed as percentage area Safranin O positive and shown as mean ± SEM of 3 separate mice from each genotype. *$P<0.05$ and ***$P<0.001$ using Two-way ANOVA with Bonferroni post-test. TMP, TNF-α-treatment generated microparticles.

These data indicate that microparticles are able to protect the cartilage matrix from integrity loss induced by IL-1β, but also indicate that ligation of Fpr2/3 is required for this protection. Thus, it was next investigated whether neutrophil microparticles can enter the cartilage matrix to interact with Fpr2/3 bearing chondrocytes.

4.4.2 Microparticles Penetrate Cartilage Matrix in *Ex Vivo* Femoral Head Explants

Were microparticles delivering protective components to the chondrocytes through the cartilage? To identify whether the protective effects were achieved by migration of microparticles through the matrix to the chondrocytes, an experiment was designed to visualise the microparticle location.

IL-1β treatment of femoral heads was carried out for 3 days (50ng/ml every day) before 100,000 Bodipy-maleimide-labelled TMP were added to the culture. Femoral heads were collected 18 hours later, sectioned, and stained with anti-human MRP-8, a protein highly abundant in neutrophil microparticles, to determine the presence of human protein. Control femoral heads and those treated with only IL-1β showed no staining for MRP-8, or any Bodipy-maleimide (green) fluorescence above background as expected (Figure 4.4.7 panels a and b). In contrast, femoral heads treated with TMP showed abundant chondrocytes positive for both Bodipy-maleimide fluorescence and MRP-8 (red) staining (Figure 4.4.7 panels c and d). In contrast, femoral heads treated with 100,000 synthetic microcapsules, which have FITC integrated into their membranes and carry a similar content of Annexin A1, with or without IL-1β stimulation, indicated presence of microcapsules on the surface of cartilage explants but showed no FITC fluorescence within the matrix or cells (Figure 4.4.7 panels e and f). Higher magnification images of TMP-treated, IL-1β-stimulated femoral heads stained with monoclonal anti-human Annexin A1 revealed double-positive staining puncta located primarily within the border of chondrocytes (detectable by wheat-germ agglutinin; Figure 4.4.7 panel g). Occasionally, these areas of double staining co-localised with chondrocyte nuclei, furthermore, Annexin A1 could also be detected within cells suggesting uptake of proteins from the microparticles followed by redistribution throughout the cytoplasm.

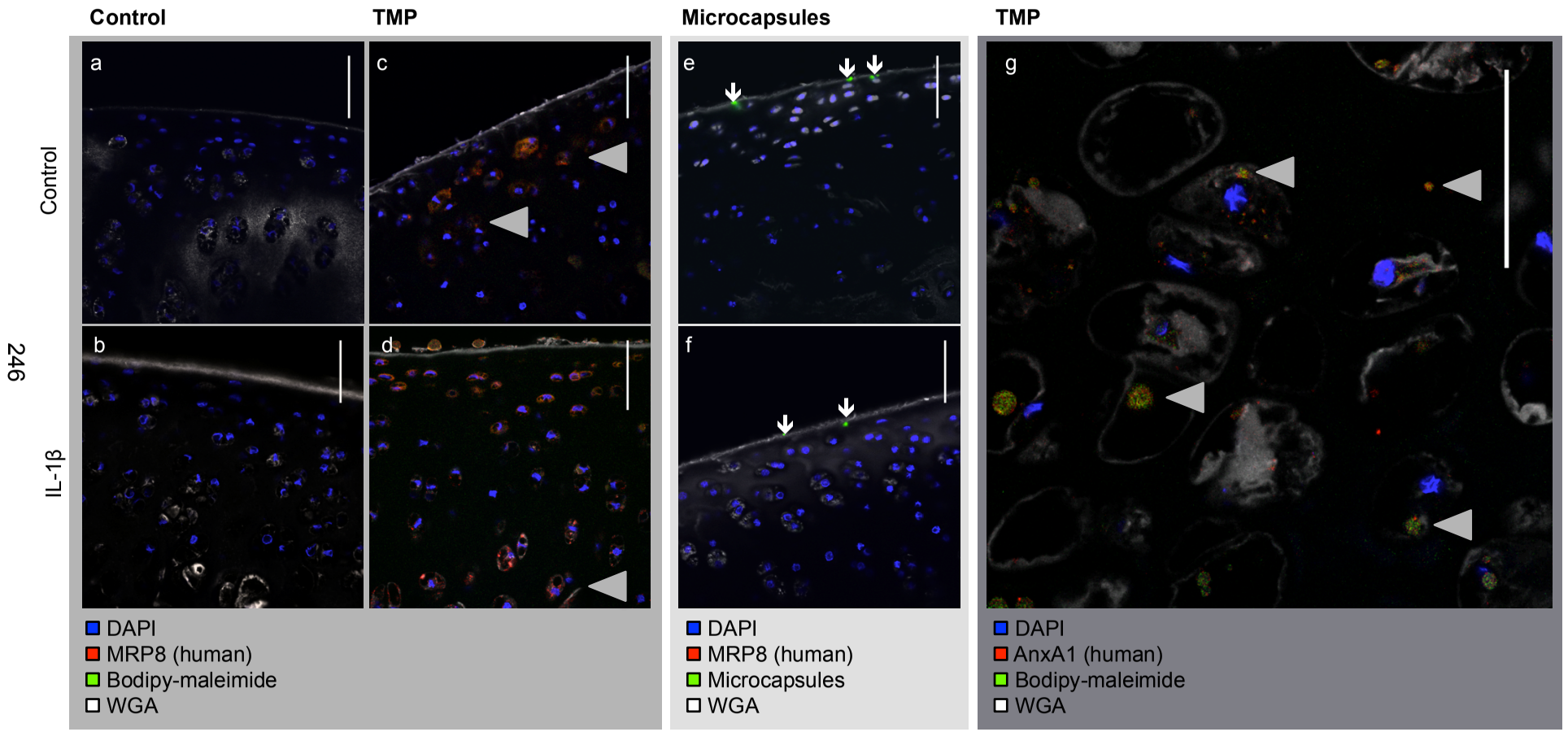
Control
TMP
Microcapsules
TMP
Control
IL-1β
a
b
c
d
e
f
g
DAPI
MRP8 (human)
Bodipy-maleimide
WGA
DAPI
MRP8 (human)
Microcapsules
WGA
DAPI
AnxA1 (human)
Bodipy-maleimide
WGA

Figure 4.4.7 Microparticles penetrate intact cartilage matrix whereas synthetic microcapsules of the same size, loaded with Annexin A1, cannot. Rat femoral head cartilage was treated with IL-1β (50ng/ml) for 3 days or left untreated before 100,000 Bodipy-maleimide-loaded TMP or synthetic microcapsules were added for 18 hours. Fixed femoral heads were sectioned and stained with monoclonal human MRP-8 antibodies (which does not cross-react with rat tissue), wheat germ agglutinin (WGA) and DAPI before confocal microscopy. (a) Untreated, (b) IL-1β (50ng/ml), (c) TMP only, (d) IL-1β (50ng/ml) and TMP treatment. Grey arrowheads denote deepest green (Bodipy-maleimide) and red (MRP8) co-localisation. (e) Microcapsules only, (f) microcapsules and IL-1β (50ng/ml) treatment. White arrows denote microcapsules that fluoresce green inherently. Scale bar denotes 50μm. (g) High magnification fluorescent confocal micrograph of Bodipy-maleimide (green) and AnxA1 (red) double positive microparticles within cartilage-resident chondrocytes. Scale bar denotes 20μm. TMP, TNF-α-treatment generated microparticles; AnxA1, Annexin 1; MRP8, myeloid-related protein 8.

Penetration of microparticles into IL-1β treated explants occurred with a higher distribution frequency compared to unstimulated explants, with microparticles reaching significantly further into IL-1β-degraded cartilage (61.8 ± 3.4 vs. 30 ± 1.9μm *P*<0.001 with two-tailed Mann-Whitney t-test; Figure 4.4.8).

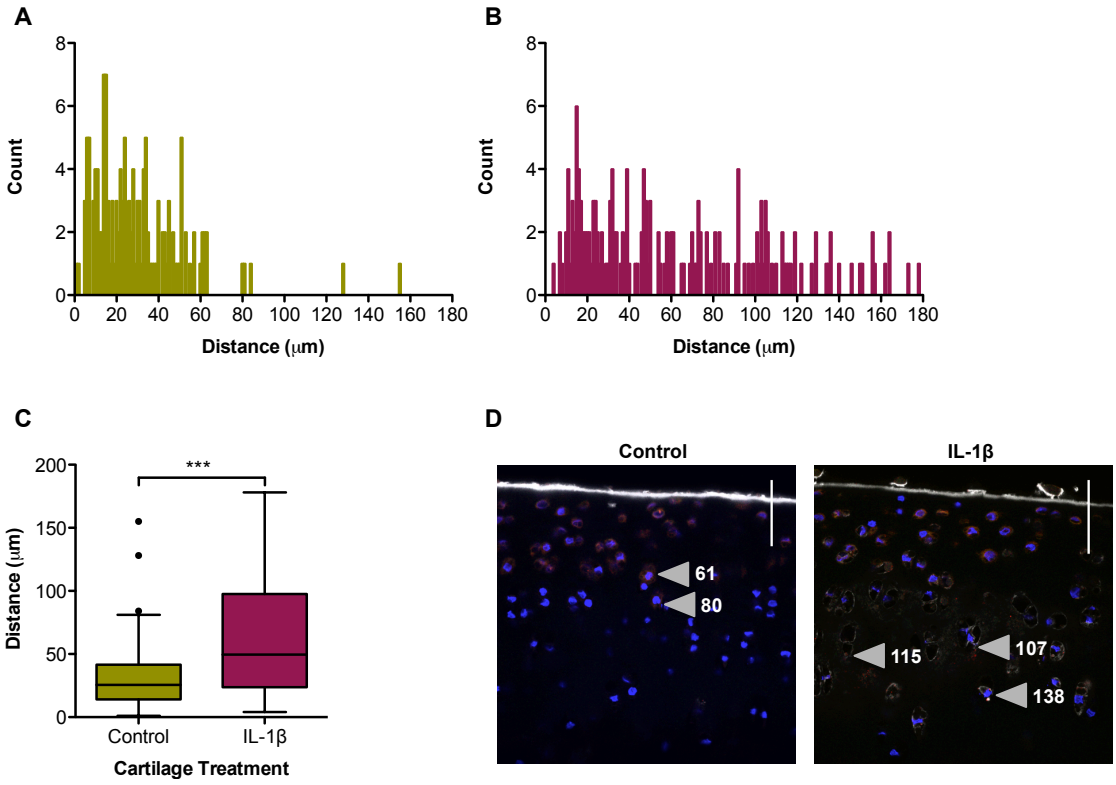

Figure 4.4.8 Microparticles penetrate further into IL-1β-treated cartilage explants. (A) Rat femoral head cartilage was either left untreated or (B) treated with IL-1β (50ng/ml) for 3 days before 100,000 Bodipy-maleimide-loaded TMP were added for 24 hours. Fixed femoral heads were sectioned and stained with monoclonal human MRP-8 antibodies (which does not cross-react with rat tissue), wheat germ agglutinin and DAPI before confocal microscopy. Each individual microparticle or double-staining cell (representing previous microparticle uptake) depth was measured using image J after calibration for pixel *vs.* distance ratio. Each graph represents 140 or 166 microparticles measured over at least 10 individual micrographs. (C) Box and whisker summary of binned data, data are shown as Bonferroni whiskers to demonstrate outliers. ***P<0.001 with Mann-Whitney t-test. (D) Representative micrographs demonstrating microparticle measurements. Grey arrowheads denote green (Bodipy-maleimide) and red (MRP8) co-localisation, with their distance (μm) from the cartilage edge denoted to the right. Scale bar denotes 50μm. TMP, TNF-α-treatment generated microparticles, MRP8, myeloid-related protein 8.

Furthermore, using high magnification confocal microscopy and acquiring a series of z-stack slices through the 10μm cartilage section it was possible to image three chondrocytes in situ with multiple microparticles within the plasma membrane of the chondrocytes (Figure 4.4.9). It was also possible to see that the human Annexin A1 was present within the cells localised to the plasma membrane. In the bottom row of photographs, a third chondrocyte appears to the right of the first two, and it is possible to see at least 7 intact microparticles within this cell.

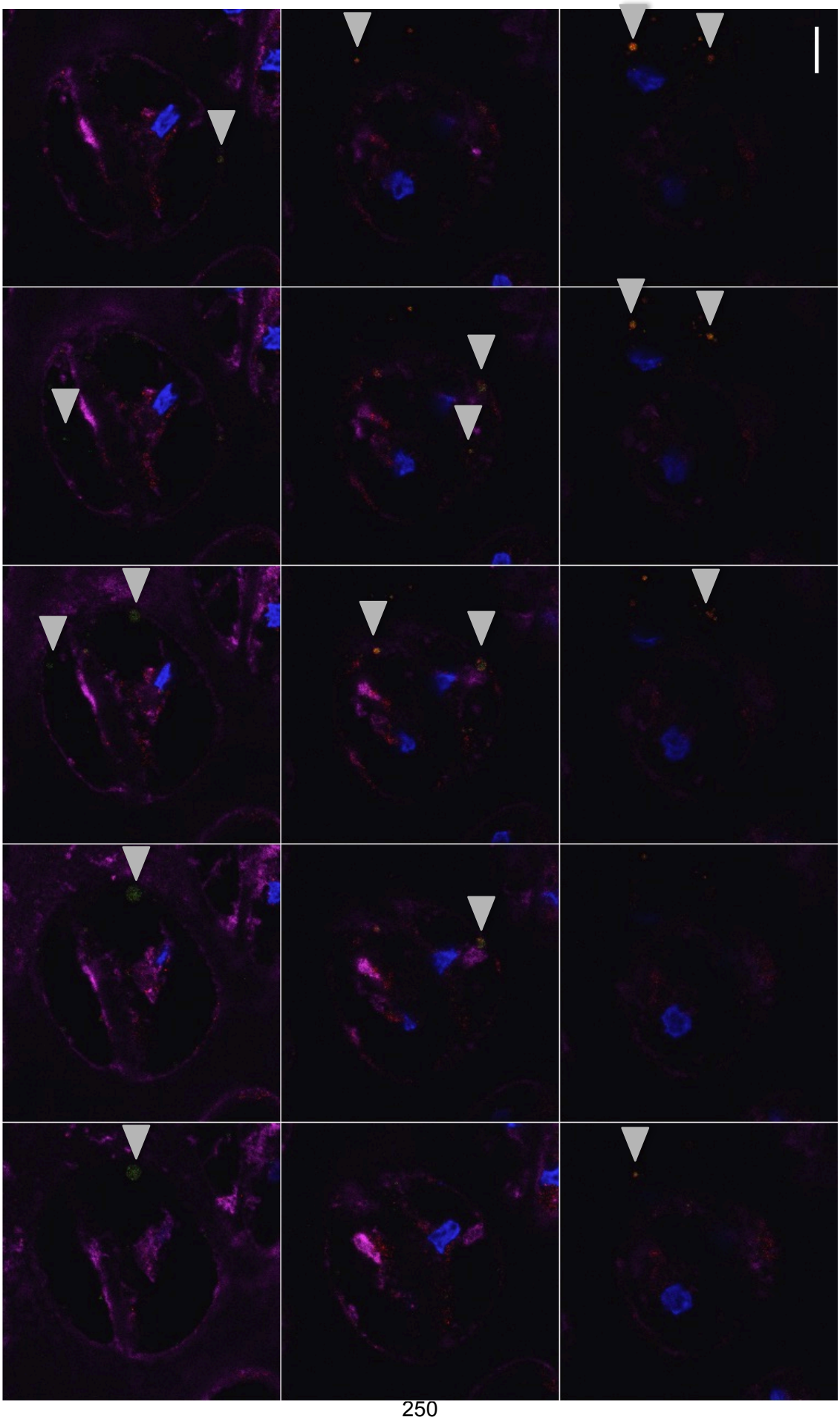

Figure 4.4.9 Multiple microparticles enter each chondrocyte. Rat femoral head cartilage was treated with IL-1β (50ng/ml) for 3 days before 100,000 Bodipy-maleimide -loaded TMP were added for 16 hours. Fixed femoral heads were sectioned and stained with monoclonal human Annexin A1 antibodies (red; which does not cross-react with rat tissue), wheat germ agglutinin (purple; WGA) and DAPI (blue) before confocal microscopy. Figure shows a serial montage produced from a 3D confocal z-stack project. Image processing was performed using ImageJ. Scale bar denotes 10μm, grey arrowheads denote microparticles. TMP, TNF-α-treatment generated microparticles; AnxA1, Annexin A1.

When the data are combined into a max projection, it is possible to see around 40 individual double-staining circular events within the three main grouped chondrocytes (Figure 4.4.10). This represents a very large transfer of protein (and other microparticle components) from one cell type to another, suggesting that the uptake of microparticles by chondrocytes is likely to have a profound effect on cell phenotype, protein repertoire and transcriptional and translational machinery.

Together, these data show that microparticles penetrate more readily into damaged cartilage to deliver their content to the resident chondrocytes likely to initiate a program that prevents the loss of proteoglycans from the matrix induced by IL-1β treatment. These data are extremely interesting, as the current view is that the cartilage is penetrable only to small molecules present within the synovial fluid. Perhaps this is not the case, and proteins previously detected in arthritic cartilage (for example MRP8, (van Lent et al., 2008)) may be present in abundance due to the penetration of neutrophil microparticles.

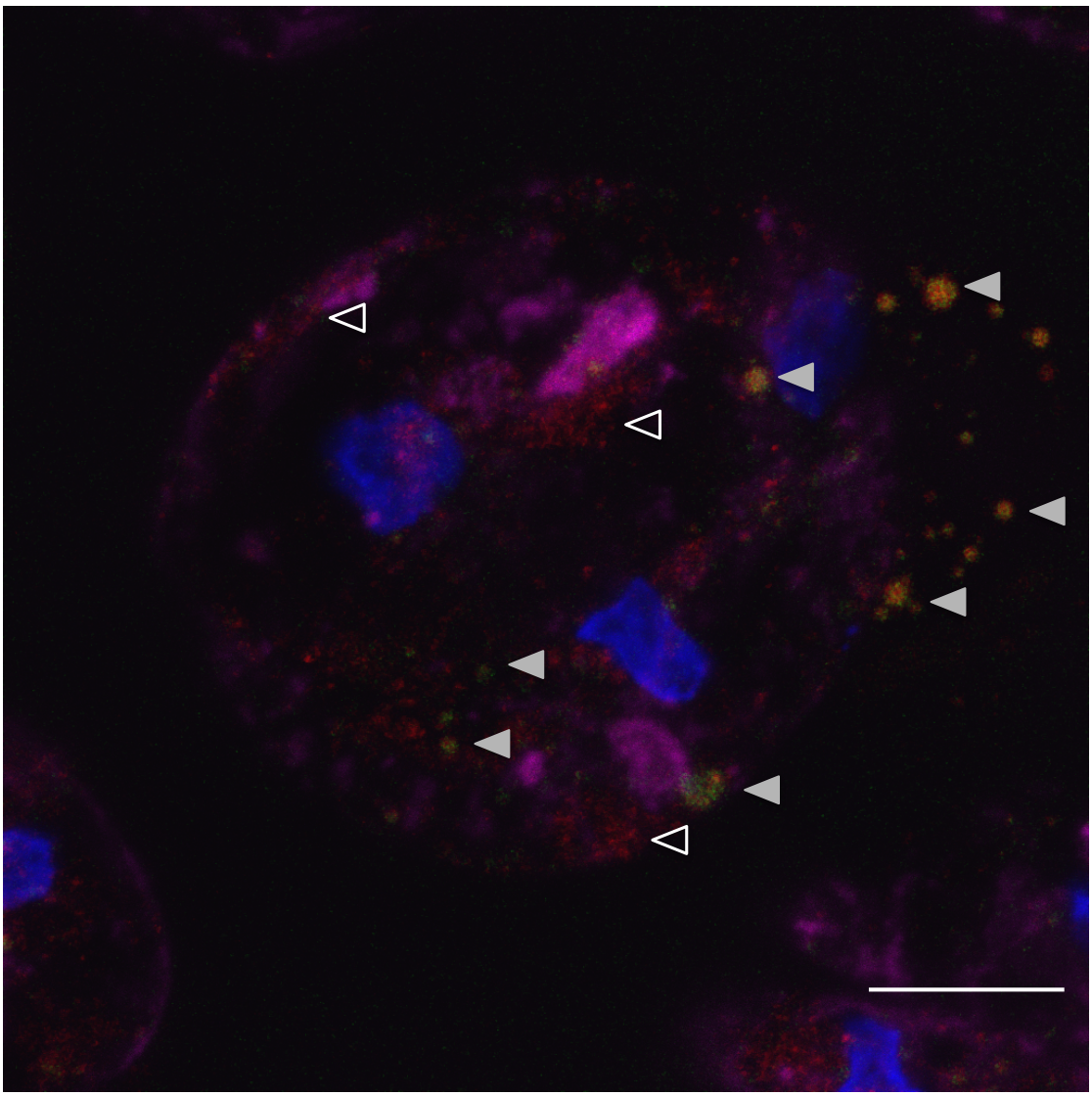

Figure 4.4.10 Microparticles enter cartilage native chondrocytes whole before being dismantled. Rat femoral head cartilage was treated with IL-1β (50ng/ml) for 3 days before 100,000 Bodipy-maleimide -loaded TMP were added for 16 hours. Fixed femoral heads were sectioned and stained with monoclonal human Annexin A1 antibodies (red; which does not cross-react with rat tissue), wheat germ agglutinin (purple; WGA) and DAPI (blue) before confocal microscopy. Figure shows a max projection image from the 3D confocal z-stack project. Images 4-20 were used to reduce WGA background. Image processing was performed using ImageJ. Scale bar denotes 10μm, grey arrowheads denote double-positive microparticles, open arrowheads denote diffuse Annexin A1 staining. TMP, TNF-α-treatment generated microparticles.

CHAPTER 5: EXAMINING THE ROLE OF NEUTROPHIL MICROPARTICLES IN AN *IN VIVO* MODEL OF ARTHRITIS

5.1 Microparticles Protect Cartilage *In Vivo*

As microparticles were found to penetrate cartilage matrix in *ex vivo* explants, and protected chondrocytes from IL-1β-induced proteoglycan loss, it was next assessed whether microparticle treatment could protect cartilage in mouse models of arthritis. Again, the cross-reactivity of human microparticles on rodent tissue was relied upon.

5.1.1 Intravenous Microparticle Treatment During K/BxN Arthritis

The K/BxN serum-transfer model of arthritis, which recapitulates the flare phase of human rheumatoid arthritis, is driven by the innate immune cells and displays early onset and high disease penetrance. In-house generated serum was employed, and arthritis experiments carried out using a previously established protocol (Patel, 2010). Mice were injected with 100μl serum on day 0 and day 2 and monitored for signs of arthritis over an 8-day period. All mice developed clinical signs of arthritis (swollen and red digits, pads, wrists or ankles; Figure 5.1.1A and B) with 100% incidence by day 3 (Figure 5.1.1C). Hind paw volume was measured for each individual using water displacement plethysmometry, to determine the extent of swelling (Figure 5.1.1D).

At the peak of arthritis (day 5) mice were treated with 100,000 human TMP intravenously. The clinical scores were similar between groups across the experiment (maximum score was 11 out of 12; Figure 5.1.1A) yet paw oedema was slightly higher in the TMP-treatment group, prior to microparticle treatment, but this difference was not statistically significant at the peak of disease on day 5 (110 ± 31.8 vs. 42.5 ± 18μl; Figure 5.1.1C). These subtle differences between groups before treatment reflects the variability of *in vivo* arthritis studies, even in mice received from the same suppliers and housed in the same room, under the same conditions.

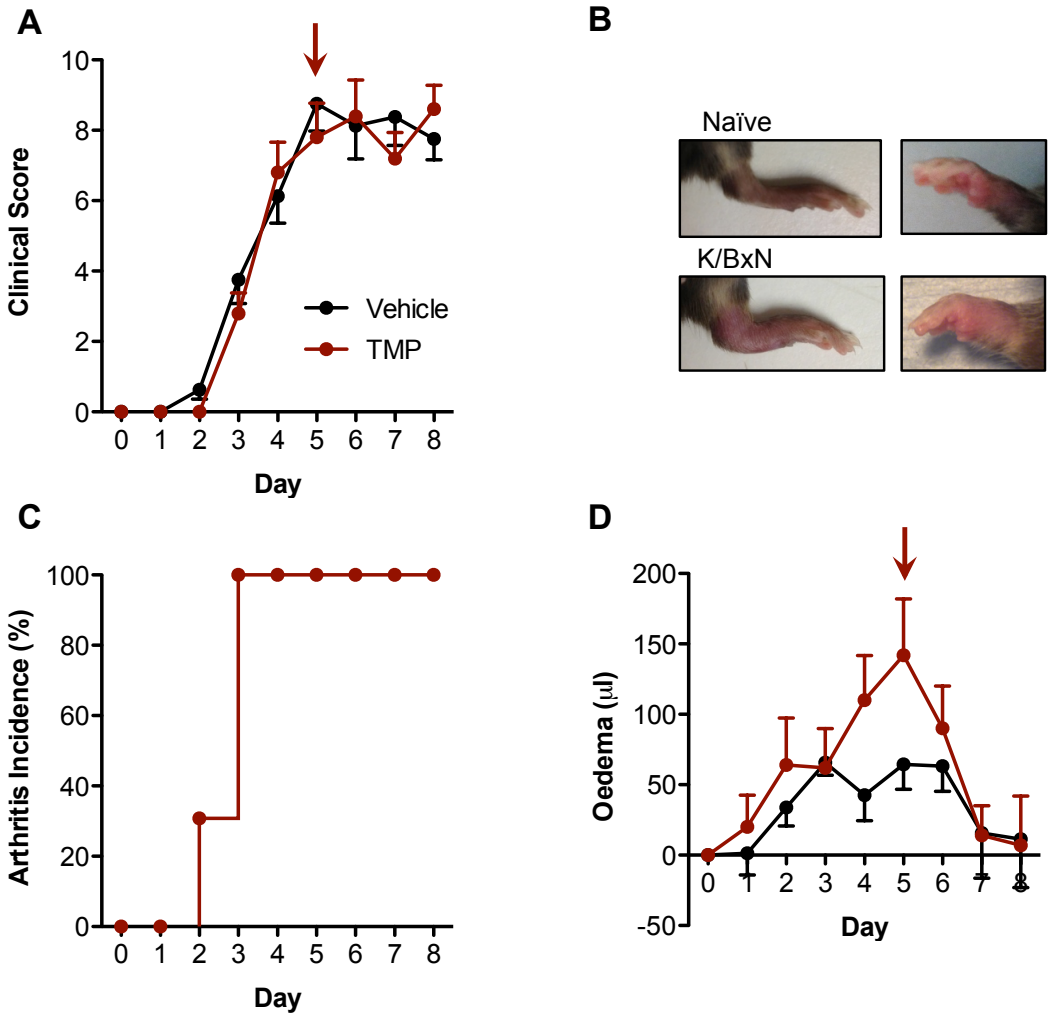

Figure 5.1.1 Disease course of K/BxN serum-transfer arthritis with intravenous microparticle treatment. Eight-week old male C57BL6 mice were administered 100µl K/BxN serum intraperitoneally day 0 and day 2. Eight mice received intravenous saline (200µl) and 5 mice received 100,000 TMP (in 200µl saline) intravenously on day 5 (red arrows). Six naïve mice were used as control. (A) Clinical arthritis score. A swollen wrist, ankle, or any swollen digits on a limb receives a score of 1; a swollen wrist and ankle and any digit on a limb receives a score of 3. All limb scores are combined to generate a score out of a possible 12. (B) Representative photographs of naïve and arthritic fore- and hind-paws, which would receive a score of 3. (C) Incidence of arthritis (a score >1). (D) Hind paw oedema volume as measured by water-displacement plethysmometry. Data shown are mean ± SEM. TMP, TNF-α generated human microparticles.

Following intravenous administration of microparticles there was no significant improvement in the clinical score of the arthritic mice compared to vehicle. Intravenous microparticle treatment did not significantly reduce histological signs of inflammation in the knees compared to vehicle (1 ± 0.5 vs. 4.1 ± 1.4; Figure 5.1.2). This could be due to the number of microparticles, or that they were only administered once during the experiment, leading to sub-optimal numbers of microparticles reaching inflammatory sites.

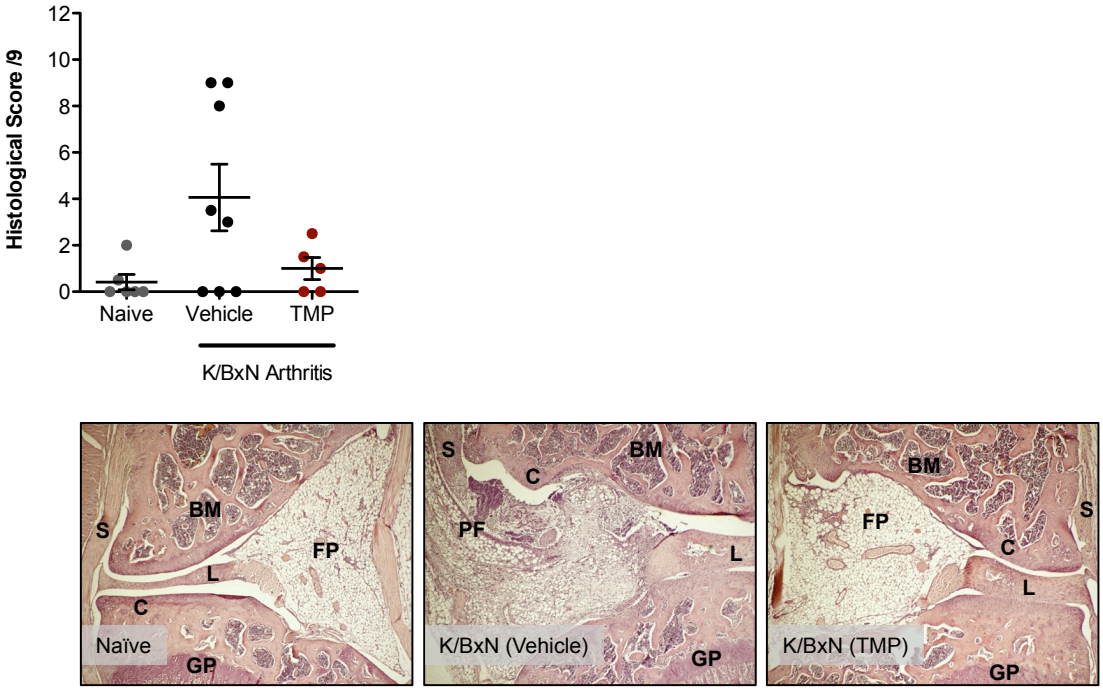

Figure 5.1.2 Intravenous administration of human microparticles had no effect in K/BxN arthritis. Eight-week old male C57BL6 mice were administered 100μl K/BxN serum intraperitoneally day 0 and day 2. Eight K/BxN mice received intravenous saline (200μl) and 5 K/BxN mice received 100,000 TMP (in 200μl saline) intravenously on day 5. Six naïve mice were used as control. Knee joints were collected for histology on day 8. H&E sections were analysed and scored by two blinded scorers. Arthritis severity was scored over three parameters with a possible total score of 3 for each: immune cell infiltration, pannus formation and disruption of cartilage structure (0=none, 1=slight, 2=moderate, 3=severe). Data shown are mean ± SEM from at least 3 separate micrographs from each knee, not significant with One-way ANOVA and Bonferroni post-test. Below are representative micrographs at 4X magnification. TMP, TNF-α generated microparticles; BM, bone marrow; S, synovium; L, ligament; FP, fat pad; C, cartilage; GP, growth plate; PF, pannus formation.

5.1.2 Intra-Articular Administration of Microparticles Protects From *In Vivo* Arthritis Cartilage Damage

Although intravenous administration of microparticles did not reduce histological signs of inflammation in the knees of K/BxN mice, the effect may have been diluted by systemic treatment. Instead, administration of microparticle treatment directly into the knee joint could reveal local effects, and may recapitulate the physiological environment in human rheumatoid arthritis, where neutrophils recruited locally to the joint would generate microparticles that act locally. Furthermore, this system was advantageous in that the contralateral knee joint could serve as an internal control for each individual mouse.

Microparticles were administered intra-articularly on day 3 of a 5-day K/BxN arthritis, before the peak of disease. The anti-inflammatory effect of intra-articular microparticle injection (30,000 human TMP into K/BxN mice) could be observed *in vivo* in live mice by IVIS bioluminescence imaging (Figure 5.1.3). Luminol sodium salt injected intra-peritoneally into mice 10 minutes before imaging is catalysed into a bioluminescent compound by extracellular neutrophil myeloperoxidase released by activated neutrophils upon degranulation. The representative images showed that naïve knees did not give any bioluminescent signal, whether injected intra-articularly with saline (0.8 ± 0.2 $x10^4$ photons/sec) or 30,000 TMP (0.2 ± 0 $x10^4$ photons/sec). Conversely, in arthritic mice discrete bioluminescent signals could be observed within the inflamed joints. In this case, bioluminescence was observed within both forepaws of each mouse, and in individual hind limb digits and/or ankles. In contrast, bioluminescence in the knees of K/BxN mice receiving 30,000 TMP (red arrowheads) were reduced compared to contralateral vehicle injected knees and release fewer photons per second (12.8 ± 5 vs. 31.8 ± 5.8 photons/sec $P<0.01$ with paired two-tailed t-test; black arrowheads). These data suggest local administration of TMP to arthritic joints protects cartilage from degradation and has potent anti-inflammatory affects by reducing neutrophil activation within the joint.

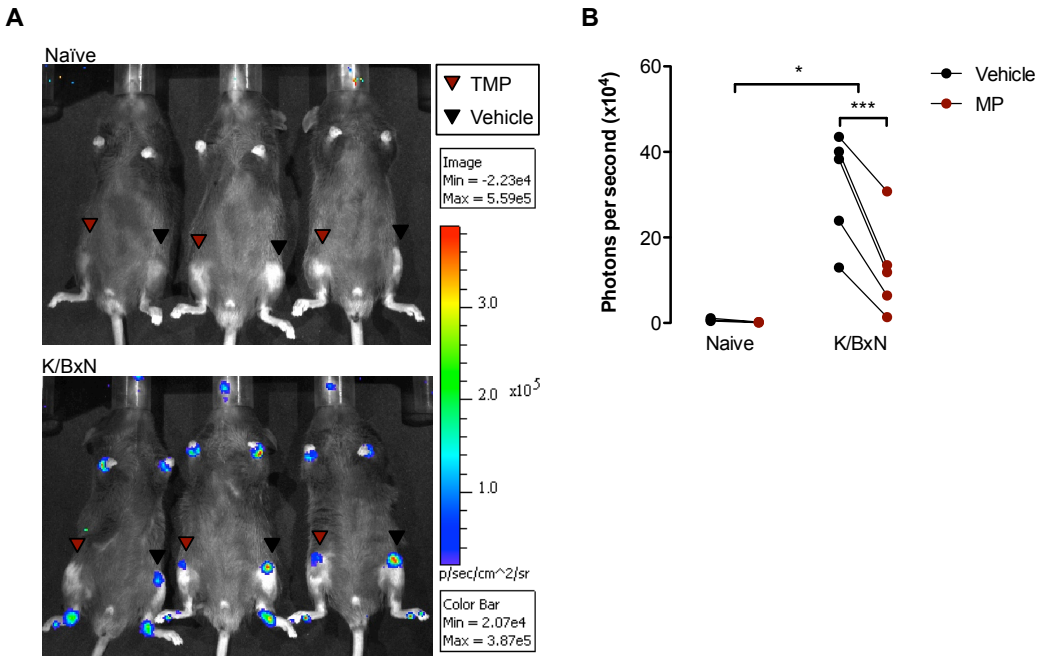

Figure 5.1.3 Live imaging indicates intra-articular administration of human microparticles locally protects from K/BxN serum-induced joint inflammation. Twelve-week old male C57BL6 mice were administered 100μl K/BxN serum intraperitoneally day 0 and day 2. Five K/BxN mice and 3 naïve mice received intra-articular TMP (30,000 in 5μl, right knee) and vehicle (5μl saline, left knee) on day 3. On day 5 mice received luminol (200mg/kg, intraperitoneally) for 10 minutes prior to bioluminescence imaging to visualize activated neutrophil myeloperoxidase activity. **P*<0.05 and ****P*<0.01 with Mixed Model Two-way ANOVA and Bonferroni post-test. Data shown are paired between each mouse. Right shows bioluminescence quantification images. Heat map denotes emission of photons per second. Burgundy arrowheads denote knees that received TMP injection, black arrowheads, vehicle injection. TMP, TNF-α generated human microparticles.

Two doses of microparticles were tested in the following experiment, 10,000 and 30,000 TMP during the onset of arthritis (day 3 of 5 of arthritis). To ensure intra-articular injections did not cause local inflammation, the knees of each mouse were measured using callipers throughout the experiment (Figure 5.1.4). Following intra-articular injection on day 3, a transient but non-significant increase in width was observed across all groups the following day (day 4), which then returned back to knee widths similar to those observed on day 3 by the end-point of the experiment (day 5). Importantly, the knee widths of naïve mice injected with microparticles did not vary significantly from the contralateral knee receiving a sham injection of saline across the time-course (5.6 ± 0.1 vs. 5.7 ± 0.2mm at day 5; Figure 5.1.4A). Similarly, arthritic mice receiving either 10,000 (5.2 ± 0.2 vs. 5.3 ± 0.2mm) or 30,000 microparticles intra-articularly (6.4 ± 0.2 vs. 6.5 ± 0.2mm) did not show any increase of knee width compared to the contralateral knees (Figure 5.1.4B and C). However the accuracy of calliper measurements was questionable, when visible differences in the knee widths could be observed between microparticle and sham-treated knees following post-mortem skin resection (Figure 5.1.4D). Injection of 30,000 TMP into the right knee of naïve mice showed no alteration in post-mortem knee appearance compared to vehicle, but interestingly, it was evident that knees receiving 30,000 TMP in K/BxN arthritic mice were not as grossly swollen as those receiving vehicle injections; and had a more pronounced effect than 10,000 TMP.

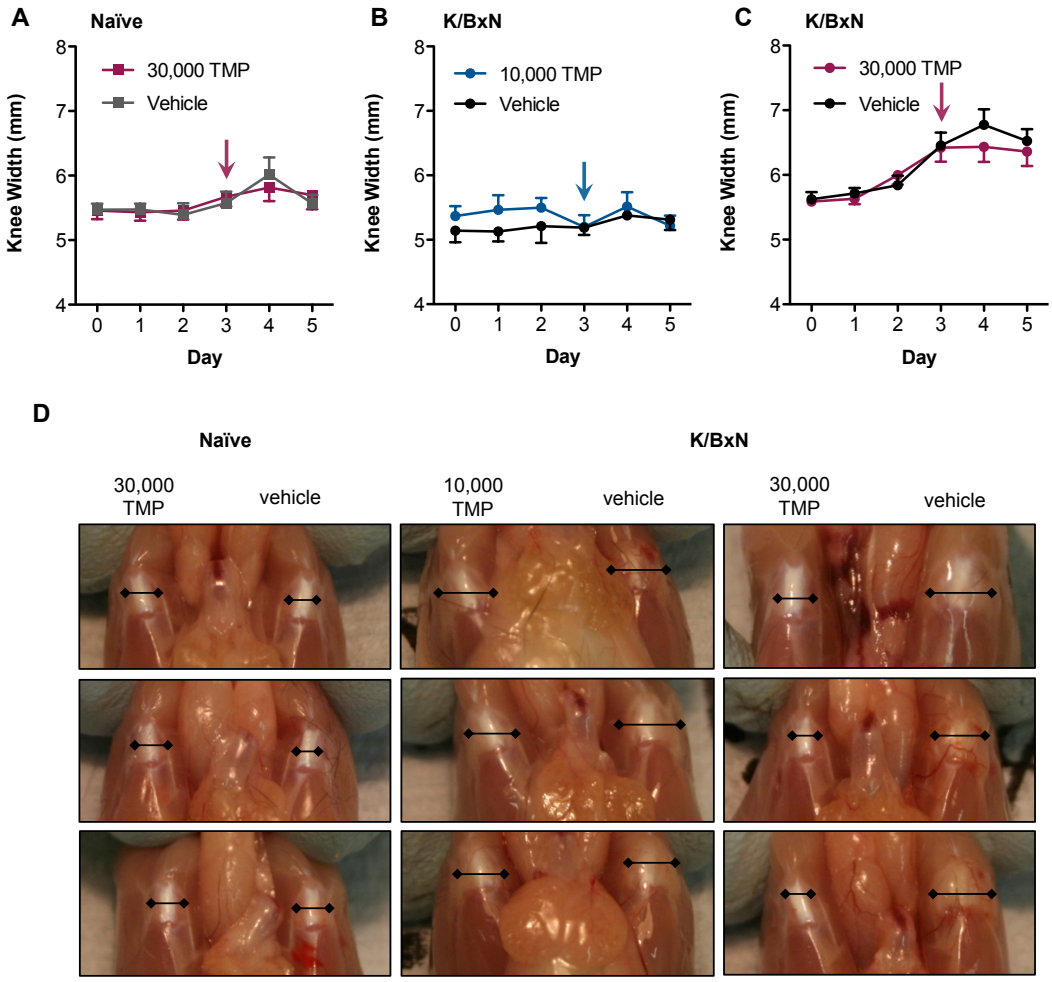

Figure 5.1.4 Calliper measurements of K/BxN serum-transfer arthritis with intra-articular microparticle administration. Twelve-week old male C57BL6 mice were administered 100μl K/BxN serum intraperitoneally day 0 and day 2. Seventeen K/BxN mice and 9 naïve mice received intra-articular TMP (30,000 in 5μl, right knee) and vehicle (5μl saline, left knee); 5 K/BxN mice received intra-articular TMP (10,000 in 5μl, right knee) and vehicle (5μl saline, left knee) on day 3 (coloured arrows). (A) Caliper measurements of naïve mice receiving TMP (30,000) and vehicle. (B) Calliper measurements of K/BxN mice receiving TMP (10,000) and vehicle. (C) Calliper measurements of K/BxN mice receiving TMP (30,000) and vehicle. (D) Representative photographs of knees following post-mortem skin resection, allowing visualisation of the extent of arthritic inflammation. Black bars highlight inflamed tissue margins. Data shown are mean ± SEM, not significant with matched Two-way ANOVA with Bonferroni post-test. TMP, TNF-α generated human microparticles.

Joint inflammation was also assessed histologically by staining with haematoxylin and eosin to measure cellular infiltrate pannus formation and cartilage integrity (Figure 5.1.5). No significant alteration in the histological appearance of knees of naïve mice injected with TMP was observed compared to contralateral vehicle injected knees (1.5 ± 0.6 vs. 1.5 ± 0.6). In contrast, K/BxN mice receiving 30,000 TMP had significantly lower histological scores compared to contralateral vehicle injected knees (2.4 ± 0.9 vs. 6.6 ± 0.7 $P<0.01$ with paired two-tailed t-test).

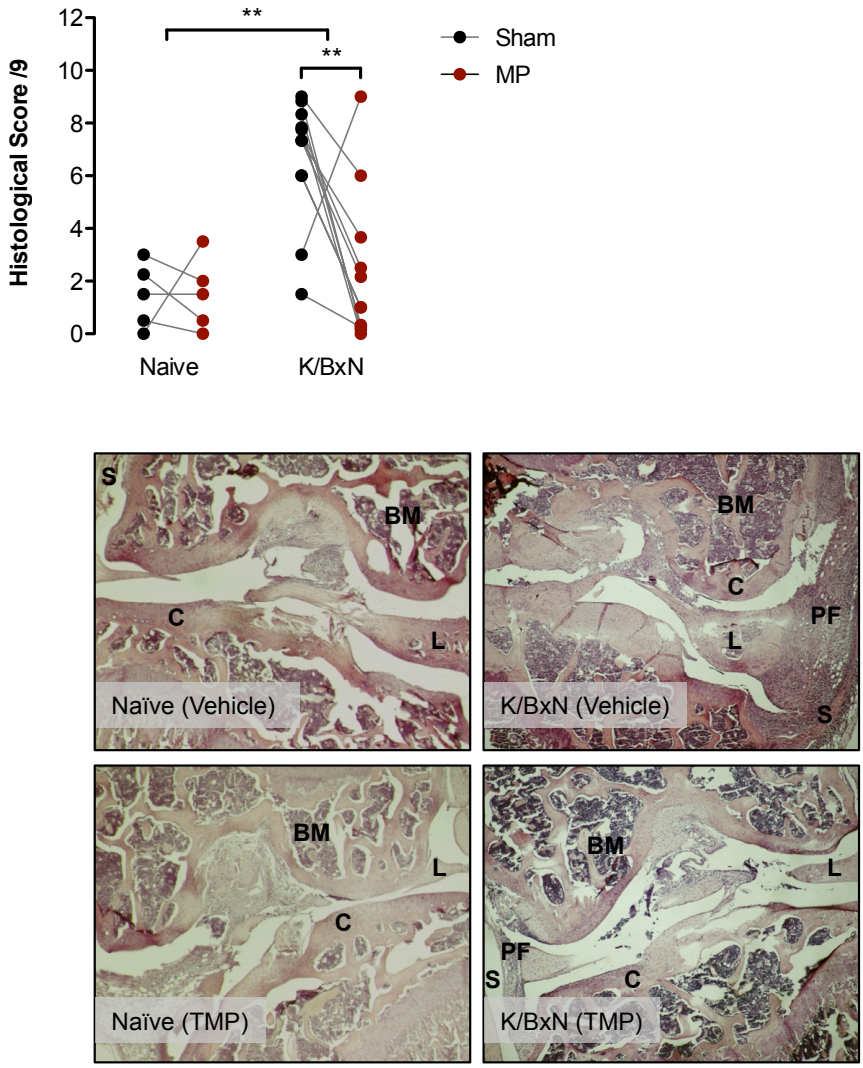

Figure 5.1.5 Intra-articular administration of human microparticles protects from K/BxN serum-induced joint inflammation. Twelve-week old male C57BL6 mice were administered 100μl K/BxN serum intraperitoneally day 0 and day 2. Eleven K/BxN mice and 5 naïve mice received intra-articular TMP (30,000 in 5μl, right knee) and vehicle (5μl saline, left knee) on day 3. Knee joints were collected for histology on day 5. H&E sections were analysed and scored by two blinded scorers. Arthritis severity was scored over three parameters with a possible total score of 3 for each: immune cell infiltration, pannus formation and disruption of cartilage structure (0=none, 1=slight, 2=moderate, 3=severe). Data shown are mean from at least 3 separate micrographs from each knee, paired to contralateral joint in each mouse. Below are representative micrographs at 4X magnification. $**P<0.01$ using Mixed Model Two-way ANOVA with Bonferroni post-test. TMP, TNF-α generated human microparticles, BM, bone marrow; S, synovium; L, ligament; C, cartilage; GP, growth plate; PF, pannus formation.

Cartilage integrity was also assessed using toluidine blue. In naïve mice no change in proteoglycan content was noted with intra-articular injections of either TMP or vehicle (82.4 ± 4 vs. 81.1 ± 3.2%). In K/BxN mice receiving 30,000 TMP had significantly higher cartilage integrity as shown by percentage area Toluidine blue positive, compared to contralateral vehicle-injected controls (78.5 ± 3.1 vs. 55.1 ± 3.2% $P<0.001$ with paired two-tailed t-test; Figure 5.1.6). This suggests that neutrophil microparticles, when injected locally into arthritic joints have both anti-inflammatory (i.e. reduce the recruitment of inflammatory cells and associated swelling and damage) and cartilage-protective effects.

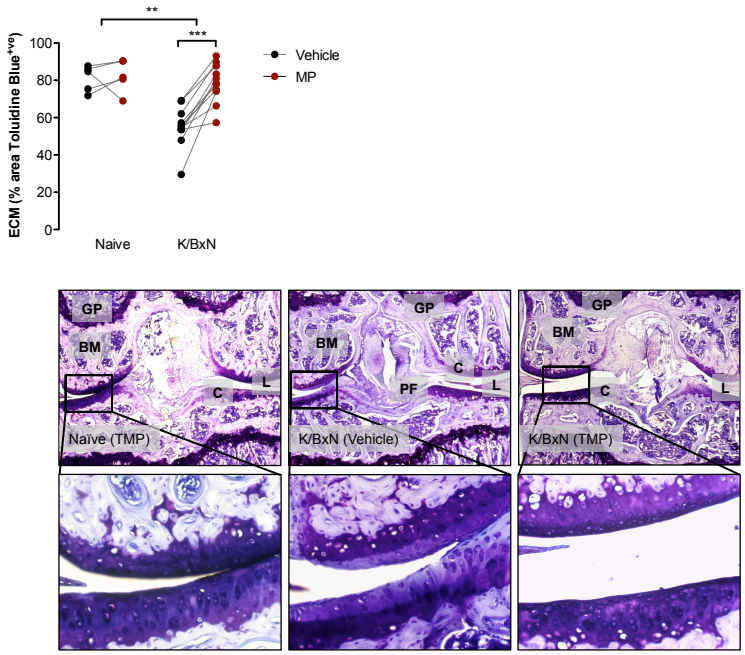

Figure 5.1.6 Intra-articular administration of human microparticles protects from K/BxN serum-induced cartilage extracellular matrix integrity loss. Twelve-week old male C57BL6 mice were administered 100μl K/BxN serum intraperitoneally day 0 and day 2. Eleven K/BxN mice and 5 naïve mice received intra-articular TMP (30,000 in 5μl, right knee) and vehicle (5μl saline, left knee) on day 3. Knee joints were collected for histology on day 5. Toluidine blue stained sections were analysed using ImageJ to determine extracellular matrix integrity. Data shown are percentage area of articular cartilage staining positively for Toluidine blue, quantified from at least six 20X magnification micrographs per section of 3 sections from each knee, paired to contralateral joint in each mouse. Below are representative micrographs at 4X and 20X magnification. **$<P<0.01$ and ***$P<0.001$ using Mixed Model Two-way ANOVA with Bonferroni post-test. TMP, TNF-α generated human microparticles; ECM, extracellular matrix; BM, bone marrow; S, synovium; L, ligament; C, cartilage; GP, growth plate; PF, pannus formation.

To investigate the potential mechanism behind the chondroprotective effects observed with intra-articular injection of microparticles into arthritic mice, RNA was extracted from paraffin embedded sections and reverse transcribed for RT-PCR (Figure 5.1.7). Although no significant *P* values were obtained, 4 out of 5 K/BxN knee samples displayed an increase in *Col2a1* expression compared to their contralateral vehicle-injected knee. On the other hand, inflammation-associated genes often appeared somewhat elevated in TMP-treated knees at this time-point.

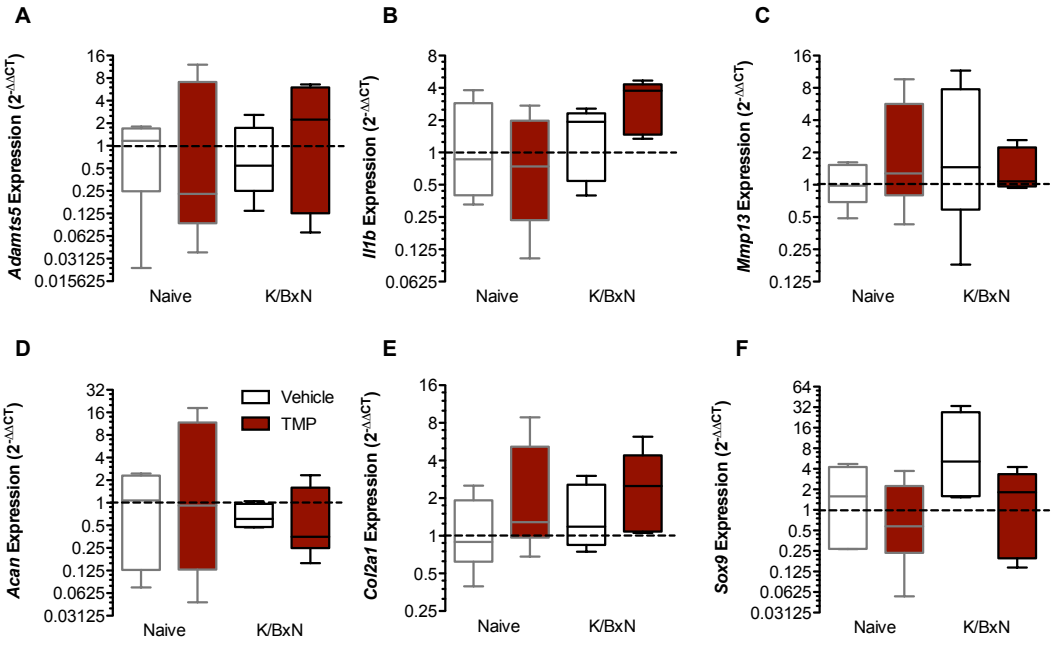

Figure 5.1.7 Intra-articular administration of human microparticles modulates mRNA expression associated with K/BxN serum-induced arthritis. Twelve-week old male C57BL6 mice were administered 100μl K/BxN serum intraperitoneally day 0 and day 2. Five K/BxN mice and 5 naïve mice received intra-articular TMP (30,000 in 5μl, right knee) and vehicle (5μl saline, left knee) on day 3. Knee joints were collected for histology on day 5. RNA was extracted from paraffin embedded sections using a commercially available kit before RT-PCR. Relative expression of pro-arthritic (A) *Adamts5*, (B) *Il1b* and (C) *Mmp13* mRNA. Relative expression of pro-anabolic (D) *Acan*, (E) *Col2a1* and (F) *Sox9* mRNA. Data shown are $2^{-\Delta\Delta CT}$ with vehicle-injected knee as calibrator and *Rpl32* as housekeeping gene, and shown as median, interquartile range and range, not significant with Two-way ANOVA and Bonferroni post-test of logged data. TMP, TNF-α generated human microparticles.

In summary, administration of microparticles intra-articularly, but not systemically, can protect the cartilage during a model of inflammatory arthritis. This protection could be monitored in live mice using bioluminescence imaging, which detects inflammatory neutrophil activity and was reduced in the knees treated with microparticles. Furthermore, these microparticles exerted both anti-inflammatory and cartilage protective effects, as observed during histological analysis. Alterations in gene expression profiles were inconclusive and require further investigation.

5.1.3 Pharmacological Antagonism of *Fpr2/3* Reduces the Chondroprotective and Anti-Inflammatory Efficacy of Neutrophil Microparticles in K/BxN Arthritis

Next I sought to determine whether the *in vivo* protection delivered by neutrophil microparticles was mediated via Fpr2/3, as observed in both *in vitro* and *ex vivo* investigations. In order to achieve this, K/BxN mice received WRW_4 (an Fpr2/3 specific inhibitor) intra-articularly together with TMP. A control group of mice received WRW_4 alone with contralateral injection of PBS to determine whether Fpr2/3 antagonism itself induced changes in inflammation and/or cartilage integrity.

From examination of skin-resected knees it was possible to tell macroscopically that knees injected with TMP plus WRW_4 had increased swelling compared to the contralateral knees injected with TMP alone. This loss in protection could also be observed microscopically using H&E staining (Figure 5.1.8).

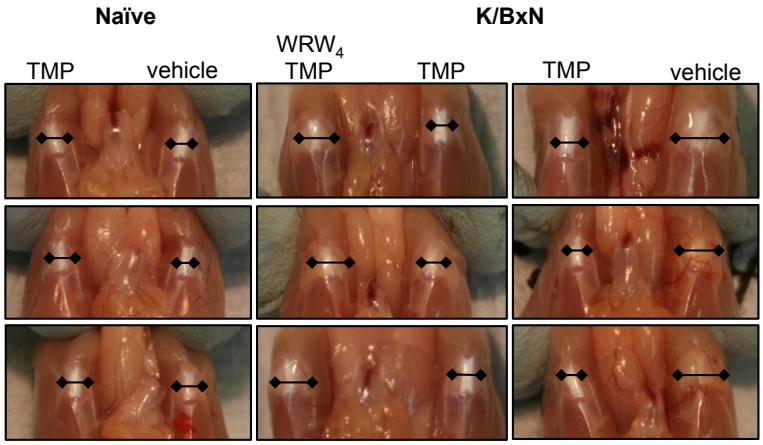

Figure 5.1.8 Description of K/BxN serum-transfer arthritis with intra-articular microparticle administration with *Fpr2/3* antagonism. Twelve-week old male C57BL6 mice were administered 100μl K/BxN serum intraperitoneally day 0 and day 2. Naïve mice received intra-articular TMP (30,000 in 5μl, right knee) and vehicle (5μl saline, left knee); K/BxN mice received intra-articular TMP (30,000, left knee) and WRW_4 (10μM) plus TMP (30,000 in 5μl, right knee); or TMP (30,000 in 5μl, right knee) and vehicle (5μl saline, left knee). Representative photographs of knees following post-mortem skin resection, allowing visualisation of the extent of arthritic inflammation. Black bars highlight inflamed tissue margins.

Paired analysis of histological sections indicated that administration of WRW_4 to naïve mice did not induce changes in histological score compared to vehicle injection (5.5 ± 2.5 vs. 4.5 ± 1.5). Administration of TMP significantly decreased clinical score compared with vehicle injection as observed previously, yet the microparticle anti-inflammatory protection was lost upon co-administration of WRW_4 (scores of 5.5 ± 1.3 vs. 1.3 ± 0.4; Figure 5.1.9).

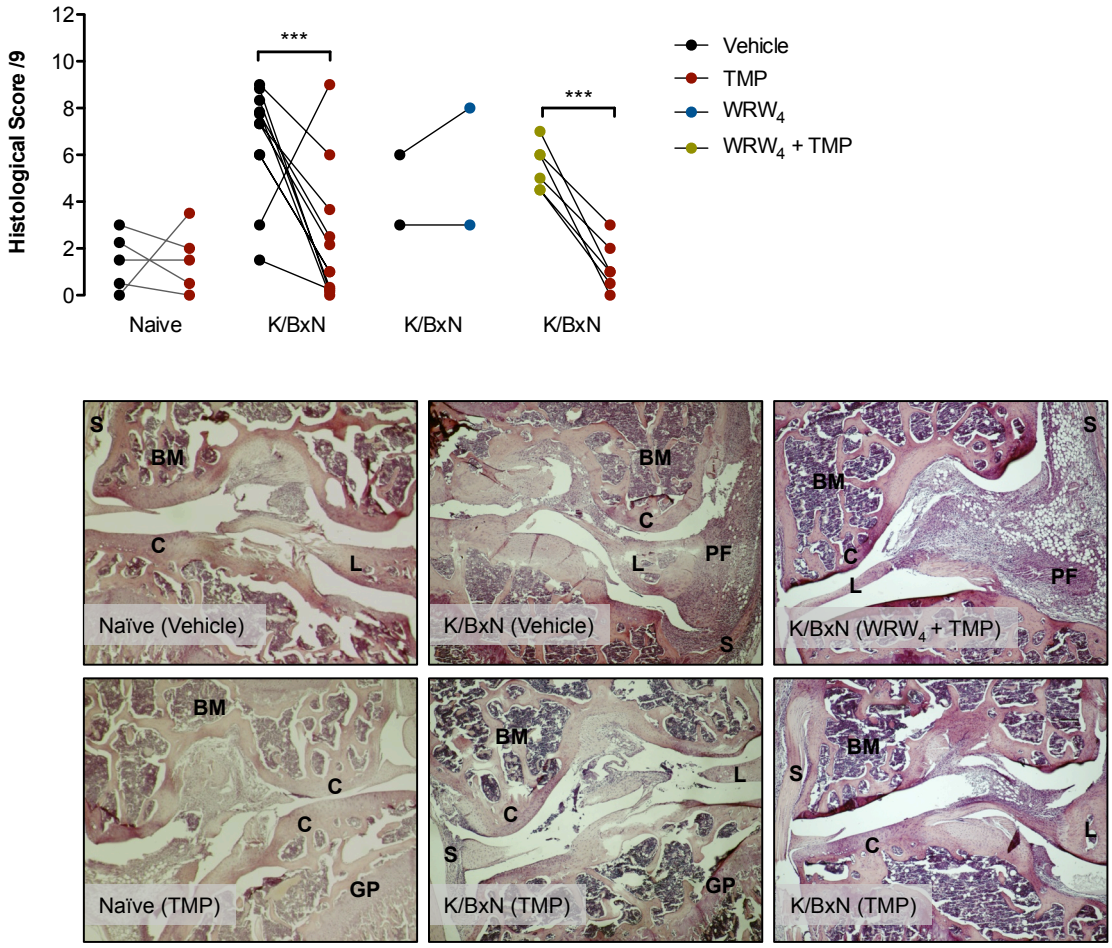

Figure 5.1.9 Pharmacological antagonism of Fpr2/3 with WRW_4 blocks microparticle protection in K/BxN serum-induced joint inflammation. Twelve-week old male C57BL6 mice were administered 100μl K/BxN serum intraperitoneally day 0 and day 2. Six K/BxN mice received intra-articular WRW_4 (10μM in 5μl) plus TMP (30,000, right knee) and TMP alone (30,000 in 5μl, left knee); 2 K/BxN mice received intra-articular WRW_4 (10μM in 5 μl, right knee) and vehicle (5μl saline, left knee). These were compared to naïve and K/BxN mice that received TMP (30,000 in 5μl, right knee) and vehicle (5μl saline, left knee) on day 3 in a parallel experiment. Knee joints were collected for histology on day 5. H&E sections were analysed and scored by two blinded scorers. Arthritis severity was scored over three parameters with a possible total score of 3 for each: immune cell infiltration, pannus formation and disruption of cartilage structure (0=none, 1=slight, 2=moderate, 3=severe). Data shown are mean from at least 3 separate micrographs from each knee, paired to contralateral joint in each mouse. Below are representative micrographs at 4X magnification ***P<0.001 using Mixed Model ANOVA with Bonferroni post-tests. TMP, TNF-α generated human microparticles; BM, bone marrow; S, synovium; L, ligament; C, cartilage; GP, growth plate; PF, pannus formation.

Furthermore, antagonism of Fpr2/3 using co-administration of WRW_4 with microparticles led to a significant decrease in proteoglycan staining by Toluidine blue compared to microparticle treatment alone (64.7 ± 3.8 vs. 82.6 ± 4.3 $P<0.05$ with paired two-tailed t-test; Figure 5.1.10).

Together, these data suggest that both the anti-inflammatory effects of microparticles and the chondroprotective action of this treatment requires Fpr2/3.

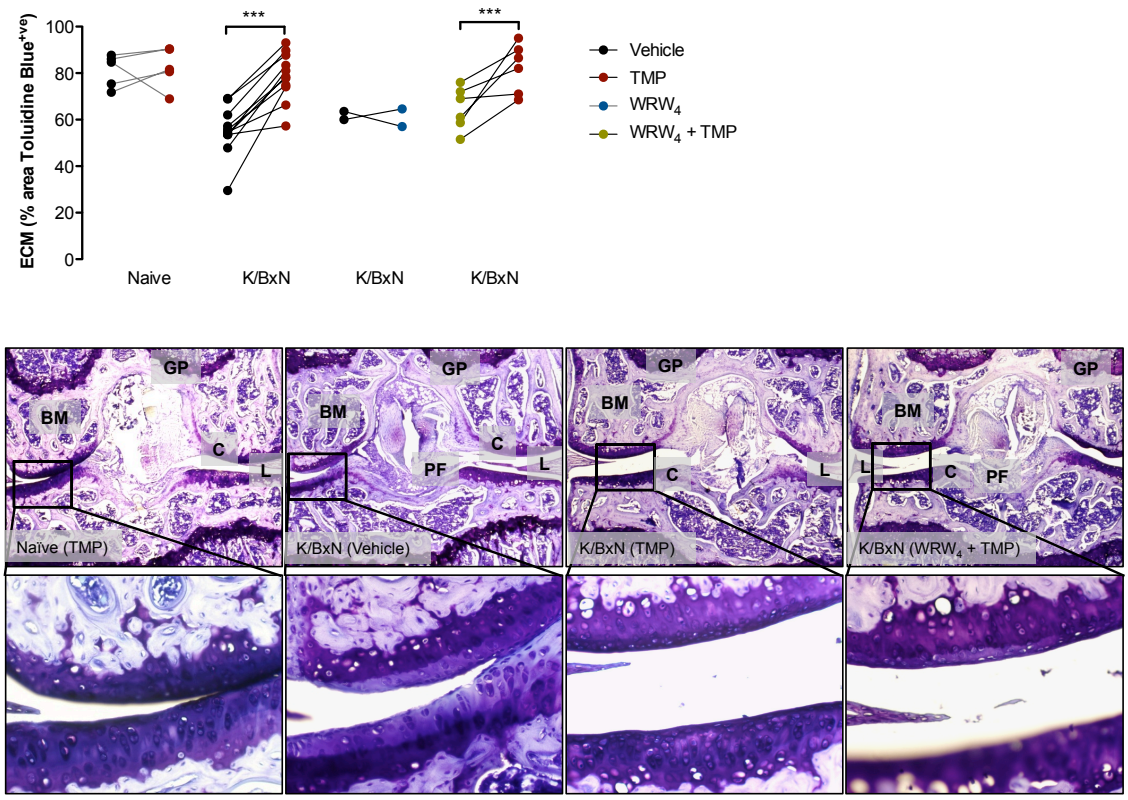

Figure 5.1.10 Pharmacological antagonism of Fpr2/3 with WRW_4 inhibits microparticle protection from K/BxN serum-induced cartilage extracellular matrix integrity loss. Twelve-week old male C57BL6 mice were administered 100μl K/BxN serum intraperitoneally day 0 and day 2. Six K/BxN mice received intra-articular WRW_4 (10μM in 5μl) plus TMP (30,000, right knee) and TMP alone (30,000 in 5μl, left knee); 2 K/BxN mice received intra-articular WRW_4 (10μM in 5 μl, right knee) and vehicle (5μl saline, left knee). These were compared to naïve and K/BxN mice that received TMP (30,000 in 5μl, right knee) and vehicle (5μl saline, left knee) on day 3 in a parallel experiment. Knee joints were collected for histology on day 5. Toluidine blue stained sections were analysed using ImageJ to determine extracellular matrix integrity. Data shown are percentage area of articular cartilage staining positively for Toluidine blue, quantified from at least six 20X magnification micrographs per section of 3 sections from each knee, paired to contralateral joint in each mouse. Below are representative micrographs at 4X and 20X magnification ***$P<0.001$ using Mixed Model ANOVA with Bonferroni post-tests. TMP, TNF-α generated human microparticles; ECM, extracellular matrix; BM, bone marrow; S, synovium; L, ligament; C, cartilage; GP, growth plate; PF, pannus formation.

5.1.4 Microparticles Do Not Protect *Fpr2/3* Null Mice from K/BxN Arthritis

For further characterisation of the requirement of the Fpr2/3 receptor in the microparticle-induced chondroprotection, K/BxN arthritogenic serum was administered to *Fpr2/3* mice, that were then monitored for alterations in disease activity, cellular infiltration and cartilage integrity. Arthritis in Fpr2/3 mice reached 100% incidence by day 2 (Figure 5.1.11A). Weight loss was significantly greater than naïve *Fpr2/3* null mice only by day 5 (-8.9 ± 1 vs. -0.5 ± 0.4% $P<0.05$ with Two-way ANOVA and Bonferroni post-test; Figure 5.1.11B) and clinical score was not different from wild type mice on day 5 (9.2 ± 0.7 vs. 10 ± 0.4; Figure 5.1.11C). Paw oedema was also not significantly different from naïve *Fpr2/3* null mice (32 ± 9 vs. -6.7 ± 9.3μl) or wild type K/BxN arthritic mice on day 5 (32 ± 9 vs. 68.2 ± 13.5μl; Figure 5.1.11D).

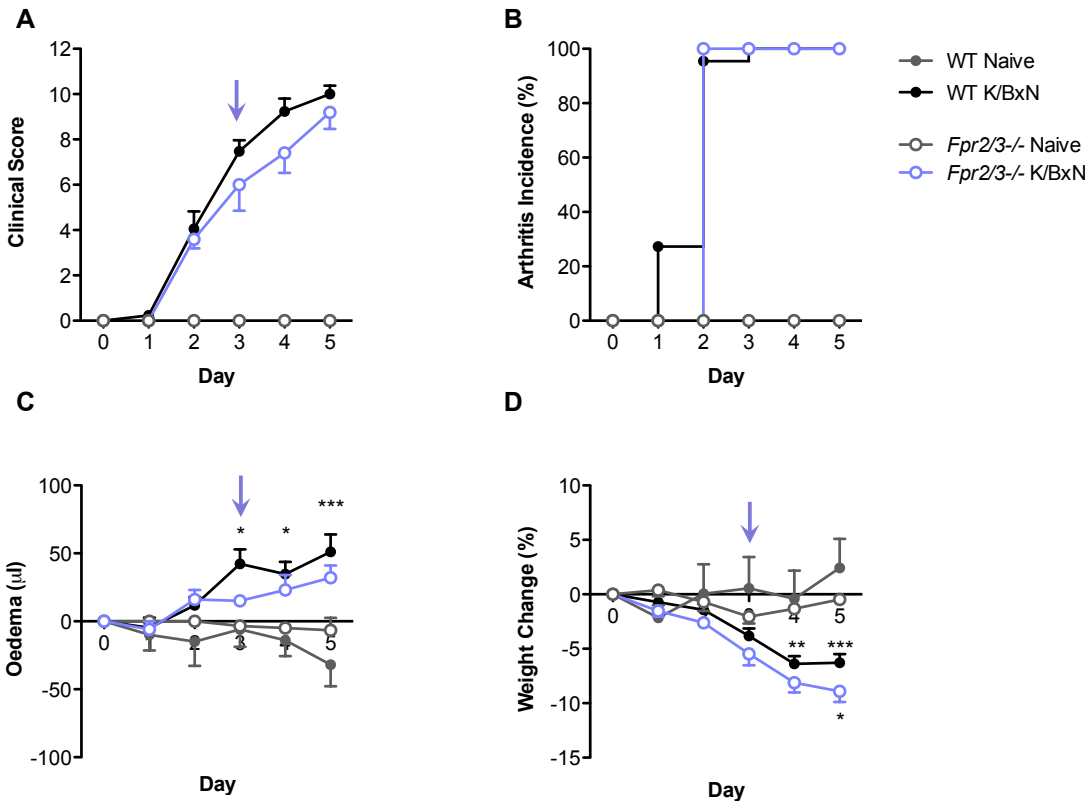

Figure 5.1.11 Description of K/BxN serum-transfer arthritis in wild type and *Fpr2/3* null mice with intra-articular microparticle administration. Twelve-week old male C57BL6 wild type and *Fpr2/3*$^{-/-}$ mice were administered 100µl K/BxN serum intraperitoneally day 0 and day 2 of arthritis. Five K/BxN *Fpr2/3*$^{-/-}$ mice and 3 naïve *Fpr2/3*$^{-/-}$ mice received intra-articular TMP (30,000 in 5µl, right knee) and vehicle (5µl saline, left knee) on day 3 (lilac arrows) and were compared to wild type mice receiving the same treatment in a parallel experiment. (A) Clinical arthritis score. A swollen wrist, ankle, or any swollen digits on a limb receives a score of 1; a swollen wrist and ankle and any digit on a limb receives a score of 3. All limb scores are combined to generate a score out of a possible 12. (B) Incidence of arthritis (a score >1). (C) Paw oedema as measured by water-displacement plethysmometry. (D) Weight change as percentage change from baseline over the course of the experiment. Data shown are mean ± SEM. **P*<0.05, ***P*<0.01 and ****P*<0.001 vs. control of the same genotype using matched Two-way ANOVA with Bonferroni post-test. TMP, TNF-α generated human microparticles.

Caliper measurements were taken daily in naïve and arthritic Fpr2/3 null mice from day 0 to day 5. Measurements were not significantly different between TMP-injected or sham-injected knees in either naïve (5.1 ± 0.1 vs. 5.8 ± 0mm) or K/BxN *Fpr2/3* mice (6.9 ± 0.3 vs. 6.4 ± 0.2mm; Figure 5.1.12). Inspection of skin resected knees post-mortem revealed no observable swelling in naïve mice. Following administration of K/BxN serum, significant swelling was observed as indicated by increased joint margins (black lines) yet no gross morphological differences were seen between vehicle and TMP treated knees. This suggests that microparticles do not provide any protection from macroscopic signs of inflammation in Fpr2/3 null mice.

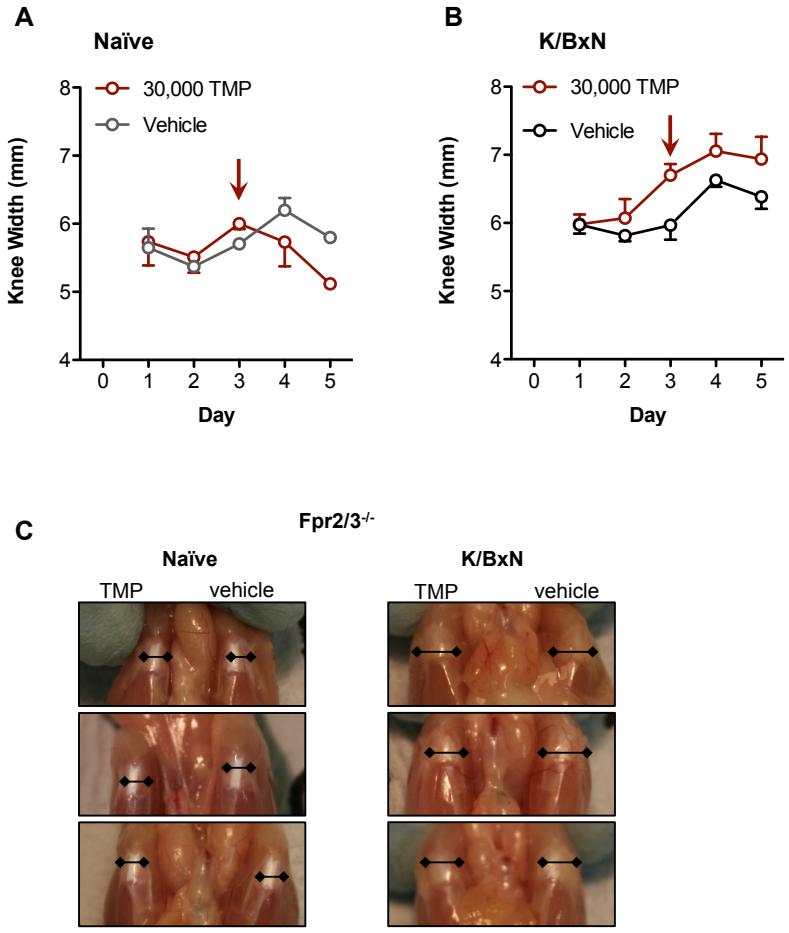

Figure 5.1.12 Caliper measurements of K/BxN serum-transfer arthritis in *Fpr2/3* null mice with intra-articular microparticle administration. Twelve-week old male C57BL6 wild type and *Fpr2/3*$^{-/-}$ mice were administered 100µl K/BxN serum intraperitoneally day 0 and day 2. Five K/BxN *Fpr2/3*$^{-/-}$ mice and 3 naïve *Fpr2/3*$^{-/-}$ mice received intra-articular TMP (30,000 in 5µl, right knee) and vehicle (5µl saline, left knee) on day 3 (red arrows). (A) Calliper measurements of naïve mice receiving TMP (30,000) and vehicle intra articular injections. (B) Calliper measurements of K/BxN mice receiving TMP (30,000) and vehicle. (C) Representative photographs of knees following post-mortem skin resection, allowing visualisation of the extent of arthritic inflammation. Black bars highlight inflamed tissue margins. Data shown are mean ± SEM, not significant with matched Two-way ANOVA and Bonferroni post-test. TMP, TNF-α generated human microparticles.

Similarly, naïve mice showed no histological differences between vehicle and TMP injected knees (1.4 ± 0.6 vs. 1.1 ± 0.2). Microparticle treatment in *Fpr2/3* null mice did not protect from serum-induced histological signs of inflammation (4.8 ± 1 vs. 4 ± 1.4, not significant with paired two-tailed t-test) compared to contralateral vehicle-injected knees (Figure 5.1.13). Therefore, the protection from inflammation afforded by microparticle treatment is lost in Fpr2/3 knockout mice.

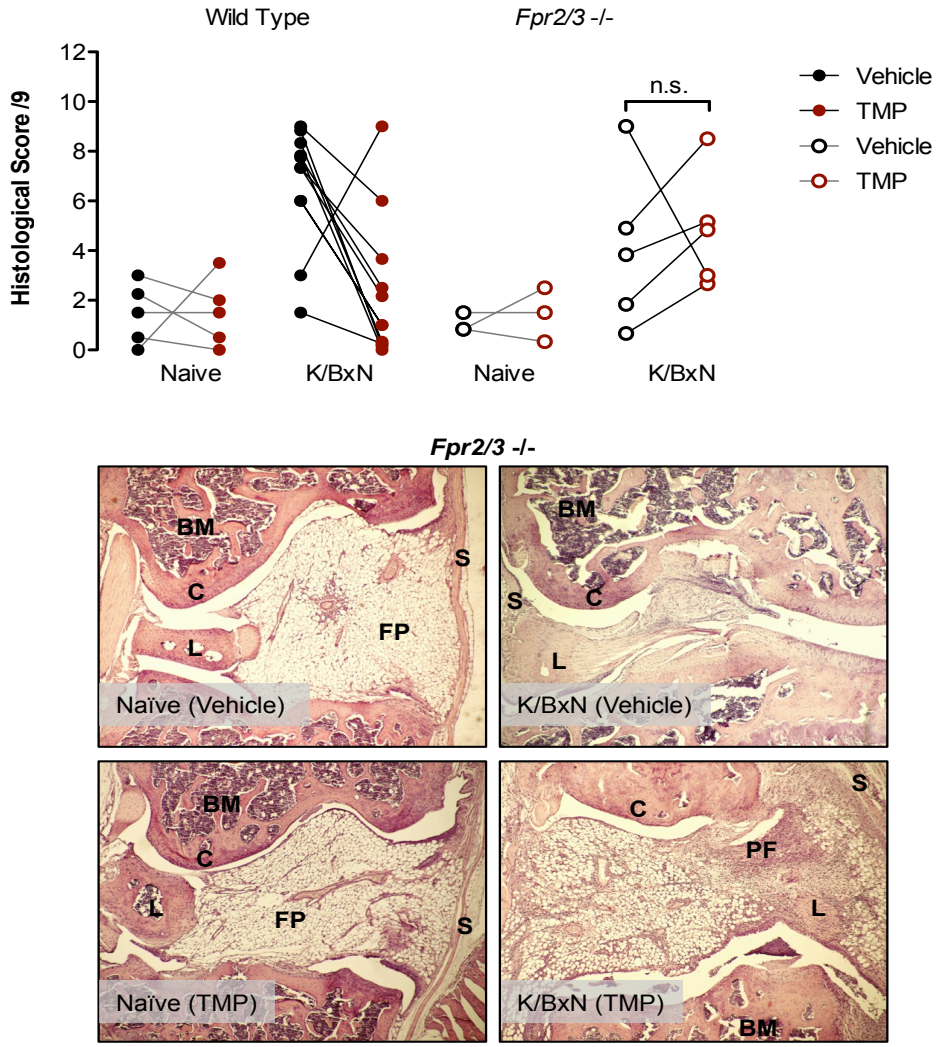

Figure 5.1.13 Intra-articular administration of human microparticles does not protect from K/BxN serum-induced joint inflammation in *Fpr2/3* null mice. Twelve-week old male C57BL6 wild type and *Fpr2/3*$^{-/-}$ mice were administered 100µl K/BxN serum intraperitoneally day 0 and day 2. Five K/BxN *Fpr2/3*$^{-/-}$ mice and 3 naïve *Fpr2/3*$^{-/-}$ mice received intra-articular TMP (30,000 in 5µl, right knee) and vehicle (5µl saline, left knee) on day 3 and were compared to wild type mice receiving the same treatment in a parallel experiment. Knee joints were collected for histology on day 5. H&E sections were analysed and scored by two blinded scorers. Arthritis severity was scored over three parameters with a possible total score of 3 for each: immune cell infiltration, pannus formation and disruption of cartilage structure (0=none, 1=slight, 2=moderate, 3=severe). Data shown are mean from at least 3 separate micrographs from each knee, paired to contralateral joint in each mouse. Below are representative micrographs at 4X magnification. Not significant using Mixed Model ANOVA with Bonferroni post-tests. TMP, TNF-α generated human microparticles; BM, bone marrow; S, synovium; L, ligament; C, cartilage; GP, growth plate; PF, pannus formation; FP, fat pad.

Similarly to wild type naïve mice, no measureable differences between TMP and vehicle injection were observed in naïve Fpr2/3 null mice (83.8 ± 3.7 vs. 82.6 ± 3.3%). Compared with wild type mice, which exhibit marked loss in proteoglycans following administration of K/BxN serum, arthritic Fpr2/3 null mice retained the majority of their proteoglycans as assessed by Toluidine blue staining (76.6 ± 3.5 vs. wild type vehicle injected knee 55 ± 3.2%), even with overt signs of inflammation both clinically, macroscopically and microscopically (Figure 5.1.14). Regardless, TMP treatment in Fpr2/3 null arthritic mice did not rescue this small loss in proteoglycans, no matter how small (70.1 ± 4.6 vs. 76.6 ± 3.5%).

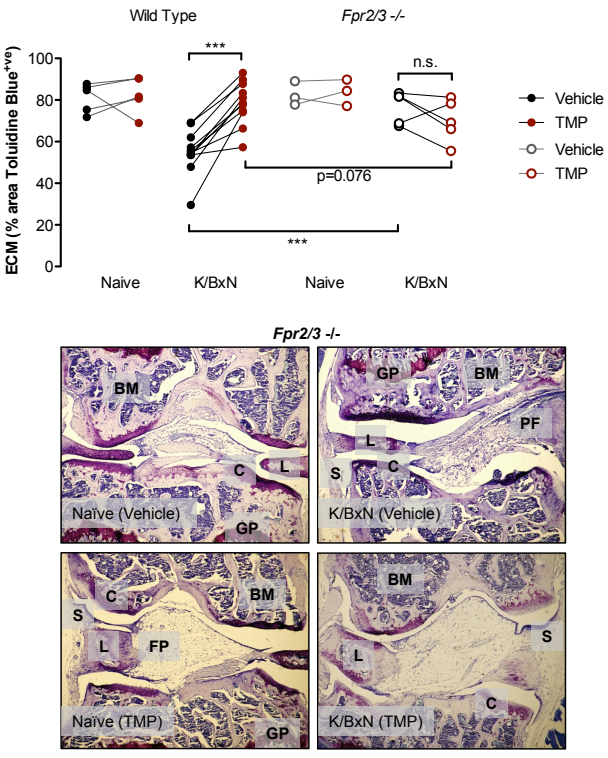

Figure 5.1.14 Intra-articular administration of human microparticles has no effect on extracellular matrix integrity in *Fpr2/3* null mice. Twelve-week old male C57BL6 wild type and *Fpr2/3*$^{-/-}$ mice were administered 100μl K/BxN serum intraperitoneally day 0 and day 2. Five K/BxN *Fpr2/3*$^{-/-}$ mice and 3 naïve *Fpr2/3*$^{-/-}$ mice received intra-articular TMP (30,000 in 5μl, right knee) and vehicle (5μl saline, left knee) on day 3 and were compared to wild type mice receiving the same treatment in a parallel experiment. Knee joints were collected for histology on day 5. Toluidine blue stained sections were analysed using ImageJ to determine extracellular matrix integrity. Data shown are percentage area of articular cartilage staining positively for Toluidine blue, quantified from at least 6 20X magnification micrographs per section of 3 sections from each knee, paired to contralateral joint in each mouse. Below are representative micrographs at 4X and 20X magnification ***P<0.001 using Mixed Model ANOVA with Bonferroni post-tests. TMP, TNF-α generated human microparticles; ECM, extracellular matrix; BM, bone marrow; S, synovium; L, ligament; C, cartilage; GP, growth plate; PF, pannus formation; FP, fat pad.

Taken together, these pharmacological and gene knockout data demonstrate that protection from cartilage loss induced by microparticles requires the expression of *Fpr2/3.* Paradoxically, *Fpr2/3* null mice retained much of their proteoglycans compared to wild type mice. This discrepancy between genotypes cannot be accounted for at this time, and requires further assessment.

5.1.5 Labelled Neutrophils Infiltrate K/BxN Arthritic Joints and Release Microparticles that are Observed to be Abundant Within the Cartilage Matrix and Chondrocytes

I needed to investigate whether microparticle penetration into the cartilage matrix is a phenomenon that occurs physiologically, as this could have important implications for the pathogenesis of rheumatoid arthritis and other cartilage-associated diseases such as osteoarthritis or injury. BODIPY-maleimide labelled mouse neutrophils were adoptively transferred into mice undergoing K/BxN arthritis on day 4, when disease was nearing its peak. Neutrophils were isolated from donor mice via zymosan peritonitis recruitment and labelled with Bodipy-maleimide (2.5μM), prior to intravenous administration into the tail vein into recipient arthritic mice. On day 5, sections from joints were obtained by freezing in OCT medium and cutting using a cryostat with no prior decalcification to preserve tissue-resident fluorescence.

Sections of wrists from naïve and arthritic mice were stained with anti-mouse monoclonal MRP-14 antibodies (red) and visualised with a confocal microscope. Surprisingly, the cartilage of wrists affected by K/BxN serum arthritis displayed abundant double-positive MRP14/Bodipy-maleimide puncta both on the surface of the cartilage, within the matrix, and contained within the chondrocytes (Figure 5.1.15). Microparticle double-fluorescence appeared to reach a certain depth before they accumulated but could not penetrate further; morphological inspection of this border appeared to be the tidemark where articular cartilage meets calcified cartilage; beyond which microparticles were unable to penetrate. Several chondrocytes contained more than one microparticle; others had diffuse staining of one fluorochrome or both, presumably where microparticle up-take had completed and the microparticle dismantled. In contrast, the wrist joint of naïve mice (the same joint visualised as in K/BxN mice) showed no positivity for MRP-14 or Bodipy-maleimide fluorescence indicating that the fluorescent neutrophils did not infiltrate the joint nor produce microparticles that entered the cartilage.

K/BxN Wrist

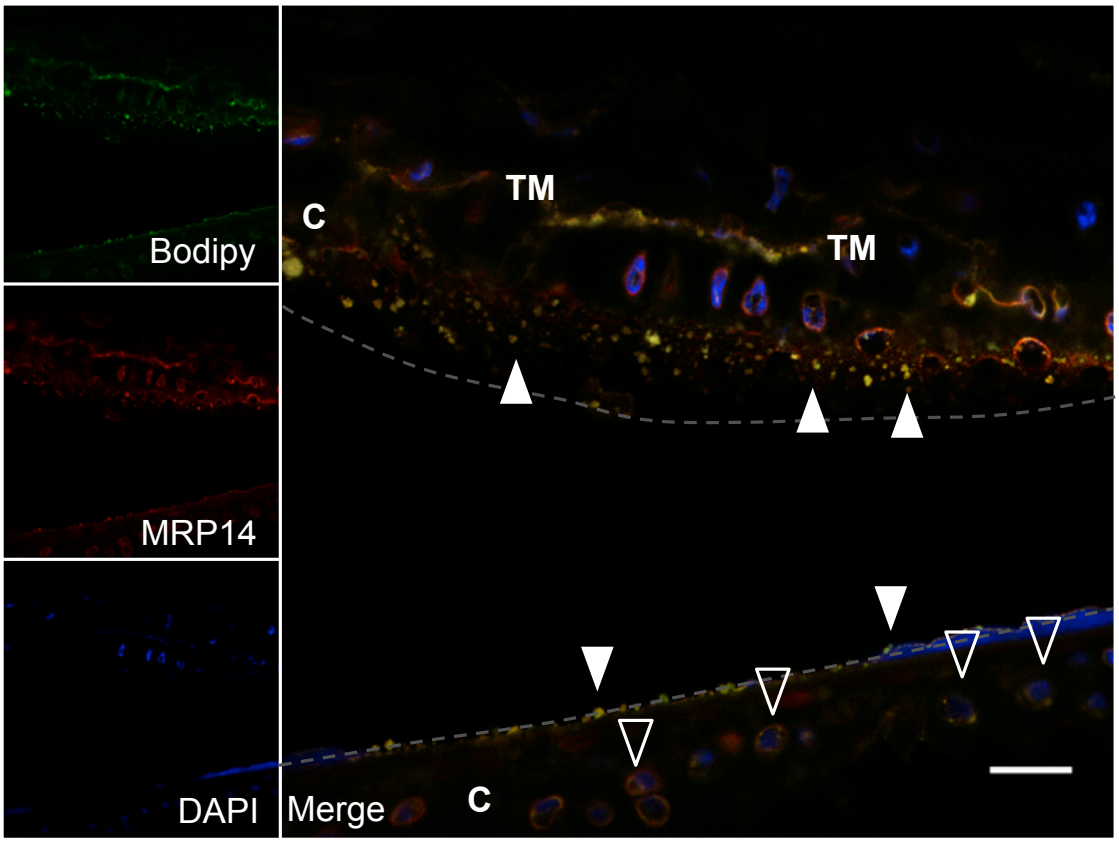

Naïve Wrist

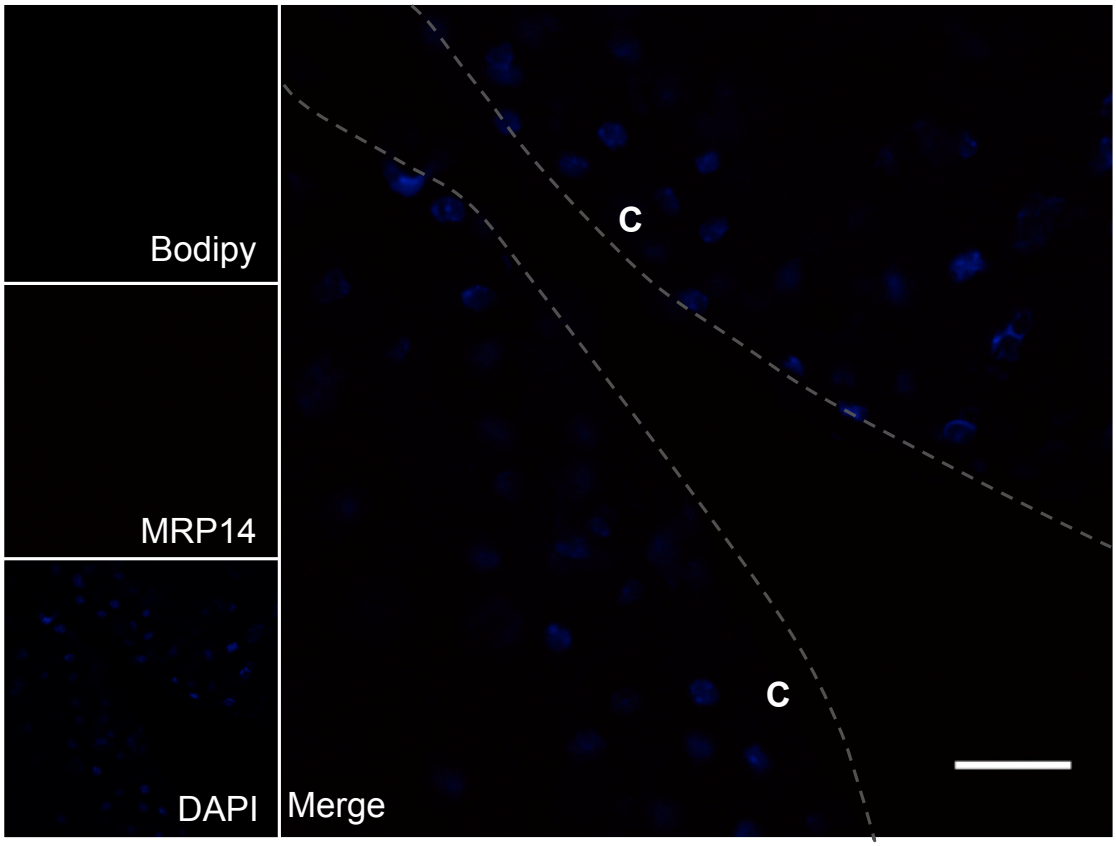

Figure 5.1.15 Adoptively transferred Bodipy-labelled neutrophils infiltrate arthritic joints and release microparticles that penetrate articular cartilage. Twelve-week old male C57BL6 mice were administered 100μl K/BxN serum intra peritoneally day 0 and day 2. Three K/BxN mice and 3 naïve mice received $1x10^6$ Bodipy-maleimide-labelled mouse neutrophils intravenously on day 3 which had been isolated from peritoneal lavages of wild type donor mice administered 1mg/mouse intraperitoneal zymosan from *Saccharomyces* for four hours. Wrist joints were collected into OCT cryo-embedding medium on day 5 and sections cut on a cryostat with no prior decalcification. Sections were stained with anti-mouse monoclonal MRP14 and DAPI prior to confocal microscopy. Grey dotted lines indicate opposing cartilage surface within the wrist, white arrows denote whole double-staining microparticles. Open arrows denote chondrocytes within lacunae containing microparticles. Scale bar denotes 20μm. Left-hand images are from a K/BxN mouse; right-hand images are from a naïve mouse receiving intravenous labelled neutrophils. C, cartilage, TM, tidemark.

In summation, the data generated during these *in vivo* experiments suggest that neutrophils generate microparticles following infiltration to the arthritic joint. The microparticles, rich in Annexin A1, penetrate the cartilage matrix and interact with *Fpr2/3* to induce a cartilage-protective programme, which is especially effective in neutrophilic arthritis such as the K/BxN model.

CHAPTER 6: DISCUSSION OF RESULTS

The aim of this project was to determine the contribution of neutrophil microparticles to the pathogenesis of inflammatory arthritis, as they are abundant in RA synovial fluid. Previous reports have uncovered pro-inflammatory roles for microparticles of platelet (Boilard et al., 2010) and immune-cell origin (Distler et al., 2005a) in the context of animal models of RA. In contrast, microparticles of specifically neutrophil origin exert anti-inflammatory effects (Gasser and Schifferli, 2004, Dalli et al., 2008, Pliyev et al., 2014, Eken et al., 2010). We found that microparticles of neutrophil origin induced a pro-anabolic phenotype in chondrocytes that were stimulated *in vitro* with proinflammatory cytokines relevant to RA (Figure 6.1). Microparticles increased ECM accumulation in chondrocyte micromasses in a dose-dependent manner and inhibited ECM release into the medium. Microparticle treatment up-regulated SOX9 transcription factor required for the expression of cartilage-associated genes; prevented chondrocyte apoptosis and abrogated the release of pro-inflammatory mediators such as IL-8, prostaglandin E_2 and IL-6. The net effect of these events resulted in a pro-anabolic, chondroprotective phenotype. We envisage a mechanism whereby neutrophils infiltrate the arthritic joint and become activated, whereupon they release microparticles, which can efficiently migrate into the cartilage and deliver a cargo of protein and lipids, which reprogram the chondrocyte into an apoptosis-resistant phenotype that produces ECM. For these effects we have shown that microparticle-derived Annexin A1 and its receptor FPR2/ALX play a role in chondroprotection (Figure 6.2).

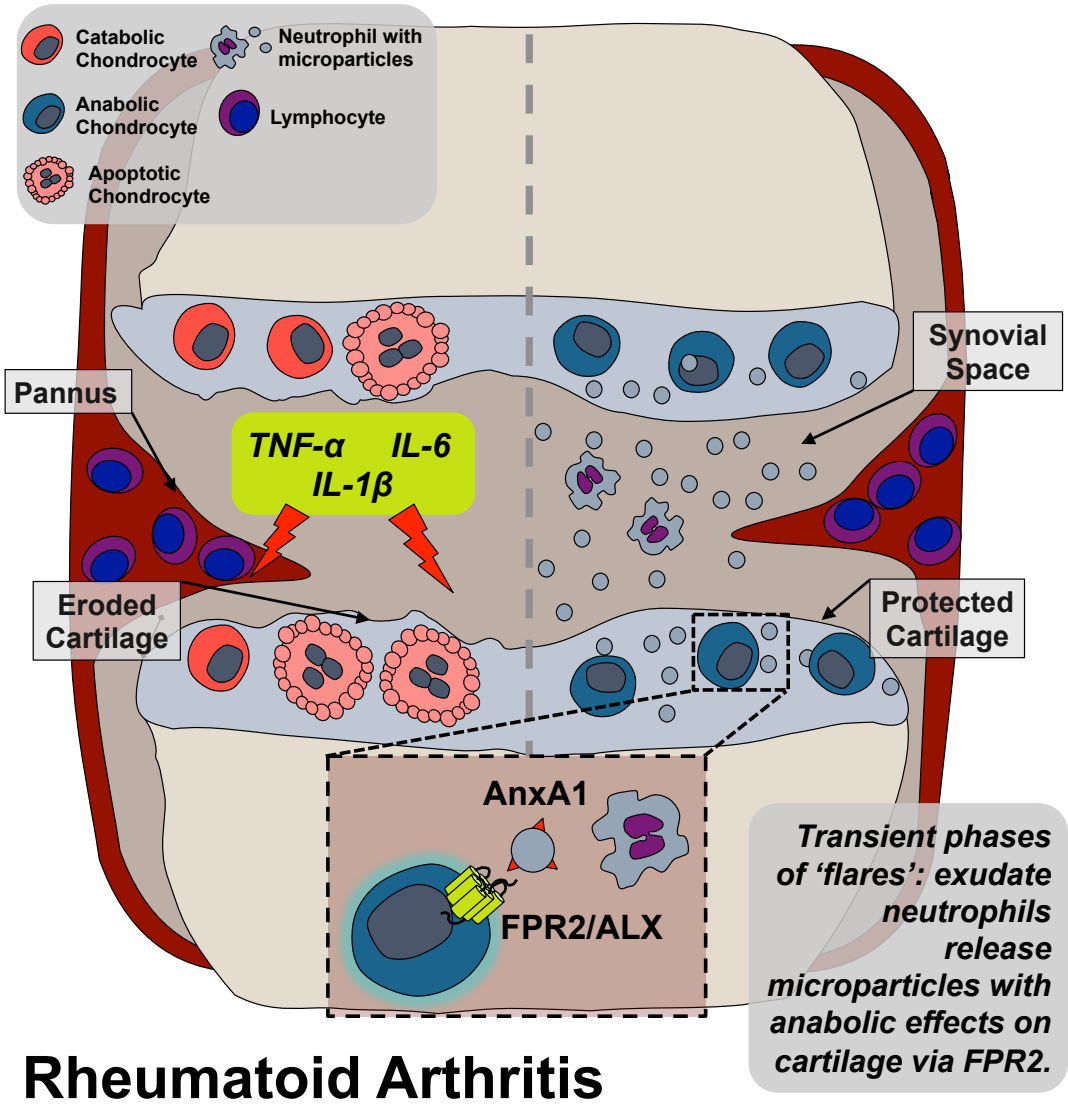

Figure 6.1 Schematic: Microparticles generated from neutrophils protect from cartilage erosion. Neutrophils migrate to the inflamed joint and are activated by inflammatory cytokines. This leads to the release of microparticles, which can migrate into the cartilage, and interact with chondrocytes. Microparticle-associated Annexin A1 ligates FPR2/ALX on the chondrocytes eliciting a chondroprotective program.

The current dogma is that cartilage is an impenetrable, dense, avascular matrix through which metabolites from the synovial fluid must diffuse (La Rocca et al., 2013). These experiments provide the first evidence that microparticles are able to cross this barrier to deliver proteins that have functional effects on the chondrocytes. The communication of chondrocytes with other cell types has not been demonstrated within the cartilage before. Previous reports have detected myeloid related protein 8 (MRP8) in arthritic cartilage (van Lent et al., 2008), and it has been linked to cartilage degradation, but the source of this myeloid protein was not confirmed to be chondrocytes themselves. We propose that MRP8, which is highly expressed by neutrophil microparticles (Dalli et al., 2013) is transferred from neutrophils to chondrocytes via microparticles as demonstrated for Annexin A1. Indeed, application of TMP to mouse femoral head cultures yielded penetration into mid to deep-zone of the cartilage layers. In our confocal analyses both human Annexin A1 and MRP8 were identified within the chondrocyte, together with co-localised immunostaining in an apparent vesicular form, indicating that the microparticles may enter the chondrocyte in their entirety, and then release their content perhaps by fusion with cytosolic elements. Studies with endothelial cells have shown that platelet microparticles are avidly engulfed and remain intact for ≥15 minutes (Dasgupta et al., 2012).

Previous reports have described the presence of several cytoskeletal proteins in neutrophil microparticles, a finding that can underlie their ability to locomote in response to stimulation (Dalli et al., 2013). Chondrocytes produce IL-8 in response to injurious stimuli and supernatants from stimulated chondrocytes are capable of inducing neutrophil chemoattraction, which can be blocked, at least in part, by anti-IL-8 antibodies (Vaamonde-Garcia et al., 2012). Neutrophils are the primary target for IL-8, and they respond with chemotaxis, degranulation and up-regulation of adhesion molecules – classical markers of neutrophil activation (Scapini et al., 2010). Data here provide speculation that IL-8 or formylated proteins released from dying chondrocytes, perhaps in analogy with that reported for damaged liver (McDonald et al., 2010), may provide the chemotactic stimulus required for these microparticles to migrate into the damaged cartilage. The details of this mechanism remain of interest, and will need to be elucidated in future studies. In pathological settings, microparticles may be effective in transporting Annexin A1 to the chondrocytes in view of their ability to migrate (Dalli et al., 2013) and selective tissue-direction may be achieved via specific adhesion molecules. Indeed, neutrophil microparticles express β_2 integrins, which are required for their anti-bacterial properties, along with α_M and β_3 integrins (Timar et al., 2013). Microparticles from other cell types have been shown to express integrins (Kapustin et

al., 2011), which could represent a common microparticle “homing” capability, allowing adhesion to specific cell types.

The stimulant that induces the production of microparticles plays a significant role in shaping the proteome of the offspring microparticles, such that they may serve separate functions. Timar et al. (2013) demonstrated that neutrophils generate elevated levels of microparticles when stimulated with opsonised Staphylococcus aureus, compared to resting neutrophils, but only those generated by this specific opsonised-bacterial stimulus effected anti-microbial properties. Neutrophils stimulated with C5a or fMLP release microparticles that have differing efficacy at reducing IL-8 production in LPS or zymosan-stimulated human macrophages (Gasser and Schifferli, 2004). Neutrophils activated in suspension, or adherent to endothelial cell monolayers, produce microparticles with differential proteomes and exert different functions (Dalli et al., 2013). Here we demonstrate an enrichment of Annexin A1 in TNF-α- and IL-8-derived neutrophil microparticles compared to those produced under resting conditions. Expression levels of ceruloplasmin, α_2-macroglobulin and heat shock protein 70 were also altered whereas MRP8 and 14 remained unchanged. This fortifies the idea that microparticle phenotype is adjusted according to setting and that content loading is prioritized, so that net protein expression is not merely a function of microparticle size or number.

Active content loading requires regulated actin and myosin cytoskeletal reorganisation, as microparticles produced under conditions of cytoskeletal destabilisation lost their protective qualities. Microparticles contain a 3D scaffold similar to that of their parent cells, the composition of which is not altered by agonist stimulation (Latham et al., 2013, Bernimoulin et al., 2009). Data reported here show that neutrophil microparticles stain positively with phalloidin, demonstrating the presence of filamental actin. It is therefore not surprising that microparticle generation was heavily affected by drugs that interfere with F-actin polymerisation. The process of microparticle production and release (vesiculation) requires the dynamic coordination of cellular components for effective destabilisation of the plasma membrane. It has been observed that during microparticle formation in cerebral microvascular endothelial cells, there is dissolution of the cortical F-actin network, followed by prominent actin stress fibre formation, and redistribution of vinculin to the newly formed fibres (Latham et al., 2013). Consistent with these findings, data presented here show that treatment of neutrophils with jasplakinolide, which promotes actin polymerisation and stabilises actin filaments into an amorphous mass, inhibits microparticle release. In contrast, treatment with

cytochalasin D, a potent inhibitor of actin polymerisation, increasing the cellular membrane fluidity, which increases microparticle release. This increase in microparticle shedding was not accompanied by an increase in chondroprotective effects in co-culture however. This suggests that regulated microparticle formation is reliant on the ability of actin to polymerise and depolymerise in a coordinated fashion.

Disrupting the interaction of actin and myosin did not lead to alterations in the number of microparticles shed. Instead, this cytoskeletal machinery may play a role in the orchestrated packing of these microparticles with protective components, as microparticles produced under these conditions also lost their chondroprotective effects. In addition, microparticle release, along with many cellular processes, is calcium-dependent. Intracellular calcium chelation led to blockade of microparticle shedding. Similarly, neutrophils treated with the calcium chelator BAPTA-AM and cultured in transwells over micromasses did not protect chondrocytes from IL-1β-induced damage. Together these data suggest that blockade of microparticle formation, or disrupting the cytoskeleton during vesiculation abrogates the protective ability of these structures, and that the neutrophils themselves are not innately chondroprotective.

Annexin A1 was partially responsible for the chondroprotective effects seen *in vitro*. Although Annexin A1 did not reduce pro-inflammatory mediator release induced by IL-1β or effectively enhance gene expression at a 6-hour time point, abundant extracellular matrix accumulation was observed in micromass culture. Annexin A1 orchestrates the resolution of inflammation by terminating leukocyte recruitment to the site of inflammation, promoting neutrophil apoptosis and efferocytosis by resident macrophages, which favours cell phenotype switching, and activates tissue repair programmes as seen in the context of gut and eye epithelia (Ortega-Gomez et al., 2013, Leoni et al., 2013). The effects of Annexin A1 treatment in chondrocytes have not been previously reported.

Annexin A1 externalisation is mediated primarily by the ATP-binding cassette ABCA1, part of a large group of transporters with varied roles that include the externalization of proteins (Omer et al., 2006). Genetic deletion of ABCA1 reduces microparticle release (Combes et al., 2005). Therefore the Annexin A1 secretion process may occur predominantly within microparticles that are copiously released from activated neutrophils via the ABCA1 transporter. To exert its biological functions Annexin A1 must bind to acid phospholipids in the presence of calcium cations to acquire the active

conformation with extrusion of the N-terminal region (Gerke et al., 2005). Thus microparticles, with their uneven segregation of phosphatidylserine on the outer leaflet (Freyssinet and Toti, 2010) and their dependence on calcium for shedding, may afford both of these fundamental requirements. Exposure of the pharmacophore N-terminal region of Annexin A1 would then allow interaction with its receptor FPR2/ALX (Bena et al., 2012a). In addition, the bivalent activity of annexins may support membrane fusion in the final stages of microparticle formation as they are released from the cell plasma membrane (Gerke et al., 2005, McNeil et al., 2006).

Annexin A1 expression is up-regulated upon neutrophil transmigration (Damazo et al., 2006), thus, neutrophil microparticles are enriched in Annexin A1 following stimulation and in the rheumatoid joint compared to paired plasma samples (manuscript in preparation). Annexin A1 lacks a signal peptide (Gerke et al., 2005) yet it is abundantly found in inflammatory exudates, including RA synovial fluids (Goulding et al., 1995). During models of inflammatory arthritis, such as K/BxN serum transfer, Annexin A1 alone is not sufficient for protection from chondrolysis (Patel et al., 2012). Proteinase 3, released by neutrophils, limits the functionality of Annexin A1 by cleaving it at its N-terminus, rendering it inactive (Vong et al., 2007). The packaging of Annexin A1 inside microparticles may preserve its functionality, making it cleavage resistant and increasing its potency, in analogy to alpha$_2$-macroglobulin loaded microparticles. These microparticles exerted greater increases of survival during a caecal-ligation and puncture model of bacterial sepsis compared to the administration of soluble alpha$_2$-macroglobulin (Dalli et al., 2014). Furthermore, cleavage-resistant Super-Annexin inhibited joint inflammation and preserved the proteoglycan content of the cartilage in this experimental arthritis setting whereas soluble un-modified Annexin A1 treatment was similar to that of vehicle (Patel et al., 2012).

The loading of microparticles with Annexins is calcium-dependent, and increasing concentrations of intracellular calcium recruits increasingly calcium-insensitive Annexins to the plasma membrane in order to protect cells from plasmalemmal injury by creating blebs and pinching off sections of damaged membrane (Potez et al., 2011). Annexin A6, possibly in analogy to Annexin A1 observed in neutrophil-derived microparticles, was expressed on both the outer and inner membrane of the microvesicles (Kapustin et al., 2011). This may account for the higher expression of Annexin A1 in IL-8 derived microparticles by flow cytometric analysis, which only detects surface-associated protein targets, but relatively lower concentrations of Annexin A1 by western blotting compared to TMP. Proportions of the vesicle-

associated annexins however are not removed by treatment with EGTA suggesting a tight calcium-independent incorporation into the plasma membrane (Kapustin et al., 2011), an interesting observation that requires further investigation.

Microparticles bear antigens from their parent cells, allowing phenotypic measurements to be made about their parent cell origin (Ettelaie et al., 2013). The experiments herein have relied heavily upon this as a strategy for corroborating microparticle identity in microscopy analyses. The exposure of phosphatidylserine, a key process in microparticle formation, was also demonstrated (Gasser and Schifferli, 2004). Microparticles contained MRP8, which is unsurprising, as this protein makes up around 40% of the total neutrophil cytosolic protein fraction (Edgeworth et al., 1991, Kerkhoff et al., 1999). Also demonstrated here was the expression of MRP8's non-covalent binding partner, MRP14. Both of these proteins are present within the cytosol of neutrophils (and also circulating monocytes, but not tissue macrophages or lymphocytes), and associate with the cytoskeleton and plasma membrane upon increases in intracellular calcium (Roth et al., 1993), for example during microparticle shedding. Although several reports have demonstrated inflammatory roles of this heterodimeric protein pair, implicating it in the increased expression of complement component C3 (Schonthaler et al., 2013), vascular inflammation and atherosclerotic plaque formation (Croce et al., 2009) and exclusively bind arachidonic acid in human neutrophils (Kerkhoff et al., 1999), MRP8/MRP14 is nevertheless required for efficient chemoattractant-induced calcium signaling (McNeill et al., 2007) and the abundance of the heterodimer in the serum of healthy patients suggests that they do not necessarily play a constitutively active pathological role in health and disease (Vogl et al., 2004). The role of these proteins in RA requires further investigation, especially in terms of expression via microparticles. It is plausible that certain controls will be exerted at the level of the receptor, i.e. receptor expression can set in motion MRP8/14 activities, of which RAGE is one example (Nacken et al., 2004); along with TLR4 (Schelbergen et al., 2012).

Other microparticle proteins may be contributing to the chondroprotective effects seen. Putative immunomodulatory proteins were found within the microparticles. Alpha$_2$-macroglobulin has in particular been harnessed by enriching in microparticles to improve the outcome in a mouse model of sepsis (Dalli et al., 2014). Alpha$_2$-macroglobulin is a tetrameric glycoprotein, which functions as a major anti-proteinase in the circulation. Alpha$_2$-macroglobulin readily traps proteinases of all classes (serine, carboxyl, thiol, metallo-) including the proteinases released by granulocytes during

inflammation. In addition, alpha$_2$-macroglobulin has major cytokine quenching abilities and changes its conformation upon protease exposure initiating high-affinity binding to several cytokines including TNF-α and IL-6, which are then cleared by endocytosis into hepatocytes, and IL-1β, whereby alpha$_2$-macroglobulin directly inhibits its functions. In contrast, TGF-β may bind to either the native form, which stabilises TGF-β and increases its half-life in the exudate, or the fast (proteinase-cleaved) form of alpha$_2$-macroglobulin which is cleared by bystander cells. Furthermore, it functions as a scavenger of peptide mediators and defensins in inflamed tissues, contributing to inflammation containment. Relevant specifically to experiments performed herein, alpha$_2$-macroglobulin has anti-apoptotic behaviour, regulated by the expression of the low-density lipoprotein receptor protein (LRP) (Rehman et al., 2013).

Chondrocytes express LRP-1, and the major ligand for this receptor, lactoferrin, has reportedly pro-proliferative effect in chondrocytes comparable to TGFβ (Brandl et al., 2010). Lactoferrin is abundant in neutrophil microparticles (Timar et al., 2013, Dalli et al., 2013). Although the expression of microparticle lactoferrin was not explored here, its effects on C28/I2 chondrocyte micromasses was assessed. Lactoferrin is an iron-chelating glycoprotein stored in the secondary granules and released upon neutrophil stimulation. Levels are elevated in the rheumatoid synovial fluid, to around 10μg/ml, compared with 0.2 to 0.6μg/ml in the circulation and correlate with CRP and disease severity (Wong et al., 2009). Lactoferrin is thought to have anti-inflammatory properties due to its iron sequestering abilities: iron accumulates within the rheumatoid synovium and acts in the conversion of hydrogen peroxide and superoxide into damaging hydroxyl radicals via the Fenton/Haber Weiss reaction (the reduction of ferric to ferrous iron by superoxide which feeds into the Fenton reaction producing ferric iron plus hydroxyl radicals and hydroxide (Haber and Weiss, 1932)). Chelation of iron could therefore remove a source of reactive oxygen intermediates (Wong et al., 2009) and could be an explanation for the reduced inflammation observed following intra-articular injection of lactoferrin into the joints of mice undergoing experimental septic and collagen induced arthritis (Guillen et al., 2000). However, lactoferrin also extends the lifespan of neutrophils (at concentrations of 50 and 100μg/ml), and depletion of lactoferrin within the synovial fluid reduces synovial fluid neutrophil lifespan (Wong et al., 2009). Furthermore, lactoferrin has been shown to induce the expression of matrix metalloproteinases in a mechanism thought to be necessary for the degradation of damaged tissue followed by the proliferation of chondrocytes for reconstruction (Brandl et al., 2010). The proliferative effects of lactoferrin were not observed in chondrocytes, and co-culture of chondrocyte micromasses with lactoferrin did not rescue IL-1β-

induced matrix degradation, possibly consistent with matrix metalloproteinase up-regulation. It would be interesting to explore whether lactoferrin prevented chondrocyte apoptosis in this setting, however.

Microparticle treatment induced chondroprotection that could be partially blocked with TGFβ neutralizing antibodies or by coating the microparticles with an excess of Annexin V to bind exposed phosphatidylserine. Both of these effects have been reported previously (Gasser and Schifferli, 2004), and may constitute a generic anti-inflammatory effect of neutrophil derived microparticles. TGFβ1 is a multifunctional growth factor that exerts pleiotropic effects in chondrocytes, which includes the stimulation of type II collagen and aggrecan synthesis (Morales and Roberts, 1988, Redini et al., 1988, Rosier et al., 1989, Shuler et al., 2000). TGF-β1 was increased in micromasses treated with microparticles alone without IL-1β, even though there was no associated increase in matrix accumulation. Cells produce TGFβ as a homodimer, which binds the latency-associated protein to confer protection and modulate its reactivity (Rossol et al., 2011, Shi et al., 2014). This latency-associated protein (LAP) is removed *in vivo* in inflammatory settings by proteases, reactive oxygen species or in low pH milieu. The cytokine bead array requires the removal of the LAP by acidification of sample supernatants, thus, the total TGFβ1 concentration is assayed, including both latent and active protein. It is possible therefore that in resting chondrocytes, microparticle treatment induces the production of TGFβ1, but matrix accumulation is not altered as the proteases required for activation of the growth factor are only minimally produced compared to IL-1β stimulation. Testing this hypothesis was attempted, by performing western blotting on the supernatants (both with and without spin-column concentration) and probing for dimerised LAP, but unfortunately the protein levels were below the limit of detection.

Analyses with Fpr2/3$^{-/-}$ mice and cartilage explant cultures, together with experiments conducted with selective antagonists, indicated unequivocal requirement of the receptor for the chondroprotection afforded by microparticles. The data produced with Annexin A1 null neutrophil microparticles provide further support to this mechanism. Although Annexin A1 was the major determinant in the microparticle chondroprotection, residual anti-catabolic effects were observed. Contributing effects of other vesicle components, from precursors of bioactive lipids (Norling et al., 2011, Dalli and Serhan, 2012) to microRNA (Bolukbasi et al., 2012), therefore cannot be excluded. In addition, neutrophil microparticles were protective during K/BxN serum transfer arthritis but this protection was not apparent in Fpr2/3 null mice. Interestingly, Fpr2/3

knockout mice were observed to retain more of their sulphated glycosaminoglycan content compared to wild type arthritic mice. How Fpr2/3 is involved in the regulation of matrix depletion in vivo is not known, however, as it is a receptor known to bind a variety of protein and non-protein ligands, including SAA, lipoxin A4 and Resolvin D1 (Ye et al., 2009), and has opposing inflammatory and anti-inflammatory functions, it is possible that as-of-yet-unappreciated GPCR associated pathways may contribute to the anabolic phenotype encountered. Furthermore, the pro-anabolic effects seen during treatment of resting human chondrocyte micromasses with Annexin A1 appears to be FPR1 mediated. This could indicate that Annexin A1 is cleaved by proteinases within the chondrocyte supernatant allowing binding to the FPR1 receptor (Hayhoe et al., 2006). The biological effects of the N-terminal cleavage peptide, Ac2-26, warrants investigation. This may also account for some of the differential effects between microparticle and Annexin A1 treatment, where packaging inside microparticles may prevent Annexin A1 cleavage. This could be tested by treatment of microparticles or Annexin A1 in parallel, with different proteases and assessing the product size by western blotting.

Downstream of FPR2/ALX receptor ligation is the activation of ERK1/2 phosphorylation and conformational changes of the receptor allowing association with G_0, G_2 and $G\alpha_{i6}$ proteins leading to receptor desensitization and recycling; interaction with $G\alpha_{ii}$, $G\alpha_{i2}$ and $G\alpha_{i3}$ leads to intracellular calcium flux, activation of phospholipase A_2 and the PI3K and MAPK pathways (Bena et al., 2012a). In myeloid cells, this receptor is responsible for chemokinesis, yet in non-myeloid cells its effects are not fully understood. The transcriptional targets of FPR2/ALX include *SGPP2, JAG1, JAM3, IKBK* and *SP1* (Renshaw et al., 2010), of which only *SGPP2* was modulated by microparticle treatment in chondrocytes. GPCR signaling is also made more complex by the propensity for receptors to hetero and homodimerise. Recently, the signaling pathway downstream of FPR2/ALX homodimerisation was characterized. Cooray et al. (2013) showed that upon FPR2/ALX homodimerisation, and following ligation of lipoxin A_4, Annexin A1 or its N-terminal derived anti-inflammatory peptide Ac2-26, p38 is phosphorylated leading to the phosphorylation of MAPKAPK2. This in turn phosphorylates Hsp27 leading to IL-10 production, to drive the resolution of inflammation. Chondrocytes do not produce IL-10, and is likely to have other intracellular signalling machinery, thus a panel of signaling molecules were probed for activation.

Microparticle treatment directly inhibited Hsp27 phosphorylation, which acts to reduce large Hsp27 oligomers (which can be as large as 700kDa, forming 24mers) into dimers and monomers, where they function to stabilize the mRNA of unstable inflammatory cytokines, such as IL-8, IL-6 and TNF-α (Lambrecht et al., 2010, Jones et al., 2009, Alford et al., 2007). Concurrently, reduced production of prostaglandin E_2, IL-8 and IL-6 was observed in microparticle co-culture with IL-1β-stimulated chondrocytes. Regulation of mRNA stability by phosphorylated Hsp27 is mediated by the 3' untranslated region of the target mRNA. Hsp27 target mRNAs (for genes such COX-2, TNF-α, GM-CSF, IL-8 and IL-6) contain a repeating pentamer sequence AUUUA (known as AU-rich elements, or AREs) that dictates stability or instability and characterizes this class of unstable cytokine mRNA species. The stability of mRNAs in microparticle/chondrocyte co-culture could be assessed by stimulating the chondrocytes with IL-1β plus microparticles whilst inhibiting protein synthesis using actinomycin D, then sampling over a time course to determine if microparticle treatment increases mRNA degradation. Investigations into how the microparticles inhibit Hsp-27 phosphorylation would be important, as the destabilisation of inflammation associated gene mRNA could prove a valuable target in the treatment of human disease.

Microparticle detection and measurement analyses were optimised extensively to ensure robust data collection. Classical flow cytometric analysis was modified to help discriminate microparticle populations from electronic noise generated within the machines by analysing the side-scatter information rather than forward scatter information traditionally used for relative cell size. This method allowed for the more accurate detection of 500nm beads, and could be used to determine the positivity of microparticles for the expression of proteins and externalisation of phosphatidylserine. However, multiple detection analyses were used to corroborate microparticle size, including nanoparticle tracking analysis and analyses with the Imagestream^X mk. II imaging cytometer. Using these techniques it was found that microparticles at a range of sizes could be detected, but only Imagestream^X analysis allowed the simultaneous detection of larger (≥1μm) and smaller (approximately 100nm) microparticle populations and parent cells. With this technology, microparticle kinetics could be measured for the first time.

The real-time temporal kinetics of microparticle production has not been reported for neutrophils. Static measurements of microparticle number have been made, for example using aliquots of cerebral vascular endothelial cell line supernatant taken and

tested by flow cytometry (Latham et al., 2013) or by spectrophotometric analysis of the supernatants of adherent glial cells stimulated with an ATP mimetic (Bianco et al., 2009). During glial cell culture, stimulation with ATP induced a plateau of microparticle production after 20 minutes, and with time-lapse microscopy, microparticle shedding could be observed (but not quantified) 1-2 minutes after stimulation (Bianco et al., 2009). Reported here, time-lapse fluorescent microscopy over a period of 10 minutes was corroborated with ImageStream^X analysis whereby freshly isolated neutrophils in suspension were stimulated with TNF-α and microparticle generation was analysed real-time over 45 minutes. Although a plateau in microparticle production was not reached over this time-point, the limiting factor of data collection was the file sizes generated during such an experiment. However, this assay could be translated to explore the real-time kinetics of microparticle generation in combination with cytoskeletal inhibitors, such as those used in single time-point experiments.

Using these techniques, in combination, allowed several new observations to be made about microparticles. Firstly, the number of microparticles generated from 98% pure neutrophil populations following stimulation increased compared to resting cells from the same donor. TNF-α stimulation induced double the amount of microparticle shedding, but counts were approximately another two-fold greater using flow cytometry compared to ImageStream^X analysis. This could be for two main reasons: firstly, the ImageStream^X analyser uses high-accuracy syringe-driven fluidics rather than vacuum driven fluidics that are prone to bubble formation, affecting analysis. Second, each of the gates used for microparticle detection can be interrogated by eye to ensure they contain only microparticles, whereas the event signals generated using flow cytometry cannot be corroborated visually. Together, even though approximately 95% of events are measured using the ImageStream^X, it is likely that these counts are more robust than the noise-prone flow cytometry data. Nanoparticle tracking analysis also revealed double the number of microparticles were present in TMP samples compared to CMP, and interpolating these data showed that for every 1 million resting neutrophils, around 2.5 million microparticles were generated basally and this rose to 4.195 million microparticles per million neutrophils upon stimulation with TNF-α. Although this analysis completely excludes microparticles 1μm in size and larger, it accurately enumerates microparticles lower than this size. Overall, a putative lower biological limit for microparticle size can only be measured using this technology, and appears to be 50nm in the TMP sample analysed by NTA, where only 3.5% of the TMP population fell below 50nm. These smaller microparticles fall below the resolution of light microscopes, and it is therefore only possible to measure the entire population of

microparticles with transmission electron microscopy, which is low through-put and in itself prone to artefacts in the sample processing.

This is the first report of the presence of the receptor FPR2/ALX, together with the cognate receptor FPR1, in chondrocytes. FPR1 expression was augmented by catabolic stimulation. Annexin A1 was also expressed in human chondrocytes but not modulated in our experimental settings. Previous reports showed *FPR2* mRNA and protein expression is increased in the joints of K/BxN arthritic mice compared to naïve mice, and could be visualised within the articular cartilage (Patel et al., 2012). We observed no alterations in the levels of *FPR2* or *FPR1* gene transcripts during stimulation of human chondrocytes *in vitro* with IL-1β for 6 hours; yet at 24 hours, FPR1 was up-regulated. The expression of GPCRs, such as those recognising formyl-methionine terminated peptides are known to be regulated at a number of levels, including modulation of receptor function, subcellular localisation and gene expression. FPR1 mRNA exhibits constitutive instability and has a half-life in resting conditions of 60 to 90 minutes. This allows the cells to rapidly modulate receptor expression by controlling transcript abundance via stabilisation (Mandal et al., 2005). Regulation of FPR2/ALX expression in non-immune cells, on the other hand, is not well understood. Synovial fibroblasts, when stimulated with TNF-α or IL-1β, up-regulate their *FPR2* mRNA expression, whereas only a modest increase was observed in IL-1β-stimulated enterocytes (Waechter et al., 2012). Hence, the lack of alteration of mRNA levels reported here might be due to a non-optimal time-point being investigated.

The murine FPR gene family is made up of at least 8 members, whereas humans express only 3 (termed FPR1, FPR2/ALX and FPR3). Both murine Fpr2 and Fpr3 genes share the lipoxin A_4 binding capacity of human FPR2/ALX (Ye et al., 2009, He et al., 2013) and knockout of both of these genes was achieved by inserting the gene cassette (and GFP reporter) in reverse orientation into intron 1 of Fpr2 thus preventing transcriptional read-through of both Fpr2 and Fpr3 genes (Dufton et al., 2010). These mice have been reported to display some degree of exacerbation of K/BxN arthritis (Dufton et al., 2010), which was not replicated fully here. This is probably due to the small number of mice used, and variation between the batches of K/BxN serum used. The scoring system employed used both *in vivo* and employed during histology analyses does not encapsulate the extent of inflammation once pannus formation or oedema is present; the pannus formation in the Fpr2/3 null mice far exceeded the severity of wild type mice for example, but as infiltration was present in both, the score ceiling was reached. Digestion of the paws and flow cytometric analysis between the

two groups could yield much more detailed analysis of the activation status and identity of the infiltrating cells. Fpr2/3 null mice did not reveal any improvement of cartilage integrity upon microparticle treatment compared to vehicle-injected knees. This supports experiments performed *in vitro* and *ex vivo* with either pharmacological inhibition or genetic deletion. Curiously, Fpr2/3 mice retained more proteoglycan content overall compared to wild type mice. This warrants further exploration. We plan to see whether Fpr2/3 nullification during osteoarthritis models, such as the destabilization of the medial meniscus (DMM) to exclude an overtly inflammatory component to the protection observed in these experiments.

The transcriptional targets after FPR2/ALX ligation were monitored for modulation by RT-PCR. Although the mRNA for the receptor itself was not drastically altered, the down-regulation of *SGPP2* mRNA was observed in co-cultures. This gene encodes sphingosine-1-phosphate phosphatase type 2, and is highly up-regulated in a number of cell types in response to inflammatory stimuli (Mechtcheriakova et al., 2007). SGPP2 functions to cleave sphingosine 1 phosphate, a bioactive lipid able to counteract the effects of IL-1β in chondrocyte co-culture (Stradner et al., 2014, Stradner et al., 2013, Moon et al., 2012, Stradner et al., 2008) and dose-dependently inhibits IL-1β-induced NF-κB p65, COX2, MMP-1, -3, -13 and -14 mRNA expression, prostaglandin E_2 synthesis and glycosaminoglycan degradation (Moon et al., 2012).

Microparticles modulated the production of Prostaglandin E_2 in micromass cultures. At lower concentrations of IL-1β stimulus, microparticles increased the level of Prostaglandin E_2 synthesis, which may be helpful in the turnover of cartilage matrix (Li et al., 2009). At higher levels of IL-1β, microparticles were able to reduce the Prostaglandin E_2 levels to similar concentrations as those seen in the low dose IL-1β stimulation. IL-8-derived microparticles were the least efficient at reducing Prostaglandin E_2, and this reflects possible different functions of this subset of microparticles. Prostaglandin E_2 is increased in osteoarthritis, but unlike other pro-inflammatory or catabolic stimuli, it can reverse aggrecan degradation induced by IL-1β and stimulate gene expression of type II collagen (Sun et al., 2011). It has been reported that the effects exerted by Prostaglandin E_2 in cartilage is very much concentration dependent. Low concentrations of Prostaglandin E_2 induce anabolic gene expression such as type II collagen and aggrecan and aids in matrix deposition (Nedelec et al., 2001, Saklatvala, 1986). High concentrations however act as a strong catabolic stimulus and induce the cells of the joint to express MMPs and ADAMTSs (Li et al., 2009). This may be why an up-regulation of Prostaglandin E_2 in micromasses

treated with both IL-1β (3ng/ml) and microparticles is observed in conjunction with increased matrix deposition. This is in contrast with observations in micromasses treated with high levels of IL-1β (30ng/ml) where much higher levels of Prostaglandin E_2 are generated – and addition of microparticles to these cultures significantly decreases the amount of Prostaglandin E_2 produced. Combined, these data suggest microparticles play a modulatory role on the production of Prostaglandin E_2 by chondrocytes. The microparticles themselves may also contribute to a shift in lipid mediators in this model by donation of bioactive lipid precursors (Dalli and Serhan, 2012). Indeed, the exogenous addition of Resolvin D1 protected chondrocytes in micromass culture from IL-1β-induced matrix degradation.

The cause of Scott syndrome, a rare bleeding disorder characterised by a reduced number of microparticles and phosphatidylserine exposure has recently been elucidated. Missense mutations in the putative scramblase TMEM16F prevent phosphatidylserine exposure and subsequently microparticle shedding in red blood cells, platelets and lymphocytes. The microparticle shedding of other cell types are likely to be affected too (Bevers et al., 1992, Kunzelmann et al., 2014). Supporting this, TMEM16F deficient mice have impaired osteoblast mineralisation resulting in reduced skeletal development (Kunzelmann et al., 2014). Ehlen et al. (2013) described skeletal abnormalities associated with absent phosphatidylserine exposure in TMEM16F null mice: hypertrophic chondrocytes present within the deep zones of the cartilage release vesicular structures, which serve as an initial nucleation site for mineral formation during embryogenesis. These matrix vesicles are derived from the phospholipid bilayer in a similar manner to microparticles and once released into the extracellular matrix, accumulate calcium and inorganic phosphate. The transformation from the amorphous to crystalline phase requires the formation of a nucleation complex involving a phosphatidylserine-associated pool of calcium, phosphate and annexins (Balcerzak et al., 2008), which leads to the formation of hydroxyapatite during bone formation. It is therefore possible that TMEM16F null mice lack the capability of releasing microparticles from a variety of cell types, in addition to platelets and red blood cells.

The calcifying properties of microparticles have been described and play pathological roles in atherosclerosis (Kapustin et al., 2011, New et al., 2013). In the atherosclerotic plaque, vascular smooth muscle cells acquire chondrogenic and osteoblastic phenotypic features and enhance mineral deposition inappropriately to enhance arterial stiffening via increases in extracellular calcium. These microparticles share phenotypic characteristics of the microvesicles released by chondrocytes during osteogenesis.

They carry similar cargo of Annexin A2, A5 and A6 and seem associated with collagen fibrils in patients with various levels of calcification in vessels. It is possible that microparticles have a generic set of roles as a function of their size, calcium-dependence and exposure of phosphatidylserine, which, in settings such as atherosclerosis have deleterious effects, whereas in cartilage and at the interface with calcified bone, are required for normal physiology.

The induction of SOX9 protein and mRNA during microparticle coculture was unexpected. ECM production is governed by the transcription factor SOX9, which directly drives the expression of type II collagen and aggrecan, the two most abundant cartilage proteins (Bi et al., 1999). SOX9 expression has also been shown to limit chondrocyte apoptosis through binding to the Pik3ca subunit of PI3K (Ikegami et al., 2011). SOX9 is a close relative of the sex-determining region Y protein (SRY) and is up-regulated in the repair phase in adult cartilage following fracture and precedes type II collagen expression (Sakano et al., 1999). Huang et al. (2000) demonstrated that phosphorylation of SOX9 enhances its ability to transactivate type II collagen. It is therefore possible that the increased molecular weight SOX9 bands observed in microparticle-micromass co-culture represent phosphorylated SOX9, accounting for increased extracellular matrix accumulation.

Although the chronic erosive progression of RA is recognised, acute inflammatory events, known as flares, also contribute to the presentation of the disease. The flare process within the synovial fluid encompasses local production of chemokines and cytokines with chemoattractive properties, as well as inflammatory mediators such as leukotriene B_4 and products of complement activation, which work in concert to attract massive amounts of neutrophils to the synovial fluid. These same agents stimulate the post capillary endothelium to become efficient at binding circulating cells. In addition, vasoactive mediators such as histamine, produced by mast cells, and prostaglandin E_2, facilitate extravasation of inflammatory cells into the synovial fluid. This phase of the disease adds a reiterative dimension to the chronic, underlying inflammation, with successive events stimulating progressive amplification of inflammation (Lipskey, 2008). Neutrophils produce a variety of matrix metalloproteinases during this phase, as well as further cytokines following phagocytosis of immune complexes within the joint, which contribute to the pathogenesis of the disease (Cassatella et al., 1997, Cassatella, 1995, Quayle et al., 1995, Quayle et al., 1994).

The involvement of neutrophils in the pathogenesis of various autoimmune diseases is well delineated. Depletion of neutrophils by Ly6G (1A8) antibody treatment in a mouse model of multiple sclerosis (experimental autoimmune encephalomyelitis, EAE) attenuated preclinical central nervous system inflammation and abrogated the development of EAE. Administration on Ly6G antibody after the clinical onset of EAE had no effect on disease incidence or severity suggesting that the contribution of neutrophils is to the onset of EAE. Furthermore, it was observed that the CNS-derived neutrophils mediated APC maturation in part by the production of reactive oxygen species (Steinbach et al., 2013). Therapeutic adsorptive granulocyte apheresis (selective depletion of cells expressing Fcγ, therefore including monocytes) in patients refractive to traditional treatments for generalised pustular psoriasis saw an improvement in area of erythroderma, pustules and oedema (Ikeda et al., 2013). Neutrophil depletion, again using the specific Ly6G antibody, in experimental epidermolysis bullosa yielded significantly lower titers of autoantibodies compared with isotype controls (Samavedam et al., 2014).

The role of neutrophils in arthritis has been historically overlooked, but more recent evidence is accumulating, implicating neutrophils in the initiation and progression of inflammatory arthritis in animal models. The molecular pathology of human rheumatoid arthritis shows strong neutrophil involvement: neutrophils are present within the synovial fluid and lining, and neutrophil-derived products can be found in joint tissues. Primed or activated neutrophils (as compared to circulating neutrophils) have an extended lifespan, synthesise inflammatory mediators and are capable of presenting antigen to T cells (Cross et al., 2003), and therefore have the ability to actively drive inflammatory processes (Wright et al., 2010). Expression of MHC II and co-stimulatory molecules (CD80 and CD86) on synovial neutrophils is equivalent to or greater than monocyte and B cell expression levels (Sandilands et al., 2005) and can be expressed rapidly during *in vitro* stimulation (Sandilands et al., 2006). Furthermore, neutrophils have been shown to synthesise and secrete IL-8 in response to TNF-α stimulation, (Fujishima et al., 1993) increasing neutrophil recruitment to the joint. Activated neutrophils also produce IL-1, IL-6, IL-12, TGF-β, TNF-α, oncostatin M and B-lymphocyte stimulator (BLyS) (Cross et al., 2003, Scapini et al., 2005, Scapini et al., 2008), thus contributing to the increased local inflammatory milieu within the rheumatoid joint.

Depletion of neutrophils in models of experimental arthritis attenuates inflammation. Elevated levels of G-CSF, important for basal and inflammatory granulopoiesis, have

been detected in RA synovial fluid and serum, and levels correlated with disease activity and severity (Nakamura et al., 2000). Depletion of Gr-1 positive cells (mainly neutrophils but also subsets of monocytes, $CD8^+$ T cells and plasmacytoid dendritic cells) reduced the clinical score of CIA mice down to 0.5, compared with isotype treated mice who retained a clinical score of >4. This was confirmed using the Ly6G (1A8) antibody, to selectively deplete neutrophils, and the score was also reduced compared to isotype, but not to the same extent (Eyles et al., 2008). Neutrophil elastase has been shown to degrade articular cartilage directly in *in vitro* assays (Moore et al., 1999). It is clear that neutrophils play important pathogenic roles in rheumatoid arthritis, but many of the reports on neutrophil function in RA models are of the overall inflammatory component of this disease. Focussing uniquely on the cartilage in this disease (of which the erosion is the causative feature of joint loss-of-function) neutrophil depletion using an irradiation protocol significantly decreased proteoglycan synthesis in zymosan-induced arthritis (ZIA) compared to non-depleted mice (Gresnigt et al., 2012). This model of ZIA is highly dependent on IL-1β, therefore this report directly relates to the data presented here, suggesting that the role of neutrophils in arthritic cartilage is not necessarily degradative. We propose that the mechanism of cartilage protection is overwhelmed in RA, thus with depletion of neutrophils and/or neutrophil microparticles, cartilage destruction may be much greater in this setting.

The concept that neutrophils play a role in limiting inflammation and contribute to the resolution of inflammation in certain settings is gaining ground. Neutrophil apoptotic bodies reprogram macrophages from M1 to M2 phenotype via efferocytosis (Hoffmann et al., 2005, Huynh et al., 2002, Li et al., 2003). Wound healing in neutrophil depletion models is delayed (Harty et al., 2010), and depletion of neutrophils in certain autoimmune diseases, such as ulcerative colitis, leads to an exacerbation of disease (Kuhl et al., 2007, Campbell et al., 2014). Although controversially reported by several authors (De Santo et al., 2010, Glowacka et al., 2010), it has been shown that human neutrophils cannot produce IL-10 as the *IL-10* genomic locus is in an inactive state (Davey et al., 2011, Tamassia et al., 2013). Mouse neutrophils do express IL-10 mRNA and protein in inflammatory contexts (Kasten et al., 2010, Doz et al., 2013), but are dispensable in survival during polymicrobial sepsis (Ocuin et al., 2011). These studies demonstrate that murine versus human biology is different, and cautions against extrapolating observations directly from mice to man. Neutrophils are also involved in nerve regeneration and protection post-injury (Kurimoto et al., 2013, Stirling et al., 2009). Neutrophil proteases, classically thought to degrade the extracellular matrices

and cells surrounding the inflammatory event, are conversely shown to deactivate inflammatory cytokines produced by mononuclear cells independently of ROS production or phagocytosis (Gresnigt et al., 2012).

Further non-redundant immunoregulatory functions of neutrophils involve their interaction with other cell types. Jaeger et al. (2012) report that the *Genista* neutrophil ($CD11b^{+}Ly6G^{high}$)-depleted mouse mutant had hyporesponsive, hyperproliferative natural killer (NK) cells with poor cellular survival and blockade at the immature stage. These mice have a point mutation in *Gfi-1* (growth factor independence-1; induced by the C/EBPα lineage-determining transcription factor; critically required for the development of mature neutrophils) leading to a termination of granulopoiesis after the metamyelocyte stage, but they do have an atypical circulating population of $CD11b^{+}Ly6G^{intermediate}$ population which retain a small proportion of mature neutrophil characteristics (Ordonez-Rueda et al., 2012). When wild type NK cells were adoptively transferred into *Genista* mice, their responsiveness was suppressed, supporting the notion that NK defects were extrinsic to the cells. *Genista* NK cells adoptively transferred into wild type mice regained full reactivity in host wild type NK cells, showing that, although NK cells express the *Gfi-1* gene modified in this mutant mouse, the point mutation was not sufficient to affect NK cell function. The maturation of NK cells through stages of CD27/CD11b positivity and negativity were terminated at the intermediate double-positive stage in *Genista* and also wild type neutrophil-depleted mice, suggesting that neutrophils are required for the final maturation of NK cells. These results were then recapitulated in human patients with severe congenital neutropenia, who displayed a higher proportion of immature, hyporeactive NK cells compared to healthy controls. It was observed that in wild type mice, NK cells and neutrophils formed conjugates in the spleen and lymph nodes far more frequently than T or B cells did with neutrophils (approximately 75% versus less than 10 percent for T and B cells). These cells can be seen with considerable plasma-membrane contact with one another, under resting conditions. These data extend the previously characterized interaction of neutrophils and NK cells under inflammatory settings (Costantini et al., 2011a, Costantini et al., 2011b).

Furthermore, there are reports that neutrophil microparticles down-regulate inflammatory cytokine production in NK cells (Pliyev et al., 2014) and induce phenotype switching of macrophages (Eken et al., 2013, Eken et al., 2010), suggesting that neutrophil microparticles may be involved in limiting chronic inflammation, adding another anti-inflammatory or pro-resolving aspect to the neutrophil repertoire. We

propose that these cells produce protective microparticles to try to limit inflammation and joint destruction, which is overwhelmed in RA. This is in analogy to the higher levels of TGF-β1 also present within the synovial fluid, thought to represent an overwhelmed protective response to inflammation, by driving regulatory T cell differentiation (Lipskey, 2008).

To recapitulate the flare phase of rheumatoid arthritis, which is when neutrophils, and therefore neutrophil microparticles are most abundant, we adopted the K/BxN serum transfer arthritis. The inflammation seen in this phenotype is entirely dependent on the innate immune cells, mainly neutrophils (Elliott et al., 2011). Serum harvested from KRN transgenic mice crossed into mice carrying the H-2^{g7} haplotype of the MHC locus, has high titres of autoantibodies to glucose-6-phosphate isomerase. Serum transfer into C57BL/6 mice initiates an aggressive, symmetrical polyarthritis, which is dependent upon neutrophils and mast cells (Monach et al., 2007, Monach et al., 2008) although the role of mast cells has recently been called into question (Elliott et al., 2011). These autoantibodies selectively deposit on the surface of the cartilage, which is detected by neutrophils via the Fcγ receptor (Elliott et al., 2011), but also fixes complement, releasing bioactive complement fragments such as C5a, initiating local inflammatory events, including recruitment of phagocytic cells to the site (Laudisi et al., 2013). The production of leukotriene B_4 leads to the infiltration of neutrophils, which in turn produce large amounts of IL-1β when stimulated by immune complexes present within the joint space. IL-1β induces chemokine production, and thus more neutrophils are recruited to the joint in a self-perpetuating inflammatory loop (Chou et al., 2010).

Systemic treatment of K/BxN mice with 100,000 TMP was unsuccessful. This is not surprising, as this is a relatively small amount of microparticles, and the dilution effect across the entire system would have been significant. Furthermore, it is not known whether neutrophil microparticles are capable of transmigrating through endothelial cells to the site of inflammation following margination, capture, rolling and adhesion to the endothelium, as their parent cells do. Importantly, however, it was possible to determine that mice receiving microparticle treatment displayed no adverse effects, and their arthritis was not worsened. Direct delivery of microparticles intra-articularly did induce chondroprotection compared to sham-injected knees. Treatment did not affect the clinical scores of mice, which are measured in peripheral, distal joints. This does not preclude microparticle treatment in human patients with rheumatoid arthritis, however, as synovial fluid aspiration is a common procedure for these patients.

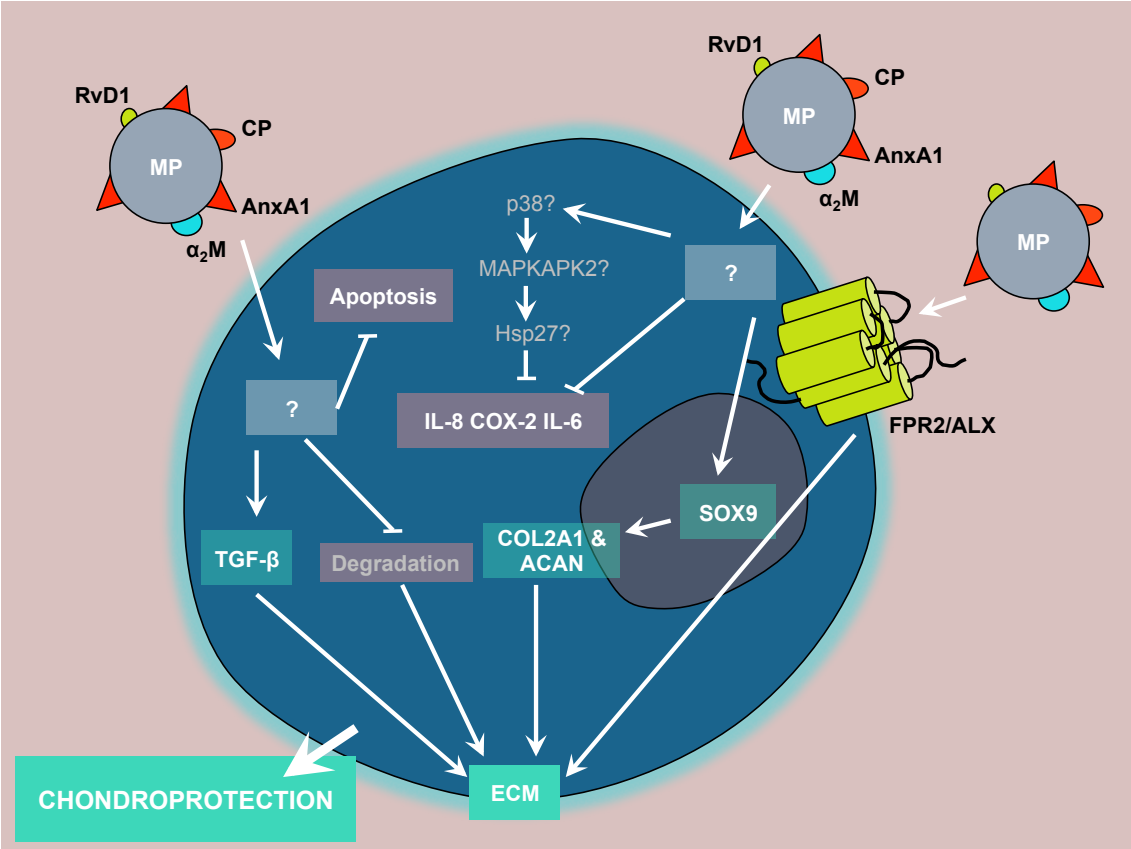

Figure 6.2 Schematic: Microparticle effects on chondrocytes. Microparticles, carrying various immunomodulatory components, have multiple effects on chondrocytes. Following ligation of FPR2/ALX, microparticles induce a program of chondroprotection and cartilage matrix accumulation via unknown mechanisms. Microparticles induce the up-regulation of SOX9, and type II collagen and aggrecan mRNA, inhibit cartilage matrix degradation and induce the production of TGF-β. Microparticle treatment also inhibits chondrocyte apoptosis and reduces levels of IL-8, IL-6 and COX-2, possibly via the inhibition of Hsp27 phosphorylation. MP, microparticles; α_2M, α_2-Macroglobulin; RvD1, Resolvin D1; CP, ceruloplasmin; AnxA1, Annexin A1; ECM, extracellular matrix.

Cartilage integrity was increased in the knees of arthritic mice injected with TMP compared to contra-lateral vehicle injected knees as determined macroscopically and by toluidine blue staining. Caliper measurements of arthritic knees were not sufficiently sensitive to distinguish arthritic from naïve knees, or treated versus vehicle knees, even when differences could clearly be seen post skin resection. In fact, the macroscopic appearance of the knee correlated to histological knee score almost 100% of the time, and provided a good measure of treatment efficacy. Decreased knee inflammation in microparticle treated knees could also be seen in live mice with bioluminescence imaging. Using luminol sodium salt, which is cleaved to a fluorescent compound when exposed to extracellular neutrophil myeloperoxidase, the inflammation induced by K/BxN serum transfer could be monitored in both peripheral joints and the knees (Gross et al., 2009). Microparticle treated knees had significantly less

inflammation compared to vehicle treated knees, and this method would allow for more long term experiments to be performed with data analysis across time points.

RNA extraction and measurement of gene expression from formalin-fixed, paraffin embedded sections did not reveal any significant results. Probably, a combination of variation within the arthritis experiment, and the low number of mice used for the study contributed to the results seen. Plus, RT-PCR is an extremely sensitive method for measuring labile RNA, thus, in future, joints prepared specifically for RNA analysis would help reduce variance.

To determine whether neutrophil microparticles were involved physiologically in the process of arthritis, two approaches were adopted. Firstly, Bodipy-maleimide labelled neutrophils transferred into mice undergoing K/BxN arthritis appeared within arthritic joints. Microparticles could be observed within the cartilage and double-stained for MRP14. This suggests that the appearance of myeloid-related proteins in human arthritic joints are localised there due to microparticles. Secondly, we attempted to block microparticle interaction in vitro to determine whether any protocols could be used in vivo. One way in which we tried, unsuccessfully, to block microparticle interaction with chondrocytes was via the addition of Annexin V in excess to coat the exposed phosphatidylserine. Although recent reports have demonstrated that the phosphatidylserine exposed by apoptotic cells down-regulates inflammation during efferocytosis, in this case, blocking exposed phosphatidylserine did not inhibit microparticle protection. This, and previous reports of similar coating experiments, suggests that although microparticles and apoptotic bodies may share overlapping anti-inflammatory qualities, their functions are separate, and that phosphatidylserine is only partially responsible for the chondroprotection observed. Inhibiting microparticle formation in a manner that is translatable in vivo has proven difficult. Neutrophils are terminally differentiated cells and can only be minimally manipulated before retransfer into live mice. Furthermore, depletion of neutrophils before K/BxN serum transfer arthritis interferes with disease onset, and is not feasible after the onset of clinical signs, as the transmigrated tissue neutrophils will remain unaffected by depletion protocols.

Analysis of microparticle number and phenotype has the potential to become a powerful biomarker in a variety of human pathologies. Our laboratory recently reported that neutrophil microparticles can be heterogeneous, identifying subtypes more abundant in plasma during systemic inflammation (Dalli et al., 2013). The results

presented in this study, although preclinical, indicate that autologous neutrophil microparticles may easily find a translational application, as has been seen with cell-based therapies, such as autologous chondrocyte implantation or stem cell-based technologies (Singh, 2012). Enrichment of a patient's neutrophil microparticle population within the joint represents a desirable therapy for RA due to the envisaged minimal side effects and low treatment cost. Autologous transplantation of patients' own microparticles to improve disease outcome represents the future of personalised medicine as these microparticles are inherently readily generated. Furthermore, in view of their ability to enter the avascular cartilage, autologous microparticles could be manipulated or engineered to transport bioactive molecules to chondrocytes, to deliver therapies by a means that cannot be achieved in current medicine. In summary, these data shed new light on our understanding of functional and cellular association between immune system and cartilage biology, delineating new strategies for innovative drug discovery approaches.

CHAPTER 7: CONCLUDING REMARKS AND FUTURE DIRECTIONS

The ascribed functions of microparticles from various cellular origins in physiological and pathophysiological settings are continuously expanding. Here, the protective roles of neutrophil microparticles specifically in terms of chondrocyte biology and physiology have been explored. To fully conclude research herein, future considerations of how to inhibit microparticle formation to demonstrate a definitive phenotype must be demonstrated experimentally. Patients with Scott syndrome have recently had the putative mutation causing their syndrome delineated, and missense mutations in TMEM16F have been shown to be pivotal in proper phosphatidylserine scrambling and therefore microparticle shedding.

I have established a collaboration with Professor Lily Jan at University of California, San Francisco who has generated TMEM16F global and TMEM16F$^{flox/flox}$ mice. My intention is to perform a K/BxN arthritis study on these recently generated TMEM16F null mice and to compare the severity in clinical score and histologic presentation of the disease with wild type littermate controls. We hypothesise that the absence of microparticles may exacerbate the loss of proteoglycans in experimental arthritis. Although neutrophil-specific TMEM16F conditional mice do not yet exist, plans are underway to obtain TMEM16F$^{flox/flox}$ mice and breed them with neutrophil-specific GC^{cre} or MRP8^{cre} mice to observe the effects of specific neutrophil microparticle deletion in various biological and pathophysiological settings. As a first step, a K/BxN model in globally TMEM16F null mice will suffice to demonstrate the role of neutrophil microparticles in arthritis, as this model is so heavily dependent on neutrophil infiltration. We envisage an overwhelmed response of neutrophil microparticle protection in rheumatoid and other inflammatory arthritides.

This report opens up other avenues for future investigation. The newly uncovered roles of Annexin A1 and the receptors FPR2 and FPR1 deserve further investigation, especially as the retention of glycosaminoglycans was noted in Fpr2/3$^{-/-}$ vehicle groups without microparticle treatment. To investigate the control of cartilage metabolism in a setting with a less overt inflammatory phenotype, a model of osteoarthritis, the destabilisation of the medial meniscus (DMM), will be employed.

The mouse model of inflammatory arthritis used during this study was purely dependent on innate immune cells. Further studies using more chronic, adaptive immunity-driven models of arthritis, such as collagen-induced arthritis and glucose-6-phosphate isomerase immunisation are underway. Whether neutrophil microparticles will ameliorate disease in these models is totally unknown, and few, if any, reports of

the effect of neutrophil microparticles interacting with lymphocytes exist. It is possible that the chondroprotective effects will still be present in chronic models, but it is not known whether neutrophil microparticles will have any bearing on the presentation of chronic inflammation.

The mechanism of neutrophil microparticle migration into the cartilage matrix is an area of pertinent interest as drug delivery strategies to target chondrocytes are currently lacking. These microparticles were able to efficiently migrate across arthritic cartilage to native chondrocytes where evidence of microparticle uptake was observed. Packing drugs into these microstructures could represent a potent new way of targeting these otherwise almost untreatable cells, and have important implications for the future of drug delivery programmes.

Bibliography

Bibliography

2010. *BD LSRFortessa Cell Analyzer User's Guide* [Online]. http://www.bdbiosciences.com/documents/BD_LSRFortessa_cell_analyzer_user_guide.pdf. [Accessed 22.02.2014 2014].

ALFORD, K. A., GLENNIE, S., TURRELL, B. R., RAWLINSON, L., SAKLATVALA, J. & DEAN, J. L. 2007. Heat shock protein 27 functions in inflammatory gene expression and transforming growth factor-beta-activated kinase-1 (TAK1)-mediated signaling. *The Journal of biological chemistry,* 282**,** 6232-41.

ALVAREZ-ERVITI, L., SEOW, Y., YIN, H., BETTS, C., LAKHAL, S. & WOOD, M. J. 2011. Delivery of siRNA to the mouse brain by systemic injection of targeted exosomes. *Nat Biotechnol,* 29**,** 341-5.

ANDALOUSSI, S. E. L., MAGER, I., BREAKEFIELD, X. O. & WOOD, M. J. 2013. Extracellular vesicles: biology and emerging therapeutic opportunities. *Nat Rev Drug Discov,* 12**,** 347-57.

BAJ-KRZYWORZEKA, M., SZATANEK, R., WEGLARCZYK, K., BARAN, J., URBANOWICZ, B., BRANSKI, P., RATAJCZAK, M. Z. & ZEMBALA, M. 2006. Tumour-derived microvesicles carry several surface determinants and mRNA of tumour cells and transfer some of these determinants to monocytes. *Cancer immunology, immunotherapy : CII,* 55**,** 808-18.

BAJ-KRZYWORZEKA, M., SZATANEK, R., WEGLARCZYK, K., BARAN, J. & ZEMBALA, M. 2007. Tumour-derived microvesicles modulate biological activity of human monocytes. *Immunology letters,* 113**,** 76-82.

BALCERZAK, M., HAMADE, E., ZHANG, L., PIKULA, S., AZZAR, G., RADISSON, J., BANDOROWICZ-PIKULA, J. & BUCHET, R. 2003. The roles of annexins and alkaline phosphatase in mineralization process. *Acta biochimica Polonica,* 50**,** 1019-38.

BALCERZAK, M., MALINOWSKA, A., THOUVEREY, C., SEKRECKA, A., DADLEZ, M., BUCHET, R. & PIKULA, S. 2008. Proteome analysis of matrix vesicles isolated from femurs of chicken embryo. *Proteomics,* 8**,** 192-205.

BANZ, Y., BELDI, G., WU, Y., ATKINSON, B., USHEVA, A. & ROBSON, S. C. 2008. CD39 is incorporated into plasma microparticles where it maintains functional properties and impacts endothelial activation. *British journal of haematology,* 142**,** 627-37.

BARON, M., LEROYER, A. S., MAJD, Z., LALLOYER, F., VALLEZ, E., BANTUBUNGI, K., CHINETTI-GBAGUIDI, G., DELERIVE, P., BOULANGER, C. M., STAELS, B. & TAILLEUX, A. 2011.

PPARalpha activation differently affects microparticle content in atherosclerotic lesions and liver of a mouse model of atherosclerosis and NASH. *Atherosclerosis,* 218**,** 69-76.

BARRY, O. P., PRATICO, D., LAWSON, J. A. & FITZGERALD, G. A. 1997. Transcellular activation of platelets and endothelial cells by bioactive lipids in platelet microparticles. *The Journal of clinical investigation,* 99**,** 2118-27.

BARRY, O. P., PRATICO, D., SAVANI, R. C. & FITZGERALD, G. A. 1998. Modulation of monocyte-endothelial cell interactions by platelet microparticles. *The Journal of clinical investigation,* 102**,** 136-44.

BEIER, F. & LOESER, R. F. 2010. Biology and pathology of Rho GTPase, PI-3 kinase-Akt, and MAP kinase signaling pathways in chondrocytes. *J Cell Biochem,* 110**,** 573-80.

BENA, S., BRANCALEONE, V., WANG, J. M., PERRETTI, M. & FLOWER, R. J. 2012a. Annexin A1 interaction with the FPR2/ALX receptor: identification of distinct domains and downstream associated signaling. *J Biol Chem,* 287**,** 24690-7.

BENA, S., BRANCALEONE, V., WANG, J. M., PERRETTI, M. & FLOWER, R. J. 2012b. Annexin A1 interaction with the FPR2/ALX receptor: identification of distinct domains and downstream associated signaling. *The Journal of biological chemistry,* 287**,** 24690-7.

BERCKMANS, R. J., NIEUWLAND, R., KRAAN, M. C., SCHAAP, M. C., POTS, D., SMEETS, T. J., STURK, A. & TAK, P. P. 2005. Synovial microparticles from arthritic patients modulate chemokine and cytokine release by synoviocytes. *Arthritis Res Ther,* 7**,** R536-44.

BERCKMANS, R. J., NIEUWLAND, R., TAK, P. P., BOING, A. N., ROMIJN, F. P., KRAAN, M. C., BREEDVELD, F. C., HACK, C. E. & STURK, A. 2002. Cell-derived microparticles in synovial fluid from inflamed arthritic joints support coagulation exclusively via a factor VII-dependent mechanism. *Arthritis Rheum,* 46**,** 2857-66.

BERNIMOULIN, M., WATERS, E. K., FOY, M., STEELE, B. M., SULLIVAN, M., FALET, H., WALSH, M. T., BARTENEVA, N., GENG, J. G., HARTWIG, J. H., MAGUIRE, P. B. & WAGNER, D. D. 2009. Differential stimulation of monocytic cells results in distinct populations of microparticles. *Journal of thrombosis and haemostasis : JTH,* 7**,** 1019-28.

BEVERS, E. M., WIEDMER, T., COMFURIUS, P., SHATTIL, S. J., WEISS, H. J., ZWAAL, R. F. & SIMS, P. J. 1992. Defective Ca(2+)-induced microvesiculation and deficient expression of procoagulant activity in erythrocytes from a patient with a bleeding disorder: a study of the red blood cells of Scott syndrome. *Blood,* 79**,** 380-8.

BEYER, C., PISETSKY, D.S. 2010. The role of microparticles in the pathogenesis of rheumatic diseases. *Nature Reviews Rheumatology,* 6**,** 21-29.

BI, W., DENG, J. M., ZHANG, Z., BEHRINGER, R. R. & DE CROMBRUGGHE, B. 1999. Sox9 is required for cartilage formation. *Nat Genet,* 22**,** 85-9.

BIANCO, F., PERROTTA, C., NOVELLINO, L., FRANCOLINI, M., RIGANTI, L., MENNA, E., SAGLIETTI, L., SCHUCHMAN, E. H., FURLAN, R., CLEMENTI, E., MATTEOLI, M. & VERDERIO, C. 2009. Acid sphingomyelinase activity triggers microparticle release from glial cells. *EMBO J,* 28**,** 1043-54.

BOILARD, E., NIGROVIC, P. A., LARABEE, K., WATTS, G. F., COBLYN, J. S., WEINBLATT, M. E., MASSAROTTI, E. M., REMOLD-O'DONNELL, E., FARNDALE, R. W., WARE, J. & LEE, D. M. 2010. Platelets amplify inflammation in arthritis via collagen-dependent microparticle production. *Science,* 327**,** 580-3.

BOLUKBASI, M. F., MIZRAK, A., OZDENER, G. B., MADLENER, S., STROBEL, T., ERKAN, E. P., FAN, J. B., BREAKEFIELD, X. O. & SAYDAM, O. 2012. miR-1289 and "Zipcode"-like Sequence Enrich mRNAs in Microvesicles. *Mol Ther Nucleic Acids,* 1**,** e10.

BORREGAARD, N. 2010. Neutrophils, from marrow to microbes. *Immunity,* 33**,** 657-70.

BRANDL, N., ZEMANN, A., KAUPE, I., MARLOVITS, S., HUETTINGER, P., GOLDENBERG, H. & HUETTINGER, M. 2010. Signal transduction and metabolism in chondrocytes is modulated by lactoferrin. *Osteoarthritis Cartilage,* 18**,** 117-25.

BURGER, D., MONTEZANO, A. C., NISHIGAKI, N., HE, Y., CARTER, A. & TOUYZ, R. M. 2011. Endothelial microparticle formation by angiotensin II is mediated via Ang II receptor type I/NADPH oxidase/ Rho kinase pathways targeted to lipid rafts. *Arterioscler Thromb Vasc Biol,* 31**,** 1898-907.

CAMPBELL, E. L., BRUYNINCKX, W. J., KELLY, C. J., GLOVER, L. E., MCNAMEE, E. N., BOWERS, B. E., BAYLESS, A. J., SCULLY, M., SAEEDI, B. J., GOLDEN-MASON, L., EHRENTRAUT, S. F., CURTIS, V. F., BURGESS, A., GARVEY, J. F., SORENSEN, A., NEMENOFF, R., JEDLICKA, P., TAYLOR, C. T., KOMINSKY, D. J. & COLGAN, S. P. 2014. Transmigrating neutrophils shape the mucosal microenvironment through localized oxygen depletion to influence resolution of inflammation. *Immunity,* 40**,** 66-77.

CASSATELLA, M. A. 1995. The production of cytokines by polymorphonuclear neutrophils. *Immunol Today,* 16**,** 21-6.

CASSATELLA, M. A., GASPERINI, S. & RUSSO, M. P. 1997. Cytokine expression and release by neutrophils. *Ann N Y Acad Sci,* 832**,** 233-42.

CASTOLDI, E., COLLINS, P. W., WILLIAMSON, P. L. & BEVERS, E. M. 2011. Compound heterozygosity for 2 novel TMEM16F mutations in a patient with Scott syndrome. *Blood,* 117**,** 4399-400.

CHALMIN, F., LADOIRE, S., MIGNOT, G., VINCENT, J., BRUCHARD, M., REMY-MARTIN, J. P., BOIREAU, W., ROULEAU, A., SIMON, B., LANNEAU, D., DE THONEL, A., MULTHOFF, G., HAMMAN, A., MARTIN, F., CHAUFFERT, B., SOLARY, E., ZITVOGEL, L., GARRIDO, C., RYFFEL, B., BORG, C., APETOH, L., REBE, C. & GHIRINGHELLI, F. 2010. Membrane-associated Hsp72 from tumor-derived exosomes mediates STAT3-dependent immunosuppressive function of mouse and human myeloid-derived suppressor cells. *The Journal of clinical investigation,* 120**,** 457-71.

CHARGAFF, E. & WEST, R. 1946. The biological significance of the thromboplastic protein of blood. *The Journal of biological chemistry,* 166**,** 189-97.

CHATTERJEE, B. E., YONA, S., ROSIGNOLI, G., YOUNG, R. E., NOURSHARGH, S., FLOWER, R. J. & PERRETTI, M. 2005. Annexin 1-deficient neutrophils exhibit enhanced transmigration in vivo and increased responsiveness in vitro. *Journal of leukocyte biology,* 78**,** 639-46.

CHOU, R. C., KIM, N. D., SADIK, C. D., SEUNG, E., LAN, Y., BYRNE, M. H., HARIBABU, B., IWAKURA, Y. & LUSTER, A. D. 2010. Lipid-cytokine-chemokine cascade drives neutrophil recruitment in a murine model of inflammatory arthritis. *Immunity,* 33**,** 266-78.

CLOUTIER, N., TAN, S., BOUDREAU, L. H., CRAMB, C., SUBBAIAH, R., LAHEY, L., ALBERT, A., SHNAYDER, R., GOBEZIE, R., NIGROVIC, P. A., FARNDALE, R. W., ROBINSON, W. H., BRISSON, A., LEE, D. M. & BOILARD, E. 2013. The exposure of autoantigens by microparticles underlies the formation of potent inflammatory components: the microparticle-associated immune complexes. *EMBO Mol Med,* 5**,** 235-49.

COMBES, V., COLTEL, N., ALIBERT, M., VAN ECK, M., RAYMOND, C., JUHAN-VAGUE, I., GRAU, G. E. & CHIMINI, G. 2005. ABCA1 gene deletion protects against cerebral malaria: potential pathogenic role of microparticles in neuropathology. *The American journal of pathology,* 166**,** 295-302.

COORAY, S. N., GOBBETTI, T., MONTERO-MELENDEZ, T., MCARTHUR, S., THOMPSON, D., CLARK, A. J., FLOWER, R. J. & PERRETTI, M. 2013. Ligand-specific conformational change of the G-protein-coupled receptor ALX/FPR2 determines proresolving functional responses. *Proceedings of the National Academy of Sciences of the United States of America,* 110**,** 18232-7.

COSTANTINI, C., CALZETTI, F., PERBELLINI, O., MICHELETTI, A., SCARPONI, C., LONARDI, S., PELLETIER, M., SCHAKEL, K., PIZZOLO, G., FACCHETTI, F., VERMI, W., ALBANESI, C. & CASSATELLA, M. A. 2011a. Human neutrophils interact with both 6-sulfo LacNAc+ DC and NK cells to amplify NK-derived IFN{gamma}: role of CD18, ICAM-1, and ICAM-3. *Blood,* 117**,** 1677-86.

COSTANTINI, C., MICHELETTI, A., CALZETTI, F., PERBELLINI, O., TAMASSIA, N., ALBANESI, C., VERMI, W. & CASSATELLA, M. A. 2011b. On the potential involvement of CD11d in co-stimulating the production of interferon-gamma by natural killer cells upon interaction with neutrophils via intercellular adhesion molecule-3. *Haematologica,* 96**,** 1543-7.

CROCE, K., GAO, H., WANG, Y., MOOROKA, T., SAKUMA, M., SHI, C., SUKHOVA, G. K., PACKARD, R. R., HOGG, N., LIBBY, P. & SIMON, D. I. 2009. Myeloid-related protein-8/14 is critical for the biological response to vascular injury. *Circulation,* 120**,** 427-36.

CROSS, A., BARNES, T., BUCKNALL, R. C., EDWARDS, S. W. & MOOTS, R. J. 2006. Neutrophil apoptosis in rheumatoid arthritis is regulated by local oxygen tensions within joints. *Journal of leukocyte biology,* 80**,** 521-8.

CROSS, A., BUCKNALL, R. C., CASSATELLA, M. A., EDWARDS, S. W. & MOOTS, R. J. 2003. Synovial fluid neutrophils transcribe and express class II major histocompatibility complex molecules in rheumatoid arthritis. *Arthritis and rheumatism,* 48**,** 2796-806.

D'ACQUISTO, F., PERRETTI, M. & FLOWER, R. J. 2008. Annexin-A1: a pivotal regulator of the innate and adaptive immune systems. *British journal of pharmacology,* 155**,** 152-69.

D'AURA SWANSON, C., PANIAGUA, R. T., LINDSTROM, T. M. & ROBINSON, W. H. 2009. Tyrosine kinases as targets for the treatment of rheumatoid arthritis. *Nature reviews. Rheumatology,* 5**,** 317-24.

DALLI, J., MONTERO MELENDEZ, T., NORLING, L. V., YIN, X., HINDS, C., HASKARD, D., MAYR, M. & PERRETTI, M. 2013. Heterogeneity in neutrophil microparticles reveals distinct proteome and functional properties. *Mol Cell Proteomics*.

DALLI, J., NORLING, L. V., MONTERO-MELENDEZ, T., CANOVA, D. F., LASHIN, H., PAVLOV, A. M., SUKHORUKOV, G. B., HINDS, C. J. & PERRETTI, M. 2014. Microparticle alpha-2-macroglobulin enhances pro-resolving responses and promotes survival in sepsis. *EMBO Mol Med,* 6**,** 27-42.

DALLI, J., NORLING, L. V., RENSHAW, D., COOPER, D., LEUNG, K. Y. & PERRETTI, M. 2008. Annexin 1 mediates the rapid anti-inflammatory effects of neutrophil-derived microparticles. *Blood,* 112**,** 2512-9.

DALLI, J. & SERHAN, C. N. 2012. Specific lipid mediator signatures of human phagocytes: microparticles stimulate macrophage efferocytosis and pro-resolving mediators. *Blood,* 120**,** e60-72.

DAMAZO, A. S., YONA, S., FLOWER, R. J., PERRETTI, M. & OLIANI, S. M. 2006. Spatial and temporal profiles for anti-inflammatory gene expression in leukocytes during a resolving model of peritonitis. *J Immunol,* 176**,** 4410-8.

DANIEL, L., FAKHOURI, F., JOLY, D., MOUTHON, L., NUSBAUM, P., GRUNFELD, J. P., SCHIFFERLI, J., GUILLEVIN, L., LESAVRE, P. & HALBWACHS-MECARELLI, L. 2006. Increase of circulating neutrophil and platelet microparticles during acute vasculitis and hemodialysis. *Kidney international,* 69**,** 1416-23.

DASGUPTA, S. K., LE, A., CHAVAKIS, T., RUMBAUT, R. E. & THIAGARAJAN, P. 2012. Developmental endothelial locus-1 (Del-1) mediates clearance of platelet microparticles by the endothelium. *Circulation,* 125**,** 1664-72.

DAVEY, M. S., TAMASSIA, N., ROSSATO, M., BAZZONI, F., CALZETTI, F., BRUDEREK, K., SIRONI, M., ZIMMER, L., BOTTAZZI, B., MANTOVANI, A., BRANDAU, S., MOSER, B., EBERL, M. & CASSATELLA, M. A. 2011. Failure to detect production of IL-10 by activated human neutrophils. *Nat Immunol,* 12**,** 1017-8; author reply 1018-20.

DE BARI, C., DELL'ACCIO, F. & LUYTEN, F. P. 2001. Human periosteum-derived cells maintain phenotypic stability and chondrogenic potential throughout expansion regardless of donor age. *Arthritis and rheumatism,* 44**,** 85-95.

DE SANTO, C., ARSCOTT, R., BOOTH, S., KARYDIS, I., JONES, M., ASHER, R., SALIO, M., MIDDLETON, M. & CERUNDOLO, V. 2010. Invariant NKT cells modulate the suppressive activity of IL-10-secreting neutrophils differentiated with serum amyloid A. *Nat Immunol,* 11**,** 1039-46.

DEREGIBUS, M. C., CANTALUPPI, V., CALOGERO, R., LO IACONO, M., TETTA, C., BIANCONE, L., BRUNO, S., BUSSOLATI, B. & CAMUSSI, G. 2007. Endothelial progenitor cell derived microvesicles activate an angiogenic program in endothelial cells by a horizontal transfer of mRNA. *Blood,* 110**,** 2440-8.

DISTLER, J. H., HUBER, L. C., GAY, S., DISTLER, O. & PISETSKY, D. S. 2006. Microparticles as mediators of cellular cross-talk in inflammatory disease. *Autoimmunity,* 39**,** 683-90.

DISTLER, J. H., JUNGEL, A., HUBER, L. C., SEEMAYER, C. A., REICH, C. F., 3RD, GAY, R. E., MICHEL, B. A., FONTANA, A., GAY, S., PISETSKY, D. S. & DISTLER, O. 2005a. The induction of matrix metalloproteinase and cytokine expression in synovial fibroblasts stimulated with immune cell microparticles. *Proc Natl Acad Sci U S A,* 102**,** 2892-7.

DISTLER, J. H., PISETSKY, D. S., HUBER, L. C., KALDEN, J. R., GAY, S. & DISTLER, O. 2005b. Microparticles as regulators of inflammation: novel players of cellular crosstalk in the rheumatic diseases. *Arthritis Rheum,* 52**,** 3337-48.

DIXIT, N. & SIMON, S. I. 2012. Chemokines, selectins and intracellular calcium flux: temporal and spatial cues for leukocyte arrest. *Front Immunol,* 3**,** 188.

DOZ, E., LOMBARD, R., CARRERAS, F., BUZONI-GATEL, D. & WINTER, N. 2013. Mycobacteria-infected dendritic cells attract neutrophils that produce IL-10 and specifically shut

down Th17 CD4 T cells through their IL-10 receptor. *Journal of immunology,* 191**,** 3818-26.

DUFTON, N., HANNON, R., BRANCALEONE, V., DALLI, J., PATEL, H. B., GRAY, M., D'ACQUISTO, F., BUCKINGHAM, J. C., PERRETTI, M. & FLOWER, R. J. 2010. Anti-inflammatory role of the murine formyl-peptide receptor 2: ligand-specific effects on leukocyte responses and experimental inflammation. *Journal of immunology,* 184**,** 2611-9.

EDGEWORTH, J., GORMAN, M., BENNETT, R., FREEMONT, P. & HOGG, N. 1991. Identification of p8,14 as a highly abundant heterodimeric calcium binding protein complex of myeloid cells. *The Journal of biological chemistry,* 266**,** 7706-13.

EHLEN, H. W., CHINENKOVA, M., MOSER, M., MUNTER, H. M., KRAUSE, Y., GROSS, S., BRACHVOGEL, B., WUELLING, M., KORNAK, U. & VORTKAMP, A. 2013. Inactivation of anoctamin-6/Tmem16f, a regulator of phosphatidylserine scrambling in osteoblasts, leads to decreased mineral deposition in skeletal tissues. *J Bone Miner Res,* 28**,** 246-59.

EKEN, C., GASSER, O., ZENHAEUSERN, G., OEHRI, I., HESS, C. & SCHIFFERLI, J. A. 2008. Polymorphonuclear neutrophil-derived ectosomes interfere with the maturation of monocyte-derived dendritic cells. *Journal of immunology,* 180**,** 817-24.

EKEN, C., MARTIN, P. J., SADALLAH, S., TREVES, S., SCHALLER, M. & SCHIFFERLI, J. A. 2010. Ectosomes released by polymorphonuclear neutrophils induce a MerTK-dependent anti-inflammatory pathway in macrophages. *The Journal of biological chemistry,* 285**,** 39914-21.

EKEN, C., SADALLAH, S., MARTIN, P. J., TREVES, S. & SCHIFFERLI, J. A. 2013. Ectosomes of polymorphonuclear neutrophils activate multiple signaling pathways in macrophages. *Immunobiology,* 218**,** 382-92.

ELLIOTT, E. R., VAN ZIFFLE, J. A., SCAPINI, P., SULLIVAN, B. M., LOCKSLEY, R. M. & LOWELL, C. A. 2011. Deletion of Syk in neutrophils prevents immune complex arthritis. *Journal of immunology,* 187**,** 4319-30.

ENJETI, A. K., LINCZ, L. & SELDON, M. 2008. Bio-maleimide as a generic stain for detection and quantitation of microparticles. *International journal of laboratory hematology,* 30**,** 196-9.

ERDBRUEGGER, U., GROSSHEIM, M., HERTEL, B., WYSS, K., KIRSCH, T., WOYWODT, A., HALLER, H. & HAUBITZ, M. 2008. Diagnostic role of endothelial microparticles in vasculitis. *Rheumatology,* 47**,** 1820-5.

ETTELAIE, C., COLLIER, M. E., MEI, M. P., XIAO, Y. P. & MARAVEYAS, A. 2013. Enhanced binding of tissue factor-microparticles to collagen-IV and fibronectin leads to increased tissue factor activity in vitro. *Thrombosis and haemostasis,* 109**,** 61-71.

EYLES, J. L., HICKEY, M. J., NORMAN, M. U., CROKER, B. A., ROBERTS, A. W., DRAKE, S. F., JAMES, W. G., METCALF, D., CAMPBELL, I. K. & WICKS, I. P. 2008. A key role for G-CSF-induced neutrophil production and trafficking during inflammatory arthritis. *Blood,* 112**,** 5193-201.

FAN, Z., SODER, S., OEHLER, S., FUNDEL, K. & AIGNER, T. 2007. Activation of interleukin-1 signaling cascades in normal and osteoarthritic articular cartilage. *The American journal of pathology,* 171**,** 938-46.

FERNANDES, J. C., MARTEL-PELLETIER, J. & PELLETIER, J. P. 2002. The role of cytokines in osteoarthritis pathophysiology. *Biorheology,* 39**,** 237-46.

FILER, A., BUCKLEY, C.D. 2010. Fibroblasts and Stromal Cells. *In:* SERHAN, C. N., WARD, P.A., GILROY, D.W. (ed.) *Fundamentals of Inflammation.* New York, NY: Cambridge University Press.

FILER, A., RAZA, K., SALMON, M. & BUCKLEY, C. D. 2008. The role of chemokines in leucocyte-stromal interactions in rheumatoid arthritis. *Front Biosci,* 13**,** 2674-85.

FOURCADE, O., SIMON, M. F., VIODE, C., RUGANI, N., LEBALLE, F., RAGAB, A., FOURNIE, B., SARDA, L. & CHAP, H. 1995. Secretory phospholipase A2 generates the novel lipid mediator lysophosphatidic acid in membrane microvesicles shed from activated cells. *Cell,* 80**,** 919-27.

FREYSSINET, J. M. & TOTI, F. 2010. Formation of procoagulant microparticles and properties. *Thromb Res,* 125 Suppl 1**,** S46-8.

FUJISHIMA, S., HOFFMAN, A. R., VU, T., KIM, K. J., ZHENG, H., DANIEL, D., KIM, Y., WALLACE, E. F., LARRICK, J. W. & RAFFIN, T. A. 1993. Regulation of neutrophil interleukin 8 gene expression and protein secretion by LPS, TNF-alpha, and IL-1 beta. *J Cell Physiol,* 154**,** 478-85.

GASSER, O. & SCHIFFERLI, J. A. 2004. Activated polymorphonuclear neutrophils disseminate anti-inflammatory microparticles by ectocytosis. *Blood,* 104**,** 2543-8.

GERKE, V., CREUTZ, C. E. & MOSS, S. E. 2005. Annexins: linking Ca2+ signalling to membrane dynamics. *Nat Rev Mol Cell Biol,* 6**,** 449-61.

GETZY, L. L., MALEMUD, C.J., GOLDBERG, V.M., MOSKOWITZ, R.W. 1982. Factors Influencing Metachromatic Staining in Paraffin-Embedded Sections of Rabbit and Human Articular Cartilage: A Comparison of the Safranin O and Toluidine Blue O Techniques. *Journal of Histotechnology,* 3**,** 111-116.

GLOWACKA, E., LEWKOWICZ, P., ROTSZTEJN, H. & ZALEWSKA, A. 2010. IL-8, IL-12 and IL-10 cytokines generation by neutrophils, fibroblasts and neutrophils- fibroblasts interaction in psoriasis. *Adv Med Sci,* 55**,** 254-60.

GOLDRING, M. B. 2012. Chondrogenesis, chondrocyte differentiation, and articular cartilage metabolism in health and osteoarthritis. *Ther Adv Musculoskelet Dis,* 4**,** 269-85.

GOLDRING, M. B., BIRKHEAD, J. R., SUEN, L. F., YAMIN, R., MIZUNO, S., GLOWACKI, J., ARBISER, J. L. & APPERLEY, J. F. 1994. Interleukin-1 beta-modulated gene expression in immortalized human chondrocytes. *The Journal of clinical investigation,* 94**,** 2307-16.

GOLDRING, M. B. & MARCU, K. B. 2009. Cartilage homeostasis in health and rheumatic diseases. *Arthritis Research & Therapy,* 11**,** 224.

GOULDING, N. J., DIXEY, J., MORAND, E. F., DODDS, R. A., WILKINSON, L. S., PITSILLIDES, A. A. & EDWARDS, J. C. 1995. Differential distribution of annexins-I, -II, -IV, and -VI in synovium. *Ann Rheum Dis,* 54**,** 841-5.

GRAVES, L. E., ARIZTIA, E. V., NAVARI, J. R., MATZEL, H. J., STACK, M. S. & FISHMAN, D. A. 2004. Proinvasive properties of ovarian cancer ascites-derived membrane vesicles. *Cancer research,* 64**,** 7045-9.

GRECO, K. V., IQBAL, A. J., RATTAZZI, L., NALESSO, G., MORADI-BIDHENDI, N., MOORE, A. R., GOLDRING, M. B., DELL'ACCIO, F. & PERRETTI, M. 2011. High density micromass cultures of a human chondrocyte cell line: a reliable assay system to reveal the modulatory functions of pharmacological agents. *Biochem Pharmacol,* 82**,** 1919-29.

GRESNIGT, M. S., JOOSTEN, L. A., VERSCHUEREN, I., VAN DER MEER, J. W., NETEA, M. G., DINARELLO, C. A. & VAN DE VEERDONK, F. L. 2012. Neutrophil-mediated inhibition of proinflammatory cytokine responses. *Journal of immunology,* 189**,** 4806-15.

GROSS, S., GAMMON, S. T., MOSS, B. L., RAUCH, D., HARDING, J., HEINECKE, J. W., RATNER, L. & PIWNICA-WORMS, D. 2009. Bioluminescence imaging of myeloperoxidase activity in vivo. *Nature medicine,* 15**,** 455-61.

GUIDUCCI, S., DISTLER, J. H., JUNGEL, A., HUSCHER, D., HUBER, L. C., MICHEL, B. A., GAY, R. E., PISETSKY, D. S., GAY, S., MATUCCI-CERINIC, M. & DISTLER, O. 2008. The relationship between plasma microparticles and disease manifestations in patients with systemic sclerosis. *Arthritis and rheumatism,* 58**,** 2845-53.

GUILLEN, C., MCINNES, I. B., VAUGHAN, D., SPEEKENBRINK, A. B. & BROCK, J. H. 2000. The effects of local administration of lactoferrin on inflammation in murine autoimmune and infectious arthritis. *Arthritis and rheumatism,* 43**,** 2073-80.

HABER, F. & WEISS, J. 1932. Über die Katalyse des Hydroperoxydes. *Naturwissenschaften,* 20**,** 948-950.

HARTY, M. W., MURATORE, C. S., PAPA, E. F., GART, M. S., RAMM, G. A., GREGORY, S. H. & TRACY, T. F., JR. 2010. Neutrophil depletion blocks early collagen degradation in repairing cholestatic rat livers. *The American journal of pathology,* 176**,** 1271-81.

HAYHOE, R. P., KAMAL, A. M., SOLITO, E., FLOWER, R. J., COOPER, D. & PERRETTI, M. 2006. Annexin 1 and its bioactive peptide inhibit neutrophil-endothelium interactions under flow: indication of distinct receptor involvement. *Blood,* 107**,** 2123-30.

HE, H. Q., LIAO, D., WANG, Z. G., WANG, Z. L., ZHOU, H. C., WANG, M. W. & YE, R. D. 2013. Functional characterization of three mouse formyl peptide receptors. *Mol Pharmacol,* 83**,** 389-98.

HEROLD, M. 2012. Rheumatoid Arthritis. *In:* SHOENFELD, Y., MERONI, P.L. (ed.) *The General Practice Guide to Autoimmune Diseases.* Berlin: Pabst.

HILLSON, E. J. & HALLETT, M. B. 2007. Localised and rapid Ca2+ micro-events in human neutrophils: conventional Ca2+ puffs and global waves without peripheral-restriction or wave cycling. *Cell Calcium,* 41**,** 525-36.

HOFFMANN, P. R., KENCH, J. A., VONDRACEK, A., KRUK, E., DALEKE, D. L., JORDAN, M., MARRACK, P., HENSON, P. M. & FADOK, V. A. 2005. Interaction between phosphatidylserine and the phosphatidylserine receptor inhibits immune responses in vivo. *Journal of immunology,* 174**,** 1393-404.

HUANG, W., ZHOU, X., LEFEBVRE, V. & DE CROMBRUGGHE, B. 2000. Phosphorylation of SOX9 by cyclic AMP-dependent protein kinase A enhances SOX9's ability to transactivate a Col2a1 chondrocyte-specific enhancer. *Mol Cell Biol,* 20**,** 4149-58.

HUGEL, B., MARTINEZ, M. C., KUNZELMANN, C. & FREYSSINET, J. M. 2005. Membrane microparticles: two sides of the coin. *Physiology,* 20**,** 22-7.

HUNG, N. D., KIM, M. R. & SOK, D. E. 2011. 2-Polyunsaturated acyl lysophosphatidylethanolamine attenuates inflammatory response in zymosan A-induced peritonitis in mice. *Lipids,* 46**,** 893-906.

HUYNH, M. L., FADOK, V. A. & HENSON, P. M. 2002. Phosphatidylserine-dependent ingestion of apoptotic cells promotes TGF-beta1 secretion and the resolution of inflammation. *The Journal of clinical investigation,* 109**,** 41-50.

HYRICH, K. L., WATSON, K. D., SILMAN, A. J. & SYMMONS, D. P. 2006. Predictors of response to anti-TNF-alpha therapy among patients with rheumatoid arthritis: results from the British Society for Rheumatology Biologics Register. *Rheumatology,* 45**,** 1558-65.

IKEDA, S., TAKAHASHI, H., SUGA, Y., ETO, H., ETOH, T., OKUMA, K., TAKAHASHI, K., KANBARA, T., SEISHIMA, M., MORITA, A., IMAI, Y. & KANEKURA, T. 2013. Therapeutic depletion of myeloid lineage leukocytes in patients with generalized pustular psoriasis indicates a major role for neutrophils in the immunopathogenesis of psoriasis. *J Am Acad Dermatol,* 68**,** 609-17.

IKEGAMI, D., AKIYAMA, H., SUZUKI, A., NAKAMURA, T., NAKANO, T., YOSHIKAWA, H. & TSUMAKI, N. 2011. Sox9 sustains chondrocyte survival and hypertrophy in part through Pik3ca-Akt pathways. *Development,* 138**,** 1507-19.

IMBODEN, J. B. 2009. The immunopathogenesis of rheumatoid arthritis. *Annu Rev Pathol,* 4**,** 417-34.

INAL, J. M., ANSA-ADDO, E. A., STRATTON, D., KHOLIA, S., ANTWI-BAFFOUR, S. S., JORFI, S. & LANGE, S. 2012. Microvesicles in health and disease. *Archivum immunologiae et therapiae experimentalis,* 60**,** 107-21.

JAEGER, B. N., DONADIEU, J., COGNET, C., BERNAT, C., ORDONEZ-RUEDA, D., BARLOGIS, V., MAHLAOUI, N., FENIS, A., NARNI-MANCINELLI, E., BEAUPAIN, B., BELLANNE-CHANTELOT, C., BAJENOFF, M., MALISSEN, B., MALISSEN, M., VIVIER, E. & UGOLINI, S. 2012. Neutrophil depletion impairs natural killer cell maturation, function, and homeostasis. *J Exp Med,* 209**,** 565-80.

JANOWSKA-WIECZOREK, A., WYSOCZYNSKI, M., KIJOWSKI, J., MARQUEZ-CURTIS, L., MACHALINSKI, B., RATAJCZAK, J. & RATAJCZAK, M. Z. 2005. Microvesicles derived from activated platelets induce metastasis and angiogenesis in lung cancer. *International journal of cancer. Journal international du cancer,* 113**,** 752-60.

JIMENEZ, J. J., JY, W., MAURO, L. M., SODERLAND, C., HORSTMAN, L. L. & AHN, Y. S. 2003. Endothelial cells release phenotypically and quantitatively distinct microparticles in activation and apoptosis. *Thrombosis research,* 109**,** 175-80.

JONES, S. W., BROCKBANK, S. M., CLEMENTS, K. M., LE GOOD, N., CAMPBELL, D., READ, S. J., NEEDHAM, M. R. & NEWHAM, P. 2009. Mitogen-activated protein kinase-activated protein kinase 2 (MK2) modulates key biological pathways associated with OA disease pathology. *Osteoarthritis Cartilage,* 17**,** 124-31.

JOSE, P. J., MOSS, I. K., MAINI, R. N. & WILLIAMS, T. J. 1990. Measurement of the chemotactic complement fragment C5a in rheumatoid synovial fluids by radioimmunoassay: role of C5a in the acute inflammatory phase. *Annals of the rheumatic diseases,* 49**,** 747-52.

JOSEPH, J. E., HARRISON, P., MACKIE, I. J., ISENBERG, D. A. & MACHIN, S. J. 2001. Increased circulating platelet-leucocyte complexes and platelet activation in patients with antiphospholipid syndrome, systemic lupus erythematosus and rheumatoid arthritis. *British journal of haematology,* 115**,** 451-9.

JUNGEL, A., DISTLER, O., SCHULZE-HORSEL, U., HUBER, L. C., HA, H. R., SIMMEN, B., KALDEN, J. R., PISETSKY, D. S., GAY, S. & DISTLER, J. H. 2007. Microparticles stimulate the synthesis of prostaglandin E(2) via induction of cyclooxygenase 2 and microsomal prostaglandin E synthase 1. *Arthritis and rheumatism,* 56**,** 3564-74.

JY, W., JIMENEZ, J. J., MAURO, L. M., AHN, Y. S., NEWTON, K. R., MENDEZ, A. J., ARNOLD, P. I. & SCHULTZ, D. R. 2002. Agonist-induced capping of adhesion proteins and microparticle shedding in cultures of human renal microvascular endothelial cells. *Endothelium : journal of endothelial cell research,* 9**,** 179-89.

KAPUSTIN, A. N., DAVIES, J. D., REYNOLDS, J. L., MCNAIR, R., JONES, G. T., SIDIBE, A., SCHURGERS, L. J., SKEPPER, J. N., PROUDFOOT, D., MAYR, M. & SHANAHAN, C. M. 2011. Calcium regulates key components of vascular smooth muscle cell-derived matrix vesicles to enhance mineralization. *Circulation Research,* 109**,** e1-12.

KAROOR, V., SHIH, M., THOLANIKUNNEL, B. & MALBON, C. C. 1996. Regulating expression and function of G-protein-linked receptors. *Prog Neurobiol,* 48**,** 555-68.

KASTEN, K. R., MUENZER, J. T. & CALDWELL, C. C. 2010. Neutrophils are significant producers of IL-10 during sepsis. *Biochemical and biophysical research communications,* 393**,** 28-31.

KERKHOFF, C., KLEMPT, M., KAEVER, V. & SORG, C. 1999. The two calcium-binding proteins, S100A8 and S100A9, are involved in the metabolism of arachidonic acid in human neutrophils. *The Journal of biological chemistry,* 274**,** 32672-9.

KNIJFF-DUTMER, E. A., KOERTS, J., NIEUWLAND, R., KALSBEEK-BATENBURG, E. M. & VAN DE LAAR, M. A. 2002. Elevated levels of platelet microparticles are associated with disease activity in rheumatoid arthritis. *Arthritis and rheumatism,* 46**,** 1498-503.

KOLACZKOWSKA, E. & KUBES, P. 2013. Neutrophil recruitment and function in health and inflammation. *Nat Rev Immunol,* 13**,** 159-75.

KOVACS, M., TOTH, J., HETENYI, C., MALNASI-CSIZMADIA, A. & SELLERS, J. R. 2004. Mechanism of blebbistatin inhibition of myosin II. *The Journal of biological chemistry,* 279**,** 35557-63.

KRISHNAMOORTHY, S., RECCHIUTI, A., CHIANG, N., YACOUBIAN, S., LEE, C. H., YANG, R., PETASIS, N. A. & SERHAN, C. N. 2010. Resolvin D1 binds human phagocytes with evidence for proresolving receptors. *Proceedings of the National Academy of Sciences of the United States of America,* 107**,** 1660-5.

KUHL, A. A., KAKIRMAN, H., JANOTTA, M., DREHER, S., CREMER, P., PAWLOWSKI, N. N., LODDENKEMPER, C., HEIMESAAT, M. M., GROLLICH, K., ZEITZ, M., FARKAS, S. & HOFFMANN, J. C. 2007. Aggravation of different types of experimental colitis by depletion or adhesion blockade of neutrophils. *Gastroenterology,* 133**,** 1882-92.

KUNZELMANN, K., NILIUS, B., OWSIANIK, G., SCHREIBER, R., OUSINGSAWAT, J., SIRIANANT, L., WANITCHAKOOL, P., BEVERS, E. M. & HEEMSKERK, J. W. 2014. Molecular functions of

anoctamin 6 (TMEM16F): a chloride channel, cation channel, or phospholipid scramblase? *Pflugers Arch,* 466**,** 407-14.

KURIMOTO, T., YIN, Y., HABBOUB, G., GILBERT, H. Y., LI, Y., NAKAO, S., HAFEZI-MOGHADAM, A. & BENOWITZ, L. I. 2013. Neutrophils express oncomodulin and promote optic nerve regeneration. *J Neurosci,* 33**,** 14816-24.

LA ROCCA, G., LO IACONO, M., CORSELLO, T., CORRAO, S., FARINA, F. & ANZALONE, R. 2013. Human Wharton's jelly mesenchymal stem cells maintain the expression of key immunomodulatory molecules when subjected to osteogenic, adipogenic and chondrogenic differentiation in vitro: new perspectives for cellular therapy. *Curr Stem Cell Res Ther,* 8**,** 100-13.

LADINSKY, J. L. & WESTRING, D. W. 1967. The effect of anticoagulants on the volume of normal and leukemic leukocytes. *Cancer research,* 27**,** 1688-95.

LAMBRECHT, S., DHAENENS, M., ALMQVIST, F., VERDONK, P., VERBRUGGEN, G., DEFORCE, D. & ELEWAUT, D. 2010. Proteome characterization of human articular chondrocytes leads to novel insights in the function of small heat-shock proteins in chondrocyte homeostasis. *Osteoarthritis Cartilage,* 18**,** 440-6.

LASA, M., MAHTANI, K. R., FINCH, A., BREWER, G., SAKLATVALA, J. & CLARK, A. R. 2000. Regulation of cyclooxygenase 2 mRNA stability by the mitogen-activated protein kinase p38 signaling cascade. *Mol Cell Biol,* 20**,** 4265-74.

LATHAM, S. L., CHAPONNIER, C., DUGINA, V., COURAUD, P. O., GRAU, G. E. & COMBES, V. 2013. Cooperation between beta- and gamma-cytoplasmic actins in the mechanical regulation of endothelial microparticle formation. *FASEB J,* 27**,** 672-83.

LAUDISI, F., SPREAFICO, R., EVRARD, M., HUGHES, T. R., MANDRIANI, B., KANDASAMY, M., MORGAN, B. P., SIVASANKAR, B. & MORTELLARO, A. 2013. Cutting edge: the NLRP3 inflammasome links complement-mediated inflammation and IL-1beta release. *Journal of immunology,* 191**,** 1006-10.

LAZARUS, A. H., ELLIS, J., SEMPLE, J. W., MODY, M., CROW, A. R. & FREEDMAN, J. 2000. Comparison of platelet immunity in patients with SLE and with ITP. *Transfusion science,* 22**,** 19-27.

LEONI, G., ALAM, A., NEUMANN, P. A., LAMBETH, J. D., CHENG, G., MCCOY, J., HILGARTH, R. S., KUNDU, K., MURTHY, N., KUSTERS, D., REUTELINGSPERGER, C., PERRETTI, M., PARKOS, C. A., NEISH, A. S. & NUSRAT, A. 2013. Annexin A1, formyl peptide receptor, and NOX1 orchestrate epithelial repair. *The Journal of clinical investigation,* 123**,** 443-54.

LEVY, B. D. 2005. Lipoxins and lipoxin analogs in asthma. *Prostaglandins Leukot Essent Fatty Acids,* 73**,** 231-7.

LEVY, B. D., CLISH, C. B., SCHMIDT, B., GRONERT, K. & SERHAN, C. N. 2001. Lipid mediator class switching during acute inflammation: signals in resolution. *Nat Immunol,* 2**,** 612-9.

LI, M. O., SARKISIAN, M. R., MEHAL, W. Z., RAKIC, P. & FLAVELL, R. A. 2003. Phosphatidylserine receptor is required for clearance of apoptotic cells. *Science,* 302**,** 1560-3.

LI, X., ELLMAN, M., MUDDASANI, P., WANG, J. H., CS-SZABO, G., VAN WIJNEN, A. J. & IM, H. J. 2009. Prostaglandin E2 and its cognate EP receptors control human adult articular cartilage homeostasis and are linked to the pathophysiology of osteoarthritis. *Arthritis and rheumatism,* 60**,** 513-23.

LIMA, L. G., CHAMMAS, R., MONTEIRO, R. Q., MOREIRA, M. E. & BARCINSKI, M. A. 2009. Tumor-derived microvesicles modulate the establishment of metastatic melanoma in a phosphatidylserine-dependent manner. *Cancer letters,* 283**,** 168-75.

LIN, Y. C., LIANG, Y. C., SHEU, M. T., LIN, Y. C., HSIEH, M. S., CHEN, T. F. & CHEN, C. H. 2008. Chondroprotective effects of glucosamine involving the p38 MAPK and Akt signaling pathways. *Rheumatol Int,* 28**,** 1009-16.

LIPSKEY, P. E. 2008. Rheumatoid Arthritis. *In:* FAUCI, A. S., BRAUNWALD, E., KASPER, D. L., HAUSER, S. L., LONGO, D. L., JAMESON, J. L. & LOSCALZO, J. (eds.) *Harrison's Principles of Internal Medicine.* 17th ed. New York: McGraw-Hill.

MACK, M., KLEINSCHMIDT, A., BRUHL, H., KLIER, C., NELSON, P. J., CIHAK, J., PLACHY, J., STANGASSINGER, M., ERFLE, V. & SCHLONDORFF, D. 2000. Transfer of the chemokine receptor CCR5 between cells by membrane-derived microparticles: a mechanism for cellular human immunodeficiency virus 1 infection. *Nature medicine,* 6**,** 769-75.

MACKENZIE, A., WILSON, H. L., KISS-TOTH, E., DOWER, S. K., NORTH, R. A. & SURPRENANT, A. 2001. Rapid secretion of interleukin-1beta by microvesicle shedding. *Immunity,* 15**,** 825-35.

MAJKA, M., ROZMYSLOWICZ, T., HONCZARENKO, M., RATAJCZAK, J., WASIK, M. A., GAULTON, G. N. & RATAJCZAK, M. Z. 2000. Biological significance of the expression of HIV-related chemokine coreceptors (CCR5 and CXCR4) and their ligands by human hematopoietic cell lines. *Leukemia : official journal of the Leukemia Society of America, Leukemia Research Fund, U.K,* 14**,** 1821-32.

MAJNO, G., JORIS, I. 1996. *Cells, Tissues, and Disease: Principles of General Pathology*, Blackwell Science.

MALLONE, R. & NEPOM, G. T. 2004. MHC Class II tetramers and the pursuit of antigen-specific T cells: define, deviate, delete. *Clin Immunol,* 110**,** 232-42.

MANDAL, P., NOVOTNY, M. & HAMILTON, T. A. 2005. Lipopolysaccharide induces formyl peptide receptor 1 gene expression in macrophages and neutrophils via transcriptional and posttranscriptional mechanisms. *Journal of immunology,* 175**,** 6085-91.

MAUSE, S. F., WEBER, C. 2010. Microparticles: Protagonists of a Novel Communication Network for Intercellular Information Exchange. *Circulation Research***,** 1047-1057.

MCDONALD, B., PITTMAN, K., MENEZES, G. B., HIROTA, S. A., SLABA, I., WATERHOUSE, C. C., BECK, P. L., MURUVE, D. A. & KUBES, P. 2010. Intravascular danger signals guide neutrophils to sites of sterile inflammation. *Science,* 330**,** 362-6.

MCNEILL, E., CONWAY, S. J., RODERICK, H. L., BOOTMAN, M. D. & HOGG, N. 2007. Defective chemoattractant-induced calcium signalling in S100A9 null neutrophils. *Cell Calcium,* 41**,** 107-21.

MECHTCHERIAKOVA, D., WLACHOS, A., SOBANOV, J., KOPP, T., REUSCHEL, R., BORNANCIN, F., CAI, R., ZEMANN, B., URTZ, N., STINGL, G., ZLABINGER, G., WOISETSCHLAGER, M., BAUMRUKER, T. & BILLICH, A. 2007. Sphingosine 1-phosphate phosphatase 2 is induced during inflammatory responses. *Cell Signal,* 19**,** 748-60.

MEDZHITOV, R. 2008. Origin and physiological roles of inflammation. *Nature,* 454**,** 428-35.

MIYOSHI, H., UMESHITA, K., SAKON, M., IMAJOH-OHMI, S., FUJITANI, K., GOTOH, M., OIKI, E., KAMBAYASHI, J. & MONDEN, M. 1996. Calpain activation in plasma membrane bleb formation during tert-butyl hydroperoxide-induced rat hepatocyte injury. *Gastroenterology,* 110**,** 1897-904.

MIZRAK, A., BOLUKBASI, M. F., OZDENER, G. B., BRENNER, G. J., MADLENER, S., ERKAN, E. P., STROBEL, T., BREAKEFIELD, X. O. & SAYDAM, O. 2013. Genetically engineered microvesicles carrying suicide mRNA/protein inhibit schwannoma tumor growth. *Mol Ther,* 21**,** 101-8.

MOJICA, F. J., DIEZ-VILLASENOR, C., SORIA, E. & JUEZ, G. 2000. Biological significance of a family of regularly spaced repeats in the genomes of Archaea, Bacteria and mitochondria. *Mol Microbiol,* 36**,** 244-6.

MONACH, P., HATTORI, K., HUANG, H., HYATT, E., MORSE, J., NGUYEN, L., ORTIZ-LOPEZ, A., WU, H. J., MATHIS, D. & BENOIST, C. 2007. The K/BxN mouse model of inflammatory arthritis: theory and practice. *Methods Mol Med,* 136**,** 269-82.

MONACH, P. A., MATHIS, D. & BENOIST, C. 2008. The K/BxN arthritis model. *Curr Protoc Immunol,* Chapter 15**,** Unit 15 22.

MOON, M. H., JEONG, J. K., LEE, Y. J., SEOL, J. W. & PARK, S. Y. 2012. Sphingosine-1-phosphate inhibits interleukin-1beta-induced inflammation in human articular chondrocytes. *Int J Mol Med,* 30**,** 1451-8.

MOORE, A. R., APPELBOAM, A., KAWABATA, K., DA SILVA, J. A., D'CRUZ, D., GOWLAND, G. & WILLOUGHBY, D. A. 1999. Destruction of articular cartilage by alpha 2 macroglobulin elastase complexes: role in rheumatoid arthritis. *Annals of the rheumatic diseases,* 58**,** 109-13.

MORALES, T. I. & ROBERTS, A. B. 1988. Transforming growth factor beta regulates the metabolism of proteoglycans in bovine cartilage organ cultures. *The Journal of biological chemistry,* 263**,** 12828-31.

MOREL, O., MOREL, N., JESEL, L., FREYSSINET, J. M. & TOTI, F. 2011. Microparticles: a critical component in the nexus between inflammation, immunity, and thrombosis. *Seminars in immunopathology,* 33**,** 469-86.

MOSKOVICH, O. & FISHELSON, Z. 2007. Live cell imaging of outward and inward vesiculation induced by the complement c5b-9 complex. *The Journal of biological chemistry,* 282**,** 29977-86.

MULLER, W. A. 2003. Leukocyte-endothelial-cell interactions in leukocyte transmigration and the inflammatory response. *Trends Immunol,* 24**,** 327-34.

MURALIDHARAN-CHARI, V., CLANCY, J. W., SEDGWICK, A. & D'SOUZA-SCHOREY, C. 2010. Microvesicles: mediators of extracellular communication during cancer progression. *Journal of cell science,* 123**,** 1603-11.

MURPHY, K., TRAVERS, P., WALPORT, M. 2008. *Janeway's Immunobiology,* New York, NY, Garland Science.

NACKEN, W., SORG, C. & KERKHOFF, C. 2004. The myeloid expressed EF-hand proteins display a diverse pattern of lipid raft association. *FEBS Lett,* 572**,** 289-93.

NAGAHAMA, M., NOMURA, S., KANAZAWA, S., OZAKI, Y., KAGAWA, H. & FUKUHARA, S. 2003. Significance of anti-oxidized LDL antibody and monocyte-derived microparticles in anti-phospholipid antibody syndrome. *Autoimmunity,* 36**,** 125-31.

NAGAHAMA, M., NOMURA, S., OZAKI, Y., YOSHIMURA, C., KAGAWA, H. & FUKUHARA, S. 2001. Platelet activation markers and soluble adhesion molecules in patients with systemic lupus erythematosus. *Autoimmunity,* 33**,** 85-94.

NAKAMURA, H., UEKI, Y., SAKITO, S., MATSUMOTO, K., YANO, M., MIYAKE, S., TOMINAGA, T., TOMINAGA, M. & EGUCHI, K. 2000. High serum and synovial fluid granulocyte colony stimulating factor (G-CSF) concentrations in patients with rheumatoid arthritis. *Clin Exp Rheumatol,* 18**,** 713-8.

NATHAN, C. & DING, A. 2010. Nonresolving inflammation. *Cell,* 140**,** 871-82.

NEBE-VON-CARON, G. 2009. Standardisation in microbial cytometry. *Cytometry,* 75A**,** 86-89.

NEDELEC, E., ABID, A., CIPOLLETTA, C., PRESLE, N., TERLAIN, B., NETTER, P. & JOUZEAU, J. 2001. Stimulation of cyclooxygenase-2-activity by nitric oxide-derived species in rat chondrocyte: lack of contribution to loss of cartilage anabolism. *Biochem Pharmacol,* 61**,** 965-78.

NEMETH, T. & MOCSAI, A. 2012. The role of neutrophils in autoimmune diseases. *Immunology letters,* 143**,** 9-19.

NEUMANN, E., LEFEVRE, S., ZIMMERMANN, B., GAY, S. & MULLER-LADNER, U. 2010. Rheumatoid arthritis progression mediated by activated synovial fibroblasts. *Trends in molecular medicine,* 16**,** 458-68.

NEW, S. E., GOETTSCH, C., AIKAWA, M., MARCHINI, J. F., SHIBASAKI, M., YABUSAKI, K., LIBBY, P., SHANAHAN, C. M., CROCE, K. & AIKAWA, E. 2013. Macrophage-derived matrix vesicles: an alternative novel mechanism for microcalcification in atherosclerotic plaques. *Circulation Research,* 113**,** 72-7.

NIELSEN, C. T., OSTERGAARD, O., STENER, L., IVERSEN, L. V., TRUEDSSON, L., GULLSTRAND, B., JACOBSEN, S. & HEEGAARD, N. H. 2012. Increased IgG on cell-derived plasma microparticles in systemic lupus erythematosus is associated with autoantibodies and complement activation. *Arthritis and rheumatism,* 64**,** 1227-36.

NILSSON, J., SKOG, J., NORDSTRAND, A., BARANOV, V., MINCHEVA-NILSSON, L., BREAKEFIELD, X. O. & WIDMARK, A. 2009. Prostate cancer-derived urine exosomes: a novel approach to biomarkers for prostate cancer. *British journal of cancer,* 100**,** 1603-7.

NOMURA, S., INAMI, N., OZAKI, Y., KAGAWA, H. & FUKUHARA, S. 2008. Significance of microparticles in progressive systemic sclerosis with interstitial pneumonia. *Platelets,* 19**,** 192-8.

NORLING, L. V., SPITE, M., YANG, R., FLOWER, R. J., PERRETTI, M. & SERHAN, C. N. 2011. Cutting edge: Humanized nano-proresolving medicines mimic inflammation-resolution and enhance wound healing. *Journal of Immunology,* 186**,** 5543-7.

OCUIN, L. M., BAMBOAT, Z. M., BALACHANDRAN, V. P., CAVNAR, M. J., OBAID, H., PLITAS, G. & DEMATTEO, R. P. 2011. Neutrophil IL-10 suppresses peritoneal inflammatory monocytes during polymicrobial sepsis. *Journal of leukocyte biology,* 89**,** 423-32.

OMER, S., MEREDITH, D., MORRIS, J. F. & CHRISTIAN, H. C. 2006. Evidence for the role of adenosine 5'-triphosphate-binding cassette (ABC)-A1 in the externalization of annexin 1 from pituitary folliculostellate cells and ABCA1-transfected cell models. *Endocrinology,* 147**,** 3219-27.

OMOTO, S., NOMURA, S., SHOUZU, A., NISHIKAWA, M., FUKUHARA, S. & IWASAKA, T. 2002. Detection of monocyte-derived microparticles in patients with Type II diabetes mellitus. *Diabetologia,* 45**,** 550-5.

ORDONEZ-RUEDA, D., JONSSON, F., MANCARDI, D. A., ZHAO, W., MALZAC, A., LIANG, Y., BERTOSIO, E., GRENOT, P., BLANQUET, V., SABRAUTZKI, S., DE ANGELIS, M. H., MERESSE, S., DUPREZ, E., BRUHNS, P., MALISSEN, B. & MALISSEN, M. 2012. A hypomorphic mutation in the Gfi1 transcriptional repressor results in a novel form of neutropenia. *Eur J Immunol,* 42**,** 2395-408.

ORTEGA-GOMEZ, A., PERRETTI, M. & SOEHNLEIN, O. 2013. Resolution of inflammation: an integrated view. *EMBO Mol Med*.

PATEL, H. B., DAWSON, B., HUMBY, F., BLADES, M., PITZALIS, C., BURNET, M., SEED, M. 2010. Animal Models of Rheumatoid Arthritis. *In:* SERHAN, C. N., WARD, P.A., GILROY, D.W. (ed.) *Fundamentals of Inflammation.* New York, NY: Cambridge University Press.

PATEL, H. B., KORNERUP, K. N., SAMPAIO, A. L., D'ACQUISTO, F., SEED, M. P., GIROL, A. P., GRAY, M., PITZALIS, C., OLIANI, S. M. & PERRETTI, M. 2012. The impact of endogenous annexin A1 on glucocorticoid control of inflammatory arthritis. *Ann Rheum Dis,* 71**,** 1872-80.

PEREIRA, J., ALFARO, G., GOYCOOLEA, M., QUIROGA, T., OCQUETEAU, M., MASSARDO, L., PEREZ, C., SAEZ, C., PANES, O., MATUS, V. & MEZZANO, D. 2006. Circulating platelet-derived microparticles in systemic lupus erythematosus. Association with increased thrombin generation and procoagulant state. *Thrombosis and haemostasis,* 95**,** 94-9.

PERRETTI, M. & D'ACQUISTO, F. 2009. Annexin A1 and glucocorticoids as effectors of the resolution of inflammation. *Nat Rev Immunol,* 9**,** 62-70.

PFAFFL, M. W. 2001. A new mathematical model for relative quantification in real-time RT-PCR. *Nucleic acids research,* 29**,** e45.

PHILLIPSON, M. & KUBES, P. 2011. The neutrophil in vascular inflammation. *Nature medicine,* 17**,** 1381-90.

PICK, R., BRECHTEFELD, D. & WALZOG, B. 2013. Intraluminal crawling versus interstitial neutrophil migration during inflammation. *Mol Immunol,* 55**,** 70-5.

PLIYEV, B. K., KALINTSEVA, M. V., ABDULAEVA, S. V., YARYGIN, K. N. & SAVCHENKO, V. G. 2014. Neutrophil microparticles modulate cytokine production by natural killer cells. *Cytokine,* 65**,** 126-9.

POTEZ, S., LUGINBUHL, M., MONASTYRSKAYA, K., HOSTETTLER, A., DRAEGER, A. & BABIYCHUK, E. B. 2011. Tailored protection against plasmalemmal injury by annexins with different Ca2+ sensitivities. *The Journal of biological chemistry,* 286**,** 17982-91.

PRINCE, L. R., ALLEN, L., JONES, E. C., HELLEWELL, P. G., DOWER, S. K., WHYTE, M. K. & SABROE, I. 2004. The role of interleukin-1beta in direct and toll-like receptor 4-mediated neutrophil activation and survival. *The American journal of pathology,* 165**,** 1819-26.

PRUZANSKI, W., KEYSTONE, E. C., STERNBY, B., BOMBARDIER, C., SNOW, K. M. & VADAS, P. 1988. Serum phospholipase A2 correlates with disease activity in rheumatoid arthritis. *The Journal of rheumatology,* 15**,** 1351-5.

PUPJALIS, D., GOETSCH, J., KOTTAS, D. J., GERKE, V. & RESCHER, U. 2011. Annexin A1 released from apoptotic cells acts through formyl peptide receptors to dampen inflammatory monocyte activation via JAK/STAT/SOCS signalling. *EMBO Mol Med,* 3**,** 102-14.

QUAYLE, J. A., ADAMS, S., BUCKNALL, R. C. & EDWARDS, S. W. 1994. Cytokine expression by inflammatory neutrophils. *FEMS Immunol Med Microbiol,* 8**,** 233-9.

QUAYLE, J. A., ADAMS, S., BUCKNALL, R. C. & EDWARDS, S. W. 1995. Interleukin-1 expression by neutrophils in rheumatoid arthritis. *Annals of the rheumatic diseases,* 54**,** 930-3.

QUAYLE, J. A., WATSON, F., BUCKNALL, R. C. & EDWARDS, S. W. 1997. Neutrophils from the synovial fluid of patients with rheumatoid arthritis express the high affinity immunoglobulin G receptor, Fc gamma RI (CD64): role of immune complexes and cytokines in induction of receptor expression. *Immunology,* 91**,** 266-73.

RATAJCZAK, J., WYSOCZYNSKI, M., HAYEK, F., JANOWSKA-WIECZOREK, A. & RATAJCZAK, M. Z. 2006. Membrane-derived microvesicles: important and underappreciated mediators of cell-to-cell communication. *Leukemia : official journal of the Leukemia Society of America, Leukemia Research Fund, U.K,* 20**,** 1487-95.

RAZA, K., FALCIANI, F., CURNOW, S. J., ROSS, E. J., LEE, C. Y., AKBAR, A. N., LORD, J. M., GORDON, C., BUCKLEY, C. D. & SALMON, M. 2005. Early rheumatoid arthritis is characterized by a distinct and transient synovial fluid cytokine profile of T cell and stromal cell origin. *Arthritis Research & Therapy,* 7**,** R784-95.

REDINI, F., GALERA, P., MAUVIEL, A., LOYAU, G. & PUJOL, J. P. 1988. Transforming growth factor beta stimulates collagen and glycosaminoglycan biosynthesis in cultured rabbit articular chondrocytes. *FEBS Lett,* 234**,** 172-6.

REHMAN, A. A., AHSAN, H. & KHAN, F. H. 2013. alpha-2-Macroglobulin: a physiological guardian. *J Cell Physiol,* 228**,** 1665-75.

REMMERS, E. F., PLENGE, R. M., LEE, A. T., GRAHAM, R. R., HOM, G., BEHRENS, T. W., DE BAKKER, P. I., LE, J. M., LEE, H. S., BATLIWALLA, F., LI, W., MASTERS, S. L., BOOTY, M. G., CARULLI, J. P., PADYUKOV, L., ALFREDSSON, L., KLARESKOG, L., CHEN, W. V., AMOS, C. I., CRISWELL, L. A., SELDIN, M. F., KASTNER, D. L. & GREGERSEN, P. K. 2007. STAT4

and the risk of rheumatoid arthritis and systemic lupus erythematosus. *N Engl J Med,* 357**,** 977-86.

RENSHAW, D., MONTERO-MELENDEZ, T., DALLI, J., KAMAL, A., BRANCALEONE, V., D'ACQUISTO, F., CIRINO, G. & PERRETTI, M. 2010. Downstream gene activation of the receptor ALX by the agonist annexin A1. *PLoS One,* 5.

REVILLE, K., CREAN, J. K., VIVERS, S., DRANSFIELD, I. & GODSON, C. 2006. Lipoxin A4 redistributes myosin IIA and Cdc42 in macrophages: implications for phagocytosis of apoptotic leukocytes. *Journal of immunology,* 176**,** 1878-88.

RIECK, M., ARECHIGA, A., ONENGUT-GUMUSCU, S., GREENBAUM, C., CONCANNON, P. & BUCKNER, J. H. 2007. Genetic variation in PTPN22 corresponds to altered function of T and B lymphocytes. *Journal of immunology,* 179**,** 4704-10.

ROOD, I. M., DEEGENS, J. K., MERCHANT, M. L., TAMBOER, W. P., WILKEY, D. W., WETZELS, J. F. & KLEIN, J. B. 2010. Comparison of three methods for isolation of urinary microvesicles to identify biomarkers of nephrotic syndrome. *Kidney international,* 78**,** 810-6.

ROOS, M. A., GENNERO, L., DENYSENKO, T., REGUZZI, S., CAVALLO, G., PESCARMONA, G. P. & PONZETTO, A. 2010. Microparticles in physiological and in pathological conditions. *Cell biochemistry and function,* 28**,** 539-48.

ROSIER, R. N., O'KEEFE, R. J., CRABB, I. D. & PUZAS, J. E. 1989. Transforming growth factor beta: an autocrine regulator of chondrocytes. *Connect Tissue Res,* 20**,** 295-301.

ROSSOL, M., HEINE, H., MEUSCH, U., QUANDT, D., KLEIN, C., SWEET, M. J. & HAUSCHILDT, S. 2011. LPS-induced cytokine production in human monocytes and macrophages. *Crit Rev Immunol,* 31**,** 379-446.

ROTH, J., BURWINKEL, F., VAN DEN BOS, C., GOEBELER, M., VOLLMER, E. & SORG, C. 1993. MRP8 and MRP14, S-100-like proteins associated with myeloid differentiation, are translocated to plasma membrane and intermediate filaments in a calcium-dependent manner. *Blood,* 82**,** 1875-83.

ROZMYSLOWICZ, T., MAJKA, M., KIJOWSKI, J., MURPHY, S. L., CONOVER, D. O., PONCZ, M., RATAJCZAK, J., GAULTON, G. N. & RATAJCZAK, M. Z. 2003. Platelet- and megakaryocyte-derived microparticles transfer CXCR4 receptor to CXCR4-null cells and make them susceptible to infection by X4-HIV. *AIDS,* 17**,** 33-42.

SAFAEI, R., LARSON, B. J., CHENG, T. C., GIBSON, M. A., OTANI, S., NAERDEMANN, W. & HOWELL, S. B. 2005. Abnormal lysosomal trafficking and enhanced exosomal export of cisplatin in drug-resistant human ovarian carcinoma cells. *Molecular cancer therapeutics,* 4**,** 1595-604.

SAKANO, S., ZHU, Y. & SANDELL, L. J. 1999. Cartilage-derived retinoic acid-sensitive protein and type II collagen expression during fracture healing are potential targets for Sox9 regulation. *J Bone Miner Res,* 14**,** 1891-901.

SAKLATVALA, J. 1986. Tumour necrosis factor alpha stimulates resorption and inhibits synthesis of proteoglycan in cartilage. *Nature,* 322**,** 547-9.

SAMAVEDAM, U. K., IWATA, H., MULLER, S., SCHULZE, F. S., RECKE, A., SCHMIDT, E., ZILLIKENS, D. & LUDWIG, R. J. 2014. GM-CSF modulates autoantibody production and skin blistering in experimental epidermolysis bullosa acquisita. *Journal of immunology,* 192**,** 559-71.

SANDILANDS, G. P., AHMED, Z., PERRY, N., DAVISON, M., LUPTON, A. & YOUNG, B. 2005. Cross-linking of neutrophil CD11b results in rapid cell surface expression of molecules required for antigen presentation and T-cell activation. *Immunology,* 114**,** 354-68.

SANDILANDS, G. P., MCCRAE, J., HILL, K., PERRY, M. & BAXTER, D. 2006. Major histocompatibility complex class II (DR) antigen and costimulatory molecules on in vitro and in vivo activated human polymorphonuclear neutrophils. *Immunology,* 119**,** 562-71.

SCAPINI, P., BAZZONI, F. & CASSATELLA, M. A. 2008. Regulation of B-cell-activating factor (BAFF)/B lymphocyte stimulator (BLyS) expression in human neutrophils. *Immunology letters,* 116**,** 1-6.

SCAPINI, P., CARLETTO, A., NARDELLI, B., CALZETTI, F., ROSCHKE, V., MERIGO, F., TAMASSIA, N., PIEROPAN, S., BIASI, D., SBARBATI, A., SOZZANI, S., BAMBARA, L. & CASSATELLA, M. A. 2005. Proinflammatory mediators elicit secretion of the intracellular B-lymphocyte stimulator pool (BLyS) that is stored in activated neutrophils: implications for inflammatory diseases. *Blood,* 105**,** 830-7.

SCAPINI, P., HU, Y., CHU, C. L., MIGONE, T. S., DEFRANCO, A. L., CASSATELLA, M. A. & LOWELL, C. A. 2010. Myeloid cells, BAFF, and IFN-gamma establish an inflammatory loop that exacerbates autoimmunity in Lyn-deficient mice. *J Exp Med,* 207**,** 1757-73.

SCHELBERGEN, R. F., BLOM, A. B., VAN DEN BOSCH, M. H., SLOETJES, A., ABDOLLAHI-ROODSAZ, S., SCHREURS, B. W., MORT, J. S., VOGL, T., ROTH, J., VAN DEN BERG, W. B. & VAN LENT, P. L. 2012. Alarmins S100A8 and S100A9 elicit a catabolic effect in human osteoarthritic chondrocytes that is dependent on Toll-like receptor 4. *Arthritis and rheumatism,* 64**,** 1477-87.

SCHIF-ZUCK, S., GROSS, N., ASSI, S., ROSTOKER, R., SERHAN, C. N. & ARIEL, A. 2011. Saturated-efferocytosis generates pro-resolving CD11b low macrophages: modulation by resolvins and glucocorticoids. *Eur J Immunol,* 41**,** 366-79.

SCHONTHALER, H. B., GUINEA-VINIEGRA, J., WCULEK, S. K., RUPPEN, I., XIMENEZ-EMBUN, P., GUIO-CARRION, A., NAVARRO, R., HOGG, N., ASHMAN, K. & WAGNER, E. F. 2013. S100A8-S100A9 protein complex mediates psoriasis by regulating the expression of complement factor C3. *Immunity,* 39**,** 1171-81.

SERHAN, C. N. & PETASIS, N. A. 2011. Resolvins and protectins in inflammation resolution. *Chem Rev,* 111**,** 5922-43.

SERHAN, C. N. & SAVILL, J. 2005. Resolution of inflammation: the beginning programs the end. *Nat Immunol,* 6**,** 1191-7.

SHEDDEN, K., XIE, X. T., CHANDAROY, P., CHANG, Y. T. & ROSANIA, G. R. 2003. Expulsion of small molecules in vesicles shed by cancer cells: association with gene expression and chemosensitivity profiles. *Cancer research,* 63**,** 4331-7.

SHI, S., CHAN, A. G., MERCER, S., ECKERT, G. J. & TRIPPEL, S. B. 2014. Endogenous versus exogenous growth factor regulation of articular chondrocytes. *J Orthop Res,* 32**,** 54-60.

SHIN, M. E., HE, Y., LI, D., NA, S., CHOWDHURY, F., POH, Y. C., COLLIN, O., SU, P., DE LANEROLLE, P., SCHWARTZ, M. A., WANG, N. & WANG, F. 2010. Spatiotemporal organization, regulation, and functions of tractions during neutrophil chemotaxis. *Blood,* 116**,** 3297-310.

SHULER, F. D., GEORGESCU, H. I., NIYIBIZI, C., STUDER, R. K., MI, Z., JOHNSTONE, B., ROBBINS, R. D. & EVANS, C. H. 2000. Increased matrix synthesis following adenoviral transfer of a transforming growth factor beta1 gene into articular chondrocytes. *J Orthop Res,* 18**,** 585-92.

SINGH, J. A. 2012. Stem cells and other innovative intra-articular therapies for osteoarthritis: what does the future hold? *BMC Med,* 10**,** 44.

SKOG, J., WURDINGER, T., VAN RIJN, S., MEIJER, D. H., GAINCHE, L., SENA-ESTEVES, M., CURRY, W. T., JR., CARTER, B. S., KRICHEVSKY, A. M. & BREAKEFIELD, X. O. 2008. Glioblastoma microvesicles transport RNA and proteins that promote tumour growth and provide diagnostic biomarkers. *Nat Cell Biol,* 10**,** 1470-6.

STANTON, H., GOLUB, S. B., ROGERSON, F. M., LAST, K., LITTLE, C. B. & FOSANG, A. J. 2011. Investigating ADAMTS-mediated aggrecanolysis in mouse cartilage. *Nat Protoc,* 6**,** 388-404.

STEINBACH, K., PIEDAVENT, M., BAUER, S., NEUMANN, J. T. & FRIESE, M. A. 2013. Neutrophils amplify autoimmune central nervous system infiltrates by maturing local APCs. *Journal of immunology,* 191**,** 4531-9.

STIRLING, D. P., LIU, S., KUBES, P. & YONG, V. W. 2009. Depletion of Ly6G/Gr-1 leukocytes after spinal cord injury in mice alters wound healing and worsens neurological outcome. *J Neurosci,* 29**,** 753-64.

STRADNER, M. H., GRUBER, G., ANGERER, H., HUBER, V., SETZNAGL, D., KREMSER, M. L., FURST, F. C., WINDHAGER, R. & GRANINGER, W. B. 2014. A5.9 Sphingosine-1-phosphate counteracts interleukin-1beta in human chondrocytes. *Annals of the rheumatic diseases,* 73 Suppl 1**,** A66-7.

STRADNER, M. H., GRUBER, G., ANGERER, H., HUBER, V., SETZNAGL, D., KREMSER, M. L., MOAZEDI-FURST, F. C., WINDHAGER, R. & GRANINGER, W. B. 2013. Sphingosine 1-phosphate counteracts the effects of interleukin-1beta in human chondrocytes. *Arthritis and rheumatism,* 65**,** 2113-22.

STRADNER, M. H., HERMANN, J., ANGERER, H., SETZNAGL, D., SUNK, I., WINDHAGER, R. & GRANINGER, W. B. 2008. Spingosine-1-phosphate stimulates proliferation and counteracts interleukin-1 induced nitric oxide formation in articular chondrocytes. *Osteoarthritis Cartilage,* 16**,** 305-11.

SUN, L., WANG, X. & KAPLAN, D. L. 2011. A 3D cartilage - inflammatory cell culture system for the modeling of human osteoarthritis. *Biomaterials,* 32**,** 5581-9.

SUZUKI, J., UMEDA, M., SIMS, P. J. & NAGATA, S. 2010. Calcium-dependent phospholipid scrambling by TMEM16F. *Nature,* 468**,** 834-8.

TAMASSIA, N., ZIMMERMANN, M., CASTELLUCCI, M., OSTUNI, R., BRUDEREK, K., SCHILLING, B., BRANDAU, S., BAZZONI, F., NATOLI, G. & CASSATELLA, M. A. 2013. Cutting edge: An inactive chromatin configuration at the IL-10 locus in human neutrophils. *Journal of immunology,* 190**,** 1921-5.

TECCHIO, C. & CASSATELLA, M. A. 2014. Neutrophil-derived cytokines involved in physiological and pathological angiogenesis. *Chem Immunol Allergy,* 99**,** 123-37.

TIMAR, C. I., LORINCZ, A. M., CSEPANYI-KOMI, R., VALYI-NAGY, A., NAGY, G., BUZAS, E. I., IVANYI, Z., KITTEL, A., POWELL, D. W., MCLEISH, K. R. & LIGETI, E. 2013. Antibacterial effect of microvesicles released from human neutrophilic granulocytes. *Blood,* 121**,** 510-8.

TROUW, L. A., HUIZINGA, T. W. & TOES, R. E. 2013. Autoimmunity in rheumatoid arthritis: different antigens--common principles. *Annals of the rheumatic diseases,* 72 Suppl 2**,** ii132-6.

TUAN, R. S., CHEN, A. F. & KLATT, B. A. 2013. Cartilage regeneration. *J Am Acad Orthop Surg,* 21**,** 303-11.

ULLAL, A. J., REICH, C. F., 3RD, CLOWSE, M., CRISCIONE-SCHREIBER, L. G., TOCHACEK, M., MONESTIER, M. & PISETSKY, D. S. 2011. Microparticles as antigenic targets of antibodies to DNA and nucleosomes in systemic lupus erythematosus. *Journal of autoimmunity,* 36**,** 173-80.

UYSAL, H., BOCKERMANN, R., NANDAKUMAR, K. S., SEHNERT, B., BAJTNER, E., ENGSTROM, A., SERRE, G., BURKHARDT, H., THUNNISSEN, M. M. & HOLMDAHL, R. 2009. Structure and pathogenicity of antibodies specific for citrullinated collagen type II in experimental arthritis. *J Exp Med,* 206**,** 449-62.

VAAMONDE-GARCIA, C., RIVEIRO-NAVEIRA, R. R., VALCARCEL-ARES, M. N., HERMIDA-CARBALLO, L., BLANCO, F. J. & LOPEZ-ARMADA, M. J. 2012. Mitochondrial dysfunction increases inflammatory responsiveness to cytokines in normal human chondrocytes. *Arthritis Rheum,* 64**,** 2927-36.

VALADI, H., EKSTROM, K., BOSSIOS, A., SJOSTRAND, M., LEE, J. J. & LOTVALL, J. O. 2007. Exosome-mediated transfer of mRNAs and microRNAs is a novel mechanism of genetic exchange between cells. *Nat Cell Biol,* 9**,** 654-9.

VAN DEN BERG, W. B. 2008. Lessons from animal models of osteoarthritis. *Curr Rheumatol Rep,* 10**,** 26-9.

VAN DER POL, E., BOING, A. N., HARRISON, P., STURK, A. & NIEUWLAND, R. 2012. Classification, functions, and clinical relevance of extracellular vesicles. *Pharmacol Rev,* 64**,** 676-705.

VAN DER POL, E., HOEKSTRA, A.G., STURK, A., OTTO, C., VAN LEEUWEN, T.G., NIEUWLAND, R., 2010. Optical and non-optical methods for detection and characterisation of microparticles and exosomes. *J Thromb Haemost,* 8**,** 2596-2607.

VAN LENT, P. L., GREVERS, L. C., BLOM, A. B., ARNTZ, O. J., VAN DE LOO, F. A., VAN DER KRAAN, P., ABDOLLAHI-ROODSAZ, S., SRIKRISHNA, G., FREEZE, H., SLOETJES, A., NACKEN, W., VOGL, T., ROTH, J. & VAN DEN BERG, W. B. 2008. Stimulation of chondrocyte-mediated cartilage destruction by S100A8 in experimental murine arthritis. *Arthritis Rheum,* 58**,** 3776-87.

VOGL, T., LUDWIG, S., GOEBELER, M., STREY, A., THOREY, I. S., REICHELT, R., FOELL, D., GERKE, V., MANITZ, M. P., NACKEN, W., WERNER, S., SORG, C. & ROTH, J. 2004. MRP8 and MRP14 control microtubule reorganization during transendothelial migration of phagocytes. *Blood,* 104**,** 4260-8.

VOISIN, M. B. & NOURSHARGH, S. 2013. Neutrophil transmigration: emergence of an adhesive cascade within venular walls. *J Innate Immun,* 5**,** 336-47.

VONG, L., D'ACQUISTO, F., PEDERZOLI-RIBEIL, M., LAVAGNO, L., FLOWER, R. J., WITKO-SARSAT, V. & PERRETTI, M. 2007. Annexin 1 cleavage in activated neutrophils: a pivotal role for proteinase 3. *The Journal of biological chemistry,* 282**,** 29998-30004.

VOSSENAAR, E. R. & VAN VENROOIJ, W. J. 2004. Citrullinated proteins: sparks that may ignite the fire in rheumatoid arthritis. *Arthritis Research & Therapy,* 6**,** 107-11.

WAECHTER, V., SCHMID, M., HEROVA, M., WEBER, A., GUNTHER, V., MARTI-JAUN, J., WUST, S., ROSINGER, M., GEMPERLE, C. & HERSBERGER, M. 2012. Characterization of the promoter and the transcriptional regulation of the lipoxin A4 receptor (FPR2/ALX) gene in human monocytes and macrophages. *Journal of immunology,* 188**,** 1856-67.

WANG, S., VOISIN, M. B., LARBI, K. Y., DANGERFIELD, J., SCHEIERMANN, C., TRAN, M., MAXWELL, P. H., SOROKIN, L. & NOURSHARGH, S. 2006. Venular basement membranes contain specific matrix protein low expression regions that act as exit points for emigrating neutrophils. *J Exp Med,* 203**,** 1519-32.

WARD, P. A. 2010. Acute and Chronic Inflammation. *In:* SERHAN, C. N., WARD, P.A., GILROY, D.W. (ed.) *Fundamentals of Inflammation.* New York, NY: Cambridge University Press.

WEYAND, C. M. & GORONZY, J. J. 2003. Ectopic germinal center formation in rheumatoid synovitis. *Ann N Y Acad Sci,* 987**,** 140-9.

WHITE, F. S., QUAYLE, J. A. & EDWARDS, S. W. 1996. Gene expression by inflammatory neutrophils: stimulation of interleukin-1 beta production by rheumatoid synovial fluid. *Biochem Soc Trans,* 24**,** 493S.

WITHERS, P. C. 1992. *Comparative Animal Physiology,* University of Michigan, Saunders College Publisher.

WITKO-SARSAT, V., RIEU, P., DESCAMPS-LATSCHA, B., LESAVRE, P. & HALBWACHS-MECARELLI, L. 2000. Neutrophils: molecules, functions and pathophysiological aspects. *Lab Invest,* 80**,** 617-53.

WOLF, P. 1967. The nature and significance of platelet products in human plasma. *British journal of haematology,* 13**,** 269-88.

WONG, S. H., FRANCIS, N., CHAHAL, H., RAZA, K., SALMON, M., SCHEEL-TOELLNER, D. & LORD, J. M. 2009. Lactoferrin is a survival factor for neutrophils in rheumatoid synovial fluid. *Rheumatology,* 48**,** 39-44.

WRIGHT, H. L., BUCKNALL, R. C., MOOTS, R. J. & EDWARDS, S. W. 2012. Analysis of SF and plasma cytokines provides insights into the mechanisms of inflammatory arthritis and may predict response to therapy. *Rheumatology,* 51**,** 451-9.

WRIGHT, H. L., MOOTS, R. J., BUCKNALL, R. C. & EDWARDS, S. W. 2010. Neutrophil function in inflammation and inflammatory diseases. *Rheumatology,* 49**,** 1618-31.

YANG, H., KIM, A., DAVID, T., PALMER, D., JIN, T., TIEN, J., HUANG, F., CHENG, T., COUGHLIN, S. R., JAN, Y. N. & JAN, L. Y. 2012. TMEM16F forms a Ca2+-activated cation channel required for lipid scrambling in platelets during blood coagulation. *Cell,* 151**,** 111-22.

YE, R. D., BOULAY, F., WANG, J. M., DAHLGREN, C., GERARD, C., PARMENTIER, M., SERHAN, C. N. & MURPHY, P. M. 2009. International Union of Basic and Clinical Pharmacology. LXXIII. Nomenclature for the formyl peptide receptor (FPR) family. *Pharmacol Rev,* 61**,** 119-61.

YIN, W., PARK, J. I. & LOESER, R. F. 2009. Oxidative stress inhibits insulin-like growth factor-I induction of chondrocyte proteoglycan synthesis through differential regulation of phosphatidylinositol 3-Kinase-Akt and MEK-ERK MAPK signaling pathways. *The Journal of biological chemistry,* 284**,** 31972-81.

ZAMZAMI, N., MARCHETTI, P., CASTEDO, M., DECAUDIN, D., MACHO, A., HIRSCH, T., SUSIN, S. A., PETIT, P. X., MIGNOTTE, B. & KROEMER, G. 1995. Sequential reduction of mitochondrial transmembrane potential and generation of reactive oxygen species in early programmed cell death. *J Exp Med,* 182**,** 367-77.

ZHOU, X., ENGEL, T., GOEPFERT, C., ERREN, M., ASSMANN, G. & VON ECKARDSTEIN, A. 2002. The ATP binding cassette transporter A1 contributes to the secretion of interleukin 1beta from macrophages but not from monocytes. *Biochemical and biophysical research communications,* 291**,** 598-604.

ZITVOGEL, L., REGNAULT, A., LOZIER, A., WOLFERS, J., FLAMENT, C., TENZA, D., RICCIARDI-CASTAGNOLI, P., RAPOSO, G. & AMIGORENA, S. 1998. Eradication of established murine tumors using a novel cell-free vaccine: dendritic cell-derived exosomes. *Nature medicine,* 4**,** 594-600.